université de BORDEAUX

THÈSE PRÉSENTÉE

POUR OBTENIR LE GRADE DE

DOCTEUR DE

L'UNIVERSITÉ DE BORDEAUX
PRÉPARÉE à l'ESTIA

ÉCOLE DOCTORALE : SCIENCES PHYSIQUES ET DE L'INGENIEUR

SPÉCIALITÉ : Mécanique

Par Gilberto FONTECHA DULCEY

Modèle paramétrique, réduit et multi-échelle pour l'optimisation interactive de structures composites

Sous la direction de : Pr. Xavier FISCHER
(Co-directeur : Pierre JOYOT)

Soutenue le : 3 décembre 2018

Membres du jury :

M. FOURQUET, Jean-Yves	Professeur des Universités ENIT	Président
M. CHINESTA, Francisco	Professeur des Universités à l'ENSAM	Rapporteur
M. YANNOU, Bernard	Professeur des Universités à CentraleSupélec	Rapporteur
M. BENNIS, Fouad	Professeur des Universités à Centrale Nantes	Examinateur
M. FISCHER, Xavier	Professeur ESTIA	Examinateur
M. FADEL, Georges	Professeur Clemson University	Examinateur
M. JOYOT, Pierre	Enseignant-Chercheur ESTIA	Examinateur
M. POSADA, Jorge	Directeur adjoint à Vicomtech	Examinateur

(This page is intentionally left blank)

Dedicada a mi amada esposa y mis dos hijos

(This page is intentionally left blank)

Titre : Modèle Paramétrique, Réduit et multi-échelle pour l'optimisation interactive de structures composites

Résumé : Concevoir une structure composite consiste à relever un défi de taille : alors qu'un ingénieur qui conçoit un produit mécanique à base de matériau métallique se concentre principalement sur le développement d'une forme qui garantira un comportement spécifique, l'ingénieur pour qui le problème de conception est celui d'un produit à base de matériaux composites doit trouver la meilleure combinaison forme - structure de matériau. Ainsi, il doit aussi concevoir simultanément un matériau et la topologie produit. La combinatoire s'avère être complexe et les espaces de solutions de très grande taille.

Les outils de CAO et de simulation par éléments finis n'offrent pas au concepteur une approche permettant d'explorer les espaces de recherche de manière interactive et rapide. Le travail de thèse conduit à une nouvelle approche numérique permettant de manipuler chaque paramètre de conception caractérisant une structure composite, quelle que soit l'échelle à laquelle il est pertinent.

Premièrement, le modèle de comportement paramétrique et réduit (Parametric and Reduced Behavior Model, PRBM) est un modèle dit séparé. Il permet :

1- une approche multi-échelle : les paramètres mécaniques de la structure sont explicitement décrits comme issus de la qualité matérielle de chaque fibre, de la matrice, de chaque couche et de la topologie même du stratifié,

2- une approche multi-physique: indépendamment le comportement mécanique de chaque couche et de chaque interface est traité pour donner lieu au comportement du stratifié. Des situations de comportements statiques et dynamiques sont étudiés. Dans le cas du comportement dynamique, le caractère visco-élastique est devenu un enjeu conceptuel.

Deuxièmement, une méthode mixant dérivées non entières et usage de la méthode PGD a permis la réalisation du PRBM. Intégré dans un modèle de connaissance paramétrique (Parametric Knowledge Model, PKM) auprès de modèles de connaissances experts, il constitue la base d'une méthode interactive d'aide à la conception.

Le PKM est traité par une méthode d'optimisation évolutionnaire. De ce fait, le concepteur peut explorer de façon interactive les espaces de conception. Pour qualifier nos modèles et notre PRBM, nous étudions 2 problèmes de conception de structures stratifiées. Les solutions déterminées sont qualifiées vis-à-vis de simulations par éléments finis ou selon une approche empirique.

Mots clés : Modèle Réduit et paramétrique, Optimisation interactive, Aide à la décision en conception, PGD, Viscoélasticité, Matériaux composites

ESTIA Recherche – I2M CNRS UMR 5295

(This page is intentionally left blank)

Title: Parametric, Reduced and Multiscale model for the Interactive Optimization of Laminated Composite Structures

Abstract: The design process of laminated composites faces a major challenge: while an engineer designing a metallic based mechanical product is mainly focusing on the development of a shape that will guarantee a specific behavior, the engineer designing a composite based product must find the best combination of the shape-material structure. Therefore, he must simultaneously create a material and the product topology. The number of design solutions can be huge since the solution space is considerable.

Standard CAE systems (CAD, Finite Element Simulation) do not provide an approach to explore these solution spaces efficiently and interactively. A new numerical procedure is proposed to allow engineers to handle each design parameter of a laminated composite structure, each at its relevant scale.

First, the Parametric and Reduced Behavior Model (PRBM) is a separated model that enables reasoning based on

1- A multiscale approach: the mechanical parameters of the structure are explicitly described as coming from the material quality of each fiber, the matrix, each layer and the topology of the laminate,

2- A multiphysical approach: independently the mechanical behavior of each layer and each interface is processed, leading to the behavior of the laminate. Some situations of static and dynamic behavior are studied. In the case of dynamic behavior, the creeping becomes a conceptual issue.

Secondly, a method mixing fractional derivatives and the Proper Generalized Decomposition (PGD) method allowed the creation of the PRBM. Integrated into a Parametric Knowledge Model (PKM) with other expert knowledge models, the PRBM makes the basis of an interactive method of design support.

The PKM is processed by an evolutionary optimization method. As a result, the designer can interactively explore the design space. To qualify our models and our PRBM, we study two problems of design of laminated composite structures. The solutions determined are qualified versus finite element simulations or according to an empirical approach.

Keywords: Parametric and reduced model, Interactive optimization, Design support system, PGD, Viscoelasticity, Composite materials

(This page is intentionally left blank)

Título: Modelo Paramétrico, Reducido y Multiescala para la Optimización Interactiva de estructuras compuestas

Resumen: El diseño de una estructura compuesta es un desafío mayor, mientras que un ingeniero que diseña un producto mecánico con materiales metálicos se concentra principalmente en el desarrollo de una geometría que garantice un comportamiento específico, el ingeniero que diseña un producto con materiales compuestos debe encontrar la mejor combinación forma – estructura del material. De esta manera, el ingeniero debe diseñar simultáneamente el material y la topología del producto, razón por la que esta combinación se vislumbra compleja, puesto que los espacios de solución son gran tamaño.

Las herramientas CAO y de simulación por elementos finitos no ofrecen al diseñador una metodología que permita explorar los espacios de solución de manera interactiva y rápida. Por lo tanto, este trabajo de tesis propone un nuevo enfoque numérico que permite manipular parámetros de diseño que caracterizan la estructura compuesta, cualquiera que sea la escala de pertinencia.

Como primera medida, el modelo de comportamiento paramétrico y reducido (Parametric and Reduced Behavior Model, PRBM) es un modelo definido de manera separada que permite:

1- Un enfoque multiescala: los parámetros mecánicos se presentan de manera explícita en términos de las propiedades de cada fibra, de la matriz, de cada capa y de la topología del mismo apilamiento.

2- Un enfoque multifísico: el comportamiento mecánico de cada capa y cada interface se modela de manera independiente para dar lugar al comportamiento del apilamiento. Se estudian situaciones de casos de comportamiento estático y dinámico. En el caso dinámico en particular, se tiene en cuenta también la característica viscoelástica de las interfaces.

Como segunda medida, un método que combina derivadas no enteras y el uso de la descomposición propia generalizada (PGD), permite la realización del PRBM. Este constituye la base de un método interactivo de ayuda al diseño, pues está integrado dentro de un modelo de conocimiento (PKM) que también incorpora mejores prácticas aprendidas por expertos.

El PKM es utilizado por un método de optimización evolucionaria. De esta manera, el diseñador puede explorar de manera interactiva los espacios de solución. Para validar nuestros modelos y el PRBM, se estudian dos problemas de diseño de estructuras apiladas. Las soluciones obtenidas se comparan con respecto a simulaciones obtenidas por el método de los elementos finitos y con respecto a resultados experimentales.

Palabras clave: Modelo reducido y paramétrico, Optimización interactiva, Ayuda a la decisión en diseño, PGD, Viscoelasticidad, Materiales compuestos

(This page is intentionally left blank)

ACKNOWLEDGMENTS

I want to express my most sincere gratitude to my thesis director, Professor Xavier FISCHER, for his guidance and advice. He has helped me expand my knowledge and challenge my perspectives.

Special thanks also to my thesis co-director Dr. Pierre JOYOT, for his willingness to teach me and develop on the fascinating PGD method.

I would also like to thank the members of the jury for their valuable time to read and evaluate this thesis.

This thesis is specially dedicated to my beloved wife, María Paula and my children Azucena and Martín. Thank you for your support, love, and patience during the process of researching and writing this thesis.

To my mother and my father, as their emphasis on education is an inspiration. To my sisters and extended family for their support. Special thanks to my sister Fabiola, for her willingness to read this manuscript.

Special thanks to M. Jean Pierre and Mme. Marie Jeanne COUZI. They gave me invaluable support and the warmth of a home in France.

I appreciate the support of all my friends and co-workers at UPB in Colombia and ESTIA in France.

Finally, I would like to thank the UPB and COLCIENCIAS for providing the funding for this work.

(This page is intentionally left blank)

SYMBOLS

E	Young's modulus (MPa).	$U_{x,y,z,p_1,p_2,\cdots,p_d}$	Approximation of the displacement field (mm).
E_f	Fiber Young's modulus (MPa)	$U(x,y,z,p_1,p_1,\cdots,p_d)$	Displacement field as a function of given parameters (mm).
E_m	Matrix Young's modulus (MPa).	C	Tensor of material properties in local coordinates.
E_l	Young's modulus of the ply in the direction of the fibers (MPa).	n	Number of enrichment modes in PGD sense.
E_t	Young's modulus of the ply in a direction transversal to the fiber direction (MPa).	$\overline{\boldsymbol{C}}$	Tensor of material properties in global coordinates.
F_y, F_z	External forces (N).	$\overline{\boldsymbol{C}}(p_1), \overline{\boldsymbol{C}}(p_2)$ $\overline{\boldsymbol{C}}(p_3), \overline{\boldsymbol{C}}(p_4)$	Tensor of material properties at plies 1, 2, 3, 4 in global coordinates.
$F(\omega)$	Force as a function of frequency (N).	$\boldsymbol{C}_{int}$	Tensor of material properties at the interfaces.
B	Body force.	D	Transformation matrix.
G	Shear modulus (MPa).	ρ	Density (kg/m^3).
v	Poisson's ratio.	ρ_f	Fiber density.
l	Length (mm).	ρ_m	Resin density.
h	Height (mm).	Ω	Geometric domain.
w	Width (mm).	θ_i	Fiber orientation of ply i (degrees).

u	Displacement in direction *x*.	V_f	Fiber volume fraction (%).
v	Displacement in direction *y*.	G_0	Short term shear modulus (GPa)
w	Displacement in direction *z*.	G_∞	Long-term shear modulus (GPa).
$\boldsymbol{\varepsilon}$	Strain tensor.	α	Fractional derivative order .
$\boldsymbol{\sigma}$	Stress Tensor (Pa).	τ	Decay time (s).
σ_{ij}	Stress tensor element (Pa).	$X, Y, Z, P1, P2, P3, P4, P5, P6, P7$	PGD functions.
F_0	Objective function.	$x, y, z, p_1, p_2, p_3, p_4, p_5, p_6, p_7$	PGD domains
ς, ξ, ψ	Weights.	T_{max}	Maximum twist.
$\mathcal{L}_{max}$	Maximum deformation to the direction *y*.		

ACRONYMS

CAD	Computer-Aided Design
CAE	Computer-Aided Engineering
CLT	Classical Lamination Theory
CM	Composite Material
CMC	Ceramic Matrix Composites
CPU	Computer Processing Unit
CZM	Cohesive Zone Model
DMSS	Decision Making Support Systems
EA	Evolutionary Algorithm
ECSW	Energy Conserving Sampling and Weighting
ESL	Equivalent Single Layer
FEM	Finite Element Method
FE^2	Two-level Finite Elements
FRF	Frequency Response Function
FSDT	First-Order Shear Deformation Theory
GA	Genetic Algorithm
HSDT	High Order Shear Deformation Theory
LW	LayerWise
MMC	Metallic Matrix Composites
NN	Neuronal Network
NTFA	Nonuniform Transformation Field Analysis

OMC	Organic Matrix Composites
PGD	Proper Generalized Decomposition
PKM	Parametric Knowledge Model
POD	Proper Orthogonal Decomposition
PRBM	Parametric and Reduced Base Model
RAM	Random Access Memory
RB	Reduced Base
ROQ	Reduced Optimal Quadrature
RS	Response Surface
RVE	Representative Volume Element
SEM	Scanning Electron Microscopy
SSM	Spatial Separated Model
TFA	Transformation Field Analysis

TABLE OF CONTENTS

RESUME ETENDU **1**

INTRODUCTION **27**

CHAPTER 1 MODELING AND DESIGN OF COMPOSITE STRUCTURES: STATE OF THE ART **31**

1.1 INTRODUCTION 31

1.2 LAMINATED STRUCTURES 32

1.2.1 Definition *32*

1.2.2 Major parameters *34*

1.3 MULTISCALE APPROACH 35

1.3.1 Analytical multiscale *37*

1.3.2 Computational multiscale *40*

1.4 REPRESENTATION OF LAMINATED STRUCTURES 41

1.4.1 Relevance of simulation *41*

1.4.2 Generalities *42*

1.5 MULTIPHYSICAL APPROACH 43

1.5.1 Multiphysical point of view in composite structures *43*

1.5.2 Viscoelasticity in composite structures *45*

1.6 SIMULATION OF COMPOSITE STRUCTURES, ADVANCES, AND LIMITATIONS 48

1.6.1 Finite element based simulation *48*

1.6.2 Simulation for multiscale and multiphysical behavior *49*

1.7 MODEL REDUCTION 55

1.7.1 Methods of reduction *55*

1.7.2 The PGD *58*

1.7.3 The PGD method for composite materials *59*

1.8 DESIGN OF COMPOSITE STRUCTURES 61

1.8.1 The design process *62*

1.8.2 Design from simulation *63*

1.8.3 Support to decision making in composite design 63
1.8.4 Optimization leading to the design of laminated composites..... 65
1.8.5 Solutions to support the design of composites..... 68
1.9 CONCLUSION 69

CHAPTER 2 REPRESENTATION, BEHAVIOR, AND DESIGN OF COMPOSITE STRUCTURES 71

2.1 INTRODUCTION..... 71
2.2 MULTISCALE MODELING OF COMPOSITE STRUCTURES 72
2.2.1 3D behavior..... 73
2.2.2 Simulation with FEM considering the interfaces between plies..... 74
2.2.3 Behavior and spatial separation..... 80
2.2.4 Our multiscale approach 81
2.3 MULTIPHYSICAL CONSIDERATION OF COMPOSITE STRUCTURES 83
2.3.1 Justification of creeping in a composite structure..... 84
2.3.2 Our multiphysical approach..... 85
2.4 A NEW MODEL TO SUPPORT DECISION MAKING DURING THE DESIGN OF COMPOSITE STRUCTURES 87
2.4.1 Fast simulation for design choices validation..... 87
2.4.2 Interactive exploration of design solution spaces from the PRBM. 89
2.4.3 Our approach for composite structure design..... 91
2.5 QUALIFICATION 93
2.6 CONCLUSION 95

CHAPTER 3 PARAMETRIZATION OF A MODEL: 97

3.1 INTRODUCTION..... 97
3.2 DETAILS OF THE PRBM MODEL 98
3.2.1 Properties..... 98
3.2.2 Definition of the PRBM 102
3.3 DETAILS AND PRINCIPLES OF THE PGD METHOD 103
3.4 MODEL SEPARATION WITH PGD 106
3.4.1 Basis of modeling..... 106
3.4.2 Parametrization with PGD..... 109
3.5 SIMULATION OF A LAMINATED COMPOSITE BEAM: THE USUAL APPROACH..... 111
3.5.1 Details of the case of study..... 111
3.5.2 FEM models 113
3.5.3 Basis: FEM simulation..... 113
3.6 PRBM BASED SIMULATION 118
3.6.1 Details about the PGD approach 119
3.6.2 PRBM results in the laminated composite beam..... 119

3.6.3 Qualification of the PRBM for static behavior 122
3.7 CONCLUSION 124

CHAPTER 4 MULTIPHYSICAL MODELING: 125

4.1 INTRODUCTION 125
4.2 VISCOELASTIC BEHAVIOR IN A LAMINATED COMPOSITE STRUCTURE 126
4.2.1 Experimental approach 126
4.2.2 Demonstration of viscoelasticity 129
4.3 PRBM CONSTRUCTION FOR A MULTIPHYSICAL APPROACH. 133
4.4 FRACTIONAL DERIVATIVE TO MODEL VISCOELASTICITY 136
4.4.1 Modeling of creeping 136
4.4.2 Modeling viscoelasticity in the PRBM 139
4.4.3 Determination of the fractional parameters from experimentation 143
4.5 PRBM BASED SIMULATION OF DYNAMIC BEHAVIOR IN A COMPOSITE STRUCTURE 145
4.5.1 Study case 145
4.5.2 A separated and reduced model of the dynamic behavior of the composite beam 145
4.5.3 Model processing for CAE 147
4.6 CONCLUSION 151

CHAPTER 5 THE PRBM SUPPORTING DECISION MAKING IN THE DESIGN OF COMPOSITE STRUCTURES 153

5.1 INTRODUCTION 153
5.2 PRBM FOR DESIGN 154
5.3 A KNOWLEDGE MODEL TO DESIGN 156
5.3.1 The parametric knowledge model 156
5.3.2 Modeling of design objectives 163
5.3.3 Modelling of design constraints 164
5.4 OPTIMIZATION: A STRATEGY TO EXPLORE DESIGN SPACES INTERACTIVELY 165
5.4.1 The choice of evolutionary approach 165
5.4.2 From the PKM to the optimization model 166
5.5 MODELING A DESIGN PROBLEM FOR AG PROCESSING 167
5.5.1 Representation of the chromosome 167
5.5.2 Description of the optimization process. 170
5.6 A DESIGN PROBLEM SOLVING 171
5.6.1 Design problem details: a laminated composite plate 171
5.6.2 Design solutions after optimization 172
5.6.3 Design of laminated composite structures from the PKM 173
5.7 QUALIFICATION 174

5.7.1 Performance of the optimization process 175
5.7.2 Qualification of the design solution having static behavior: validation from a FEM simulation 175
5.7.3 Qualification of the design solution having dynamic behavior: validation from experiments 177
5.8 CONCLUSION 185

CHAPTER 6 CONCLUSIONS AND PERSPECTIVES 187

6.1 CONCLUSIONS 187
6.2 PERSPECTIVES 189

PERSONAL PUBLICATIONS 191

REFERENCES 193

RESUME ETENDU

MODELE PARAMETRIQUE ET REDUIT POUR LA CONCEPTION OPTIMALE DE STRUCTURES COMPOSITES

1. L'ENJEU DE LA CONCEPTION DE PRODUITS A BASE DE MATERIAUX COMPOSITES STRATIFIES

1.1. La conception de produits

Traditionnellement, la conception d'un produit suit un processus établi sur 3 phases majeures (Figure 0.1) :

- La conception préliminaire construite autour de l'étape de spécification, et de la phase de créativité ou de recherche de concepts,
- La conception architecturale qui consiste à identifier, agencer (ou assembler) et pré-dimensionner les composants qui vont constituer le produit final,
- La conception détaillée qui fournit une représentation fine et avancée du produit, la plupart du temps sous sa forme virtuelle ; la simulation des comportements physiques y prend une place centrale permet de :
    - Remettre en cause les choix de conception architecturale et les concepts,
    - Améliorer les choix de conception par l'usage de méthodes d'optimisation,

- Préparer la phase d'industrialisation et de production ou de fabrication.

Le processus de conception est donc fortement itératif.

L'approche traditionnelle que nous venons de synthétiser est complètement adaptée à la conception de produits à base de matériaux métalliques., Dans ce processus, dès que les matériaux sont choisis, les ingénieurs se concentrent ensuite principalement sur la définition de la topologie (forme, des composants et sur la forme de l'assemblage de ces éléments).

Géométries, structures fonctionnelles et quantité de matière conditionnent la rigidité du produit, et donc déterminent son comportement physique. La conception détaillée cherche à déterminer les choix qui assureront le comportement physique attendu : cet enjeu, qui requiert une utilisation avancée de la simulation de comportements physiques, est la cause de la propriété itérative du processus de conception. Ce processus de conception itératif a fait l'objet de nombreux modèles (Scaravetti [1]): la Figure 0.1 présente l'un de ces modèles (Ullman [2]).

1.2. Concevoir un matériau composite

Lorsqu'il s'agit de la conception d'un produit fait de matériaux composites, le processus s'assimile à celui décrit précédemment. Cependant, une boucle itérative s'ajoute Figure 0.1 et les temps de développement se rallongent sensiblement

Quelle est la cause de cette itérativité additionnelle ?

La conception d'un produit à base de matériaux composites ne se focalise pas que sur le problème de topologie. En effet, les ingénieurs ont aussi la lourde tâche de définir une structure du matériau. En somme, l'ingénieur a ici une triple mission :

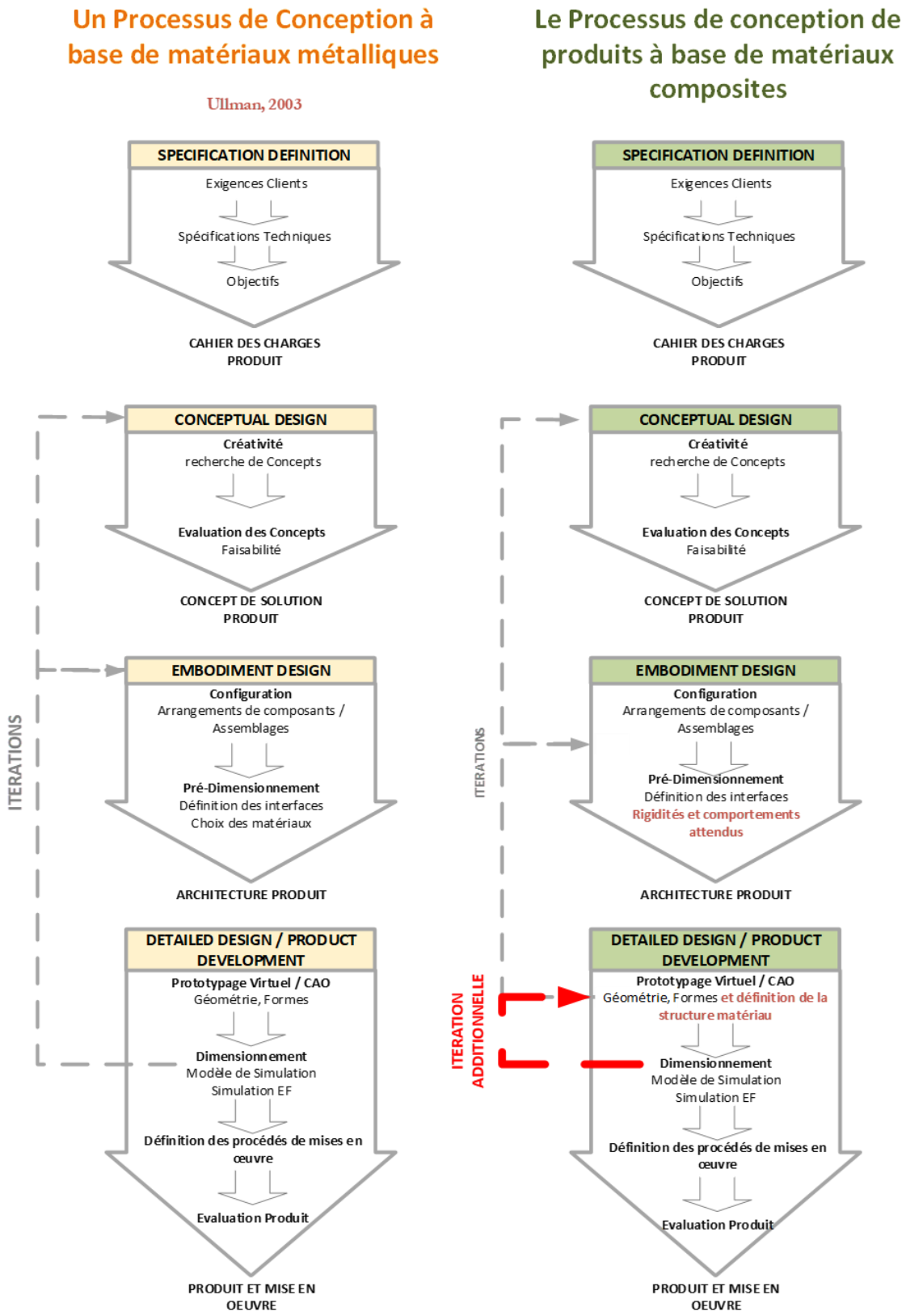

Figure 0.1, les processus de conception

1. déterminer une géométrie du produit,
2. définir aussi la macro-structure du composite ou du stratifié : la structure conditionne la loi de comportement du matériau,
3. et surtout, présenter la meilleure combinaison « géométrie - structure matériau » qui assume le comportement attendu, sans pour autant oublier les objectifs économiques.

La conception change donc ici de sens : l'ingénieur conçoit le produit mais aussi le matériau. Le mécanicien, qui habituellement, laisse aux spécialistes de la chimie et des matériaux le fait de définir ces propriétés, se voit donc l'objet d'un nouvel enjeu de conception. Or, le nombre de solutions et de combinaisons « géométrie - structure matériau »est généralement très grand. Explorer cet espace de solutions modifie sensiblement la configuration du processus de conception : dans la phase de conception détaillée s'insère (1) l'opération de conception du matériau et (2) une nouvelle boucle itérative requise pour la validation de choix opérés sur la structure de ce matériau (Figure 0.1).

Le processus de conception de produits à base de matériaux composites comporte donc une étape supplémentaire de dimensionnement. Pour contourner cette limitation, 2 solutions :

- Disposer de solutions de « **simulation rapide** », plus rapides qu'elles ne le sont aujourd'hui, et permettant de conduire une analyse fine des comportements aux différentes échelles de la structure : **le calcul devient multi-échelles**.
- Disposer d'une **solution d'aide à la conception** permettant, dès la conception architecturale, d'explorer les espaces de recherche de façon interactive. Il s'agit d'une approche synthétique qui à partir de la définition des comportements attendus conduit à des structures matériaux. Pour être exhaustif, ce processus doit prendre en compte tous les effets physiques induits à chaque échelle de la structure, même s'ils sont d'ordre et de physiques différentes (déformation,

frottements aux interfaces, contacts et délaminages, etc.) : **le problème** est **multiphysique**.

La thèse ici présentée, fournit des solutions répondant simultanément aux deux enjeux précédents. Nous allons ici faire le résumé des solutions développées.

2. L'ENJEU D'UN MODELE PARAMETRIQUE ET REDUIT

2.1. Les propriétés majeures d'un nouveau modèle

Nos travaux sont tournés vers la problématique de la conception de structures composites stratifiées. Obtenues par la superposition de plis, ces structures répondent à un comportement en déformation grâce à des caractéristiques de raideur induites par des choix de conception réalisés au niveau de chaque pli. Ces choix concernent à la fois la nature des , l'agencement et le drapage de ces fibres (orientation et tissages à l'échelle du pli), la fraction volumique de fibres, la nature de la colle, la forme des interfaces entre les plis, le nombre de plis.

Le comportement global de la structure est induit par les comportements de chaque pli, et donc par les choix réalisés pour constituer chaque pli. Pour concevoir la structure du matériau il faut donc nécessairement mener une analyse multi-échelle. Réaliser une approche multi-échelle ne signifie pas qu'il suffit de concentrer son intérêt sur les plis. En effet, les interfaces entre les plis, souvent négligées, jouent un rôle dans le comportement physique du produit : l'interaction physique entre les plis est bien réelle. Au niveau de, chaque interface existent des comportements élastiques, de fluage et de fatigue, combinées à des phénomènes de frottement. Nous démontrons dans le manuscrit l'importance des comportements aux interfaces : notre approche est aussi multi-physique.

Les argumentations précédentes ont mobilisé notre intérêt et ont conduit notre objectif principal : développer un modèle nouveau, multi-échelle et multi-

physique, permettant à la fois la simulation rapide des solutions de conception ou l'exploration interactive des espaces de recherche.

De nombreux auteurs ont travaillé sur la problématique de simulation multi-physique de comportements de structures multi-échelles : nous citerons notamment Bognet [3], Couégnat [4], Carrera [5] et Cheng [6], Prulière [7] et Chinesta [8] qui ont largement inspiré nos travaux.

Aujourd'hui, la plupart des modèles numériques et de simulation sont développés avec la méthode des éléments finis : beaucoup sont déjà disponibles dans les outils modernes de simulation. Mais, ils ont leurs limites :

1- Ces modèles sont fondés sur le calcul d'une rigidité globale de la structure composite, elle-même déterminée à partir des caractéristiques de conception déterminées à des échelles inférieures de la structure : nombre de couches, orientation des fibres dans chaque pli, fraction volumique de fibres, la nature des fibres et de la matrice, etc. De ce fait, deux structures matériaux différentes exigent 2 modèles de simulation différents : la simulation par éléments finis n'est pas paramétrique dans le sens où tous les paramètres qui définissent la structure du matériau ne sont pas explicitement des variables d'entrée du modèle numérique.

2- L'approche globale mise en œuvre avec une approche par éléments finis ne permet pas d'analyser finement les comportements aux interfaces (entre les plis). Ce comportement, qui fait l'objet de glissements transverses est appelé le comportement en zig-zag. Sans développements spécifiques additionnels, l'approche par éléments finis ne convient pas à la représentation multi-physique induite par ce phénomène,

3- Même si nous avons réussi à réaliser un modèle numérique par éléments finis (présentés dans la thèse) permettant de fournir une

vision multi-physique et multi-échelle du comportement d'un stratifié nous avons conclu que :

- Le nombre de non linéarités induites par la représentation des phénomènes aux interfaces conduit à de grandes difficultés numériques (convergence, pertinence des résultats) et augmente de manière très significative les temps de calcul,
- Le modèle numérique multi-échelle est de très grande taille et devient couteux à mettre en œuvre pour des comportements statiques, voire impossible à traiter lorsque les comportements sont dynamiques (approche explicite),
- La modélisation des phénomènes visqueux aux interfaces conduisant au comportement en zig-zag augmente aussi la taille du modèle en introduisant par endroit des singularités.

Pour éviter les difficultés citées, nous avons développé un nouveau modèle nouveau mobilisé par 3 propriétés majeures :

Propriété 1 **le modèle est paramétrique et multi-échelle :**
Notre modèle rend explicite les paramètres de conception propres à chaque échelle et permet d'analyser indépendamment le comportement physique dans chaque pli et de chaque interface.

Propriété 2 **le modèle est une représentation multi-physique**
Notre modèle numérique est de taille modérée (réduite vis-à-vis d'un modèle éléments finis) et permet la mise en œuvre de simulations rapides en conception détaillée, ou l'exploration tout aussi rapide des espaces de conception durant la phase de conception architecturale.

Propriété 3 **le modèle est une représentation multi-physique :** Tout en rendant explicite les paramètres de conception propres à chaque échelle, notre modèle peut tout aussi bien traiter de comportements statiques que dynamiques, capables de représenter des phénomènes dont les physiques sont différentes et quel qu'en soit le lieu de réalisation au sein même de la structure.

2.2. Méthodes de modélisation

Pour développer un modèle ayant les 3 propriétés précédentes, nous avons mis en œuvre un certain nombre de méthodes :

Propriété 1 **un modèle paramétrique et multi-échelle :**

Avoir une approche multi-échelle consiste à la fois :

- de de traiter chaque pli indépendamment,
- de mener une approche globale regardant un résultat issu de l'assemblage de ces plis.

Pour cela, nous avons choisi de construire un modèle fondé sur le principe de séparation. Nous appellerons ce modèle le modèle spatial séparé ou **Spatial Separated Model (SSM).**

Disposer de ce modèle séparé permet :

- De considérer séparément les lois constitutives créées au niveau de chaque plis et consécutifs aux choix de conception suivants :
  - Nature des fibres.
  - Orientation des fibres.
  - Nature des tissages.
  - Densité volumique de fibres.
  - Nature de la colle.
- De traiter de façon explicite du nombre de plis constituant le stratifié,

- De représenter les comportements du stratifié à chaque échelle du stratifié : plis, interfaces et structure,

Avec cette vision, tous les paramètres de conception qui définissent la structure du matériau, et cela qu'elle qu'en soit l'échelle, sont les variables d'entrée du modèle. Nous avons donc caractérisé ce modèle comportemental de **modèle paramétrique**.

En matière d'information de sortie : le SSM fournit une approximation $U^n(x,y,z,q)$ du champ réel de déplacement $U\,(x,y,z,q)$ subit par la structure au cours d'une déformation. Il décrit le champ de déplacement comme étant une fonction des d variables d'entrée (les paramètres de conception) $q_i\,,\ i \in \{1,\cdots,d\}$ (Figure 0.2).

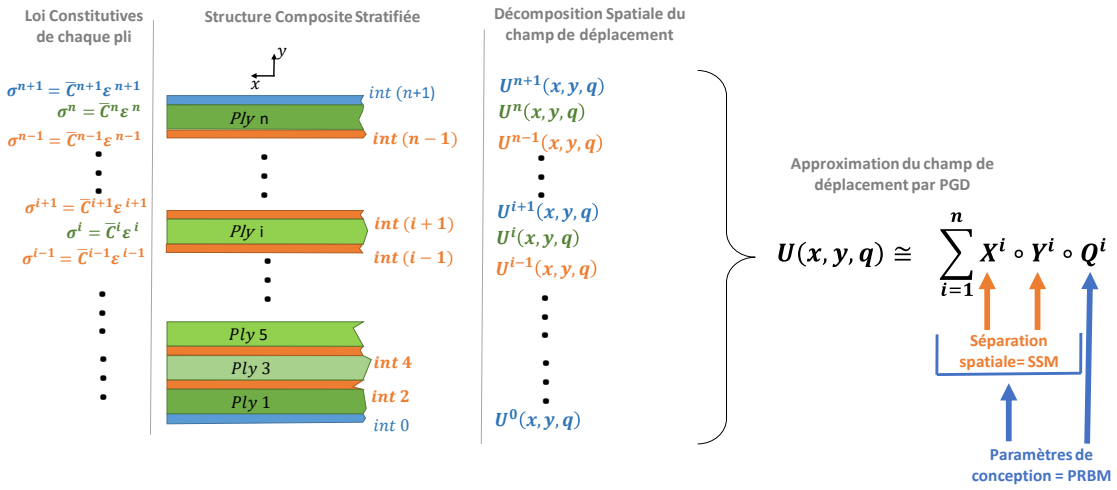

Figure 0.2. Principe de séparation spatiale : le SSM

Pour développer le SSM, nous avons utilisé une méthode de réduction de modèles : la méthode PGD (Proper Generalized Decomposition). La PGD (Bognet et al. [3], Pluriere et al. [7]) permet aux différentes dimensions de l'espace d'être séparées, et de donner lieu à l'expression de fonctions représentant chacune des dimensions spatiales (équation 0.1).

$$U(x,y,q) \cong U^n(x,y,q) \cong \sum_{i=1}^{n} X^i \circ Y^i \circ Q^i \qquad 0.1$$

Les paramètres de conception définis dans différentes dimensions de l'espace, donnent lieu eux aussi à l'expression de fonctions séparées $(Q^1, Q^2, Q^3, \cdots)$

Propriété 2 un modèle réduit

Le seul usage de la méthode PGD permet de garantir l'expression d'un modèle réduit (Chinesta et al. [9]).

Ainsi, le SSM donne lieu à l'expression d'un modèle de comportement paramétrique et réduit dont le nom sera le **Parametric and Reduced Behavioral Model (PRBM).**

Propriété 3 une représentation multi-physique

Le modèle séparé a l'avantage de permettre à l'utilisateur d'analyser séparément :

- Les comportements au sein de chaque pli,
- Les déplacements relatifs qui se produisent aux interfaces entre les couches,
- Le comportement global de la structure.

Grâce au PRBM nous répondons à une tendance industrielle actuelle qui vise à comprendre le comportement des interfaces et les phénomènes de transfert de contraintes en ces endroits. Ces transferts peuvent être affectés par de mauvaises adhérences et des délaminages (Chattopadhyay et al. [10], Lei et al. [11]) aussi bien pour des comportements statiques que dynamiques (Liu et al. [12], Budiman et al. [13], Ramos and Pesce [14], Cheng et al. [6], Lenci and Warminski [15]). Au niveau des interfaces se produisent des comportements ne faisant pas appel aux théories de la déformation : glissements, fluages et

endommagement qui sont liés au phénomène de zig-zag. De nombreux modèles ont permis de modéliser ce phénomène : ils sont détaillés dans le Tableau 0-1. Grâce à la séparation, nous pouvons traiter de ces physiques au niveau de chaque interface

Tableau 0-1. Théories pour la représentation du phénomène de zig-zag dans les starifiés

Théorie	Équations de base	Illustration	Commentaires
Théorie de stratification classique, (CLT) (2D) Kirchhoff (Reddy [16])	$\mathrm{u}(x,y,z) = \mathrm{u}_0(x,y) - z\frac{\partial \omega_0}{\partial x}$ $\mathrm{v}(x,y,z) = \mathrm{v}_0(x,y) - z\frac{\partial \omega_0}{\partial x}$ $\omega(x,y,z) = \omega_0(x,y)$	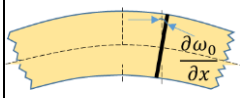	Très faible coût de calcul. Réduit à la simulation des structures à déformations infinitésimales
Théorie du premier ordre : déformations et cisaillement (FSDT) (2D) Reissner-(Reddy [16])	$\mathrm{u}(x,y,z) = \mathrm{u}_0(x,y) + z\phi_x(x,y)$ $\mathrm{v}(x,y,z) = \mathrm{v}_0(x,y) + z\phi_y(x,y)$ $\omega(x,y,z) = \omega_0(x,y)$	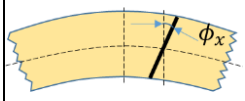	Faible coût de calcul. Des facteurs de correction corrigeant le cisaillement sont requis : leur obtention est complexe.
Théorie d'ordre élevé : déformations et cisaillement (HSDT) (2D) (Reddy [16])	$\mathrm{u}(x,y,z) = \mathrm{u}_0(x,y) + z\phi_x(x,y) + z^3\left(-\frac{4}{3h^2}\right)\left(\phi_x + \frac{\partial \omega_0}{\partial x}\right)$ $\mathrm{v}(x,y,z) = \mathrm{v}_0(x,y) + z\phi_x(x,y) + z^3\left(-\frac{4}{3h^2}\right)\left(\phi_y + \frac{\partial \omega_0}{\partial y}\right)$ $\omega(x,y,z) = \omega_0(x,y)$	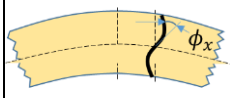	Précision accrue, ne nécessitent pas des facteurs de. Coût de calcul augmente avec l'ordre
Zig-zag (2D) (Carrera [5])	$\mathrm{u}(x,y,z) = \mathrm{u}_0(x,y) + \sum_{k=1}^{N_l-1}(z - z_{k-1})a_k H(z - z_k)$	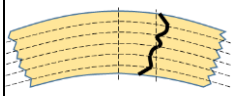	Bonne précision, Difficulté d'interpolation.
Théorie Layer Wise (3D) (Carrera[5])	$\mathrm{u}(x,y,z) = \sum_{I=1}^{N} U_I(x,y,t)\Phi_j^k(z)$ $\mathrm{v}(x,y,z) = \sum_{I=1}^{N} V_I(x,y,t)\Phi_j^k(z)$ $\mathrm{w}(x,y,z) = \sum_{I=1}^{M} W_I(x,y,t)\Psi_j^k(z)$	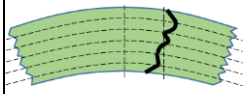	Des résultats précis au niveau des plis, avec un coût de calcul maitrisé. Des rigidité transverses parasites peuvent apparaitre et les matrices sont mal conditionnées

2.3. Un modèle pour soutenir la la conception de structures composites stratifiées

Le PRBM constitue une représentation fidèle du comportement d'une structure composite stratifiée : elle est multi-échelle et multi-physique.

Si dans la plupart des cas les modèles de simulation sont utilisés pour valider des choix de conception, peu de modèles sont exploités pour synthétiser des solutions. Cette situation est induite par la seule forme des modèles. Nous avons été mobilisés par l'idée de disposer d'un modèle utile dans la phase de dimensionnement, mais aussi au cours de la phase de conception architecturale (ou pré-dimensionnement).

A l'exception de Irrisari [17], peu de travaux fournissent des solutions en matière d'exploration des espaces de conception. Lorsqu'il s'agit d'explorer un espace la plupart des études se cantonnent à l'usage d'une méthode d'optimisation couplée à la méthode des éléments finis. Mais dans ce cas, le nombre de paramètres de conception exploités est nécessairement restreint, du fait de l'approche globale (échelle la plus haute) des modèles (éléments finis) mis en jeu : les éléments finis ne sont pas adaptés immédiatement à une approche multi-échelle.

Nous utilisons le PRBM pour explorer les espaces de solution. Ce modèle paramétrique devient pour nous l'outil essentiel d'une approche d'aide à la conception basée sur une méthode d'optimisation évolutionnaire.

3. Quelques éléments sur la méthode de construction du PRBM

3.1. La séparation spatiale : vers le modèle SSM

Pour construire le modèle SSM, nous utilisons la méthode PGD. Il s'agit aussi d'une méthode de réduction.

L'approche est largement détaillée dans le manuscrit principale.Afin d'illustrer le principe, nous présentons ici méthode de séparation dans le cas d'un comportement en déformations planes ou dit 2D (en référence à une approche par éléments finis). Voulant représenter la déformation de la structure composite stratifiée, toute notre approche est fondée sur l'expression du champ de déplacement, ou autrement dit des fonctions spécifiant le mouvement de chaque particule formant la structure. Les équations 0.2, 0.3 et 0.4 représente le principe de décomposition de ce champ.

$$U(x,y) \cong U^n(x,y) \qquad 0.2$$

$$U^n(x,y) = \sum_{i=1}^{n} X^i \circ Y^i \qquad 0.3$$

$$U^n(x,y) = \sum_{i=1}^{n} \begin{Bmatrix} X_{\mathrm{u}}^i \cdot Y_{\mathrm{u}}^i \\ X_{\mathrm{v}}^i \cdot Y_{\mathrm{v}}^i \end{Bmatrix} \qquad 0.4$$

X et Y sont des fonctions représentent les 2 domaines étudiés. u et v représentent respectivement les composantes de déplacements horizontaux et verticaux de chaque particule. Le symbole «°» est le produit de Hadamard.

Les fonctions, pour être connues « a priori » sont construites à partir d' une « stratégie de direction de remplacement » . Cette stratégie implique qu'à partir d'une condition initiale établie par $(n-1)$ solutions déjà connus, la solution suivante n est obtenu par itération de telle sorte que à l'itération p il est possible de calculer le vecteur à 1 dimension $\begin{Bmatrix} X_{\mathrm{u}}^p \\ X_{\mathrm{v}}^p \end{Bmatrix}$ selon un traitement non déterministe des fonctions $\begin{Bmatrix} Y_{\mathrm{u}}^{p-1} \\ Y_{\mathrm{v}}^{p-1} \end{Bmatrix}$ issue de l'itération $(p-1)$ (équation 0.5).

$$U_{(x,y)}^{n-1,p} = \left(\sum_{i=1}^{n-1} X^i \circ Y^i \right) + X^p \circ Y^{p-1} \qquad 0.5$$

Le champ de déplacement est reconstruit en additionnant les produits de Kronecker (équation 0.5 : $\sum_{i=1}^{n} X^i \circ Y^i$) des fonctions spatiales calculées et issues de ce que nous appelons communément des modes de calculs.

Au cours de nos travaux, la méthode PGD a fait l'objet d'un développement spécifique (code déployé à ESTIA). Le code mis en œuvre permet de définir chaque fonction spatiale séparément selon un maillage unidimensionnel. Dans le cas présent chaque déplacement de particule, horizontaux u et verticaux v, sont traités selon un comportement en déformation planes. La Figure 0.3 illustre ce principe.

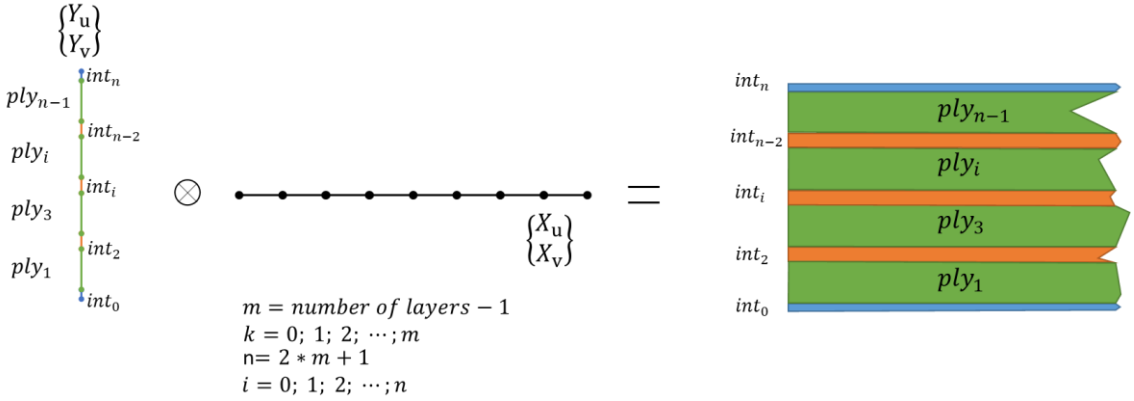

Figure 0.3. La séparation spatiale par PGD

3.2. Le principe de paramétrisation : le modèle PRBM

Au sens de la PGD, paramétriser le modèle consiste à ajouter une ou plusieurs dimensions au modèle approché afin de représenter le champ de déplacement. Nous avons ajouté au modèle PGD des dimensions représentants les paramètres de conception. Dans les équations 0.6 et 0.7, Q représente des fonctions issues d'un domaine q rassemblant les différents paramètres de conception. Les équations 0.6 et 0.7 représentent une nouvelle forme approchée du champ de déplacement, que nous caractérisons par conséquent de paramétrique.

$$U(x,y,q) \cong U^n(x,y,q) \quad (0.6)$$

$$U^n(x,y,q) = \sum_{i=1}^{n} X^i \circ Y^i \circ Q^i \quad (0.7)$$

La stratégie de direction de remplacement consiste à retrouver la solution : $U^n(x,y,q)$

Le nouveau modèle PGD est représenté à présent par l'équation 0.8

$$U_{(x,y,q)}^{n-1,p} = \sum_{i=1}^{n-1} \begin{Bmatrix} X_{\mathrm{u}}^i \cdot Y_{\mathrm{u}}^i \cdot Q_{\mathrm{u}}^i \\ X_{\mathrm{v}}^i \cdot Y_{\mathrm{v}}^i \cdot Q_{\mathrm{v}}^i \end{Bmatrix} + \begin{Bmatrix} X_{\mathrm{u}}^p \cdot Y_{\mathrm{u}}^{p-1} \cdot Q_{\mathrm{u}}^{p-1} \\ X_{\mathrm{v}}^p \cdot Y_{\mathrm{v}}^{p-1} \cdot Q_{\mathrm{v}}^{p-1} \end{Bmatrix} \quad (0.8)$$

Les paramètres de conception déterminés à chaque échelle n'apparaissent pas encore explicitement dans le modèle PGD. Or, les propriétés orthotrope du matériau qui nous motive sont établies par des modules d'Young E_{ii}, d'abord définies à l'échelle de la structure : équations 0.9, 0.10 et 0.11.

$$E_{xx} = E_{x\mathrm{u}} \cdot E_{y\mathrm{u}} \quad (0.9)$$

$$E_{x\mathrm{u}} = 1 \quad (0.10)$$

$$E_{y\mathrm{u}} = \begin{cases} E_{xxn} \; if \; y = subspace_n \\ \vdots \\ E_{xxi} \;\; if \;\; y = subspace_i \\ \vdots \\ E_{xx0} \;\; if \;\; y = subspace_0 \end{cases} \quad (0.11)$$

La paramétrisation et la séparation spatiale conduit alors au modèle 0.12

$$
\begin{aligned}
J \cdot \Bigg\{ & \int_{\Omega} (1-\vartheta_{yz}\vartheta_{zy}) E_{xx} \cdot \left(\left[\frac{dX_{\mathrm{u}}^{p}}{dx} \cdot \frac{dX_{\mathrm{u}}^{*}}{dx} \right] \cdot dx \times \left[Y_{\mathrm{u}}^{p-1} \cdot Y_{\mathrm{u}}^{p-1} \right] \cdot dy \right) \\
& + \int_{\Omega} (\vartheta_{yx} - \vartheta_{zx}\vartheta_{yz}) E_{xx} \cdot \left(\left[X_{\mathrm{v}}^{p} \cdot \frac{dX_{\mathrm{u}}^{*}}{dx} \right] \cdot dx \times \left[\frac{dY_{\mathrm{v}}^{p-1}}{dy} \cdot Y_{\mathrm{u}}^{p-1} \right] \cdot dy \right) \quad \Big\} \; from\ \boldsymbol{\sigma}_{xx} \cdot \boldsymbol{\varepsilon}_{xx}^{*} \\
& + \int_{\Omega} (1-\vartheta_{xz}\vartheta_{zx}) E_{yy} \cdot \left(\left[X_{\mathrm{v}}^{p} \cdot X_{\mathrm{v}}^{*} \right] \cdot dx \times \left[\frac{dY_{\mathrm{v}}^{p-1}}{dy} \cdot \frac{dY_{\mathrm{v}}^{p-1}}{dy} \right] \cdot dy \right) \\
& + \int_{\Omega} (\vartheta_{yx} - \vartheta_{zx}\vartheta_{yz}) E_{xx} \cdot \left(\left[\frac{dX_{\mathrm{u}}^{p}}{dx} \cdot X_{\mathrm{v}}^{*} \right] \cdot dx \times \left[\cdot Y_{u}^{p-1} \cdot \frac{dY_{\mathrm{v}}^{p-1}}{dy} \right] \cdot dy \right) \quad \Big\} \; from\ \boldsymbol{\sigma}_{yy} \cdot \boldsymbol{\varepsilon}_{yy}^{*} \\
& + \int_{\Omega} \Bigg\{ G_{xy} \left(\left[X_{\mathrm{u}}^{p} \cdot X_{\mathrm{u}}^{*} \right] \cdot dx \times \left[\frac{dY_{\mathrm{u}}^{p-1}}{dy} \cdot \frac{dY_{\mathrm{u}}^{p-1}}{dy} \right] \cdot dy + \left[X_{\mathrm{u}}^{p} \cdot \frac{dX_{\mathrm{v}}^{*}}{dx} \right] \cdot dx \right. \\
& \times \left[\frac{dY_{\mathrm{u}}^{p-1}}{dy} \cdot Y_{\mathrm{v}}^{p-1} \right] \cdot dy + \left[\frac{dX_{\mathrm{v}}^{p}}{dx} \cdot X_{\mathrm{u}}^{*} \right] \cdot dx \times \left[Y_{\mathrm{v}}^{p-1} \cdot \frac{dY_{\mathrm{u}}^{p-1}}{dy} \right] \cdot dy + \left[\frac{dX_{\mathrm{v}}^{p}}{dx} \cdot \frac{dX_{\mathrm{v}}^{*}}{dx} \right] \\
& \left. \cdot dx \times \left[Y_{\mathrm{v}}^{p-1} \cdot Y_{\mathrm{v}}^{p-1} \right] \cdot dy \right) / J \Bigg\} \quad \Big\} \; from\ \boldsymbol{\sigma}_{xy} \cdot 2\boldsymbol{\varepsilon}_{xy}^{*}
\end{aligned}
\tag{0.12}
$$

La méthode PGD sépare donc aussi les paramètres que l'espace. Le comportement est donc bien déterminé par les comportements induits à chaque échelle dépendant des paramètres de conception issus de chaque Figure 0.4.

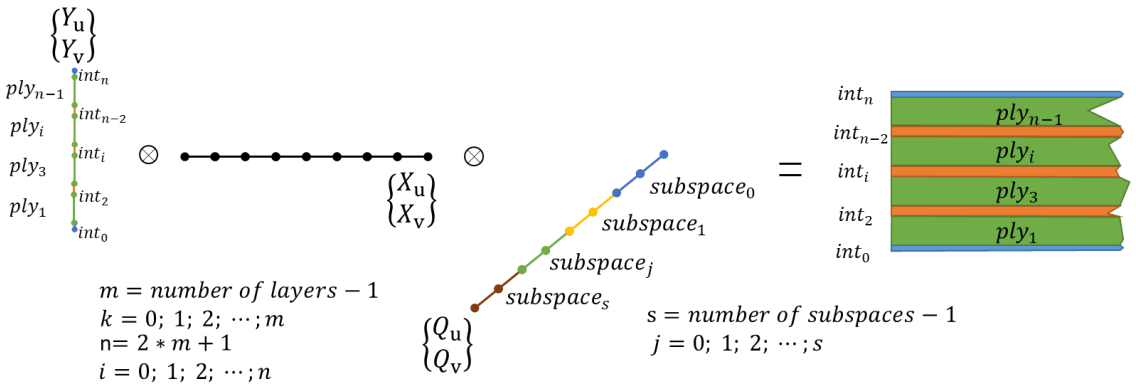

Figure 0.4. Le principe de paramétrisation : le modèle PRBM

Les équations 0.13 permettant d'intégrer dans le modèle PGD les paramètres de conception déterminés à chaque échelle.

$$\sigma_{xx}\cdot\varepsilon^{*}_{xx}=J\cdot\left(E_{xx}\left(\left(\sum_{i=1}^{n-1}\left(\frac{dX^{i}_{\mathrm{u}}}{dx}\right)\cdot Y^{i}_{\mathrm{u}}\right)+\left(\frac{dX^{p}_{\mathrm{u}}}{dx}\right)\cdot Y^{p-1}_{\mathrm{u}}\right)\left(1-\vartheta_{yz}\vartheta_{zy}\right)\right.$$
$$\left.+E_{xx}\left(\left(\sum_{i=1}^{n-1}X^{i}_{\mathrm{v}}\cdot\left(\frac{dY^{i}_{\mathrm{v}}}{dy}\right)\right)+X^{p}_{\mathrm{v}}\cdot\left(\frac{dY^{p-1}_{\mathrm{v}}}{dy}\right)\right)\left(\vartheta_{yx}-\vartheta_{zx}\vartheta_{yz}\right)\right)\cdot\left(\frac{dX^{*}_{\mathrm{u}}}{dx}\right)\cdot Y^{p-1}_{\mathrm{u}}$$

$$\sigma_{yy}\cdot\varepsilon^{*}_{yy}=J\cdot\left(E_{yy}\left(\left(\sum_{i=1}^{n-1}X^{i}_{\mathrm{v}}\cdot\left(\frac{dY^{i}_{\mathrm{v}}}{dy}\right)\right)+X^{p}_{v}\cdot\left(\frac{dY^{p-1}_{\mathrm{v}}}{dy}\right)\right)\left(1-\vartheta_{xz}\vartheta_{zx}\right)\right. \qquad 0.13$$
$$\left.+E_{xx}\left(\left(\sum_{i=1}^{n-1}\left(\frac{dX^{i}_{\mathrm{u}}}{dx}\right)\cdot Y^{i}_{\mathrm{u}}\right)+\left(\frac{dX^{p}_{\mathrm{u}}}{dx}\right)\cdot Y^{p-1}_{\mathrm{u}}\right)\left(\vartheta_{yx}-\vartheta_{zx}\vartheta_{yz}\right)\right)\cdot X^{*}_{\mathrm{v}}\cdot\left(\frac{dY^{p-1}_{\mathrm{v}}}{dy}\right)$$

$$\sigma_{xy}\cdot 2\varepsilon^{*}_{xy}=G_{xy}\left(\left(\sum_{i=1}^{n-1}\left(X^{i}_{\mathrm{u}}\cdot\frac{dY^{i}_{\mathrm{u}}}{dy}+\frac{dX^{i}_{\mathrm{v}}}{dx}\cdot Y^{i}_{\mathrm{v}}\right)\right)+X^{p}_{\mathrm{u}}\cdot\frac{dY^{p-1}_{\mathrm{u}}}{dy}+\frac{dX^{p}_{\mathrm{v}}}{dx}\cdot Y^{p-1}_{\mathrm{v}}\right)$$
$$\cdot\left(X^{*}_{\mathrm{u}}\cdot\left(\frac{dY^{p-1}_{\mathrm{u}}}{dy}\right)+\left(\frac{dX^{*}_{\mathrm{v}}}{dx}\right)\cdot Y^{p-1}_{\mathrm{v}}\right)$$

La méthode de construction du PRBM est largement détaillé dans le cœur de la thèse. Nous retiendrons à cette étape du manuscrit que le PRBM :

- Séparé bien l'espace et considère les différentes échelles de la structure,
- Considère les paramètres de conception de chaque couche.

4. Simulation centrée PRBM et premières qualifications

Différentes structures stratifiées ont été simulées avec le PRBM. Ces études sont détaillées dans la thèse. Pour justifier l'efficacité du modèle, nous nous appuyons, à ce niveau du manuscrit, sur une approche comparative : elle porte sur la simulation du comportement d'une plaque composite stratifiée décrite dans la (Figure 0.5).

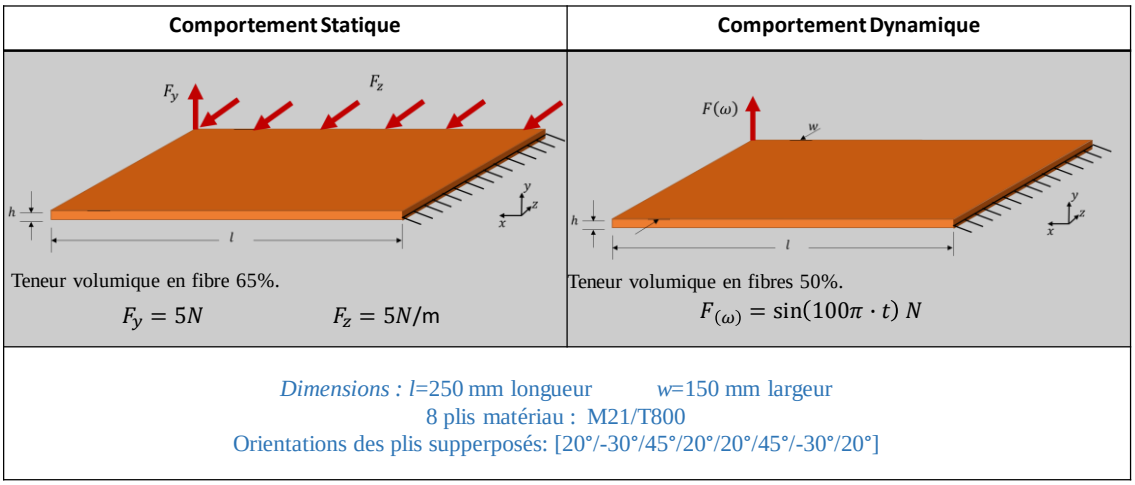

Figure 0.5. La plaque étudiée

Cette plaque est soumise à des cas de charges spécifiés dans la Figure 0.5.

4.1. Simulation rapide de comportements statiques

Pour simuler le comportement de la plaque, le PRBM est a été exploité. Le processus de simulation/modélisation se se construit en 2 temps :

1- Un temps caché, ou de pré-traitement, qui consiste à construire le modèle réduit (le PRBM),
2- Un temps de traitement pour déterminer le champ de déplacement, à partir du PRBM nourri par des valeurs données au paramètres de conception. , en fonction de toute valeur numérique d'entrée.

Nous avons appliqué donc ce processus pour construire un modèle réduit et paramétrique du comportement statique de la dite plaque stratifiée (Figure 0.5, gauche).

Le temps de pré-traitement requis pour disposer du PRBM a été de 25 minutes.

Le temps de construction a été de 25 minutes. Cependant, le modèle construit, les temps de traitement deviennent négligeables : le champ de déplacement pour la plaque présentée précédemment a été de 3 secondes.

Quant au temps de traitement il est négligeable : le champ de déplacement pour la plaque présentée précédemment a été de 3 secondes.

Nous mettons l'accent sur le fait que, après pré-traitement, les valeurs des paramètres de conception peuvent être modifiées à l'infini dans le modèle (dans la limite de validité physique du modèle) : les temps de traitements restent petits. Inutile de repasser par une phase de pré-traitement, contrairement aux éléments finis ou cela serait nécessaire. Le modèle est générique.

Par ailleurs, le PRBM fournit une représentation du phénomène de zig-zag.

Pour justifier la pertinence du PRBM, et dans l'esprit de modéliser par d'autres biais numériques le phénomène de zig-zag, nous avons construit un modèle à base d'éléments finis fait :

- D'une superposition d'éléments de coques représentant chaque pli,
- De modèles de liaisons permettant de représenter le comportement aux interfaces. Le comportement en zig-zag est ainsi modélisé.

Ce modèle est de grande taille 18 minutes ont été requises pour fournir la simulation d'une structure matériau établie et figée : une autre conception requiert la construction d'un nouveau modèle et d'un nouveau traitement numérique : les temps de calcul s'additionnent.

La Figure 0.6 montre finalement que les 2 approches donnent des résultats comparables en matière de simulation du zig-zag. Cependant, le PRBM reste paramétrique et générique. Construit, il est inutile de réitérer quelque approche de traitement numérique que ce soit.

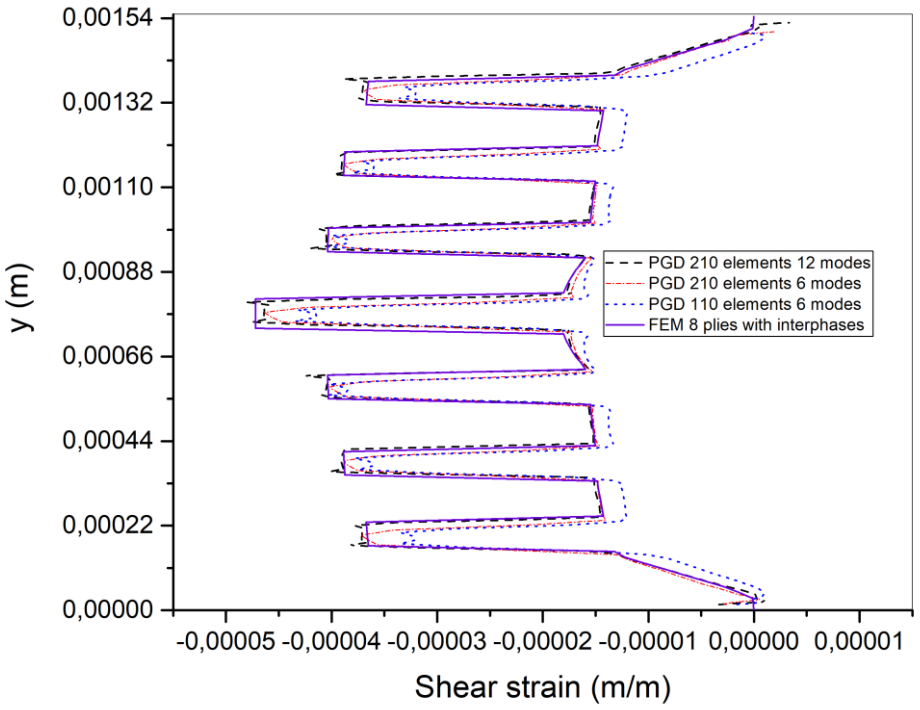

Figure 0.6. Le comportement en zig-zag obtenus avec les modèles éléments finis et le PRBM.

Finalement, une analyse comparative montre que les résultats de simulation obtenus par éléments finis et par le PRBM ne diffèrent que de 5,5% (Figure 0.7). Nous retenons cependant la force du modèle PRBM qui réside en sa paramétrisation.

	PRBM	Analyse Eléments Finis
Résultats de Simulation	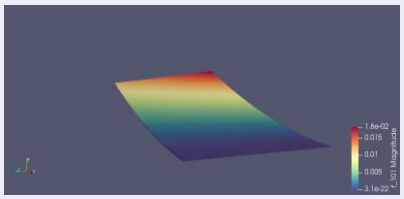 Déplacement max: 18 mm	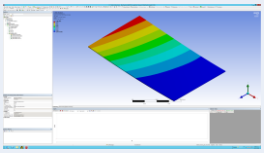 Déplacement max : 17 mm

Figure 0.7. Résultats comparatifs quant à la simulation du comportement statique.

4.2. Simulation rapide de comportements dynamiques

Les structures composites stratifiées sont capables d'amortissement.

Une approche expérimentale, détaillée dans le manuscrit principal, nous a conduit à démontrer les capacités de fluage des structures composites stratifiées. Ce phénomène opère au niveau des interfaces entre les plis : la colle a un comportement viscoélastique.

Pour modéliser ce comportement, nous avons été conduits à ajouter une nouvelle dimension dans le modèle séparé. Cette dimension est liée à l'usage d'une dérivée non entière. Les paramètres et ordres de dérivation de la dérivée fractionnaire sont directement définis par les capacités viscoélastiques de la colle. La séparation opérée est décrite dans la (Figure 0.8).

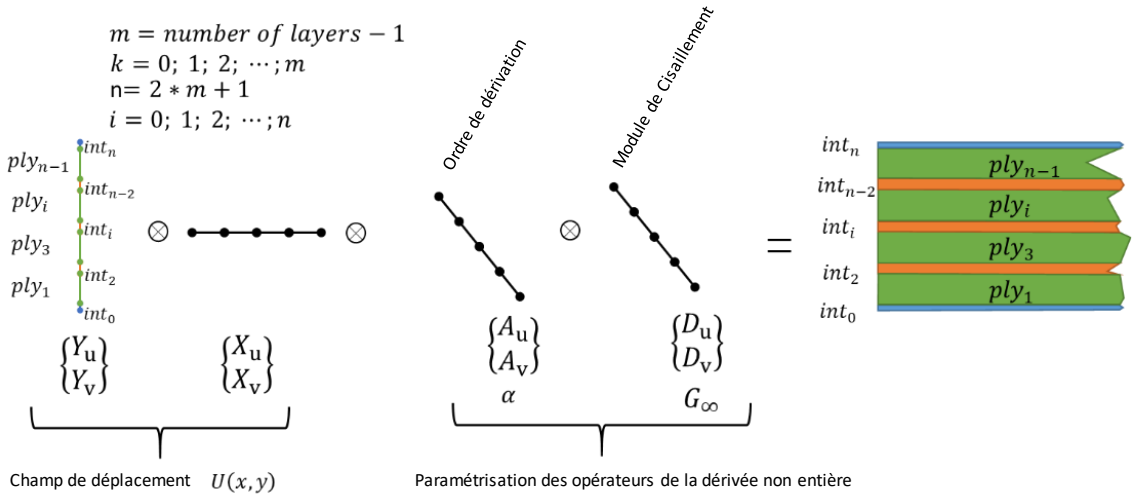

Figure 0.8. Paramétrisation de la viscoélasticité

Afin de qualifier le PRBM représentant le comportement dynamique multi-échelle et multi-physique de la structure composite, il nous fallait une référence. En référence au calcul statique, nous avons entrepris de construire un modèle éléments finis multi-échelle.

Nous n'avons pas pu mener une simulation par éléments finis : Le modèle de grande taille, affichant des non linéarités majeures, et traité selon une

approche explicite, n'a pas pu converger en des temps raisonnables (arrêt volontaire du traitement numérique au bout de 9 jours de calculs).

Cependant, le PRBM a donné ses résultats. Le modèle paramétrique à été disponible au bout de 360 minutes.

Quant au temps de traitement, il demeure tout aussi petit : 4 secondes pour obtenir la simulation du comportement dynamique de la plaque stratifiéeLes résultats sont présentés dans la Figure 0.9.

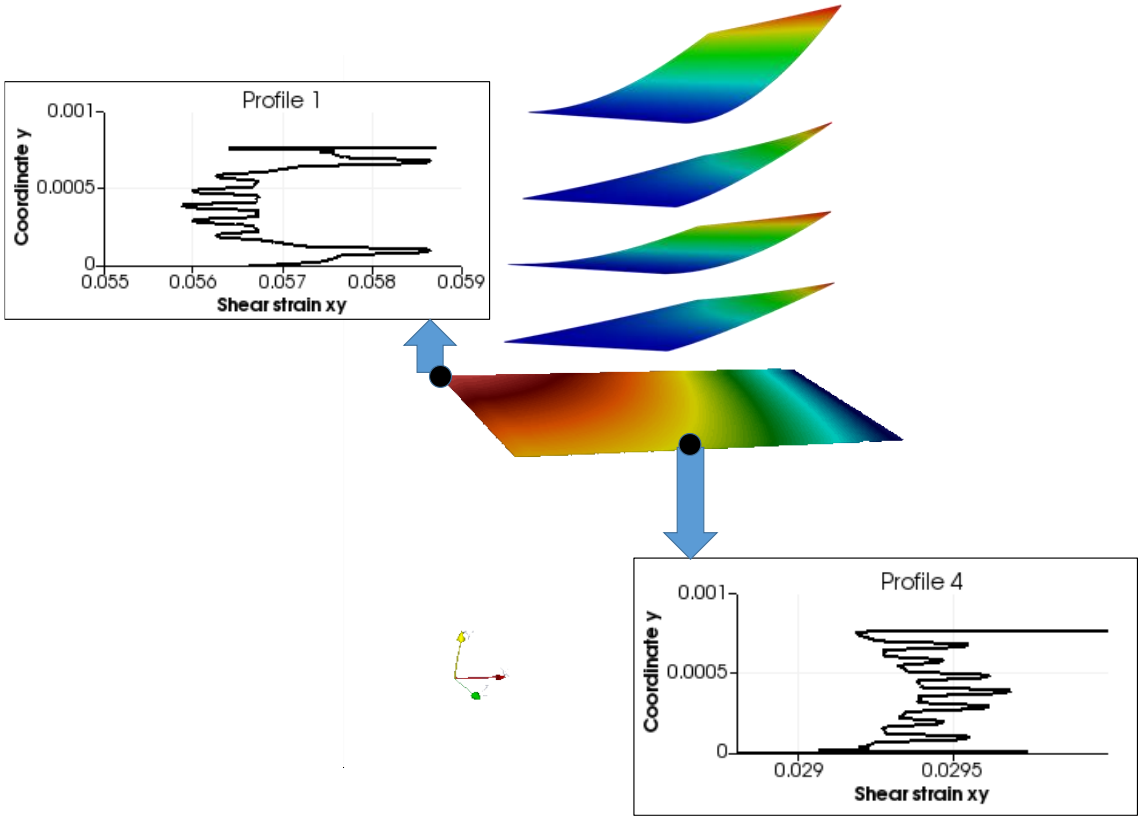

Figure 0.9. Simulation du comportement dynamique par le PRBM.

Nous avons entrepris de qualifier la pertinence du PRBM grâce à une approche expérimentale. Des plaques dont la configuration est celle présentée en début de section ont été fabriquées spécialement. Elles, ont fait l'objet d'un plan expérimental détaillé dans le corps principal du manuscrit (Figure 0.9 et Figure 0.10).

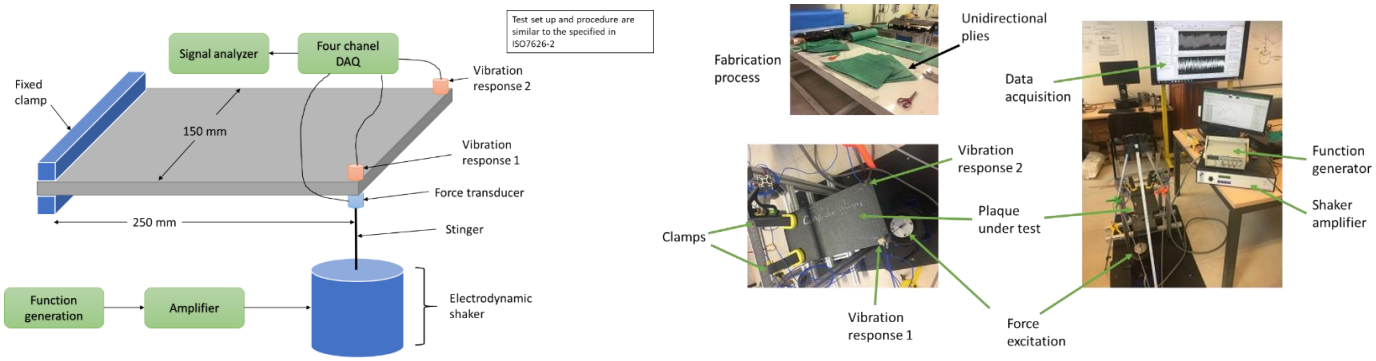

Figure 0.10. Schéma de principe du banc de test et plan expérimental

Les résultats issus de l'expérimentation et de l'usage du PRBM ont été comparés : la figure Figure 0.11 présente ces résultats.

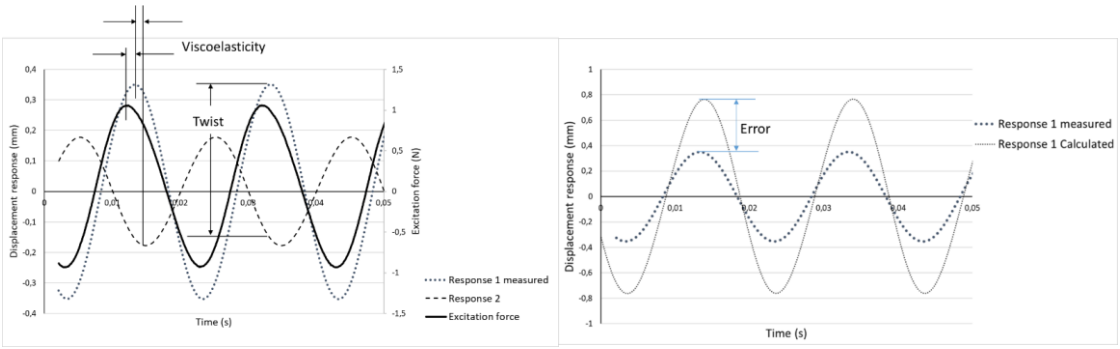

Figure 0.11. Comparaison des résultats calculés aux expérimentations

Si en matière de mesure de flèche (déformation) les résultats sont décevants - mais ont été justifiés (cf ; manuscrit principal) - le PRBM montre parfaitement le phénomène de fluage : le déphasage entre réponse et application des efforts harmoniques est réel. Mais surtout nous retiendrons que ce déphasage est quasiment identique en valeur lorsque nous comparons les résultats issus du PRBM et ceux issus de l'expérimentation.

5. Le PRBM et aide à la conception

Le PRBM est un modèle paramétrique. Il a donc l'avantage de pouvoir être traité par une méthode d'optimisation.

Pour se faire nous avons construit un modèle de connaissance. Ce modèle de connaissance est traité avec une méthode de traitement évolutionnaire. Le PRBM il fait partie du_ modèle de connaissance (Figure 0.12).

Modèle de Connaissance paramétrique (PKM)

PRBM	$U_{x,y,z,p1,p2,p3,p4,p5,p6,p7}$
Loi constitutive	$\boldsymbol{\sigma} = \overline{\boldsymbol{C}}\boldsymbol{\varepsilon}$
Comportement géométrique	$\boldsymbol{\varepsilon}(U) = \frac{1}{2}(\nabla U + (\nabla U)^T)$
Loi constitutive de chaque pli	$E_x^i = f(E_l, E_t, \theta_i)$ $E_y^i = f(E_l, E_t, \theta_i)$
Objectifs de conception	F_0
Viscoelastic behavior at the interfaces	$P = f(G_0, G_\infty, \alpha, \tau)$

Figure 0.12. un modèle de connaissance paramétrique.

Les algorithmes génétiques ont été utilisés. Nous présentons en détail le modèle génétique dans le cœur du manuscrit. Ainsi, grâce à ce modèle nous recherchons des solutions optimales de structures composite et stratifiée (Figure 0.13).

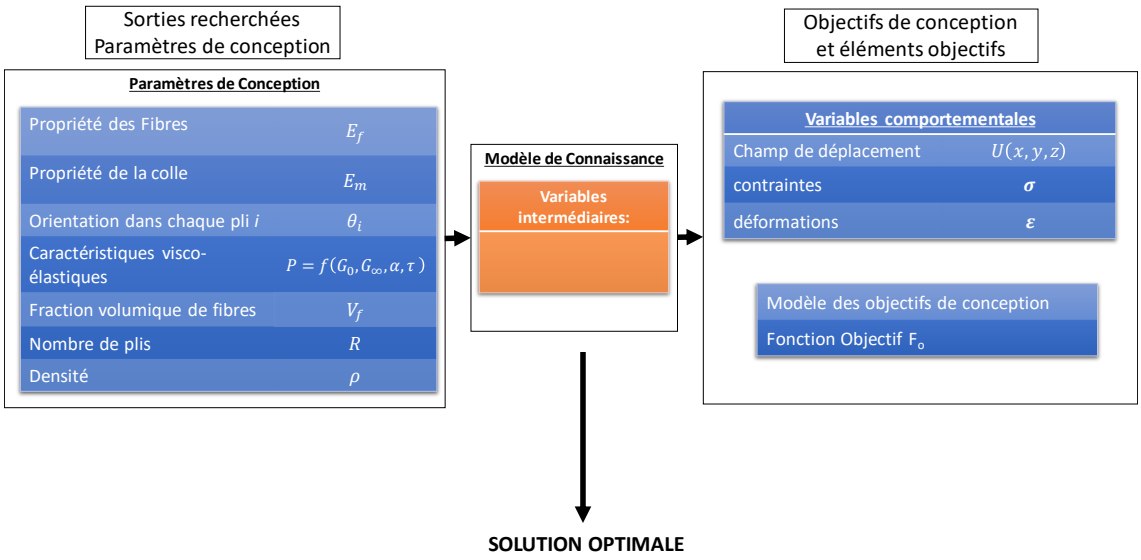

Figure 0.13. Les variables du problème d'optimisation.

Les temps requis pour explorer les espaces de recherche sont précisés dans le Tableau 0-2.

Tableau 0-2. Temps de recherche de solution

	Comportement statique	Comportement dynamique
Temps de construction du PRBM	25 min	360 min
Temps d'exploration de l'espace de recherche	75 min	520 min

Ces temps d'exploration ont conduit à la plaque présentée dans la section précédente. les simulation ayant été validées, nous pouvons en déduire que la méthode de conception l'est aussi. Le détail de ces conclusions est fait dans le mansucrit.

6. Conclusion

Nous présentons un modèle réduit et paramétrique capable de représenter le comportement de structures composites stratifiées : le PRBM.

Ce modèle a l'avantage de pouvoir être traité par des méthodes d'optimisation, sans devoir recourir à la construction de bases de cas.

L'originalité de notre approche réside dans une solution d'aide à la conception qui est celle (Figure 0.14) :

- Une approche multi-échelle,
- Une approche multiphysique,
- Une approche paramétrique,
- Une méthode d'exploration interactive des espaces de recherche d'optimisation évolutionnaire.

Notree modèle est un modèle séparé. Mais notre vision de la conception l'est aussi : nous proposons de concevoir en permet de considérant séparément les différentes échelles de conception (Figure 0.14).

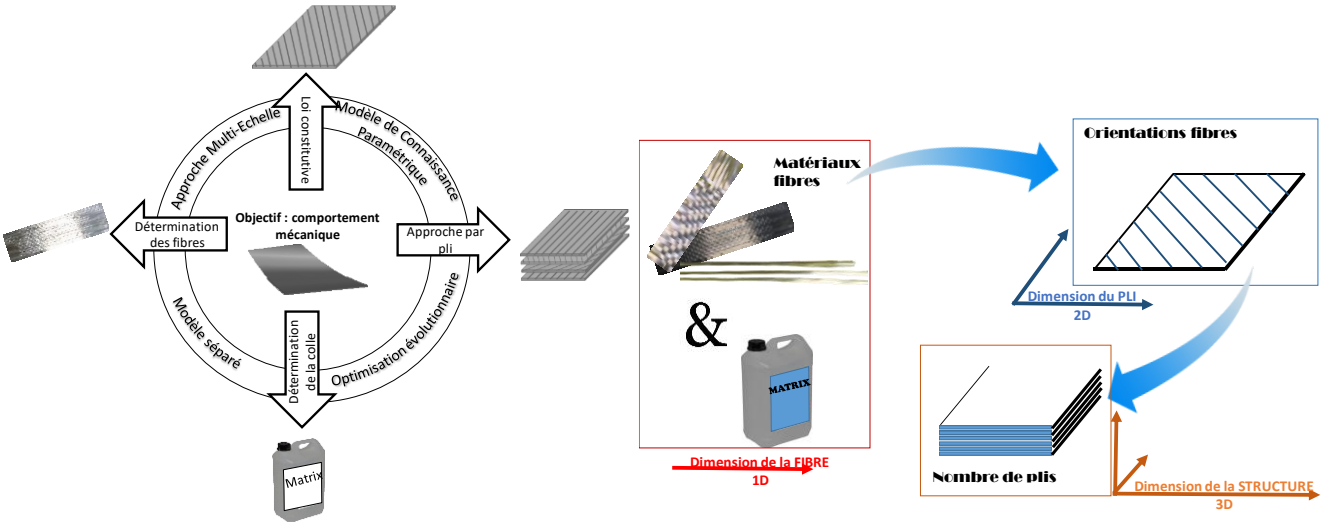

Figure 0.14. La conception séparée

Nous traitons avec détail des différents éléments présentés dans ce chapitre, dans la cadre d'un manuscrit écrit en anglais.

INTRODUCTION

Laminated composite materials are used mainly on applications where both high strength and low density are required. However, their benefits go far beyond these characteristics; when using composites, it is possible to obtain mechanical properties on demand, in particular, it is possible to obtain given desired responses by defining a stacking sequence of layers, orienting the maximum strength of each ply towards strategic directions. Moreover, due to the resin used as matrix, these materials also exhibit a higher damping characteristic than those observed on metals, resulting in a better capacity to dissipate vibrations (Galuppi and Royer [18]). These and many other characteristics besides the mechanical ones, make laminated composites attractive for critical structures, increasing the to rely on simulations to predict their mechanical behavior during the engineering design phases. Nevertheless, the mismatch of properties between fibers and matrix produces localized strains. For this reason, it is essential to be able to develop simulations, not only at the highest scales to account for global effects, but also in lower scales to develop advanced and optimized properties.

This thesis is concerned with the design of laminated composite structures responding either to static or dynamic load. Contrary to the design of metallic structures, an engineer designing a structure made by laminated composites has to consider a wide diversity of parameters and variables. Moreover, load responses are developed not only at the level of its components, said fibers and

matrix, but also on the interactions between them. The complication is observed at the level of the microscale with the details of these interactions because ideally, any numerical simulation method should account for every detail.

The finite element method (FEM) is mainly used to solve numerical models; its application includes diverse fields including the mechanical simulation of laminated composites. However, including every microstructural detail of fibers, matrix and interfaces within the models involves an enormous amount of computational capacities not readily available.

In order to overcome the limitations of the FEM, design engineers have used simplifications, assumptions and reduction techniques such as homogenizing the composite structure to treat it as an equivalent metallic material. The trend is to develop more complex models as the computational improvements become available. In the meantime, the uncertain phenomena occurring between fibers and matrix shifts a portion of the design decision making to manufacturing engineering; where testing, prototyping or trial and error procedures cause economic consequences, asset risks, ecological impacts or even worst, human hazards.

Nowadays, the demand for optimized solutions is growing faster than the improvements in computational capacities. The objective is not only to develop simulation models able to fit into current computational capacities but also include the physical phenomena required to analyze the essential details in a laminated composite structure.

Instead of the typical FEM approach, in this thesis we developed a PRBM, a Parametric and Reduced Based Model. The PRBM basis is the separation of variables used by the Proper Generalized Decomposition method (PGD). It embeds multi-physical behavior laws in a separated approach of plies and interfaces between plies, all within a predefined interval of design parameters. Consequently, the PRBM is reduced, because the operations to compute a particular solution are not based on tensor operations, but on simple function multiplications, therefore it can run fast in light computational resources.

Within this work, first the simulations may separate the elastic response of plies and their interfaces, leading to the development of a Separated Spatial Model (SSM). Then, from the SSM basis, several PRBM's are developed to perform fast simulations both in static and dynamic cases, becoming multi-physic because of the addition of viscoelasticity at the level of the interfaces between plies. A PRBM is then linked to an evolutionary optimization algorithm to provide solutions in a decision support scheme to design engineers. Therefore, the optimized solution provides information about the fiber density ratio, stacking sequence ply orientations, and the number of plies.

This manuscript is organized as follows:

Chapter 1 includes a theoretical background and state of the art about multiscale and multi-physical modeling of laminated composites.

Chapter 2 analyses the problem designing a laminated composite structure, it is based on numeric experiences and experimental data, and defines the objectives of this work.

Chapter 3 proposes the problem of a laminated composite under static load, based on a Spatial Separated Model (SSM).

Chapter 4 makes a PRBM multi-physical incorporating viscoelasticity in the interfaces between the plies; then it is used to solve a dynamic problem.

Chapter 5 configures a decision support scheme using a PRBM to find optimized solutions, both for a static and a dynamic problem.

Chapter 6 are the conclusions and future perspectives

(This page is intentionally left blank)

Chapter 1

MODELING AND DESIGN OF COMPOSITE STRUCTURES: STATE OF THE ART

1.1 Introduction

The design of composite materials faces significant challenges. The main challenge is the vast amount of parameters which are often not fully understood and affect the performance of the final product. Modeling every detail of the fibers, matrix and the interactions between them at the microscale could be an infinite task. Therefore, the engineering process usually makes simplifications, assumptions, and approximations to bring the computation cost to affordable limits. The consequence is the loss of accuracy and reliability, and the resulting increase of costly experimental validations.

This chapter presents a review of multiscale and multiphysical approaches, model reduction methods and decision making support systems for composite materials.

1.2 Laminated structures

1.2.1 Definition

Definition: **Composite structure**

> Two or more non-miscible materials joined together form a composite structure. The materials have different properties. Therefore, the global performance of the assembled structure is improved when compared to each of the individual materials.

Most of the composite structures are made of two materials, a high strength material acting as reinforcement and a matrix joining together the reinforcement. The matrix is used in bulk form, so it also transfers stresses among the reinforcement. Composite structures are grouped generally by the type of matrix: ceramic matrices (CMC) for high-temperature applications, metallic matrices (MMC) for high-performance applications and organic matrices (OMC), characterized by high strength and lower density than metals (Figure 1.1). The reinforcement can be in particulates or fibers.

Using fibers as reinforcement provides an advantage, they are stronger than the same material in bulk because they tend to contain fewer defects (Buncel and Renard [19]). The fibers may be short and unidirectional or distributed randomly over the matrix; or long and unidirectional, woven or bidirectional, generating a directionality of properties on the composite structure.



Figure 1.1. Applications of composite materials. Left: CMC on a jet turbine [1]. Center: MMC on automobile spares [2]. Right: OMC on a sailing ship[3]

Definition: **Laminated structure**

> A laminated structure is an array of several fiber-reinforced plies. They are stratified in a sequence, such that each ply is providing a specific characteristic in a given orientation to contribute to a particular global mechanical performance.

The most essential characteristic of laminated composite materials is their ability to obtain enhanced mechanical properties “on demand”; as a result, rather than adjusting the design of a product to available materials, as it is done typically for metals, a composite might be produced to supply specific design needs. The challenge is to find the right sequence of plies to achieve a particular performance. Among other benefits such as superior fatigue and corrosion resistance, laminated composites have significantly lower weight compared to

[1] Used under authorization from The Industry Today http://theindustrytoday.com

[2] Used under authorization from the Foundry Gate portal http://foundrygate.com

[3] Used under authorization from COMPOSITADOUR – ESTIA

metals, although at considerably higher prices, reducing their applications to mainly aerospace and automotive industries (Bunsell and Renard [19]).

1.2.2 Major parameters

The analysis of a laminated composite may be viewed at different scales. By this way, if we consider the ply as the fundamental building element, two key parameters are identified during their design phase.

- The number of plies in the lamination.
- The orientation of each ply relative to the principal direction of the lamination.

These two elements imply a constitutive law for each of the plies, altogether resulting in a global behavior of the structure. The properties of a ply are presented in Figure 1.2 and explained in Table 1-1.

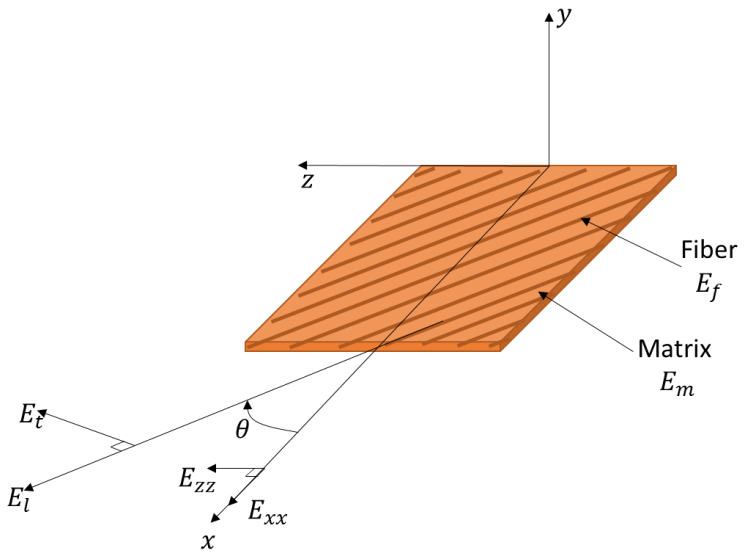

Figure 1.2. Major parameters of a laminae

Table 1-1. Description of the parameters in a laminae

E_f, G_f, υ_f	Young's modulus, shear modulus, Poisson's ratio of the fiber
E_m, G_m, υ_m	Young's modulus, shear modulus, Poisson's ratio of the matrix
V_f	Fiber volume ratio; $V_f = \frac{Volume\ of\ the\ fibers}{Volume\ of\ the\ ply}$
E_l, E_t	Equivalent ply Young's modulus relative to ply coordinates
G_{lt}	Equivalent ply shear modulus relative to ply coordinates
$\upsilon_{lt}, \upsilon_{tl}$	Equivalent ply Poisson's ratio relative to ply coordinates
E_{xx}, E_{yy}, E_{zz}	Equivalent ply Young's modulus relative to the lamination coordinates
G_{xy}, G_{yz}, G_{xz}	Equivalent ply shear modulus relative to the lamination coordinates
$\upsilon_{xy}, \upsilon_{yz}, \upsilon_{xz}$ $\upsilon_{yx}, \upsilon_{zy}, \upsilon_{zx}$	Equivalent ply Poisson's modulus relative to the lamination coordinates
θ	The orientation angle of the principal ply coordinate relative to the principal lamination coordinate

1.3 Multiscale approach

In practice, an engineer designing a composite structure is led both to:

- Designing the product morphology, and
- Designing the material to allow the final product to respond to the desired behavior.

Designing a composite structure consists of manipulating some parameters and variables that are well-known for manufacturing experts. Such manipulation of parameters leads the engineers to mix three points of view or scales (Figure 1.3).

1. A 1D point of view:

   The first choice to make is to select the type of fibers. By choosing a fiber, the engineer is determining the essential elements that will settle the constitutive law of the laminated structure. The Material properties represent these essential elements ($E_f,\ G_f, v_f$). At the same time, the matrix is defined, this choice will also act on the final constitutive law of the structure (E_m, G_m, v_m).

2. A 2D point of view:

   The fibers and the matrix joined together are forming a ply. A ply is considered a 2D structure. The volume fiber rate constituting the ply (V_f) and the orientation of the fibers (θ) inside the ply are defining a specific orthotropic law. These characteristics determine the capacity of a ply to react to the solicitations with a specific behavior.

3. A 3D point of view:

   The stacking of the multiple plies forms the Laminated Composite Structure. In our approach, we only consider mirror stacking: a symmetry plane exists with same ply orientation on each side of the plane. The primary parameter being considered at that point of view is the number of layers.

In the simulation of composite structures, the mechanical behavior is a consequence of the intrinsic heterogenic microstructure causing a non-uniform response throughout its domain. From the Finite Element Method (FEM), the introduction of every microscopic detail is not only a computational complication but also, the vast amount of required work to settle a FEM model does not satisfy the requirements of design in engineering regarding specialization and accuracy. Therefore; a better approach is to separate the scales of description; this strategy is known as multiscale modeling. The basis of a multiscale approach is homogenization and localization, considering the composite material as an equivalent homogeneity at each scale.

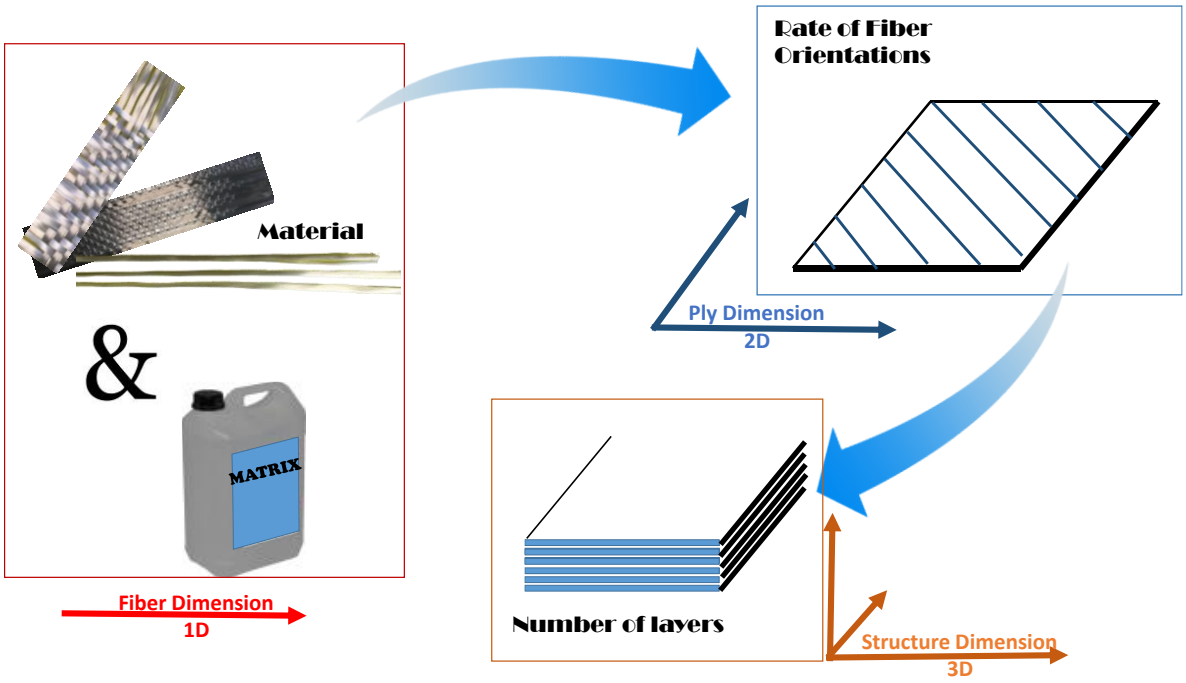

Figure 1.3. The design of a laminated composite

The multiscale approach has roughly two categories:

- Analytical multiscale, where continuous functions are introduced to model the displacement field through the thickness direction,
- Computational multiscale, where representative volumes in the microscale are modeled numerically, and the results are coupled to higher scales.

1.3.1 Analytical multiscale

Within the macroscale, the simplest method to simulate a laminated composite structure is to use the same models originally developed for homogeneous materials. This approach is known as the Classical Lamination Theory (CLT), and it is based on the Kirchhoff assumptions, where transverse shear is zero, meaning that all the layers in the structure are assumed to be in a state of plane stress. Today, the CLT is available in every Finite Element based CAE system. In this case, equivalent mechanical properties at the macroscale

may be estimated by homogenization of the properties from the lower scales. Particularly for the case of shells and beams, when thickness is small compared to the in-plane dimensions, it is common to approximate the unknown displacement field through the thickness direction by an estimated function which may be explicitly integrated, therefore the problem is solved only in 1D in the case of beams or 2D in the case of shells and plates. Reddy [16], analyses the estimation of transverse functions, both in homogenous materials and in laminated composites, concluding that the accuracy is good enough, as long as localized effects are not required within the analysis. These functions are known as Equivalent Single Layer theory (ESL), commonly used in plates when the ratio $\frac{tickness}{lenght} < 0{,}05$

Essentially, ESL theories are known to work well in metals, because they are considered homogeneous materials, however, on laminated composites, their application is limited to the macroscale because at the ply level and deeper in the fiber level the homogenization smoothes out the mismatch of mechanical properties typical of these structures.

Alternatively, layerwise theories are used when the relative displacements through the thickness direction are considered necessary. This theory is based on introducing piecewise continuous functions representing these relative displacements at the ply level, assuming C^0 continuity. Using the layer wise concept, Carrera and Ciuffreda [20] propose a unified formulation to assess theories for multilayered plates; an extensive work has been done under the name zig-zag theories as in Carrera [21], Carrera [22], Carrera and Brishetto [23], Brishetto and Carrera [24], Carrera and Petrolo [25], Carrera et al. [26] Carrera and Petrolo [27], Carrera and Miglioretti [28], Filippi and Carrera [29], Carrera et al. [30]. Other layer-wise approaches are also used in Robbins et al. [31] and Yas et al. [32]. The drawback of all of these theories is that the designer has to deal with choosing among a complex and wide diversity of layerwise functions prior to performing a simulation. The ESL theories are summarized in Table 1-2.

Table 1-2. Equivalent single layer theories

Theory	Base equations	Illustration	Comments
Classical Lamination Theory, (CLT) (2D) Kirchhoff-Love [33]	$u(x,y,z) = u_0(x,y) - z\frac{\partial \omega_0}{\partial x}$ $v(x,y,z) = v_0(x,y) - z\frac{\partial \omega_0}{\partial x}$ $\omega(x,y,z) = \omega_0(x,y)$	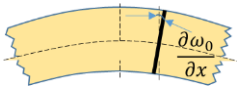	Very low computational cost. Useful for Very small deformations
First Order Shear deformation theory (FSDT) (2D) Reissner-Mindlin [33]	$u(x,y,z) = u_0(x,y) + z\phi_x(x,y)$ $v(x,y,z) = v_0(x,y) + z\phi_y(x,y)$ $\omega(x,y,z) = \omega_0(x,y)$	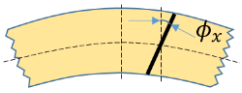	Low computational cost. It needs shear correction factors not easy to determine
High order shear deformation theory (HSDT) (2D) Reddy [33]	$u(x,y,z) = u_0(x,y) + z\phi_x(x,y) + z^3\left(-\frac{4}{3h^2}\right)\left(\phi_x + \frac{\partial \omega_0}{\partial x}\right)$ $v(x,y,z) = v_0(x,y) + z\phi_x(x,y) + z^3\left(-\frac{4}{3h^2}\right)\left(\phi_y + \frac{\partial \omega_0}{\partial y}\right)$ $\omega(x,y,z) = \omega_0(x,y)$	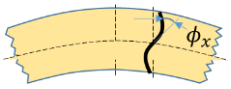	Enhanced accuracy, do not need shear correction factors. Computational cost increases as the order do.
Zig-Zag theory (2D) Carrera [5]	$u(x,y,z) = u_0(x,y) + \sum_{k=1}^{N_l-1}(z - z_{k-1})a_k H(z - z_k)$	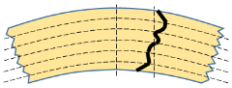	Good accuracy, Difficulty to choose among theories at the layer level and interpolation functions.
Layer wise (3D) Carrera [5]	$u(x,y,z) = \sum_{I=1}^{N} U_I(x,y,t)\Phi_j^k(z)$ $v(x,y,z) = \sum_{I=1}^{N} V_I(x,y,t)\Phi_j^k(z)$ $w(x,y,z) = \sum_{I=1}^{M} W_I(x,y,t)\Psi_j^k(z)$	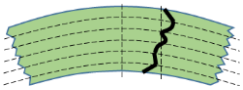	Accurate results at the ply level, not too high computational cost because it uses separated numerical integration. In thin laminates, it can exhibit spurious transverse shear stiffness, spurious transverse normal stiffness, and ill-conditioned stiffness matrices

1.3.2 Computational multiscale

Computational multiscale refers to the use of computational capacities together with mathematical models, allowing to account for the structural details of the microscale and coupling them to the macroscale. Computational multiscale approaches are either hierarchical or concurrent. In the hierarchical multiscale the properties are brought from the micro to the macroscale in one direction by Representative Volume Elements (RVE). The concurrent approach is about reevaluating the effects of the microscale at designated conditions; this is the idea behind the two-level Finite Elements (FE^2)

Andreassen and Andreassen [34], Sun et al. [35] and De Souza Neto [36] evaluated the theory of elasticity with RVE. Mosby and Matous [37] perform computational homogenization from the microscale using RVE on a high-performance computation (HPC) to simulate mode I delamination. The use RVE to analyze flaws and reinforcements on laminated composites applying the FEM has been adopted by Kushnir and Rabinovitch [38], Puel and Aubry [39], Willot and Jeulin [40], Hu et al. [41], Savvas and Papadopoulos [42], Sakata et al. [43]

The FE^2 was presented by Feyel [44] to model the viscoelastic behavior of composite materials coupling microscale representations to macroscopic levels. Unger [45] uses an FE^2 on an HPC system to solve an improved procedure to reduce computational time.

The multiscale systems have been largely studied. The book edited by Soutis and Beaumont [46], exposes a good overview of the problems encountered by those interested in the design of composite structures. Notably, most of the authors are regarding the problematic of damage prediction inside the laminate structures. For example:

- Galiotis and Paipetis [47] propose that the damage may occur at the level of interfaces between plies, developing specific criteria to locate the risk of delamination.

- McCartney [48] proposes that the damage may start either with the cracking of the fibers or inner in the matrix, presenting a micro-mechanical model in order to locate the origin of the damage

Some other authors consider that damage in laminated structures may be uncertain (Bogdanor et al. [49]), even when it frequently is the consequence of a cyclic behavior (Hosseini et al. [50]), the damage leads to some significant problems of material integrity occurring during the material design process (Beaumont [51]). Consequently, the problem of damage may be modeled better by a micromechanical approach (Wang [52] and Ivancevic [53]).

1.4 Representation of laminated structures

1.4.1 Relevance of simulation

From the identification of tasks, specifications, and constraints, to the production of the desired result; the design of a laminated composite follows a standard process similar to the specified by Pahl et al. [54]. This process is illustrated in Figure 1.3 and explained in detail in section 1.8.1

Figure 1.3 also shows the support of simulation capabilities in order to perform many of the computations required by the designer, given the extensive amount of parameters conforming the constitutive laws. During the dimensioning phase, mechanical simulations of composites are a crucial tool, but because of the significant complexity, the reliability of the simulations is still under high uncertainties impacting the costs of experimentation to validate results. For this reason, many researchers have focused their interest in contributing to the improvement of simulation capacities.

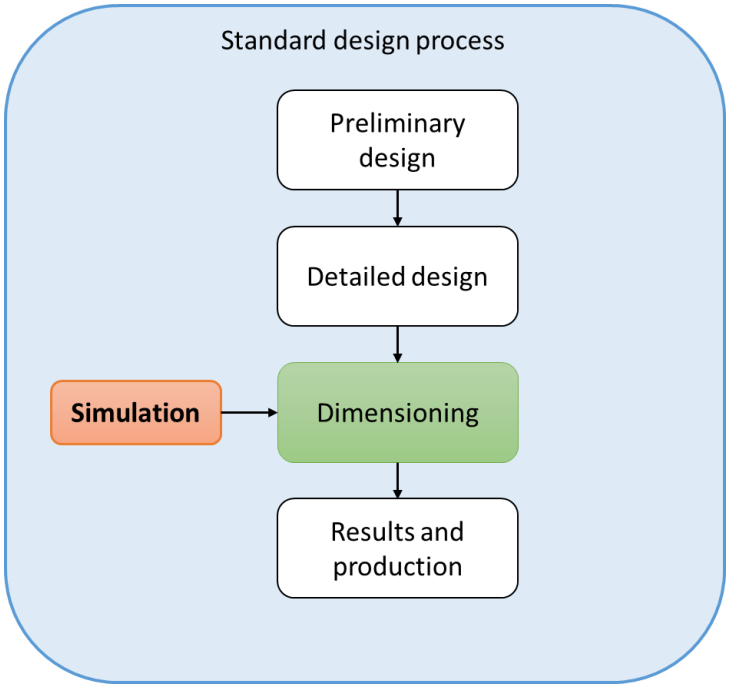

Figure 1.4. The design process of a laminated composite

1.4.2 Generalities

A basic simulation of a laminated composite structure may be performed by implementing the elasticity theory. In the simulations, body motion is assumed to have small geometric changes. Thus, the strain tensor ε as a function of the displacement vector field U for each body (ply) i with n plies is presented in equation 1.1.

$$\boldsymbol{\varepsilon}^i(U) = \frac{1}{2}\left(\nabla U^i + \left(\nabla U^i\right)^T\right) \qquad 1.1$$

Then, equation 1.2 represents the kinetics relating the stress tensor σ_i for each body i, and the body force B.

$$-\sum_{i=0}^{n} \nabla \cdot \boldsymbol{\sigma}^i = B \qquad 1.2$$

$$\nabla = \left(\frac{\partial}{\partial x}, \frac{\partial}{\partial y}, \frac{\partial}{\partial z}\right)^T$$

Moreover, the constitutive equation relating the stresses and strains is implemented by Hooke's law in equation 1.3

$$\boldsymbol{\sigma}^i = \boldsymbol{H}^i \cdot \boldsymbol{\varepsilon}^i \qquad 1.3$$

Where $\boldsymbol{H}^i$ is the stiffness tensor for each body i. However, instead of introducing every detail of the structure, it is common to use a multiscale approach where equivalent orthotropic materials are obtained at each body i. Equation 1.4 is presenting the form of the stiffness tensor.

$$J = \frac{1}{1 - \vartheta_{xy}\vartheta_{yx} - \vartheta_{yz}\vartheta_{zy} - \vartheta_{zx}\vartheta_{xz} - 2\vartheta_{yx}\vartheta_{zy}\vartheta_{xz}}$$

$$[\boldsymbol{H}^i] = J \begin{bmatrix} E_{xx}(1-\vartheta_{yz}\vartheta_{zy}) & E_{xx}(\vartheta_{yx}-\vartheta_{zx}\vartheta_{yz}) & E_{xx}(\vartheta_{zx}-\vartheta_{yx}\vartheta_{zy}) & 0 & 0 & 0 \\ E_{xx}(\vartheta_{yx}-\vartheta_{zx}\vartheta_{yz}) & E_{yy}(1-\vartheta_{xz}\vartheta_{zx}) & E_{yy}(\vartheta_{zy}-\vartheta_{xy}\vartheta_{zx}) & 0 & 0 & 0 \\ E_{xx}(\vartheta_{zx}-\vartheta_{yx}\vartheta_{zy}) & E_{yy}(\vartheta_{zy}-\vartheta_{xy}\vartheta_{zx}) & E_{zz}(1-\vartheta_{xy}\vartheta_{yx}) & 0 & 0 & 0 \\ 0 & 0 & 0 & G_{yz}/J & 0 & 0 \\ 0 & 0 & 0 & 0 & G_{zx}/J & 0 \\ 0 & 0 & 0 & 0 & 0 & G_{xy}/J \end{bmatrix}^i \qquad 1.4$$

1.5 Multiphysical approach

1.5.1 Multiphysical point of view in composite structures

A multiphysical approach is considered when the structure exhibits different physical properties, for example, electrical, thermal or mechanical, (Yuan et al. [55]). Within the scope of this thesis, the multiphysical approach is mechanical and goes through the thickness direction in a laminated composite. In this sense, a multiphysical research trend is devoted to understanding the behavior of the interfaces and the effects on the stress transfer (Geers et al. [56]). These effects are interlaminar normal stresses tending to separate the plies, and interlaminar shear stresses tending to slide one ply over the adjacent ones, either because of weak or non-adhesion, both in static and dynamic applications.

Separation and slippage have been studied mainly in laminated structures, for example by Cheng et al. [6] using a spring-layer model, Ramos and Pesce [14] assuming frictionless interfaces in a riser tube, Chattopadhyay et al. [10] introducing fictitious linear springs, Lei et al. [11] experimentally evaluating interface interaction models using micro-Raman spectroscopy, Budiman et al. [13] proposing a fragmentation model or Liu et al. [12] developing a nonlinear cohesive/frictional coupled model. They all use the FEM with contact elements to guarantee continuity. This approach achieves good accuracy, but the consequence is the high computational cost and computing time, this is the reason why these works are concentrated on localized effects.

Among localized effects, delamination is keeping the interest of many research works. Delamination is known to appear in the normal direction to the interface surfaces (mode I) and the in-plane direction to the interfaces (mode II and mode III). The simulation of delamination modes is achieved better by using the Cohesive Zone Model (CZM) because it uses a cohesive zone before the crack tip to avoid the singularity caused by its sharp shape (Figure 1.5).

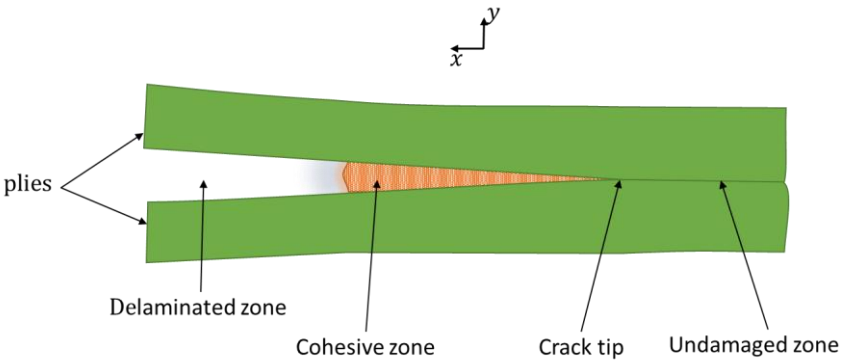

Figure 1.5. Delamination according to the CZM

The CZM concept introduced the idea of non-prefect bonding and several cohesive force models, holding together two different plies have been proposed according to the type of matrix. Some of these force models have a nonlinear elastic shape before the yield stress with accurate results (Barenblatt [57], Needleman [58], Aduloju [59]), but resin based interfaces are well represented by linear elastic shapes (Kumar [60]) with lower computational cost.

1.5.2 Viscoelasticity in composite structures

Fictitious thin layers have also been used to introduce viscous interfacial effects. Mostly, they are used to model imperfect bonding between plies caused by delamination and they may behave as linear spring, viscous or viscoelastic characteristics. Using this approach, the review by Carrera [5] explains that such insertions improve the accuracy of zig-zag models. Similarly, Lenci and Warminski [15] studied two layers of structural glass bonded together by a thin elastic joint, they analyzed the first analytical natural frequency concluding that it decreases as a function of amplitude due to the nonlinearity, thus the strong relationship between the stiffness of each ply and the viscoelastic coefficients of the fictitious layers to the natural frequencies. The difficulty as already mentioned is that using zig-zag theories force the designer to choose among a wide variety of functions while configuring the simulation before it is run.

Additionally, Venkatachalam, and Balasivanandha [61], and Sahoo and Ray [62] highlighted the relevance of viscoelastic properties of a composite part using FEM and a mesh-free method. However, the main problem is also the simulation cost. Lisandrin and van Tooren [63] aimed at making lower computing costs by reducing a dynamic model of a composite beam.

Differential models commonly represent viscoelasticity; these are combinations of uni-dimensional elastic elements and viscous dashpots (Gutierrez [64]). In these models, there is a linear relationship between the stress σ with its derivatives and strain ε with its derivatives. In the general case, assuming characteristic mechanical properties a and b, with n combinations of dashpots in series and m combinations of dashpots in parallel (having $n \leq m$) is given by Equation 1.5,

$$b_0\sigma(t) + \sum_{i=1}^{n} b_i \frac{d^i\sigma(t)}{dt^i} = a_0\varepsilon(t) + \sum_{i=1}^{m} a_i \frac{d^i\varepsilon(t)}{dt^i} \qquad 1.5$$

A combination of both a Kelvin-Voigt model (a spring in parallel with a dashpot, where $a_0 \neq 0$, $n = 0$ and $m = 1$ representing a viscous solid) and a

Maxwell model (a spring in series with a dashpot, $a_0 = 0$ and $n = m = 1$ representing a viscous fluid) are more suitable to represent the internal friction, characteristic of viscoelasticity in a solid structure. This representation includes creep, stress relaxation, hysteresis, recovery response and stress dependence on strain rate. In this sense, the Standard Linear Viscoelastic Solid model or simply the Zener model is responding to this characteristic (Assie et al. [65]). Particularly, for an isotropic viscoelastic material, with constant Poisson ratio and considering only viscoelastic shear strain, the Zener model is represented in Figure 1.6

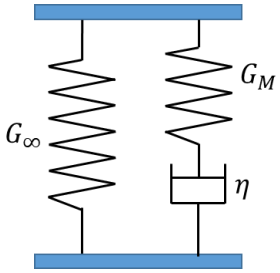

Figure 1.6. Representation of the Zener model

The following arguments configure the Zener model,

$G_0 = G_\infty + G_M$	Short term shear modulus, this is the unrelaxed shear modulus
G_∞	Long-term shear modulus, this is the relaxed shear modulus
$\tau = \eta / G_0$	Relaxation time with viscosity η
$n = m = 1;\ b_0 = 1;\ b_1 = \tau;\ a_0 = G_0;$ $a_1 = \tau G_\infty$	From equation 1.5

Moreover, equation 1.5 becomes equation 1.6.

$$\sigma_{xy}(t) + \tau \frac{d\sigma(t)}{dt} = G_0 \varepsilon_{xy}(t) + G_\infty \tau \frac{d\varepsilon_{xy}(t)}{dt} \qquad 1.6$$

Beyond the Zener model, additional elastic elements and dashpots may be used in more complex models with the intention to gain accuracy; however experimental results show a weaker frequency dependence than the effect of a viscous dashpot with constant loss factor for all frequencies (Pritz [66]). For this reason, especially in the case of metals and polymers, it is known that viscous friction is not the actual character of their viscoelastic behavior. Several research works are reporting that the stress in a dashpot representing structural internal friction is not entirely related to a derivative of integer order, as it is used in fluids, but instead, it could be related in a diminished extent to the time variation of strain or a fractional derivative of the strain.

Pritz [66] describes the advantages of assuming a fractional four-parameters Zener model, versus the five-parameters (Pritz [67]). These advantages are explained regarding the satisfaction of the thermodynamic constraints if $\alpha = \beta$, being α the order of the stress derivatives and β the order of the strain derivatives. The consequence is a wider frequency range of application. Therefore, equation 1.6 becomes equation 1.7,

$$\sigma_{xy}(t) + \tau^{\alpha} \frac{d^{\alpha}\sigma(t)}{dt^{\alpha}} = G_0 \varepsilon_{xy}(t) + G_{\infty}\tau^{\alpha} \frac{d^{\alpha}\varepsilon_{xy}(t)}{dt^{\alpha}} \qquad 1.7$$

Monte Carlo simulations have been frequently used by different authors to construct models to identify the four viscoelastic parameters from experimental FRF measurements (Lenci [15], Ventakatachalam and Balasivanandha Prabu [61] and Sahoo [62]).

By this way, several discrete simulations are selected with carefully selected points of the parameters to be found, so the solution has to be computed several times, with consequences over the computing time.

1.6 Simulation of composite structures, advances, and limitations

1.6.1 Finite element based simulation

From the mechanical point of view, the FEM problem is solved by the reformulation of the governing equation 1.2 into its variational form as shown in equation 1.8,

$$-\int_{\Omega}(\nabla\sigma)u^{*}d\Omega=\int_{\Omega}B\cdot u^{*}d\Omega \qquad 1.8$$

Where Ω is the domain and u^{*} is a test function belonging to a discrete test space V, which is used to find the approximated solution of the displacement field u in a discrete trial space with the condition that the test function vanishes in the boundaries where the displacement is known (Bathe [68]). Assuming good governing equation models, the advantage of the FEM is the accuracy. Conversely, the complication in the case of laminated composites is the elevated computational cost and computing time, because of the inherent micro structural details. Including microstructural details in the simulation result on enormous matrices when the problem is solved in full 3D having, $u=u(x,y,z)$ (Qu [69], Chinesta [9]).

Full 3D FEM simulations are accepted as an accurate solution, and therefore they are used as a reference to evaluate the performance of new simulation techniques.

- Han et al. [70] use finite elements with a zig-zag function through the thickness direction to model vibration in a multilayered composite beam and compares the solution to a high order shear deformation function elements and full 3D FEM solution.
- Kussmaul et al. [71] evaluate the effectiveness of a 2D shear lag model to model interlaminar effects in patched laminates, by comparing the

solution to a full 3D solid brick simulation. They conclude that the 2D elements are not able to calculate interlaminar stresses with accuracy.

- Yan et al. [72] apply a meshless analysis with layerwise theories evaluating the results against full 3D solutions.
- Bognet et al. [3] argue that only full 3D FEM simulations may numerically validate 3D PGD simulations of composite plates.

Localized effects on laminated composites are also simulated by full 3D simulations, inserting contact elements between bodies. These simulations include delamination and friction in joints and interfaces and the structural effects under impacts.

- Bedon and Fragiacomo [73] perform a full 3D FEM simulation to analyze composite joints, inserting contact elements with a CZM
- Sápi et al. [74] use a CZM to analyze filler materials in joints, concluding that more in-depth details of the microstructure are needed to improve reliability on the simulations.
- Sun et al. [75] compare three solid element technologies applied to thermoplastic and thermoset laminated composites under low-velocity impact.
- Dong et al. [76] use brick elements to model carbon fiber composites damage under lighting strikes.

1.6.2 Simulation for multiscale and multiphysical behavior

Reducing CPU time when modeling laminated composites is a priority, instead of costly 3D simulations. Therefore, the properties at low scales are homogenized to higher scales. A review of computational multiscale and multiphysical methods is presented by Matous [77].

Furthermore, using shell and plate theories,

- Kim and Lee [78] analyze the fatigue effects of laminated composites by the use of 8 node shell elements.

- Song et al. analyze [79] aircraft laminated composites under ice impacts using brick elements to model the ice bullets and shell elements to model the composite plates.
- Raju et al. [80] evaluate the use of microscale representative volume elements on the FE modeling of laminated composites, using the rule of mixture to predict the effective elastic properties
- Molker et al. [81] use first-order shear deformation shell elements to analyze failures caused by loads perpendicular to laminated composite plates
- Carrera et al. [82] develop a zig-zag power function, comparing the results to high-order shear deformation theories and layerwise theories.
- De Miguel et al. [83] and Entezari et al. [84] implement 1D layerwise elements on shell and beam elements to reduce the CPU time and obtain similar accuracy than full 3D simulations of laminated composites under mechanical load.

New simulation techniques are incorporating multiphysical capacities, specially intended to understand the behavior of the interfaces, whether at the microscale between fibers and matrix or the mesoscale in the interfaces between plies. These interfaces are modeled to respond with friction, viscoelasticity or cohesive forces.

- Yang et al. [85] model a sandwich composite structure under vibration by finite shell elements considering the viscoelastic behavior of the core. They use the Rayleigh-Ritz approach to model the frequency dependency of viscoelasticity by its complex representation.
- Assarar et al. [86] use the modal strain energy approach to analyze the response of a laminated composite with a viscoelastic core, using the FEM
- Filippi et al. [87] study the effects of a viscoelastic core in a multilayer structure by finite zig-zag elements embedding a fractional order viscoelastic model.

- Hirsekorn et al. [88] study woven composites considering the viscoelastic response by homogenization from the micro to the macro structure, using the Maxwell model to represent viscoelasticity.
- Hazzard et al. [89] develop homogenized solid bricks with an embedded CZM to account for interface effects of composites under impact tests.
- Stojcevski et al. [90] experimentally analyze the impact of localized interfacial properties on laminated composites to improve response performance under load.
- Berton et al. [91] conclude that the evolution of cracks is dependent on the viscoelastic property where the matrix response is dominant. They use a thermodynamics-based constitutive model to analyze creep deformation using finite RVE.
- Covezzi et al. [92] analyze elastoplasticity and viscoplasticity on CM using RVE with Transformation Field Analysis (TFA) homogenization.

Computational advances have also been achieved on hierarchical and concurrent multiscale, Ullah et al. [93] uses a computational homogenization to analyze textile composites by the use of RVE. Wulfinghoff et al. [94] use Hashing-Shtrikman homogenization approach to perform refinements at the microstructure level similarly to the FE^2 approach. Hiemstra et al. [95] describe the rules of a Reduced Optimal Quadrature ROQ to reduce the computing time of the mass and stiffness matrix, and Oliver et al. 2017 [96] use an FE^2 approach to better integrate RVE on the analysis of fracture, applying Proper Orthogonal Decomposition (POD) and ROQ.

Furthermore, simulation for analysis within an affordable CPU time requires parametric studies. In order to do so Shakya et al. [97] made a parametric study on wind turbine blades subject to flutter using shell elements with CLT, Gul et al. [98] on a Timoshenko beam, Li et al. [99] on a FGPM using FOSDT, Kumar et al. [100] assuming plane strain on quadrilateral elements to evaluate local damage on laminated ceramic composites to account for the

influence of geometry, and Ahmadi and Rahimi [101] using RVE on a grid stiffened composite panel.

Besides, Khan and Kim, [102] analyze delamination on smart composites by implementing artificial intelligence, and the FEM with layerwise theory elements and Zhou et al. [103] use RVE to perform reliability analysis on composite materials and Liang et al. [104] Propose a Koiter-Newton order reduction technique to analyze nonlinear buckling of composite plates applying the FEM

Within simulation for design Li et al. [105] perform a surrogate assisted optimization of a laminated composite problem under vibration. The CPU time is reduced by implementing the FEM with shell elements using the first order shear deformation theory. Savran and Aydin [106] optimize the stacking sequence of laminated composites in a multi-objective problem, by using GA and the FEM with zig-zag theory shell elements. Montemurro et al. [107] perform a multi-scale optimization to design laminated composites by the use of zig-zag FEM elements obtaining specially oriented stacking sequences. Gonzalez Lozano et al. [108] propose a design for the manufacturing process of laminated composites to align the fibers with the principal stress direction, optimizing the stiffness distribution with specialized fiber orientations. In order to reduce CPU time, they use structural approximations of the FEM, and Scheffold et al. [109] propose a model order reduction method based on ECSW and Galerkin projection to optimize jointed structures, achieving more than four times less time than the full order method. Table 1-3 synthetizes the references cited in this section.

Table 1-3. Synthesis of references on simulation of composite structures

Type of simulation	Method	References	Advantage	Limitation
Global simulation	Full 3D FEM	Bedon and Fragiacomo [73] Sápi et al. [74] Sun et al. [75] Dong et al. [76] Kussmaul et al [71]	Enhanced accuracy and through the thickness resolution	Extremely high computational cost
Multiscale simulation	FSDT	Molker et al. [81]	Improved CPU time	Poor through the thickness resolution
	HSDT	Kim and Lee [78] Song et al. [79] Raju et al. [80]	Improved accuracy and through the thickness resolution	A wide diversity of basis functions to be chosen before the simulation is run
	Zig-zag	Han et al. [70] Yan et al. [72] Carrera et al. [82] De Miguel et al. [83] Entezari et al. [84]		
Multiphysical	HSDT	Yang et al. [85]	Improved accuracy and through the thickness resolution	A wide diversity of basis functions to be chosen before the simulation is run
	Zig-zag	Filippi et al. [87]		
	Modal strain energy	Assar et al. [86]	Enhanced accuracy and through the thickness resolution	High computational cost
	FEM and CZV	Hazzard et al. [89]		
	RVE	Berton et al. [91] Hirsekorn et al. [88] Covezzi et al. [92] Ullah et al. [93] Zhou et al. [103]		
	ROQ-FE^2	Wulfinhoff et al. [94] Hiemstra et al. [95] Oliver et al. [96]		

Table 1 3. (Continuation) Synthesis of references on simulation of composite structures

Simulation for analysis	CLT	Shakya et al. [97] Gul et al. [98]	Low CPU cost, low specialization.	Details of the microscale are smoothed out
	FSDT	Li et al. [99]		
	Layer-wise	Khan and Kim [102]	Improved accuracy and through the thickness resolution	A basis function must be chosen before the simulation is run.
	Square elements and plain strain	Kumar et al. [100]	Improved through the thickness resolution	Plain strain is a 2D simulation
	RVE	Zhou et al. [103] Ahmadi and Rahimi [101]	Enhanced accuracy	High CPU cost
	FEM	Liang et al. [104]		
Simulation for design	FSDT	Li et al. [105]	Low CPU cost. Easy.	Details of the microscale are smoothed out
	Zig-Zag	Savran and Aydin [106] Montemurro et al. [107]	Improved accuracy and through the thickness resolution	A basis function must be chosen before the simulation is run.
	FEM	Gonzalez L et al. [108]	Enhanced accuracy and through the thickness resolution	High CPU cost
	ECSW	Scheffold et al. [109]		

Most of the simulation techniques that we presented are costly in term of computing time. Even if a large number of authors aim at reducing the time processing, the results are not persuasive. Some authors achieve time processing reduction developing some reduced models. We are presenting the relevance of reduced models in the next section. So, from this section, we realize that our implementation requires a model reduction method to save

computational cost and computing time, yet considering the details at lower scales.

1.7 Model reduction

Definition: **Reduced model**

> A reduced model is obtained by projecting representative basis functions of the full order model onto a lower dimensional subspace. They are intended to reduce both, the CPU time and the computational cost.

Under the definition above, multiscale methods might be considered reduced models, including ESL theories, RVE, FE^2 or even ROQ. However, in the literature, it is common to talk about model reduction referring to those methods allowing to build a reduced model offline to be used later online.

1.7.1 Methods of reduction

Definition: **Method of reduction**

> The methods of reduction allow building a reduced model offline where expensive computations are usually run. Then the reduced model may be used online to compute less expensive and in a fraction of the time.

The methods of reduction are divided into two groups; depending on whether the reduced model is constructed after the definition of the representative basis functions (“aposteriori”) or before, so the representative functions are

defined along the model construction procedure (“apriori”). Figure 1.7 illustrates this classification; it also illustrates how a meta-modeling of knowledge may use the resulting reduced models as a vademecum of solutions (Cagin [110])

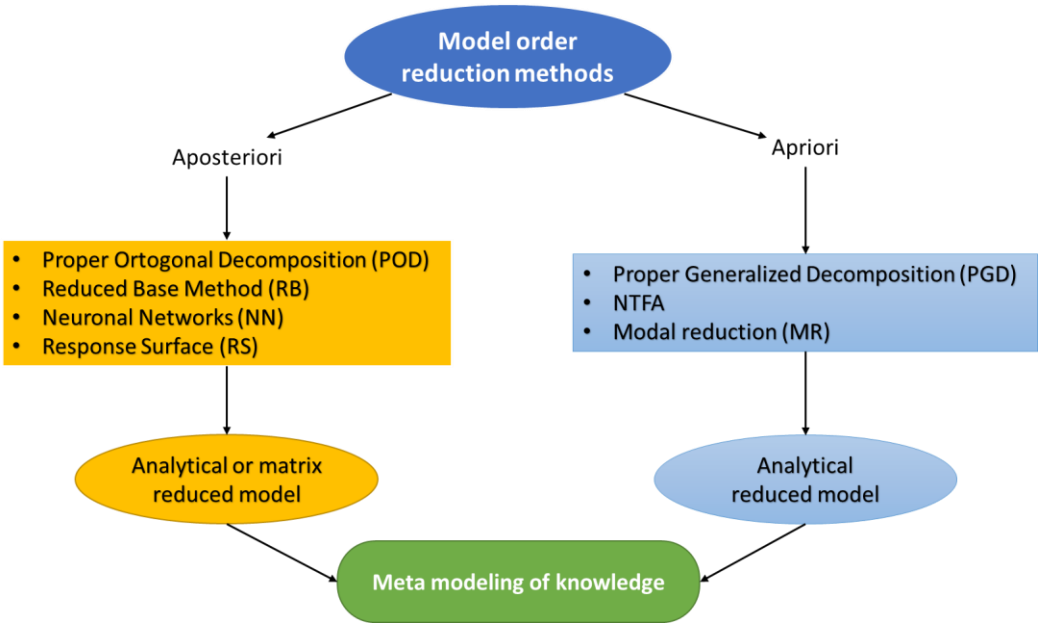

Figure 1.7. Classification of model order reduction methods

While working with aposteriori methods, Zaghi et al. [111] use response surfaces to simulate the nonlinear response of CM and Limongelli [112] to find damage in plates, Bhattacharjee and Matous [113] and Bessa et al. [114] develop a database based on RVE to train an NN based machine learning system. Later, a review on state of the art NN as model order reduced methods is made by Bostanabad et al. [115]. RB methods have been utilized by Liu et al. [116] for linear elastic problems, and Milani et al. [117] extend the application to problems with multiple parameters, then Iapichino and Volkwein [118] analyze the method on an optimization problem and Lu et al. [119] use the RBM and POD to create time depending solutions on thermo-mechanical problems. Currently one of the most developed approach is the Proper Orthogonal Decomposition (POD). Hernández et al. [120] performs a hyper-reduction model applying POD, proposing a cubature approach to simulate CM under quasi-static and resonant

load and Samir et al. [121] applies POD for crack identification in CM using Genetic Algorithms (GA). However, the POD has been used rather to model fluids. Indeed, the complication with the apriori methods is the high computational cost to solve the constitutive equations needed to feed the departing snapshot functions.

Apriori methods do not require previous assumptions. Therefore the basis functions are rather deduced by the method meanwhile the reduced model is built. Chang et al. [122] applied modal order reduction for structural health monitoring using NN and Hudson, and Sinha [123] using linearization to the assessment of defects. Michel and Suquet [124] and Leuschener and Fritzen [125] present a reduced order technique based on decomposition on a basis of modes called Nonuniform Transformation Field Analysis NTFA, used to preserve the effects of the micromechanics and responding in a viscoelastic manner.

The Proper Generalized Decomposition (PGD) is also an apriori method, we will discuss it in the next section. Table 1-4 synthetizes the references cited so far.

Table 1-4. Synthesis of references about model order reduction

	Method	**Reference**	**Advantage**	**Limitation**
Aposteriori	Response surface	Zaghi et al. [111] Limongelli [112]	Low specialization	Linear responses are preferred
	Neuronal Networks	Bhattacharjee and Matous [113] Bessa et al. [114] Bostanabad et al. [115]	Good accuracy	The high computational cost to construct the reduced model
	Reduced base	Liu et al. [116] Milani et al. [117] Iapichino and Volkwein [118]		
	POD	Lu et al. [119] Hernández et al. [120] Samir et al. [121]		

Table 1 4. (Continuation) Synthesis of references about model order reduction

Apriori	Modal order	Chang et al. [122] Hudson and Sinha [123]	Low specialization	Limited to linear responses
	NTFA	Michel and Suquet [124] Leuschener and Fritzen [125]	Good accuracy	The high computational cost to construct the reduced model
	PGD	Discussed in next section		

1.7.2 The PGD

Within the apriori model reduction methods, the Proper Generalized Decomposition (PGD) has been developed as an alternative solution method to the FEM (Chinesta [9]), whether in 3D solids, Bognet et al. [3] or high dimensional spaces, Pruliere [7]. The PGD method has been validated in a diversity of applications, from control as in González et al. [126] and Nadal et al. [127]), to optimal temperature for fiber placement in composites (Bur et al. [128]), 3D printing (Sibileau et al. [129]), and fracture mechanics (Giner et al. [130]), among others.

The PGD method is based on the separation of variables as shown in equation 1.9 and equation 1.10

$$U(x,y) \cong U^n(x,y) \qquad 1.9$$

$$U^n(x,y) = \sum_{i=1}^{n} X^i \cdot Y^i \qquad 1.10$$

Where X and Y represent basis functions along each separated domain x and y. By this manner, the separation of space variables approximates the solution by a sum of n functional products called “Modes” (Chinesta [9]).

The first attractive characteristic of this method is that it does not need to know apriori the basis functions. Instead, they are constructed from an "alternative direction strategy" during the construction of the reduced model.

The second most important characteristic of PGD is the consequence of the separation of space domains; it implies that the number of equations to be solved are $N \times D$ at each iteration, being N the number of nodes in a mesh and D the dimensions. Therefore, in PGD the computational time of each iteration grows linearly with the number of dimensions, instead of exponentially as in the FEM.

The third and perhaps the most remarkable characteristic of the PGD method is its ability to handle parametric computations as a separated extra domain (Pruliere et al. [7]), as shown in equation 1.11 and equation 1.12.

$$U(x, y, q) \cong U^n(x, y, q) \tag{1.11}$$

$$U^n(x, y, q) = \sum_{i=1}^{n} X^i \cdot Y^i \cdot Q^i \tag{1.12}$$

In this case, Q represents basis functions in a domain q, these basis functions might represent the variation of an input quantity such as design parameters and variables. The basis functions Q allow the reduced model to become a parametric model. In addition, the parametrization in PGD is not only set within the nodes of the additional domain, but also for the whole domain by interpolation in a post-processing routine, requiring a very low computational cost. This property is different and more efficient than other parametric analysis as the Monte Carlo method, where a solution has to be computed several times, each with different input quantities to obtain a set of solutions, having as consequence the increase in computational time.

1.7.3 The PGD method for composite materials

In a lamination, the PGD might also be seen as a multiscale method (Ammar et al., [8], Halabi et al. [131], and Metoui et al. [132]). The method finds

a solution first at low scales, considering the details through the thickness direction to iterate basis functions, and then coupling the results at the macro scale along the in-plane direction. Table 1-5 Synthetizes references using the PGD method in laminated composites.

Table 1-5. Synthesis of references about the PGD method in laminated composites

Application	**Reference**
Simulation of laminated composite structures by the separation of the 3D field into an in-plane 2D and through the thickness 1D space	Prulière [133]
Squeeze flow of thermoplastic composites during the forming process	Ghnatios et al. [134]
Use RVE to apply a multiscale formulation using the PGD method	Halabi et al. [135]
The development of a PGD model of composite laminates considering thin elastic layers through the thickness direction.	Zghal et al.[136]
Response under the low-speed impact of laminated composites, including a CZM to incorporate delamination within the analysis.	Metoui et al. [137]
Finding low error differences between the FEM and the PGD method on the multiscale and separated simulation of laminated composites.	Metoui et al. [132]
Using wavelets to generate PGD basis functions better.	Leon et al. [138]

PGD reduced models for composite materials have also been parametrized. This way, rather than a single solution, the method produces a reduced model, that provides solutions within a scenario inside the boundaries of a weight function. Table 1-6 Synthetizes references about parametrized PGD reduced models.

Table 1-6. Synthesis of references using PGD parametric models.

Application	**Reference**
Parametric orientations of elastic laminated composites	A. Ammar et al. [139]
Error evaluation of PGD solution of parametrized 2D and 3D problems.	Chamoin et al. [140]
Harmonic exited structure, developing a frequency parametrized and separated model.	Malik et al. [141]

By the same manner as variables may be introduced as parameters in additional domains, time also may be introduced as an additional domain, producing a model that is not time incremental as in the Newmark time integration method, but continuous within the defined time interval. Table 1-7 synthetizes references about the separation of time in the PGD method.

Table 1-7. Synthesis of references about the separation of time in the PGD method

Application	**Reference**
General application	Ammar et al. [8]
Linear viscoelasticity	Ammar et al. [142]
Large Time Increment Method (LATIN-PGD) to solve a nonlinear non-incremental time-dependent structural problem.	Ladevèze [143]

1.8 Design of composite structures

The design of products based on metals leads the designer to explore a limited and discrete space of possibilities, regarding the problem of material choice. Indeed, the material is chosen well before the dimensioning phase. In contrast, the design process of laminated composites is different; the designer must make decisions at the same time on the product morphology and the

composite structure. In other words, the designer is not only defining the morphology of the product, but also simultaneously designing the product and the material. Therefore, the amount of acceptable combinations becomes vast.

Two approaches are addressed in this section: a standard approach having defined sequential phases, and an approach assisted by a decision support system, allowing the designer to skip intermediate phases resulting in an optimal solution produced directly.

1.8.1 The design process

The design of a laminated composite structure goes in sequential order through preliminary design, detailed design, dimensioning, and production of the resulting composite (Pahl et al. [54], Ullman [2]). Figure 1.8 explains these phases, showing that the process may reconsider preliminary or detailed design concepts iteratively, to finally send a solution to production.

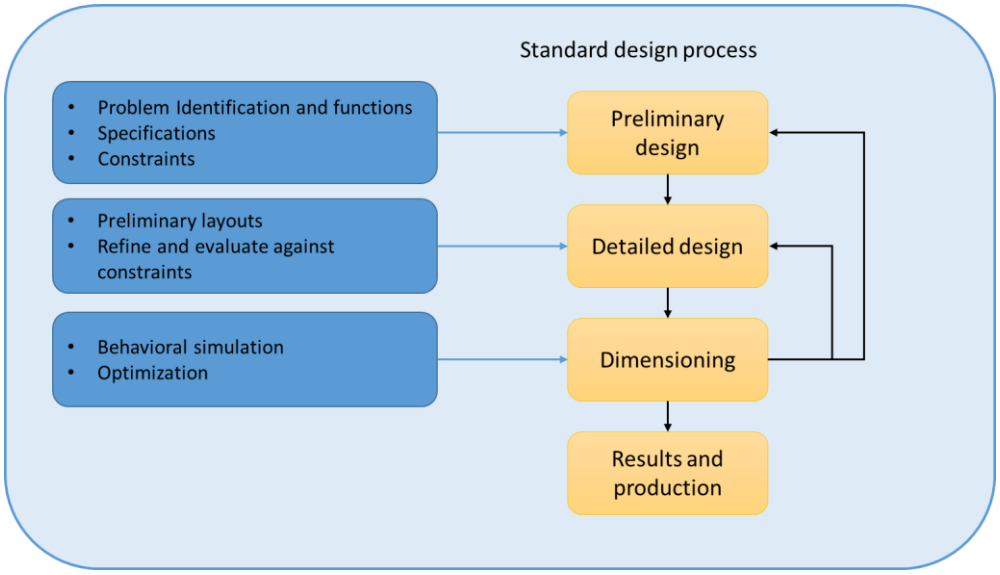

Figure 1.8. The design process according to Pahl et al. [54]

1.8.2 Design from simulation

From the mechanical point of view, FEM simulations are used primarily to validate and optimize the displacement field and global stress state. In a typical dimensioning phase of a laminated composite structure, the simulation begins with the selection of fiber and matrix, then the fiber volume fraction, the number of plies and the orientation of each ply, and stacking sequence. Therefore, multiple refinements might be required back to the detailed design or even reconsidering specifications and constraints in the preliminary design if possible. This iteration process is illustrated in Figure 1.9

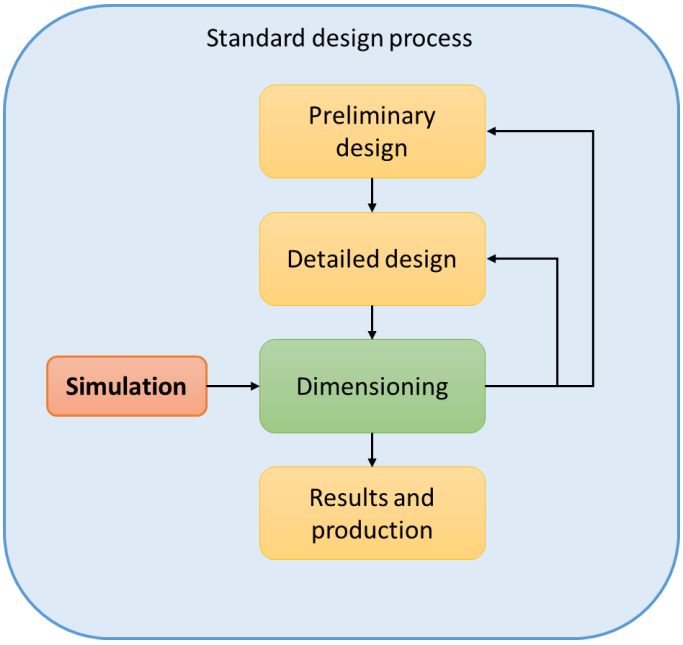

Figure 1.9 Standard design process

1.8.3 Support to decision making in composite design

Along with the design process, engineers make use of available knowledge to take decisions for the solution to technical problems. The decision-making process also considers requirements and constraints to obtain optimized solutions. Further, the engineer may also use computer support to model and

collect information, this is known as Decision Making Support Systems (DMSS) (Pahl et al. [54] Gutierrez et al. [144], Fischer et al. [145]). This concept is represented in Figure 1.10.

A DMSS embeds rational models, relevant information or features to assist the engineering decision making, which otherwise would be numerous or impossible for human processing (Bouyssou [146]). By doing so, DMSSs are developed for specific design phases of a composite. For example, in predesign, Hambali et al. [147] developed a DMSS of material selection of composite bumper beams by a hierarchy process; similarly Corona et al. [148] analyse the impact of natural fibers on the life cycle of a composite and Calado et al. [149] worked on a DMSS to select composite materials during the early phases of aircraft structure design. Within the production of composite solutions, Srinivasan et al. [150] use a DMSS to understand composite manufacturing interactions, Sanz-Corretge [151] proposes a decision tree algorithm with many possible laminate combinations and Coronado et al. [152] use a DMSS to evaluate the impact over the supply chain of end products. The attempt to develop a DMSS including all design phases is commonly known as a multiplatform that integrates software modeling the micromechanics and selection of components, CAD, FEM and simulation of enterprise resource planning. Instead of such multiplatform integration, Gascons et al. [153] propose a DMSS integrating all design phases based on a single variable reduction with better efficiency. Moreover, in this thesis (Chapter 5) we use a parametric knowledge model to explore a solution space in the pre-design phase to directly obtain an optimized solution ready to be sent to production.

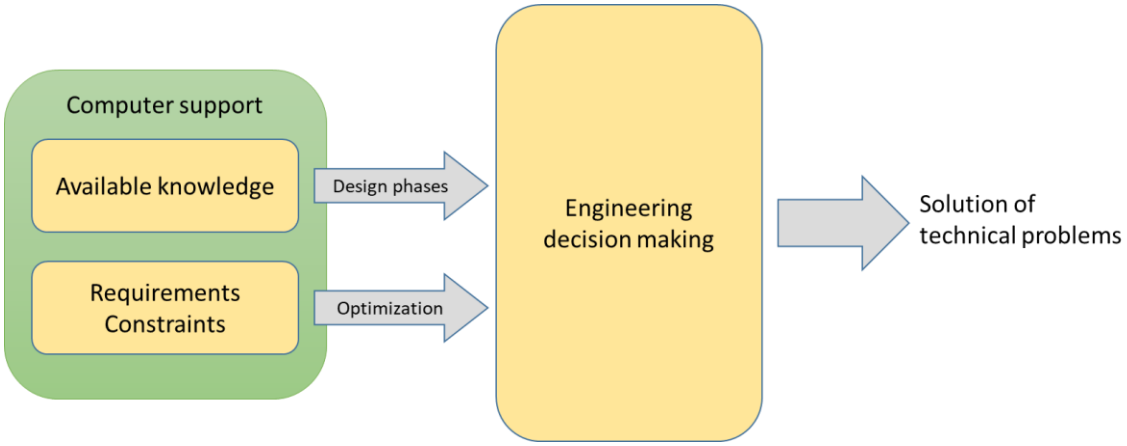

Figure 1.10. Decision-making process

1.8.4 Optimization leading to the design of laminated composites

Under the idea of a DMSS and beyond the interest of damage prediction, an excellent way to avoid damage consists in providing the engineers with virtual solutions to support the design of non-damageable laminated structures. To achieve such an objective, some authors present new parametrized models of behavior that explicitly characterize the design choices realized at different levels of the structure. These models may be processed through an optimization approach in order to lead to some stacking sequence of layers responding to design requirements. Some of the parametrized models are,

- Response-Surface-based gradient optimization approach.

  This approach ties the optimization to a response surface obtained from the FEM analysis at specific points and using the derivatives of the responses concerning the design parameters. These derivatives are indicators of the sensitivity of the response to a change in parameters and are usually obtained using the finite difference method. Several authors use this approach to optimize the stacking sequence in a laminate. Macquart et al. [154] for example, first restrict the design domain using their practical experience and then use the Classical Lamination Theory (CLT) to efficiently but approximately compute

responses within that domain at discrete intervals and generate a feasibility map. The speed of computing the derivatives using finite differences is therefore increased, and single objective gradient-based optimization is carried out. On the other hand, Dutra and de Almeida [155] use First-Order Shear Deformation Theory (FSDT) to improve the shear prediction through the thickness direction and also use their practical experience to constrain the design space and to create feasibility maps to compute responses derivatives and then perform a multi-objective weight based gradient optimization. Similarly, other authors are developing new ways to look for optimized stacking sequences from FEM based methods (Ranaivomiarana et al. [156], Tong et al. [157], Monte et al. [158]).

The advantage of this strategy is the moderate user specialization because commercial FEM software is available to perform the analysis and optimization procedure.

The limitation is the use of Equivalent Single Layer (ESL) theories, as for the CLT or the FSDT, smoothing out the properties through the thickness direction. Although from a global perspective the accuracy of the displacement field is acceptable with ESL theories, the price to pay after the homogenization of the mismatched properties up to the macroscale level, is the loss of details at lower scales, say the ply level or fiber-matrix level, as discussed by Reddy [159].

- Discrete approach

  Several Heuristic approaches including evolutionary algorithms are described in the literature. The Ant Colony optimization, the Particle Swarm, the Simulated Annealing, the Imperialistic Competitive algorithm, and the Firefly algorithm are some examples. However, the most widely used heuristic approach is the Evolutionary Genetic Algorithm as cited by Nikbakt et al. [160].

Whether a discrete design parameter is present or not within the model, evolutionary algorithms are a widely used alternative in the optimal design of

laminate composites. Almeida et al. [161] used a Genetic Algorithm (GA) to find the optimal stacking sequence of a ten ply laminated composite tube under internal pressure, simplifying the model by the application of an Equivalent Single Layer (ESL) theory on a shell element and assuming plane stress to reduce the computational cost of every solution. In the same way, Irisarri et al. [162] used CLT on shell elements to perform a multi-objective optimization procedure to avoid buckling on laminated composite structures, limiting the search to a previously generated feasibility map, including selected stacking sequences that respect commonly used constraints in the industry.

The advantage of the feasibility map, providing a solution space, is that it consideres solutions with a specific number of plies and selected stacking sequences, at an acceptable computing cost.

However, the limitation implies that every searching point requires a new FEM solution. Thus, similarly to the previous case, ESL theories are used to simplify the FEM solutions and save computational time. Conversely, if the interest of the analysis relies on lower scales, the model size quickly becomes prohibitive regarding computational cost and computing time, due to the inherent inhomogeneity of a laminate and the number of elements required to represent them. Additionally, restricting the search for optimal solutions to selected stacking sequences included in the feasibility map implies that better solutions may exist but are left outside the solution space if the solution map is not populated enough.

- Other approaches to optimization

  Additional approaches to the optimization of composite structures are known as trial and error, local search and random search. These are included in a review on optimization approaches of composite structures presented by Nikbakt et al. [160]. Similarly, Miki and Sugiyamat [163] and Jing et al. [164] propose some analytical behavioral models that can aid to the determination of the number of layers in a laminated structure, such models are continuous and do not consider the different behaviors that are occurring at the different scales of the structure.

The advantages of the approaches above are the continuous advance of optimization strategies and computation capacities, allowing complex and extensive evaluation of compromises between objectives, resulting in better decision support during the design phases.

Despite the increased computation capacities, the limitation extending the analysis to the micro-scale using FEM involves expensive models, which also must be solved multiple times depending on the model nature, optimization strategy and design parameters.

1.8.5 Solutions to support the design of composites

Table 1-8 synthetizes the references used to analyze the state of the DMSS

Table 1-8. Synthesis of references about DMSS

Application	Reference		Advantage	Limitation
DMSS for pre-design	Gascons et al. [153]		Enhanced DMSS	Requires high CPU capacity or a reduced model
DMSS for design	Hambali et al. [147] Corona et al. [148] Calado et al. [149]		Allows optimization in design	
DMSS for production	Srinivasan et al. [150] Sanz-Corretge [151] Coronado et al. [152]		Allows optimization in manufacturing	
Optimization	Continuous	- Macquart et al. [154] - Dutra and de Almeida [155] - Ranaivomiarana et al. [156] - Tong et al. [157] - Monte et al. [158]	Moderate user specialization	The details at the microscale are smoothed out.
	Discrete	- Nikbakt et al. [160] - Almeida et al. [161] - Irisarri [162]	Acceptable computing cost	Every searching point requires a new solution
	Other	- Miki and Sugiyamat [163] - Jing et al. [164]	Allows complex and extensive evaluation of compromises	High computational cost

1.9 Conclusion

In conclusion, a DMSS to produce detailed, and optimized solutions of laminated composite structures, but based on the use of a reduced and separated model is a research trend. Some authors have already proposed reduced and separated models. First, the reduction has the advantage to make the simulation run faster (Ladevèze [165]). Second, the separation makes possible the independent analysis of each scale of the structure (Llorca et al. [166]). However, most of the authors motivated by the problematic of separated and reduced models are mainly focusing on the behavioral simulation of structures and not on supporting the decision making, in a similar concept to the DMSS described by Cluzel et al. [167], Sirin et al. [168] and Yannou and Petiot [169]

Sonmez [170] lists 1007 approaches that contribute directly or indirectly to aid the engineer to design a composite material based product. We noted that none of the optimization process based on a parametric and reduced model was developed. Moreover, most of the design problems aim at dimensioning a composite under static behavior. Even if some authors have developed parametrized models to represent the viscoelastic dynamic behavior (Hiemstra et al. [95], Oliver et al. [96], Shakya et al. [97], Gul et al. [98] and Li [99]), all of them have supplied specialized models: any parametrized model can address both a static and a dynamic behavior.

(This page is intentionally left blank)

Chapter 2

REPRESENTATION, BEHAVIOR, AND DESIGN OF COMPOSITE STRUCTURES

2.1 Introduction

The problem designing a laminated composite material is the different material properties acting at different scales of the product. The overall mechanical behavior is determined by the product shape and by all constitutive laws involved at each ply and even deeper in the microstructure. For this reason, the designer encounters a situation of multiscale and multiphysical design.

This chapter presents the analysis of the problem addressed in this thesis, from the multiscale approach, to solve the case of a composite structure under static load, to a multiphysical approach, solving a dynamic load case. Finally, a decision-making support system is proposed, capable of finding quick optimal solutions.

2.2 Multiscale modeling of composite structures

Our multiscale approach is illustrated in Figure 2.1; it is described as follows:

1. The ply, where fibers and matrix joined together play a fundamental role.
2. The stacking sequence, where interstitial delamination and sliding effects must be mastered.
3. Linking interfaces between substructures and joints with strong singular behaviors where the laws of contact, local damage and friction might be necessary.
4. Large assembled structures, resulting from assemblages of plies, laminates, and joints whose last character is to resist the stress distribution and any solicitation from their environment.

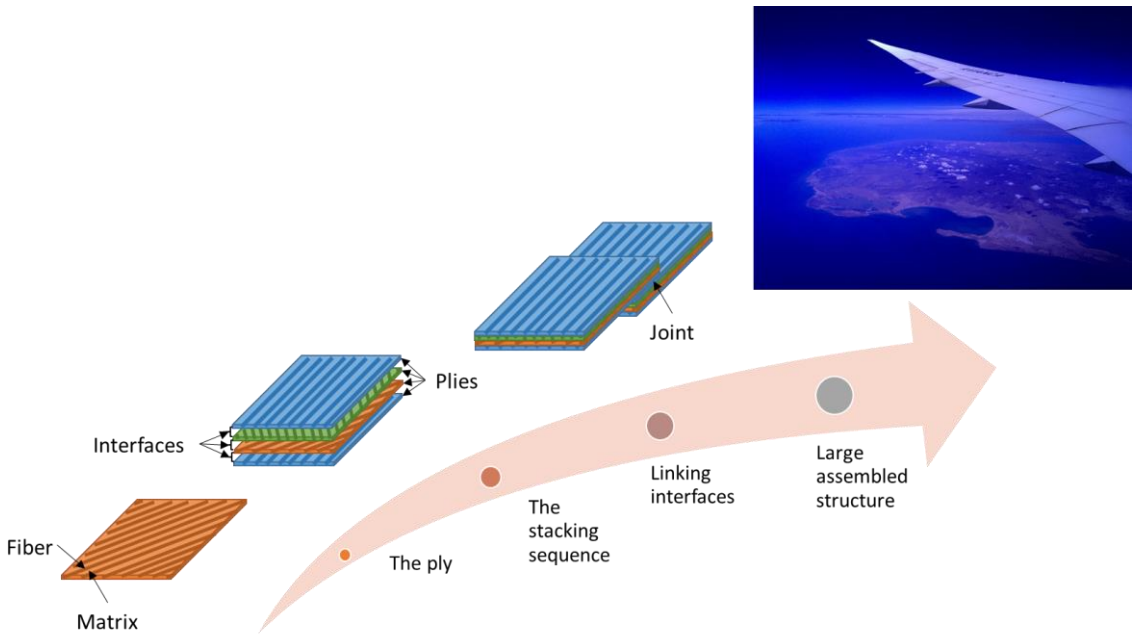

Figure 2.1. Our multiscale approach. (The picture is taken entering the north of Colombia from my window seat, showing the wing of an Avianca Boeing 787 Dreamliner)

We presented in section 1.2.2 the main parameters of a composite structure. In Figure 2.2, the problem is how to obtain a global constitutive law,

without handling each low scale parameter independently and considering the role of plies and interfaces.

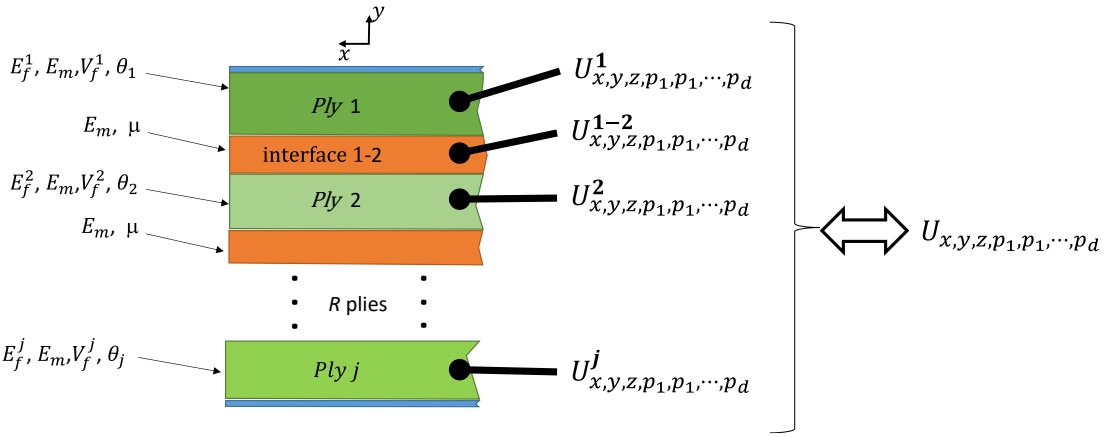

Figure 2.2. Global constitutive law

2.2.1 3D behavior

Definition: **3D behavior**

> The stress state in a solid continuum is behaving in 3D when it is deforming in every direction in the three-dimensional Euclidean space.

Definition: **2D behavior**

> When there is a constant cross-section, normal to a given direction in a structure, it is possible to simplify a simulation to a 2D continuum, assuming either zero stress (plane stress) or zero strain (plane strain) in the normal direction of the 2D continuum.

We intend to understand the physical phenomena at the ply level and the interfaces between plies, producing a zig-zag displacement effect through the thickness direction, as represented in Figure 2.3. Zig-zag theories modeling the zig-zag behavior by basis functions was already introduced in section 1.3.1 however, instead of making the designer choose among a diversity of functions before running a simulation, we aim to run a model equivalent to a full 3D FEM simulation, where the behavior is deduced from the constitutive equations.

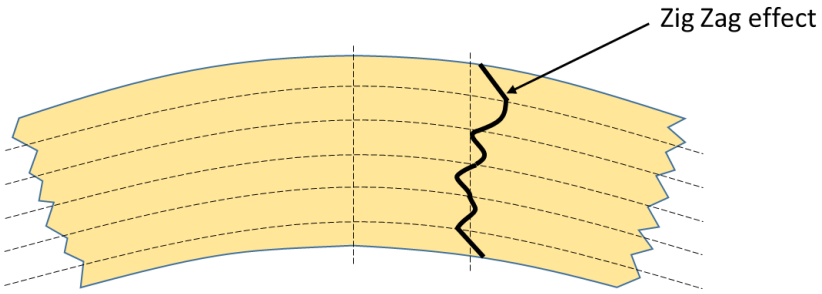

Figure 2.3 The zig-zag effect

2.2.2 Simulation with the FEM considering the interfaces between plies.

Currently, some efficient numerical models processed with the FEM are available in the usual CAE tools. We use standard CAE software to simulate a composite structure under static load by considering plies and interfaces. However, immediately found the following limitations:

a) Usual FEM models are based on a global stiffness of the composite structure being computed from the design characteristics, determined at some lower scales of the structure: the number of plies, the orientation of fibers in each ply, the volume fraction of fibers, nature of fiber material, nature of the matrix. A Finite Element Model is highly specialized regarding design description; as a matter of fact, two different designs of structures require two different models of simulation. A FEM model is not considered as a parametric approach in the sense of design.

b) The global approach implemented with the FEM does not allow to consider the shear behavior that may occur at the level of the interface between the plies. Each ply has its particular behavior, and it can slide relative to each other. This behavior, named zig-zag, cannot be easily modeled with the FEM. The FEM is not suitable for a multi-scale representation of the composite structure behavior.
c) Even if we succeeded in developing a shell based FEM model in order to represent the behavior of each ply and each interface, we concluded that the implementation of a non-global simulation with the FEM is not suitable because:
   - Modeling contacts and friction is complex and adds significant non-linearites that make the computation expensive.
   - Computing such a multiscale model is costly when the behavior is static and even more if the behavior is dynamic (explicit model); the computing time would become enormous.
   - The interface introduces a viscous behavior in the situation of dynamic behavior, and we have to analyze the problem using a multiphysical approach that cannot be easily computed with the FEM.

In order to illustrate the statements listed above, a cantilever beam under static load is used to perform the simulation involving friction on the interfaces. We used isotropic plies with Young's Modulus $E = 2{,}6x10^{11}\ Pa$ and Poisson ratio $v = 0{,}3$, by this manner we can concentrate our analysis on the internal friction occurring at the interfaces. The dimensions were $480\ mm\ x\ 45\ mm\ x\ 2\ mm$ as represented in Figure 2.4. The beam is also split into four equal layers through the thickness direction.

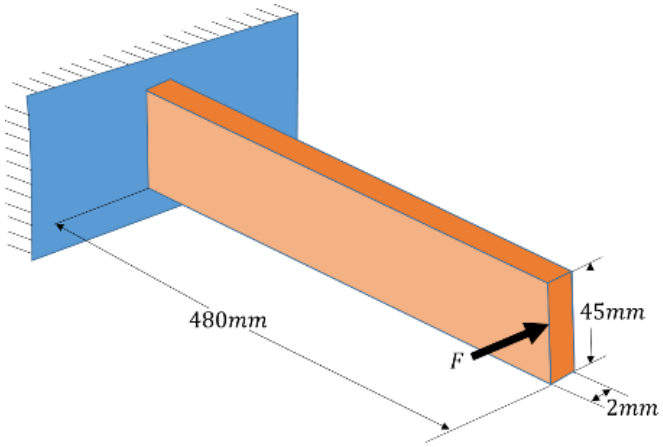

Figure 2.4 Cantilever beam solved by the FEM

All the simulations were carried out using a server with Intel Xeon E5-16 cores processor, 64 GB in RAM and Windows 2012 server. The software used was ANSYS® APDL 17.2, and the simulations are in the 3-D domain so brick elements were used to mesh the whole beam. The boundary condition is set by a fixed support in one of the ends, and a static force is applied at the free end in the z direction. Then, contact elements were used as an interface between the plies. The contact elements were tested using two different behaviors:

- Bonded, therefore having a linear response of the interfaces.
- Frictional, representing the internal friction occurring between plies.

The frictional behavior is based on the Coulomb model by equation 2.1:

$$f_f = \mu \cdot N + b \qquad 2.1$$

Where f_f is the friction force, μ is the friction coefficient, N is the normal force and b represents the cohesion between layers. This cohesion force is based on the idea of the cohesive zone model proposed by Dugdale [171], where a given uniform cohesive force is assumed to be the behavior of an adhesive.

Solving the frictional nonlinear problem required implicit integration. The FEM solver uses the trapezoidal rule proposed by Newmark [172]. As recommended by Bathe [68], the parameters used to gain accuracy and stability were set constant, having $\alpha = 1/4$ and $\beta = 1/2$. Finally, the Newmark method

requires the force to be applied progressively in steps rather than all at once and it uses equation 2.2 to equation 2.5 (Bathe [68], ANSYS [172] [68], [172]).

$$\widehat{K} = K + a_0 M \tag{2.2}$$

$$\hat{R}_{t+\Delta t} = R_{t+\Delta t} + M\left(a_0 U_t + a_2 \dot{U}_t + a_3 \ddot{U}_t\right) \tag{2.3}$$

$$\ddot{U}_{t+\Delta t} = a_0 (U_{t+\Delta t} - U_t) - a_2 \dot{U}_t - a_3 \ddot{U}_t \tag{2.4}$$

$$\dot{U}_{t+\Delta t} = \dot{U}_t + a_6 \ddot{U}_t + a_7 \ddot{U}_{t+\Delta t} \tag{2.5}$$

With integration constants (equation 2.6 to 2.10),

$$a_0 = \frac{1}{\alpha \cdot \Delta t^2} \tag{2.6}$$

$$a_2 = \frac{1}{\alpha \cdot \Delta t} \tag{2.7}$$

$$a_3 = \frac{1}{2\alpha} - 1 \tag{2.8}$$

$$a_6 = \Delta t(1 - \beta) \tag{2.9}$$

$$a_7 = \beta \cdot \Delta t \tag{2.10}$$

From equation 2.2, $\widehat{K}$ is the effective stiffness, from equation 2.3, $\hat{R}$ is the effective load, and M the mass matrix. The variable t should not be seen as time, but rather as a variable to introduce the concept of solving the problem by progressive steps Δt. In addition, the Newton-Raphson iteration method is used by the Newmark method at each solution step (ANSYS [172]), implying that the stiffness matrix is assumed linear to compute a trial force and recalculated from the previous iteration until a residual drops to within a reasonable limit. Table 2-1 illustrates three of the cases analyzed according to the simulation described herein.

Table 2-1. Configuration of the contact elements in three different cases

		The configuration of the contact elements
Case 1	Perfectly bonded contacts	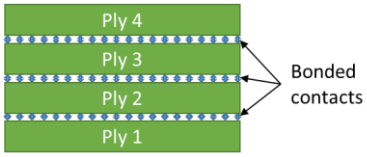
Case 2	Only the central contact has a frictional behavior; the other two are perfectly bonded	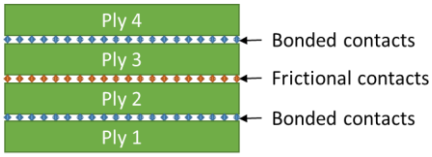
Case 3	All the three contacts have frictional behavior	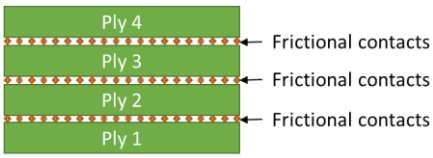

Figure 2.5 represents the calculated deformation results at the free end of the four-layer cantilever beam. A force $F = 5\ N$ is applied for each of the three cases analyzed.

Dots in the curves of Figure 2.5 indicate a solution step, so it is possible to get a sense of the computational time. Each solution step involves a recalculation of the stiffness matrix using a symmetrization algorithm. This is the case of perfectly bonded contacts as described in ANSYS [172]. By contrast, when frictional contacts were included, the nonlinearities required the process to compute more iterations at each step, or even increasing the solution steps when no convergence was achieved. Increasing the solution steps extended the computing time and in extreme cases, the simulation was aborted requiring restarting the solver. The inconvenience of aborted simulations was improved by enforcing the use of the unsymmetric matrix; hence, even if took longer to compute each step, the probability of achieving convergence increased.

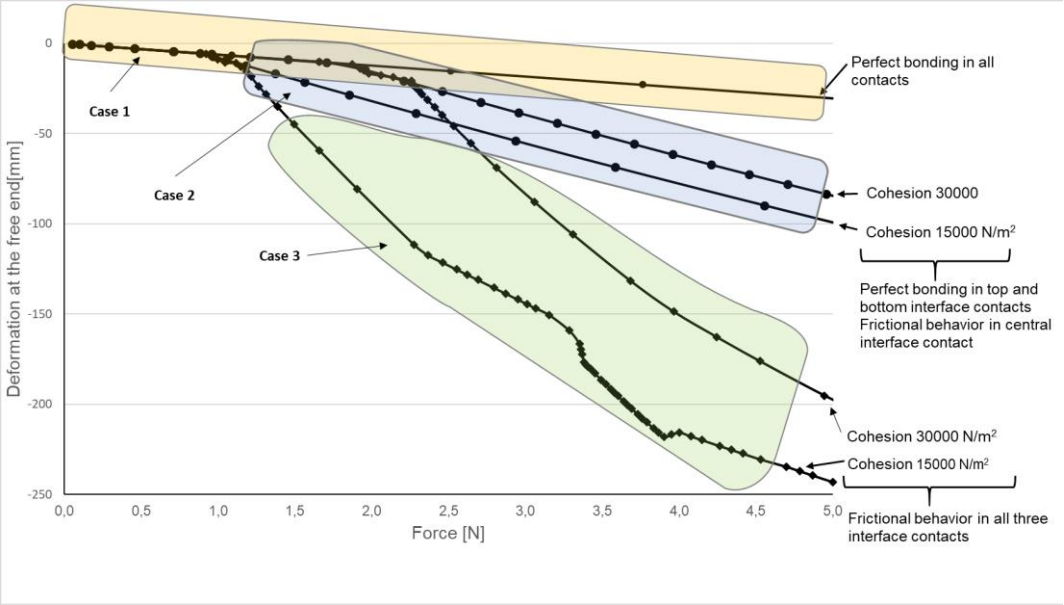

Figure 2.5 Displacement of the free end of a cantilever beam

Table 2-2 summarizes the implications in the FEM solver, configuring the contact elements on each of the three cases.

The difficulty of incorporating the internal friction in the analysis lies in the discontinuity produced by the relative motion between sliding surfaces; in order to enforce continuity, contact elements between layers were introduced. In the in-plane direction, these contact elements use the penalty method, as shown by Konyukhov and Izi [173], according to equation 2.11.

$$\Pi_{p(u)} = \Pi + {}^{1}/_{2}\,\varepsilon p_{(u)}^{2} \qquad 2.11$$

With Π being the potential energy, ε as penalty parameter and $p_{(u)}$ as penetration function. Similarly, in the direction normal to the layers, the same elements use the augmented Lagrange method as shown in equation 2.12, being λ the Lagrange multiplier.

$$L_{(u)} = \Pi + \lambda p_{(u)} + {}^{1}/_{2}\,\varepsilon p_{(u)}^{2} \qquad 2.12$$

Table 2-2. Solver outputs for the different cases solving the beam under test

	Solver output, advantages, and difficulties
Case 1	- Computing time: 5 minutes - Solution steps: 11 steps - Iterations at each step: one or two - Large deflection and symmetric matrix was set - Easy to configure
Case 2	- Computing time: up to 24 hours - Solution steps: up to 24 steps - iterations at each step: 6 to 12 - Large deflection and symmetric matrix was set - Due to not convergence, some computations were aborted before achieving the final load. The situation was improved increasing the solution steps.
Case 3	- Computing time: up to 4 days - Solution steps: up to 55 steps - Large deflection was set - Iterations at each step: 6 to 12 - Due to no convergence, many computations were aborted before achieving the final load. The situation was improved using asymmetric matrix and increasing the solution steps.

The consequence of using these contact models is the significantly higher computational cost; not only on the additional degrees of freedom but also on the difficulties to achieve convergence given the nonlinearities introduced by the frictional contact elements.

2.2.3 Behavior and spatial separation

In this thesis, our first objective is to develop a model of a composite structure that explicitly integrates the number of plies and the elastic parameters driven by the structure. We call this model a Spatial Separated Model (SSM).

The SSM uses the principle of separation of domains to integrate the properties at different scales by applying the Proper Generalized Decomposition method (PGD).

Definition: **Spatial Separated Model (SSM)**

> The SSM is a multiscale and parametrized model-based simulation allowing the user to have:
>
> 1. A macro-information detailing the global behavior of the composite structure under static load.
> 2. A layer-by-layer behavior representation.
> 3. Information about the elastic behavior of interfaces between the plies.

Our SSM, with multiscale, separated and parametric capabilities is needed to fit into current computational capabilities, which otherwise would need significant technological improvements. However, at the same time, the SSM has to model the effects of geometrical imperfections, inclusions, cracks, or low bonding which are impossible to eliminate, despite the remarkable improvements achieved on the production of laminated composite techniques.

2.2.4 Our multiscale approach

Definition: **Design parameters**

> Design parameters are quantities defining instances of a composite structure. They are the quantities being handled by the designer when creating the laminated structure.

Definition: **Behavior variables**

> Behavior variables are the quantities directly describing the mechanical behavior, which is determined by stresses and strains. A second order tensor represents the stresses at each point of the domain, this tensor is also named the Cauchy's tensor and describes three values of normal stresses and three values of shear stress. The behavior variables are linked to design parameters through mechanical laws.

Problematic 1

> From the Spatial Separation using the PGD method, we make explicit the design parameters at each scale of the composite structure.
>
> This separation is also a behavior separation allowing the plies and the interfaces between plies to be considered.
>
> A simulation model named the Spatial Separation Model (SSM) is developed.

Figure 2.6 represents the first development approach illustrating how, based on a numeric experience, we identify design parameters and behavior variables to develop our SSM. The development of the SSM is presented in Chapter 3; this study led to a publication (see section personal publications). Also in Figure 2.6, further developments remain shaded, and they are presented in the next sections.

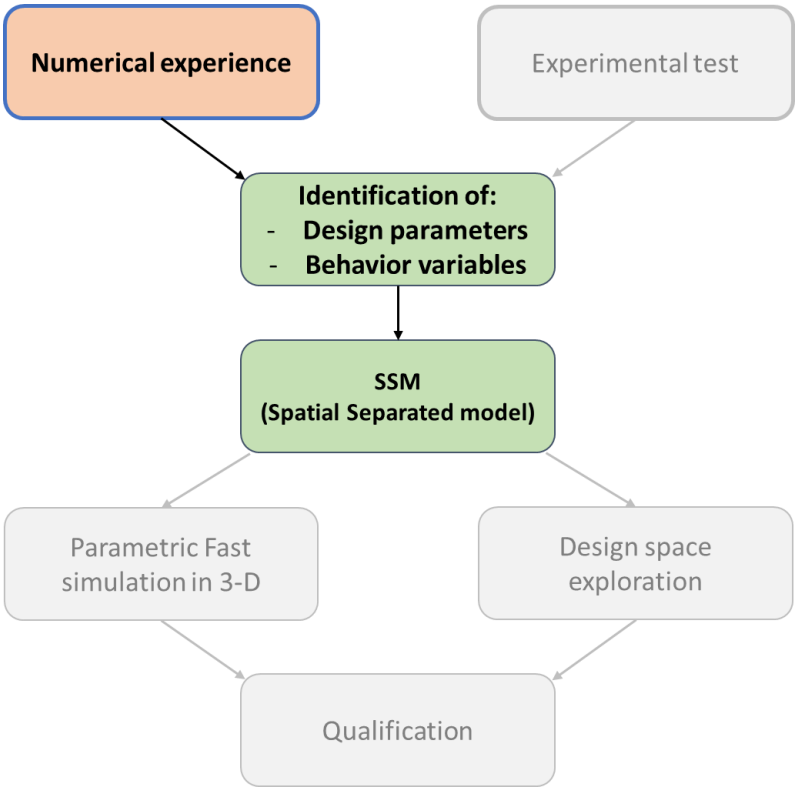

Figure 2.6 First development approach, further developments are shaded

2.3 Multiphysical consideration of composite structures

So far, our SSM considers only materials responding to linear elastic behavior in a multiscale and separated approach. Moreover, our SSM may become multi-physical incorporating different specificities and behavioral characteristics as a response to a dynamic load. The behavior of the plies remains elastic, while the interfaces generate vibration damping.

Contrary to elasticity where vibration energy is stored, damping is a mechanism of energy dissipation. We consider the dissipation of energy occurs at the interfaces between plies, caused by the internal friction developed at small scales due to inclusions, pores, delamination or crystallization of the matrix conforming these interfaces. When a structure develops internal friction, there is a tendency to find new equilibrium positions. In this case, the dynamic

characteristic of stress may be modeled by a fading memory approach which depends on the strain rate. This phenomenon is known as viscoelasticity, a rheological behavior of materials known as anelastic deformation. Figure 2.7 shows samples of flaws in the interfaces between plies on a carbon fiber laminated composite, causing the internal friction. These pictures are taken using SEM microscopy; the samples were previously subject to gold sputter deposition.

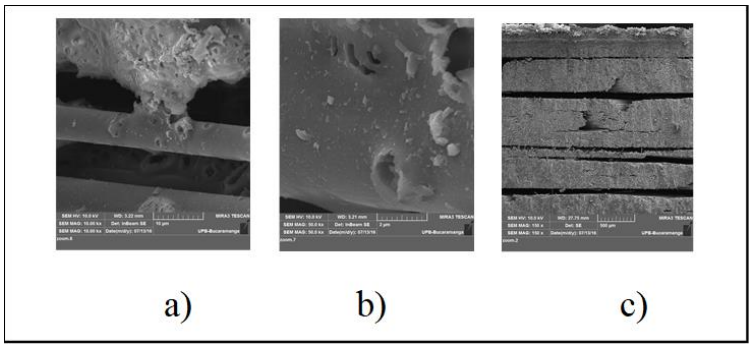

Figure 2.7 Flaws in a carbon fiber laminated composite sample. a) Poor adhesion. b) inclusions and pores. c) Debonding. (SEM microscopy conducted at UPB – Bucaramanga – Colombia)

2.3.1 Justification of creeping in a composite structure

We conducted a dynamic experiment on a carbon fiber laminated composite structure, which is described in detail section 4.2. In that experiment, away from the resonance frequencies, we found a recurrent phase lag between the force excitation and the vibration response of the laminated structure under test. This phase lag is characteristic of the viscoelastic behavior and a preliminary result is presented in Figure 2.8. Agreeing with the state of the art, we modeled the viscoelastic behavior in the interfaces because it is composed principally by the matrix. Thus, the matrix is responsible for the relative shear displacement between plies.

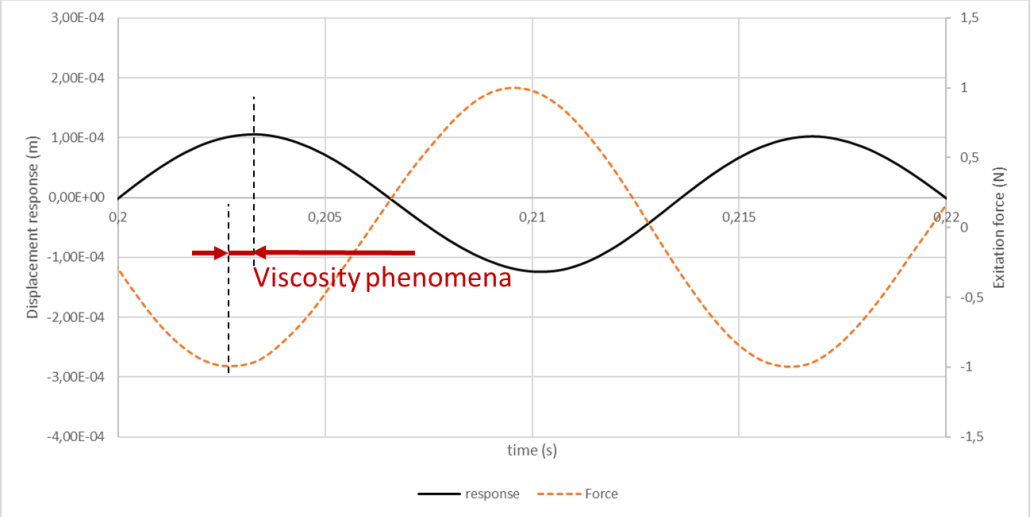

Figure 2.8 Justification of viscoelastic response

2.3.2 Our multiphysical approach

Our second objective is making our SSM able to model the response of a laminated composite beam under dynamic load. The difficulty resides in having a model allowing fast simulations. Therefore the model needs to be reduced, but also separated and multiphysical, because it considers pure elastic response within the plies while a viscoelastic behavior is tied to the interfaces. Our SSM is now named a Parametric and Reduced Base Model (PRBM).

Definition: **Parametric and Reduced Behavior Model (PRBM)**

The PRBM is a multiscale and parametrized model based simulation allowing the user to have:

1. A macro-information detailing the global behavior of the composite structure under dynamic load
2. A layer-by-layer behavior representation
3. Information about the viscoelastic behavior of interfaces between the plies.

Problematic 2

> Having explicit design parameters in a composite structure from the SSM, we now incorporate a viscoelastic behavior separately in the interfaces between plies.
>
> A simulation model named the Parametric and Reduced Base Model (PRBM) is developed.

Figure 2.9 shows the second development approach, incorporating new design parameters and behavior variables to develop the new PRBM. These new capabilities are based on data gathered from a dynamic experimental test on a carbon reinforced laminated structure. The development of the PRBM is detailed in Chapter 3; this study led to a Publication (see section personal publications). Also in Figure 2.9, further developments remain shaded and they are presented in the next sections.

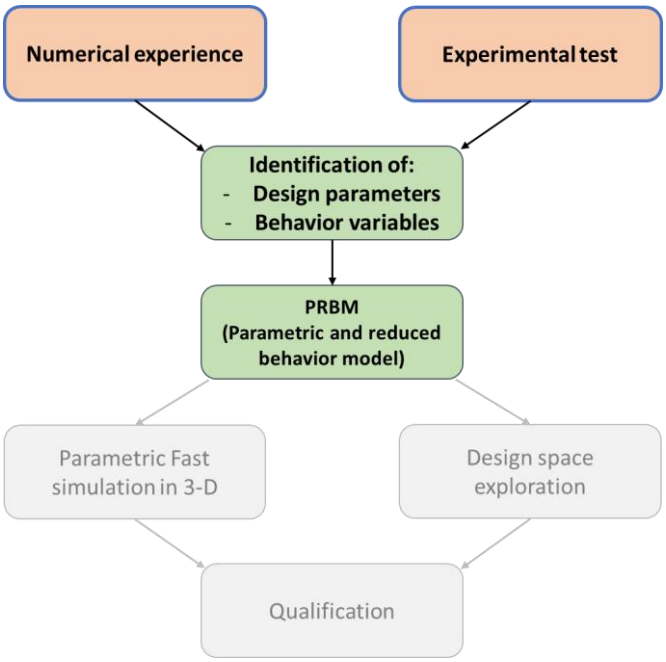

Figure 2.9 Second development approach, further developments are shaded

2.4 A new model to support decision making during the design of composite structures

Usual CAE systems (CAD, Finite Element Simulation) do not offer any solution that could allow the exploration of solution spaces interactively by manipulating specific design parameters that are handled usually during manufacturing. This limitation leads engineers to have a separate and multiscale view of the composite structure:

- At the level of the structure; where the number of layers determines the stiffness of the structure.
- At the level of the layer, where the engineer has to separately consider the ply because the orientation of fibers can lead to different behavior.
- At the level of the interface, having consequences during a dynamic behavior due to the viscosity property of the matrix.
- At the level of the fiber, because the fiber properties lead the engineer to decide on the fiber material and the volume rate of fibers in each ply.

2.4.1 Fast simulation for design choices validation

The mismatch in material properties represents a significant difficulty when performing design optimization of laminated composites. Typically, in FEM analyses, the simulations are simplified, homogenizing the details at the ply level to keep the computational time and cost affordable, but that analysis must remain at the macroscale level, missing localized details at lower scales.

We also want to use our PRBM as a fast solver on a standard design process of a composite structure, in this case, the PRBM is used during the dimensioning phase[4] as shown in Figure 2.10. By this way, interactively, a designer may quickly perform virtual tests with acceptable combinations of design

[4] The design phases are described in section 1.8.1, based on the definition by Pahl [54]

parameters in a multiscale point of view: a number of plies, type of ply, ply orientation or interface behavior.

Therefore, we aim to develop a parametric model, reduced, multiscale and multiphysical; this is a PRBM, producing fast 3D dynamic simulations of a composite structure plaque, for further validation of an optimized solution.

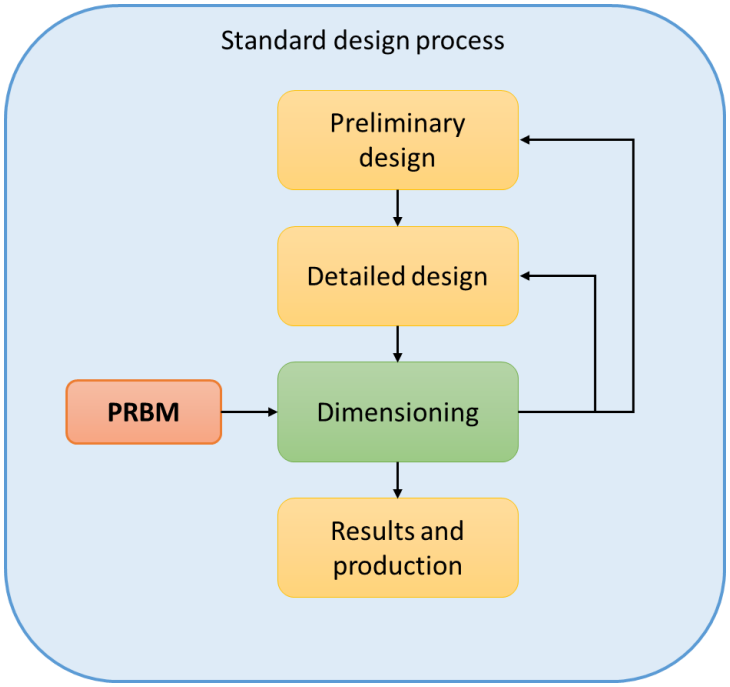

Figure 2.10 Standard design process using the PRBM

Figure 2.11 represents the third development approach, we incorporate in our PRBM parameters that usually are not handled in the simulation but during manufacturing. This development is detailed in Chapter 5; the study led to a publication (see section personal publications). Also in Figure 2.11, further developments remain shaded, and they are presented in the next sections.

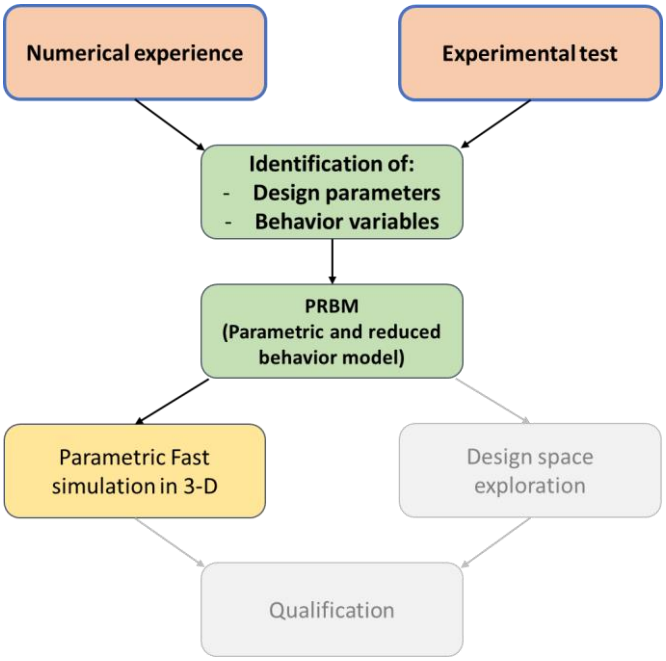

Figure 2.11 Third development approach

2.4.2 Interactive exploration of design solution spaces from the PRBM

We have demonstrated that the limitations of the FEM diminish the capacity of exploration and optimization over improved stacking sequences, imposed conditions or uncertainties at lower scales, so virtual testing is also limited, and therefore a designer needs to overestimate security factors and perform expensive experimental validations. Indeed, standard CAE systems (CAD, Finite Element Simulation) do not offer an approach to explore these solution spaces efficiently and interactively.

The design process of laminated composites faces two challenges: the engineer designs the product and its morphology, but also, simultaneously, the material. The number of design solutions can be huge since the solution space is immense.

We propose a specific process in order to support decision making during the design of a laminated composite structure. We implement an inverted design approach that leads to some design solutions from a desired mechanical

behavior. This mechanical behavior is characterized by objectives of displacements, strains and stresses. The exploration of design solution spaces is based on:

1. The PRBM.
2. Specific knowledge models related to the conditions of damage, know-how and specific dynamic behavioral considerations, leading to an original parametric knowledge model.
3. The expression of design objectives already tested in a situation of static and dynamic behavior of the laminated composite structure.

By using an evolutionary optimization approach, we implement a design process that allows the designers to avoid a classical trial and error process, usually implemented in standard industrial practices (Figure 2.12). Moreover, our approach can lead to innovative solutions, being able to provide different characteristics for each ply.

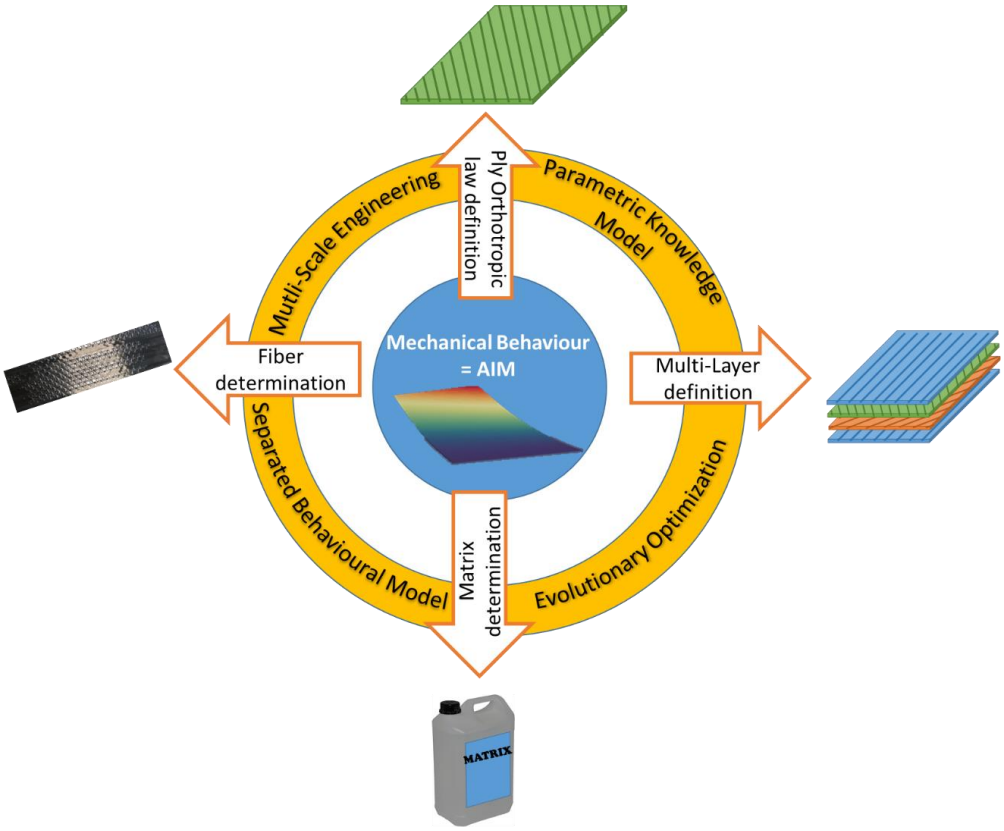

Figure 2.12 Supporting decision making during design of composite laminated structures

2.4.3 Our approach for composite structure design

This section provides a possible procedure for engineers creating a laminated composite product. It presents an approach that allows combining specific variables to usual morphological design parameters, typically the domain of composite experts and manufacturing experts. Therefore, a Decision Making Support System (DMSS) is supporting the preliminary design phase directly, using an optimization approach, which is based on an evolutionary algorithm and coupled to a PRBM (Figure 2.13).

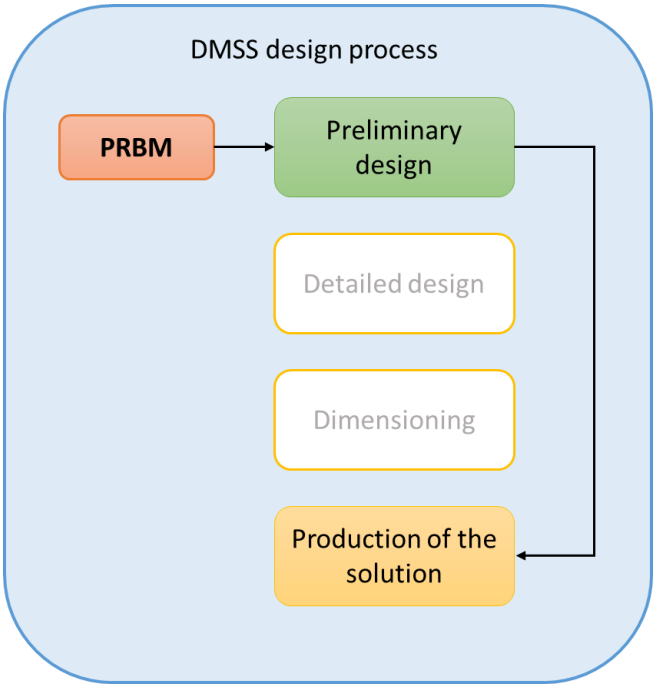

Figure 2.13 DMSS supported on a PRBM

The numeric approach proposed allows the engineer to explore design spaces:

- From a mechanical behavior objective.
- From a new parametric and reduced model that renders explicit parameters and variables commonly used by composite experts.

- From a separated model that enables reasoning based on a multiscale approach, where the engineer can implement reasoning either at the scale of the fiber, or the ply, the interfaces, the lamination or at the scale of the structure. Also a multiphysical approach, where the engineer can independently manage the mechanical effect of each ply and each interface, either in static or dynamic cases; in the latter, the creeping behavior can be considered.

Problematic 3

> We aim to use a Knowledge Model, supporting the decision making during the preliminary design phase of a composite structure. A genetic algorithm generates the computation of the fitness of every candidate solution, and it is evolved towards an optimum, while the computational cost remains reasonable despite the costly 3D simulations.

Figure 2.14 represents the fourth development approach described above, where a genetic algorithm integrates capabilities on design space exploration. The development of this additional integration is detailed in Chapter 5; the study led to a publication (see section personal publications). In the same figure, the final qualification remains shaded, and it is presented in the next section.

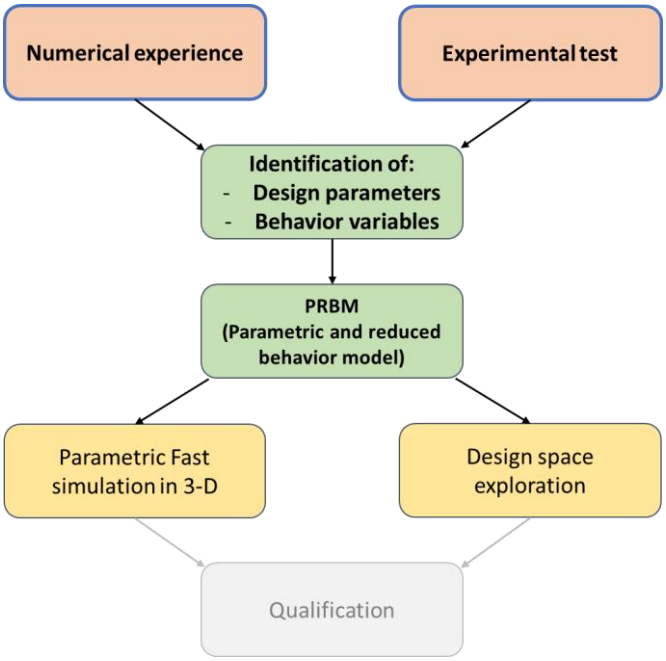

Figure 2.14 Fourth development approach

2.5 Qualification

In the last section, we proposed a design space exploration model; as a result in section Chapter 5, we obtain an optimized plaque, both under a case of static load and also under dynamic load. The final aim is to qualify our model against:

- FEM results in the static case
- Experimental results in the dynamic case

The qualification evaluates parsimony, accuracy, precision, specialization and computing time. This qualification approach is known as PEPS, introduced by Ordaz-Hernández [174] and improved by Cagin [110]. The parsimony is related to the numerical discretization of the equations needed to simulate the problem. The accuracy measures the difference in the result to a given reference. The precision gives a sense of the variance of the results. The specialization describes the degree of specialized knowledge required by the designer to carry out the simulation, and the computing time is the time needed to run the simulation.

Problematic 4

> We aim to qualify the solutions given by our DMSS according to the PEPS approach. The qualification is made against a numerical solution in the static case, and an experimental test in the dynamic case

Figure 2.15 represents the full development integrating qualification.

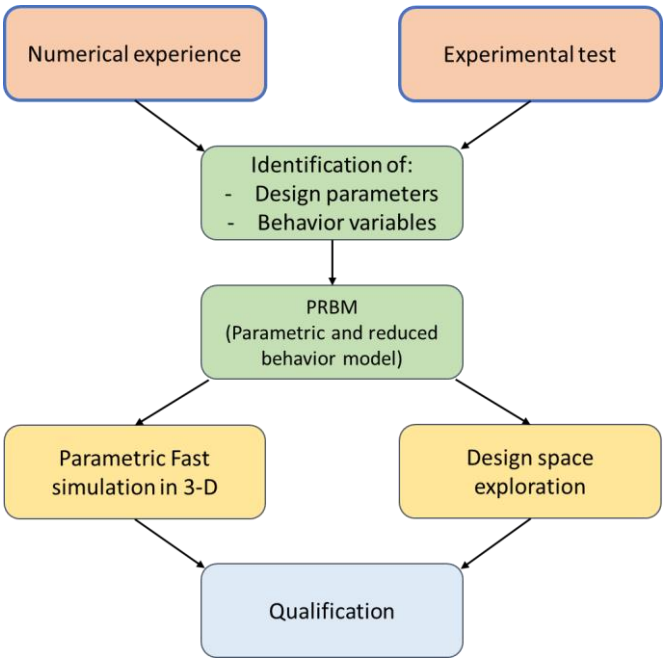

Figure 2.15 The full development

2.6 Conclusion

This chapter makes evident the difficulties and limitations of common CAE tools generally used by engineers to design composite structures. The first case presented is a numerical solution, where immediately our server capacities were overloaded. Then, we used a dynamic experimental test to demonstrate the viscoelastic character of the composite structure. We failed in our attempt using the FEM to simulate the dynamic behavior including viscoelasticity in the interfaces between plies.

Our approach is encompassed by the development of a PRBM, a reduced model for simulation that makes explicit usual and new design parameters and variables. The objective is to propose a parametric knowledge model linked to the PRBM to generate optimized solutions, computed from an evolutionary algorithm. We also aim at qualifying the optimized composite structures both, by a FEM model and by a dynamic experimental test.

In the following chapter, we start our development by the presentation of the case of a laminated composite under static load.

(This page is intentionally left blank)

Chapter 3

PARAMETRIZATION OF A MODEL: THE PRBM TO SIMULATE THE BEHAVIOR OF A COMPOSITE STRUCTURE UNDER STATIC LOAD

The work described in this chapter has been admitted for publication in the international journal Applied Composite Materials. (See section personal publications).

3.1 Introduction

This chapter presents a new model allowing a laminated composite structure to be simulated with low computational cost. The model is an alternative to full 3D simulations.

In order to tackle the problem of computing time, the model is based on three main specifications:

1. It is parametrized and multi-scale, making explicit the main elements being handled during the design of the composite laminated structure. The parametrization is independent for each layer and ply interfaces.
2. It is reduced, the size of the model is light, making it possible to implement a fast simulation.

3. It can be a multiphysical model, regarding the global behavior from each ply and interfaces, having each, different specificities or behavior characteristics.

The numerical method leading to our model is also presented in this chapter.

3.2 Details of the PRBM model

3.2.1 Properties

We aim to provide a model with the properties described in this section.

Property 1: Multiscale model

The model is representing the global behavior of the laminated composite structure by processing:

- The behavior of each layer
- The behavior of the interfaces between plies, therefore the mechanical behavior of the contact between the plies

---

The model is based on the principle of spatial separation. At this stage, we named it the Spatial Separated Model (SSM). The SSM allows to independently compute the different kind of behavior at each layer of the structure (either a ply or interfaces). The simulation is becoming multi-physical and permits the realization of the property 1.

The principle of the SSM is represented in Figure 3.1. This model leads to an approximation of the real displacement field $U(x, y, z, q)$. This function is representing the movement of every element in position (x, y, z) with the different material properties constituting the composite structure. The SSM is represented by the functions $U^j(x, y, z, q)$ describing the displacement field as a function of

the d variables and parameters $q_i \quad i \in \{1, \cdots, d\}$, describing the design of the structure.

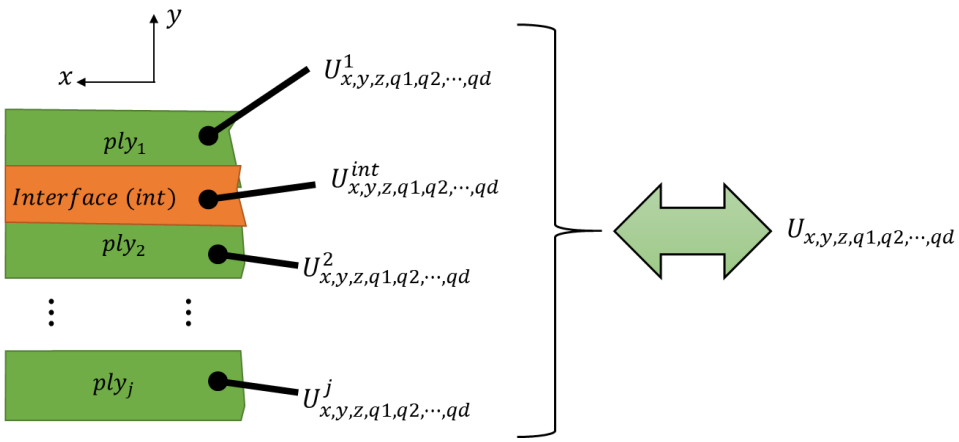

Figure 3.1. The principle of the Spatial Separated Model SSM

Property 2: Parametric model

As a result of the spatial separation, the constitutive laws and their parameters are explicit within the model. All design parameters referring to the stiffness of the laminated composite structure are explicit, regardless of the scale of application.

In the SSM, the design parameters of the composite laminated structure appear; for this reason, we characterize the SSM as being also a parametrized behavior model, as represented in Figure 3.2. This model is useful to implement fast simulations even when the design of the structure is changing.

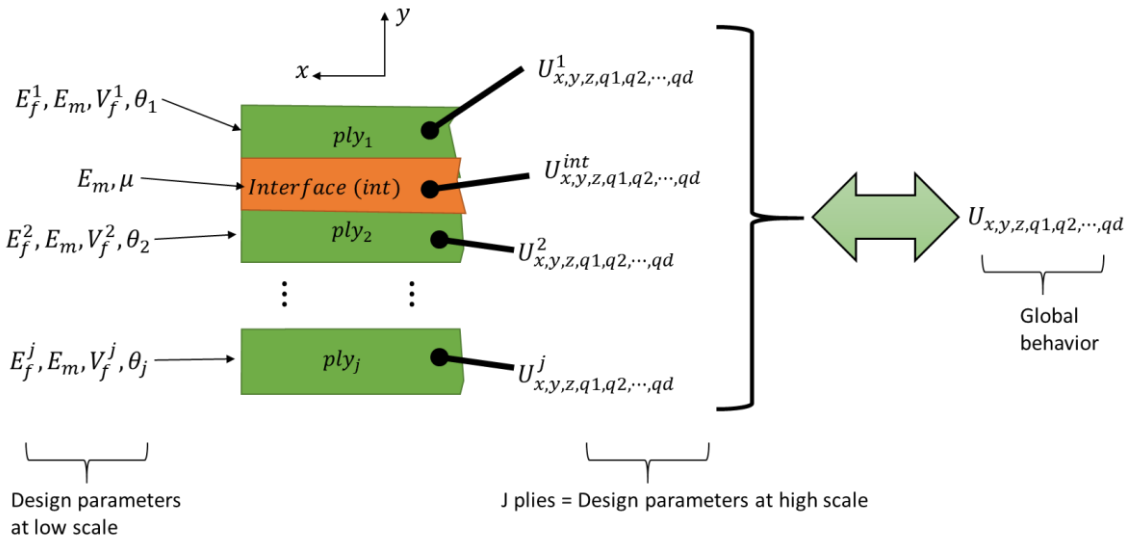

Figure 3.2. Parametrization of the SSM model

Property 3: Reduced model

In order to build the SSM, we use the Proper Generalized Decomposition (PGD) method. The advantage of the resulting model is that it is reduced, allowing a particular simulation to run fast.

The Spatial Separated Model (SSM) is presenting the advantage to consider the behavior of each layer of the laminated composite structure. So, the global behavior of the structure is coming from (Figure 3.3):

- The mechanical behavior of each ply that is dependent on the constitutive laws of the design of the ply.
- The mechanical behavior of the interfaces between plies, where shearing is occurring.

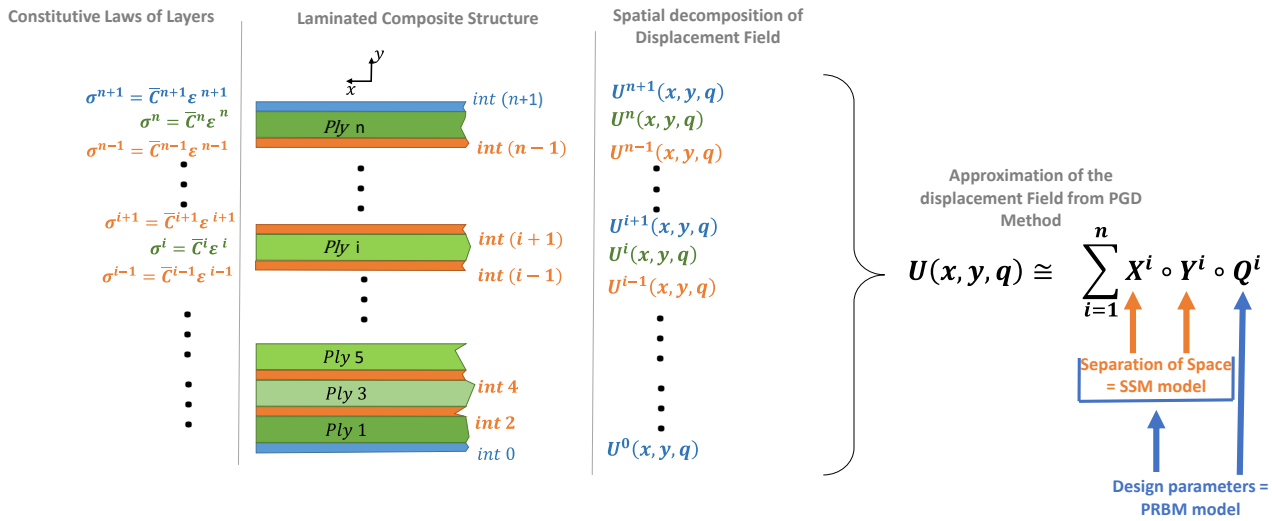

Figure 3.3 Principle of the PGD method towards the SSM and the PRBM models

We used the Proper Generalized Decomposition (PGD) method, leading to a reduced model. The resulting SSM is reduced because the displacement field is no longer computed from tensor operations relating stresses and strains. Instead, the displacement field is reconstructed by adding simple Kronecker products of the basis functions at each enrichment mode n as shown in equation 3.2. The sum of all the n PGD modes allows the displacement field to be approximated.

Property 4: Multiphysical model

The SSM considers the behavior at the level of the interfaces between plies. This property makes the elastic contact assumed by the matrix to be computed efficiently.

Making possible a layer by layer analysis allows highlighting the behavior of the interfaces between plies that produce a zig-zag effect altogether. This effect was analytically demonstrated by Pagano [175] in an analytical full 3D approach. It consisted of a 2D-3D point of view, and it was analyzed by Carrera [5] and [176]. He aimed to create finite shell elements and was able to represent

this phenomenon saving computational cost. However, a selection of an appropriate function through the thickness has to be done by the designer before the simulation. Instead, our PRPM runs 3D simulations able to handle the zig-zag discontinuities caused by the mismatch of material properties.

3.2.2 Definition of the PRBM

The stiffness of the structure depends on the design choices being realized at the 1D, 2D and 3D levels. In order to allow an engineer to have such an approach, we propose the following process:

1. To make explicit required design parameters and variables describing a composite structure at each level or dimension of the laminated structure (1D, 2D, and 3D). For this reason, we developed a Separated Spatial Model (SSM).
2. To rapidly process the SSM, it is based on the Proper Generalized Decomposition (PGD), so the model has a reduced form. The reduced model is an approximation of the real displacement field, and it enables the multiscale analysis of the design problem.
3. To make the SSM being multiphysical, it also leads to a separate representation of the mechanical behavior. The representation of the behavior can be provided at the level of:
   - Each ply being dependent on its orthotropic constitutive law,
   - The interfaces between plies, where the matrix itself has a specific role, mainly during dynamic behavior where creeping is evident.

By this way, the SSM turns into the PRBM. This new model integrates a knowledge model as shown in Figure 3.4, having design parameters as input and behavior variables, ply properties and ply orientation as output.

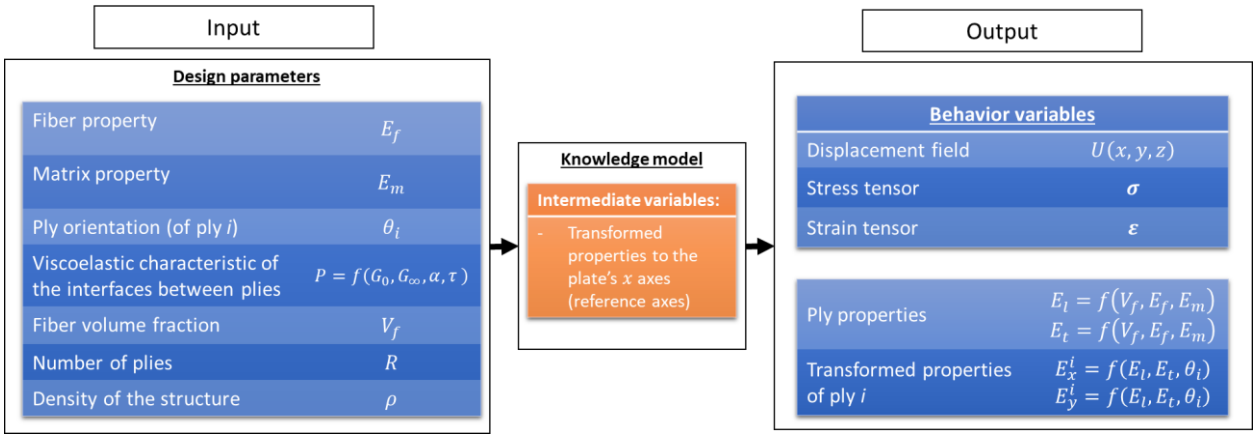

Figure 3.4 Design parameters processing. (The sub-indexes f and m refer for fiber and matrix)

3.3 Details and principles of the PGD method

For simplicity in the presentation of equations, 2D plane strain is assumed in a given structure, so that the displacement field U may be approximated as in equation 3.1,

$$U(x,y) \cong U^n(x,y) \tag{3.1}$$

$$U^n(x,y) = \sum_{i=1}^{n} X^i \circ Y^i \tag{3.2}$$

$$U^n(x,y) = \sum_{i=1}^{n} \begin{Bmatrix} X_{\mathrm{u}}^i \cdot Y_{\mathrm{u}}^i \\ X_{\mathrm{v}}^i \cdot Y_{\mathrm{v}}^i \end{Bmatrix} \tag{3.3}$$

Where X represent basis functions along the in-plane domain x, and Y represent basis functions along the thickness domain y. The symbol " $\circ$ " in equation 3.2 represents the Hadamard product in a vector space, so the products are performed in each direction u and v as shown in equation 3.3.

At this point, the application of the alternative direction strategy begins at an initial condition of $(n-1)$ modes already known, so the next mode n is obtained by iteration so that in iteration p it is possible to compute the 1D $\begin{Bmatrix} X_{\mathrm{u}}^p \\ X_{\mathrm{v}}^p \end{Bmatrix}$

vector space from a random guess of basis functions in the 1D $\begin{Bmatrix} Y_{\mathrm{u}}^{p-1} \\ Y_{\mathrm{v}}^{p-1} \end{Bmatrix}$ vector space in the previous iteration $(p-1)$ as shown in equation 3.4

$$U_{(x,y)}^{n-1,p} = \left(\sum_{i=1}^{n-1} X^i \circ Y^i \right) + X^p \circ Y^{p-1} \qquad 3.4$$

The strain tensor $\boldsymbol{\varepsilon}(U)$ becomes in the form of equation 3.5 and the test function $\varepsilon(U^*)$ in the form of equation 3.6

$$\boldsymbol{\varepsilon}(n-1,p) = \left(\sum_{i=1}^{n-1} \begin{Bmatrix} \dfrac{dX_{\mathrm{u}}^i}{dx} \cdot Y_{\mathrm{u}}^i \\ X_{\mathrm{v}}^i \cdot \dfrac{dY_{\mathrm{v}}^i}{dy} \\ X_{\mathrm{u}}^i \cdot \dfrac{dY_{\mathrm{u}}^i}{dy} + \dfrac{dX_{\mathrm{v}}^i}{dx} \cdot Y_{\mathrm{v}}^i \end{Bmatrix} \right) + \begin{Bmatrix} \dfrac{dX_{\mathrm{u}}^p}{dx} \cdot Y_{\mathrm{u}}^{p-1} \\ X_{\mathrm{v}}^p \cdot \dfrac{dY_{\mathrm{v}}^{p-1}}{dy} \\ X_{\mathrm{u}}^p \cdot \dfrac{dY_{\mathrm{u}}^{p-1}}{dy} + \dfrac{dX_{\mathrm{v}}^p}{dx} \cdot Y_{\mathrm{v}}^{p-1} \end{Bmatrix} \qquad 3.5$$

$$\boldsymbol{\varepsilon}^*(p-1) = \begin{Bmatrix} \dfrac{dX_{\mathrm{u}}^*}{dx} \cdot Y_u^{p-1} \\ X_{\mathrm{v}}^* \cdot \dfrac{dY_{\mathrm{v}}^{p-1}}{dy} \\ X_{\mathrm{u}}^* \cdot \dfrac{dY_{\mathrm{u}}^{p-1}}{dy} + \dfrac{dX_{\mathrm{v}}^*}{dx} \cdot Y_{\mathrm{v}}^{p-1} \end{Bmatrix} \qquad 3.6$$

Then, from the just computed basis functions $\begin{Bmatrix} X_{\mathrm{u}}^p \\ X_{\mathrm{v}}^p \end{Bmatrix}$, it is possible to obtain the basis functions $\begin{Bmatrix} Y_{\mathrm{u}}^p \\ Y_{\mathrm{v}}^p \end{Bmatrix}$ in iteration p from equation 3.7

$$U_{(x,y)}^{n-1,p} = \left(\sum_{i=1}^{n-1} X^i \circ Y^i \right) + X^p \circ Y^p \qquad 3.7$$

Moreover, the test function becomes now equation 3.8

$$\boldsymbol{\varepsilon}^*(p-1) = \begin{Bmatrix} \frac{dX_{\mathrm{u}}^p}{dx} \cdot Y_u^* \\ X_{\mathrm{v}}^p \cdot \frac{dY_{\mathrm{v}}^*}{dy} \\ X_{\mathrm{u}}^p \cdot \frac{dY_{\mathrm{u}}^*}{dy} + \frac{dX_{\mathrm{v}}^p}{dx} \cdot Y_{\mathrm{v}}^* \end{Bmatrix} \qquad 3.8$$

Within the computation of each mode, the iteration process stops when the norm ϵ_p (equation 3.9) of the difference between the obtained mode at iteration p and the last incorporated mode $(n-1)$ is small.

$$\epsilon_p = \frac{\int_\Omega \left((X^p \circ Y^p) - (X^{n-1} \circ Y^{n-1})\right)^2 \cdot dx \cdot dy}{\int_\Omega (X^p \circ Y^p)^2 \cdot dx \cdot dy} \qquad 3.9$$

Further, the approximated solution $U^n(x,y)$ is achieved when the sum of all modes results in a sufficiently small residual ϵ_{res} in equation 3.10

$$\epsilon_{res} = \frac{\int_\Omega \left(div\left(\mathcal{C} \cdot \boldsymbol{\varepsilon}\,(U^n)\right) - B\right)^2 \cdot dx \cdot dy}{\int_\Omega B^2 \cdot dx \cdot dy} \qquad 3.10$$

Similarly, if the displacement field is parametrized by a basis function Q on a domain q, the reduced model is represented by equation 3.11 and equation 3.12,

$$U\,(x,y,q) \cong U^n(x,y,q) \qquad 3.11$$

$$U^n(x,y,q) = \sum_{i=1}^{n} X^i \cdot Y^i \cdot Q^i \qquad 3.12$$

Then, the alternative direction strategy to obtain the solution $U^n(x,y,q)$ becomes,

From a Random guess of $\begin{Bmatrix} Y_{\mathrm{u}}^{p-1} \\ Y_{\mathrm{v}}^{p-1} \end{Bmatrix}$ and $\begin{Bmatrix} Q_{\mathrm{u}}^{p-1} \\ Q_{\mathrm{v}}^{p-1} \end{Bmatrix}$, compute $\begin{Bmatrix} X_{\mathrm{u}}^{p} \\ X_{\mathrm{v}}^{p} \end{Bmatrix}$ by equation 3.13.

$$U_{(x,y,q)}^{n-1,p} = \sum_{i=1}^{n-1} \begin{Bmatrix} X_{\mathrm{u}}^{i} \cdot Y_{\mathrm{u}}^{i} \cdot Q_{\mathrm{u}}^{i} \\ X_{\mathrm{v}}^{i} \cdot Y_{\mathrm{v}}^{i} \cdot Q_{\mathrm{v}}^{i} \end{Bmatrix} + \begin{Bmatrix} X_{\mathrm{u}}^{p} \cdot Y_{\mathrm{u}}^{p-1} \cdot Q_{\mathrm{u}}^{p-1} \\ X_{\mathrm{v}}^{p} \cdot Y_{\mathrm{v}}^{p-1} \cdot Q_{\mathrm{v}}^{p-1} \end{Bmatrix} \qquad 3.13$$

Then, from the just computed $\begin{Bmatrix} X_{\mathrm{u}}^{p} \\ X_{\mathrm{v}}^{p} \end{Bmatrix}$ and the assumed $\begin{Bmatrix} Q_{\mathrm{u}}^{p-1} \\ Q_{\mathrm{v}}^{p-1} \end{Bmatrix}$, obtain $\begin{Bmatrix} Y_{\mathrm{u}}^{p} \\ Y_{\mathrm{v}}^{p} \end{Bmatrix}$

Finally, from the just computed $\begin{Bmatrix} Y_{\mathrm{u}}^{p} \\ Y_{\mathrm{v}}^{p} \end{Bmatrix}$ and the previously computed $\begin{Bmatrix} X_{\mathrm{u}}^{p} \\ X_{\mathrm{v}}^{p} \end{Bmatrix}$, obtain $\begin{Bmatrix} Q_{\mathrm{u}}^{p} \\ Q_{\mathrm{v}}^{p} \end{Bmatrix}$ until an error convergence is reached

3.4 Model separation with PGD

3.4.1 Basis of modeling

The process will be developed in 2D assuming plane strain, in this way it also may be compared to equivalent FEM results. Further, the PGD model will be extended to 3D.

In a lamination similar to the one analyzed in this work, the PGD method finds a solution first at the mesoscale, considering the detail of plies and interphases through the thickness direction and then at the macro scale along the in-plane directions. In the code, each domain x and y must be created separately, each by a 1-D mesh, which at the same time shall be defined in each direction u and v, as shown in equation 3.14 and illustrated in Figure 3.5.

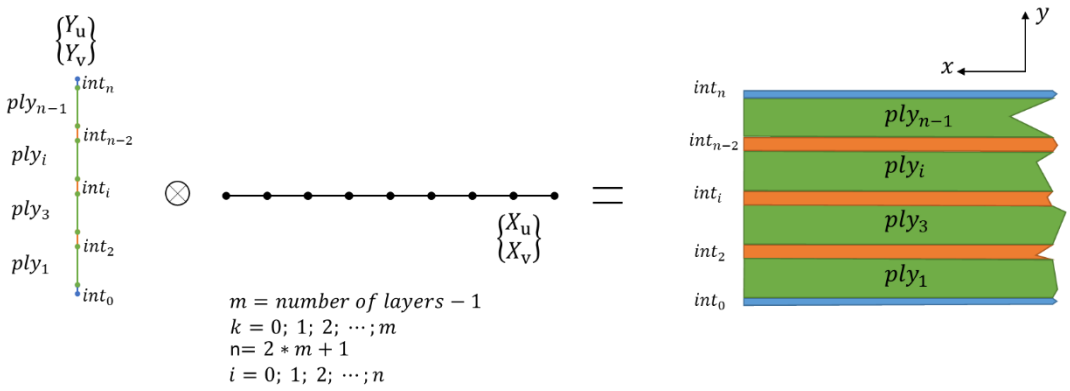

Figure 3.5 Separation of variables in a lamination

Similarly, mechanical properties are assigned separately, first through the thickness direction at the layer scale as a discrete function in domain y (see equation 3.16 and Figure 3.5). Then as a constant function equal to 1 through the x domain (equation 3.15). Consequently, when multiplying, the result we obtain is a 2D function, with constant properties on x and changing properties on y mirroring a laminate composite material.

Only the procedure for the Young's modulus E_{xx} is presented here, the other properties are handled in a similar manner.

$$E_{xx} = E_{xu} \cdot E_{yu} \qquad 3.14$$

$$E_{xu} = 1 \ ; \qquad 3.15$$

$$E_{yu} = \begin{cases} E_{xxn} \ if \ y = subspace_{int2} \\ \vdots \\ E_{xxi} \ \ if \ \ y = subspace_{ply1} \\ \vdots \\ E_{xx0} \ \ if \ \ y = subspace_{int0} \end{cases} \qquad 3.16$$

In this case, from the constitutive equation relating stress to strain for orthotropic materials, we determine the equation 3.17.

$$\boldsymbol{\sigma}_{xx} = J \cdot \left(E_{xx}\boldsymbol{\varepsilon}_{xx}\left(1 - \vartheta_{yz}\vartheta_{zy}\right) + E_{xx}\boldsymbol{\varepsilon}_{yy}\left(\vartheta_{yx} - \vartheta_{zx}\vartheta_{yz}\right)\right)$$

$$\boldsymbol{\sigma}_{yy} = J\left(E_{yy}\boldsymbol{\varepsilon}_{yy}(1 - \vartheta_{xz}\vartheta_{zx}) + E_{xx}\varepsilon_{xx}\left(\vartheta_{yx} - \vartheta_{zx}\vartheta_{yz}\right)\right)$$

$$\boldsymbol{\sigma}_{xy} = G_{xy} \cdot 2\boldsymbol{\varepsilon}_{xy} \qquad 3.17$$

$$J = \frac{1}{1 - \upsilon_{xy}\upsilon_{yx}}$$

Moreover, from the kinetics, we get equation 3.18.

$$\int_{\Omega} \boldsymbol{\sigma}_{xx} \cdot \boldsymbol{\varepsilon}^{*}_{xx} \cdot dx \cdot dy + \int_{\Omega} \boldsymbol{\sigma}_{yy} \cdot \boldsymbol{\varepsilon}^{*}_{yy} \cdot dx \cdot dy + \int_{\Omega} \boldsymbol{\sigma}_{xy} \cdot 2\boldsymbol{\varepsilon}^{*}_{xy} \cdot dx \cdot dy = \int_{\Omega} B \cdot u^{*} \cdot dx \cdot dy + \int_{\Gamma} R \cdot u^{*} \cdot d\Gamma \qquad 3.18$$

Then, incorporating equation 3.5, equation 3.6 and equation 3.17 on equation 3.18, we obtain the equation 3.19.

$$\sigma_{xx} \cdot \varepsilon^{*}_{xx} = J \cdot \left(E_{xx} \left(\left(\sum_{i=1}^{n-1} \left(\frac{dX^{i}_{\mathrm{u}}}{dx} \right) \cdot Y^{i}_{\mathrm{u}} \right) + \left(\frac{dX^{p}_{\mathrm{u}}}{dx} \right) \cdot Y^{p-1}_{\mathrm{u}} \right) \left(1 - \vartheta_{yz}\vartheta_{zy}\right) + E_{xx} \left(\left(\sum_{i=1}^{n-1} X^{i}_{\mathrm{v}} \cdot \left(\frac{dY^{i}_{\mathrm{v}}}{dy} \right) \right) + X^{p}_{\mathrm{v}} \cdot \left(\frac{dY^{p-1}_{\mathrm{v}}}{dy} \right) \right) \left(\vartheta_{yx} - \vartheta_{zx}\vartheta_{yz}\right) \right) \cdot \left(\frac{dX^{*}_{\mathrm{u}}}{dx} \right) \cdot Y^{p-1}_{\mathrm{u}}$$

$$\sigma_{yy} \cdot \varepsilon^{*}_{yy} = J \cdot \left(E_{yy} \left(\left(\sum_{i=1}^{n-1} X^{i}_{\mathrm{v}} \cdot \left(\frac{dY^{i}_{\mathrm{v}}}{dy} \right) \right) + X^{p}_{v} \cdot \left(\frac{dY^{p-1}_{\mathrm{v}}}{dy} \right) \right) \left(1 - \vartheta_{xz}\vartheta_{zx}\right) + E_{xx} \left(\left(\sum_{i=1}^{n-1} \left(\frac{dX^{i}_{\mathrm{u}}}{dx} \right) \cdot Y^{i}_{\mathrm{u}} \right) + \left(\frac{dX^{p}_{\mathrm{u}}}{dx} \right) \cdot Y^{p-1}_{\mathrm{u}} \right) \left(\vartheta_{yx} - \vartheta_{zx}\vartheta_{yz}\right) \right) \cdot X^{*}_{\mathrm{v}} \cdot \left(\frac{dY^{p-1}_{\mathrm{v}}}{dy} \right) \qquad 3.19$$

$$\sigma_{xy} \cdot 2\varepsilon^{*}_{xy} = G_{xy} \left(\left(\sum_{i=1}^{n-1} \left(X^{i}_{\mathrm{u}} \cdot \frac{dY^{i}_{\mathrm{u}}}{dy} + \frac{dX^{i}_{\mathrm{v}}}{dx} \cdot Y^{i}_{\mathrm{v}} \right) \right) + X^{p}_{\mathrm{u}} \cdot \frac{dY^{p-1}_{\mathrm{u}}}{dy} + \frac{dX^{p}_{\mathrm{v}}}{dx} \cdot Y^{p-1}_{\mathrm{v}} \right) \cdot \left(X^{*}_{\mathrm{u}} \cdot \left(\frac{dY^{p-1}_{\mathrm{u}}}{dy} \right) + \left(\frac{dX^{*}_{\mathrm{v}}}{dx} \right) \cdot Y^{p-1}_{\mathrm{v}} \right)$$

Before solving, a final important step is to reorganize equation 3.19, such that the domain x is apart from the domain y and the unknowns remain at the left part of the equation. For simplicity, only the left part is presented in equation 3.20

$$
\begin{aligned}
J \cdot \Bigg\{ \int_{\Omega} & \left(1-\vartheta_{yz}\vartheta_{zy}\right)E_{xx} \cdot \left(\left[\frac{dX_{\mathrm{u}}^{p}}{dx} \cdot \frac{dX_{\mathrm{u}}^{*}}{dx} \right] \cdot dx \times \left[Y_{\mathrm{u}}^{p-1} \cdot Y_{\mathrm{u}}^{p-1} \right] \cdot dy \right) \\
& + \int_{\Omega} \left(\vartheta_{yx}-\vartheta_{zx}\vartheta_{yz}\right)E_{xx} \cdot \left(\left[X_{\mathrm{v}}^{p} \cdot \frac{dX_{\mathrm{u}}^{*}}{dx} \right] \cdot dx \times \left[\frac{dY_{\mathrm{v}}^{p-1}}{dy} \cdot Y_{\mathrm{u}}^{p-1} \right] \cdot dy \right) \Bigg\} \quad \text{from } \boldsymbol{\sigma}_{xx} \cdot \boldsymbol{\varepsilon}_{xx}^{*} \\
& + \int_{\Omega} \left(1-\vartheta_{xz}\vartheta_{zx}\right)E_{yy} \cdot \left(\left[X_{\mathrm{v}}^{p} \cdot X_{\mathrm{v}}^{*} \right] \cdot dx \times \left[\frac{dY_{\mathrm{v}}^{p-1}}{dy} \cdot \frac{dY_{\mathrm{v}}^{p-1}}{dy} \right] \cdot dy \right) \\
& + \int_{\Omega} \left(\vartheta_{yx}-\vartheta_{zx}\vartheta_{yz}\right)E_{xx} \cdot \left(\left[\frac{dX_{\mathrm{u}}^{p}}{dx} \cdot X_{\mathrm{v}}^{*} \right] \cdot dx \times \left[\cdot Y_{u}^{p-1} \cdot \frac{dY_{\mathrm{v}}^{p-1}}{dy} \right] \cdot dy \right) \quad \text{from } \boldsymbol{\sigma}_{yy} \cdot \boldsymbol{\varepsilon}_{yy}^{*} \\
& + \int_{\Omega} \Bigg\{ G_{xy} \left(\left[X_{\mathrm{u}}^{p} \cdot X_{\mathrm{u}}^{*} \right] \cdot dx \times \left[\frac{dY_{\mathrm{u}}^{p-1}}{dy} \cdot \frac{dY_{\mathrm{u}}^{p-1}}{dy} \right] \cdot dy + \left[X_{\mathrm{u}}^{p} \cdot \frac{dX_{\mathrm{v}}^{*}}{dx} \right] \cdot dx \right. \\
& \times \left[\frac{dY_{\mathrm{u}}^{p-1}}{dy} \cdot Y_{\mathrm{v}}^{p-1} \right] \cdot dy + \left[\frac{dX_{\mathrm{v}}^{p}}{dx} \cdot X_{\mathrm{u}}^{*} \right] \cdot dx \times \left[Y_{\mathrm{v}}^{p-1} \cdot \frac{dY_{\mathrm{u}}^{p-1}}{dy} \right] \cdot dy + \left[\frac{dX_{\mathrm{v}}^{p}}{dx} \cdot \frac{dX_{\mathrm{v}}^{*}}{dx} \right] \\
& \left. \cdot dx \times \left[Y_{\mathrm{v}}^{p-1} \cdot Y_{\mathrm{v}}^{p-1} \right] \cdot dy \right) / J \Bigg\} \quad \text{from } \boldsymbol{\sigma}_{xy} \cdot 2\boldsymbol{\varepsilon}_{xy}^{*}
\end{aligned}
\tag{3.20}
$$

3.4.2 Parametrization with PGD

The PGD method allows parametrizing properties by the introduction of an additional domain. We name this additional domain q. In this case, q holds the information about how the mechanical properties defined on domain y will change. Further, it is possible to define an individual change for each ply, interface or group of these by specifying the properties in separated terms. Equation 3.21 shows the case for the Young's modulus, but the same methodology is used for the shear modulus and Poisson's ratio. Figure 3.6 illustrates how an additional dimension is used for the parametrization of properties and the Young's modulus E_{xx} is developed in equations 3.21, 3.22, and 3.23.

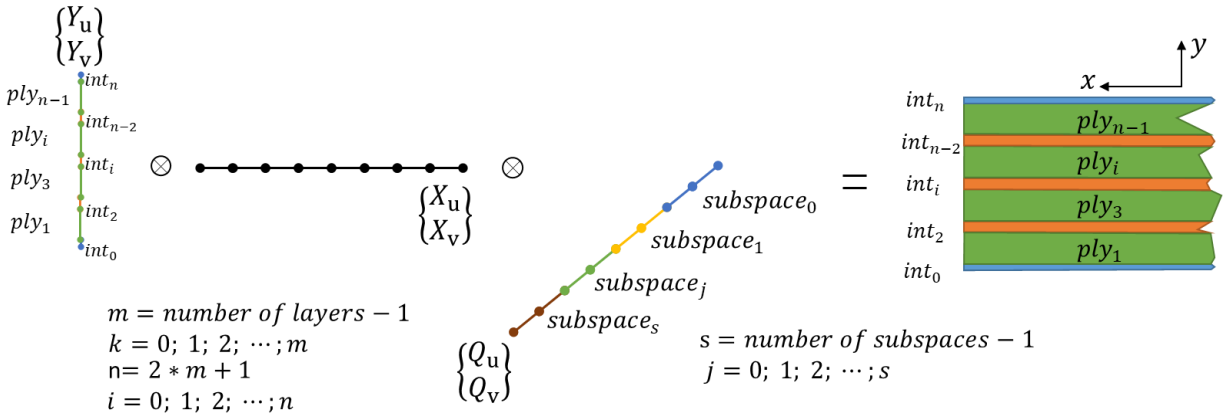

Figure 3.6 Separation of variables in a lamination with a parametrized domain.

$$E_{xx} = E_{xu} \cdot E_{yu0} \cdot E_{qu0} + \cdots + E_{xu} \cdot E_{yui} \cdot E_{qui} + \cdots + E_{xu} \cdot E_{yun} \cdot E_{qun} \quad 3.21$$

$$E_{yui} = \begin{cases} E_{xxi}\ if\ \ y = body_i \\ 0 \quad if\ \ y \neq body_i \end{cases} \quad 3.22$$

$$E_{qui} = \begin{cases} C_n\ if\ q = subspace_n \\ \vdots \\ C_j\ if\ q = subspace_i \\ \vdots \\ C_0\ if\ \ q = subspace_0 \end{cases} \quad 3.23$$

Where the C_j are the changing ratio of the properties, by this manner if $C_j = 1$ the property in y related to the body i will not change along this particular subspace of q; likewise in the case of $C_j = 0{,}5$ the property will have half the original value, moreover if $C_n \ll 1$, the property could be small enough to make a specific ply not to have a significant influence over the overall response. Considering this idea, it is possible to perform a parametrization of the stacking sequence (fiber orientation), type of fiber, fiber volume fraction or even more, the parametrization of the number of plies if the properties of the appropriate plies are made negligible.

The method proposed here introduces discrete functions describing the change of each group of bodies, and all the functions are along the same domain q. If more degrees of freedom are needed, it is also possible to include additional domains but even if linearly, an increase of computing time will be also expected to generate the reduced model.

3.5 Simulation of a laminated composite beam: the usual approach

3.5.1 Details of the case of study

For this work a laminated composite beam is studied, it is restrained at one end and loaded at the other end as shown in Figure 3.7. The beam is considered, having eight unidirectional plies symmetrically stacked as [0/90/90/0/0/90/90/0], the mechanical properties are presented in Table 3-1, and the lamination is represented in Figure 3.8.

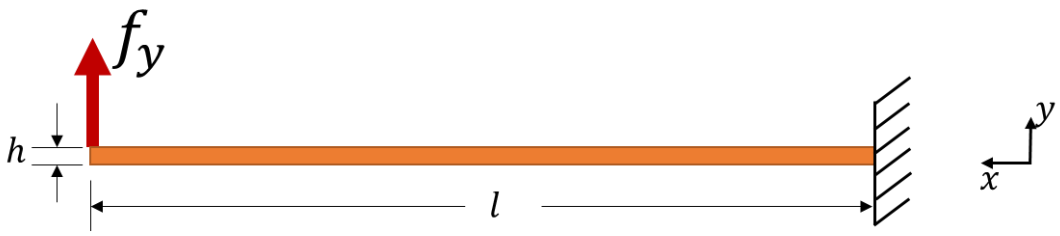

Figure 3.7 Beam under static load.

Table 3-1. Properties of the lamination under study.

Property	Units	Interface (epoxy)	Ply (fibers)	Layer (fibers + epoxy)
Young's module (E_{xx}) (in-plane direction)	GPa	3,5	294	170
Young's module (E_{yy}) (thickness direction)	GPa	3,5	15	15
Poisson's ratio (v_{xy})		0,35	0,24	0,27
Shear modulus G_{xy}	GPa	1,85	4,8	4,8
Layer thickness	mm			0,193
Total thickness for eight layers (h): 1,544 mm				
Length (l): 250 mm				
Stacking sequence: [0, 90, 90, 0, 0, 90, 90, 0]				
Force $f_y = 2{,}5\ N$				

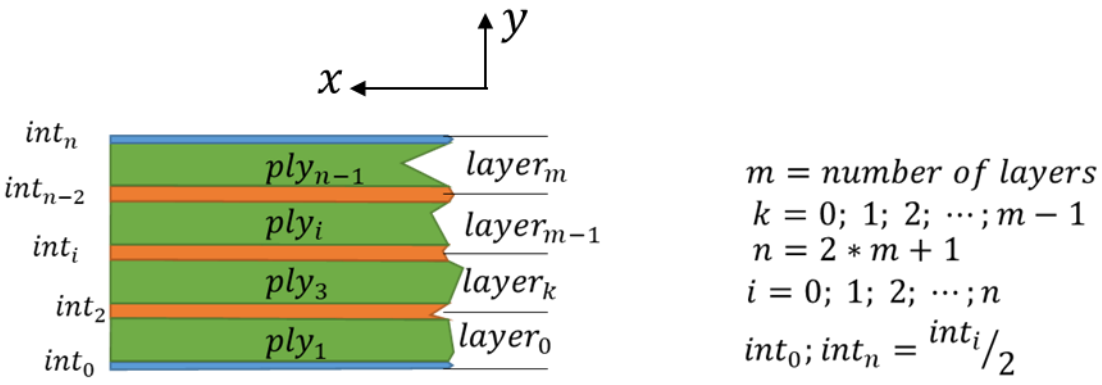

Figure 3.8 Representation of the lamination.

In this chapter, the interest is to analyze the relative displacements occurring within the interfaces between plies.

3.5.2 FEM models

Modeling the details of the mechanics through the thickness direction requires very fine meshes. When FEM is used, the consequence is the high computational cost and time required to obtain a solution. In order to illustrate these consequences, the assessment of four models is presented in Table 3-2, regarding computational cost and computing time.

The most noticeable result in Table 3-2, is the significant amount of maximum allocated memory needed to solve the problems, especially in the 3D case (Model 0). This limitation is generated in the FEM because of the aspect ratio required throughout the mesh. In other terms, it means that none of the faces of a solid element should be significantly larger than the smallest one. As an example, if a full 3D FEM model was run including the details of plies and interfaces, it might require more than 136 million elements, thus more than 3 TB of allocated memory which is not available in our server computing capacity. However, a 3D FEM model (model 0) with fewer elements was executed to account for computing cost and time, but it can only model a single equivalent layer, so no details about the lamination are obtained. Model 1 and model 2 use fewer allocated memory, thus a faster computing time. Further, the details of layers and interfaces are solved in model 3, but all these are 2D models assuming plane strain.

3.5.3 Basis: FEM simulation

The problem running this simulation was that we had only information to configure model 2. As explained in the last section, model 2 was run using FEM in an arrangement of 8 layers stacked as specified in Table 3-1. It allowed to obtain a maximum reference deformation; then this result was used to obtain a single layer orthotropic property in model 1, as well as the thickness of the interfaces between plies on model 3, resulting in the same maximum deformation than model 2. These results are presented in Table 3-3..

.

Table 3-2. Assessment modeling with the FEM.

	Server and software	**FEM Software: Ansys® academic research Distributed parallel processes used at each solution: 16**		
	Description	Mesh representation	Computing cost	
Model 0	Full 3D model, One equivalent single layer Elements through the thickness direction: 10	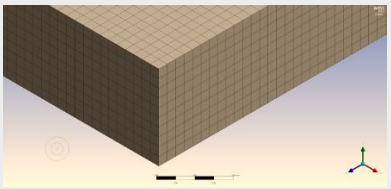	Elements: Nodes: Max allocated memory: Computing time:	2.622.780 2.904.660 23,6 GB 364 sec
Model 1	2D plane strain, One equivalent single layer. Elements through the tickness direction: 40	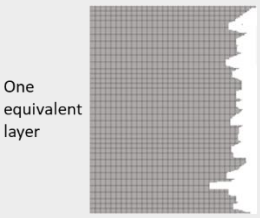	Elements: Nodes: Max allocated memory: Computing time:	256.000 262.000 17,5 GB 30 sec
Model 2	2D plane strain, 8 Layers. Elements through the tickness direction: 40	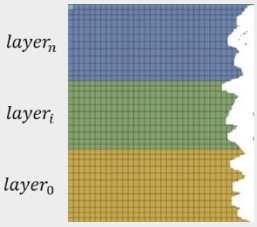	Elements: Nodes: Max allocated memory: Computing time:	256.000 307,248 17,5 GB 70 sec
Model 3	2D plane strain, 8 plies + 9 interphases Elements through the thickness direction: 105	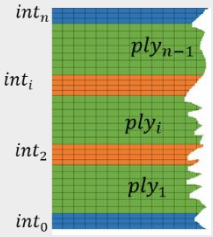	Elements: Nodes: Max allocated memory: Computing time:	840.000 976.122 19,5 GB 269 sec

Table 3-3. Deducting properties for model 1 and model 3

	Model	Properties	Max deformation
Model 1	Single equivalent layer (2D)	$E_{xx} = 108\ GPa$ $E_{yy} = 15\ GPa$ $G_{xy} = 4{,}8\ GPa$ $v_{xy} = 0{,}3$	15,6 mm
Model 2	8 equivalent layers (2D)	As in Table 3-1 , column of layer properties	15,6 mm
Model 3	8 Plies and seven interphases (2D)	As in Table 3-1, column interphase and column ply. Ply thickness = 0,113 mm Interphase thickness = 0,08 mm	15,7 mm

The beams just described were manufactured for a dynamic experimental test, presented in Chapter 4. We used a sample of the beams to measure the thickness of plies and interfaces between plies under SEM microscopy. The sample was previously sent to gold sputter deposition, and the results are presented in Figure 3.9. The measurements made by the microscope are consistent with the results given in Table 3-3. Therefore these values are used in the PRBM.

Under these configurations, Figure 3.10 shows the shear strain ε_{xy} computed for model 1, model 2 and model 3 through the thickness direction in a location 2mm away from the fixed support. Based on the shape of the shear strain curves, we observe that model 2 might have a good agreement with a second order ESL theory, whereas a layer wise behavior is seen in model 2 when 8 equivalent layers are modeled, and a stronger layer wise behavior when plies and interphases are taken into account in model 3. This explains the high

sensitive influence of the interface thickness over the resulting maximum deformation on model 3, presented in Table 3-3.

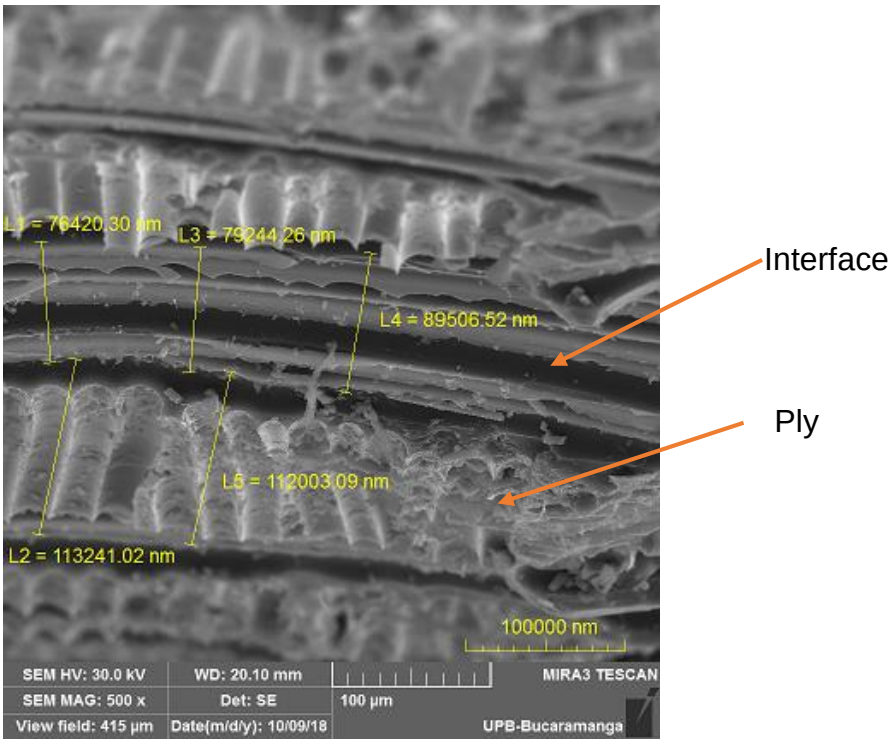

Figure 3.9. SEM microscopy of a sample of the beam under study, showing plies and interface between plies. Measurements are in nm

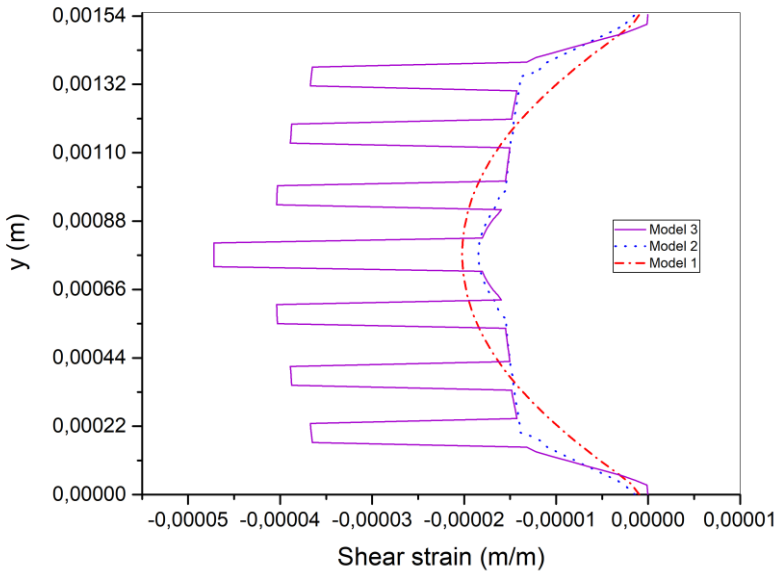

Figure 3.10 Shear strain resulting from different models

Similarly, Table 3-4 shows representations on a broader perspective of the resultant shear strain in the three configuration models presented so far. Particularly in model 3, it is shown the critical role played by the interphases in the mechanical behavior when modeling at lower scales.

Table 3-4. Shear strain computed in FEM for model 1, model 2 and model 3

	Model	Shear strain
Model 1	2D equivalent single layer	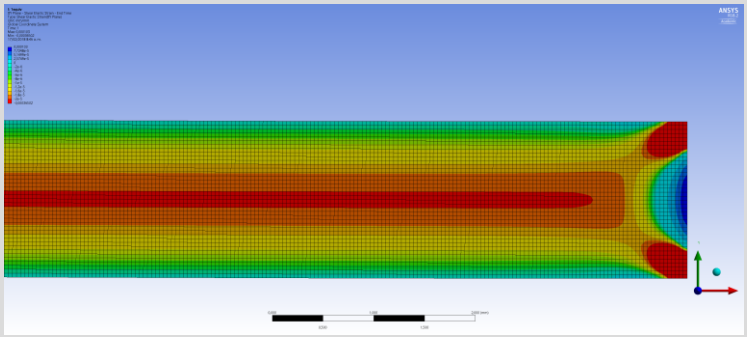
Model 2	2D, 8 layers	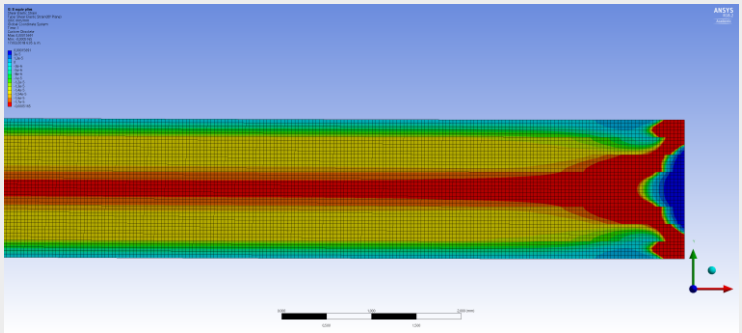
Model 3	2D, 8 plies and interphases	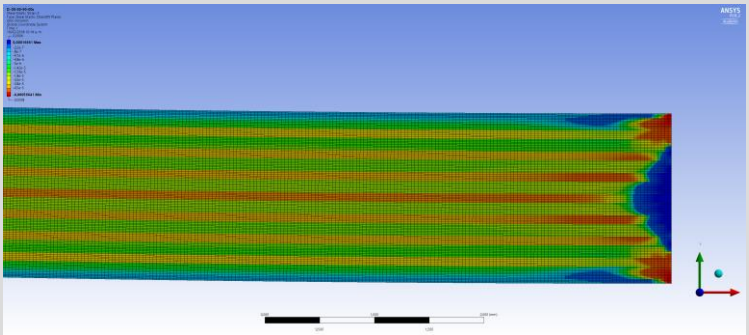

3.6 PRBM Based simulation

In order to develop the PRBM, the PGD method was implemented in a code developed as part of this work, it uses a PGD library made in ESTIA Research and the DOLFIN finite element library, all of these running on Python, on a state of the art laptop.

After converging to a solution, from the 1D solutions, a new solution is mapped in 2D towards the x direction and another one towards the y direction. Finally, in Fenics, the 2D solution may be projected either to separated 2D function spaces or combine them to a 2D vector function space.

Although the PGD method is based on several iterations, it quickly achieves convergence using light computational resources because each domain is 1D. Similarly occurs if the model is extended to 3D, indeed a separation of space variables is carried out onto 1D domains, so the solution is approximated by a sum of functional products called “modes.”

The determination of a mode requires the availability of a previous mode already computed by the iterative method. In order to initialize the process to compute the first mode, we need a previous artificial mode. This artificial mode can be either be:

- Equal to zero,
- A random number, adding numerical noise.

Falco [177] demonstrated that for all mode $(i-1)$, the following mode i is obligatory determined because such elliptic problem always converges. The iteration process requires, for all the problem we considered between 8 and 10 iterations to converge.

3.6.1 Details about the PGD approach

Before obtaining results using the PGD method, the alternative direction strategy requires two criteria to stop the construction of a model: the first is the error ϵ_p indicating when should the iteration stops during the computation of each mode, the second is the residual ϵ_{res} indicating that enough modes have been computed to achieve a convergence. The definition of these two criteria in this work is based on several runs made with different error and residual values. Figure 3.11 (left) shows the resulting deformation and computing time, setting to the same value the error and the residual, and Figure 3.11 (right) shows the same kind of results as a function of the residual, but fixing $\epsilon_p = 1 \times 10^{-15}$. This is how, we decided to use $\epsilon_{res} = 1 \times 10^{-8}$ because the convergence is in good agreement with the FEM results and no further significant improvement is achieved with a smaller residual. This error and residual values generate 10 to 12 modes and the computing time is between 60 and 70 seconds.

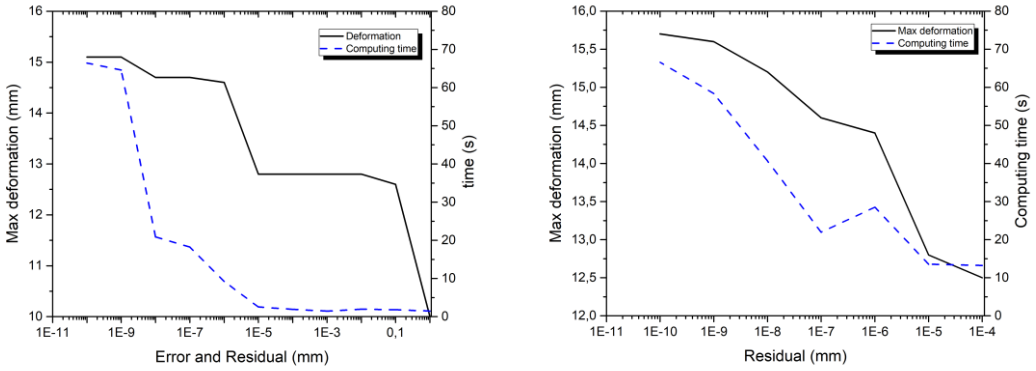

Figure 3.11 Computing time as a function of error (left) and residual (right)

3.6.2 PRBM results in the laminated composite beam

In Figure 3.12, the shear strain ε_{xy} obtained from the FEM model (model 3) is compared to the results using the PRBM at different amount of modes and different amount of elements; it is observed that accuracy is not only a function of the modes, but also sufficient elements are needed at each of the domains. These additional elements generate a little increase of computing time since they

are 1D. Additionally, Figure 3.13 shows also a wider perspective of the shear strain, which agrees quite well with those presented for model 3, Table 3-4.

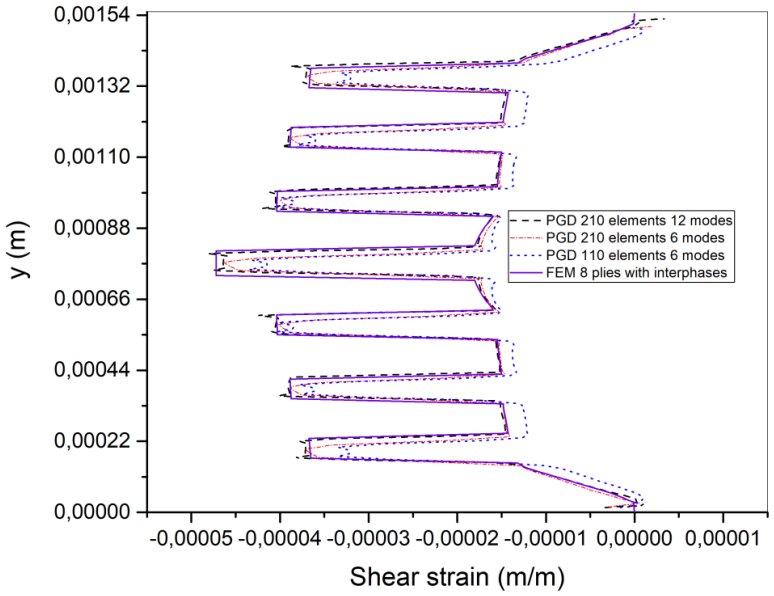

Figure 3.12 FEM vs BRPM model shear strain through the thickness direction for model 3. The curves are taken 2 mm away from the fixed support

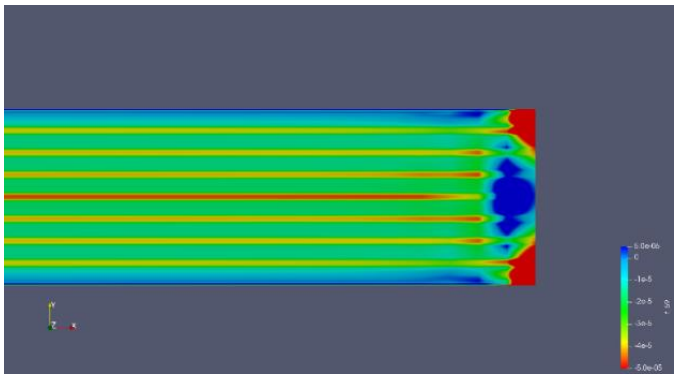

Figure 3.13 Shear strain using the PRBM model that was developed with the PGD method.

Finally, with the same properties and settlement used so far, a PGD simulation 3D was run. In Figure 3.14, the directional deformation in the y direction and the shear strain ε_{xy} are presented. This solution uses 12 modes and takes 151 seconds in a normal laptop to be completed, it was run with 1000

elements in the longitudinal direction, 340 elements through the thickness direction and 50 elements through the depth direction. However, plotting these results in our code requires projecting the PGD solution to Fenics function spaces which would need more than 12 GB in RAM and about 2 minutes of post processing for a mesh for about 170.000 nodes.

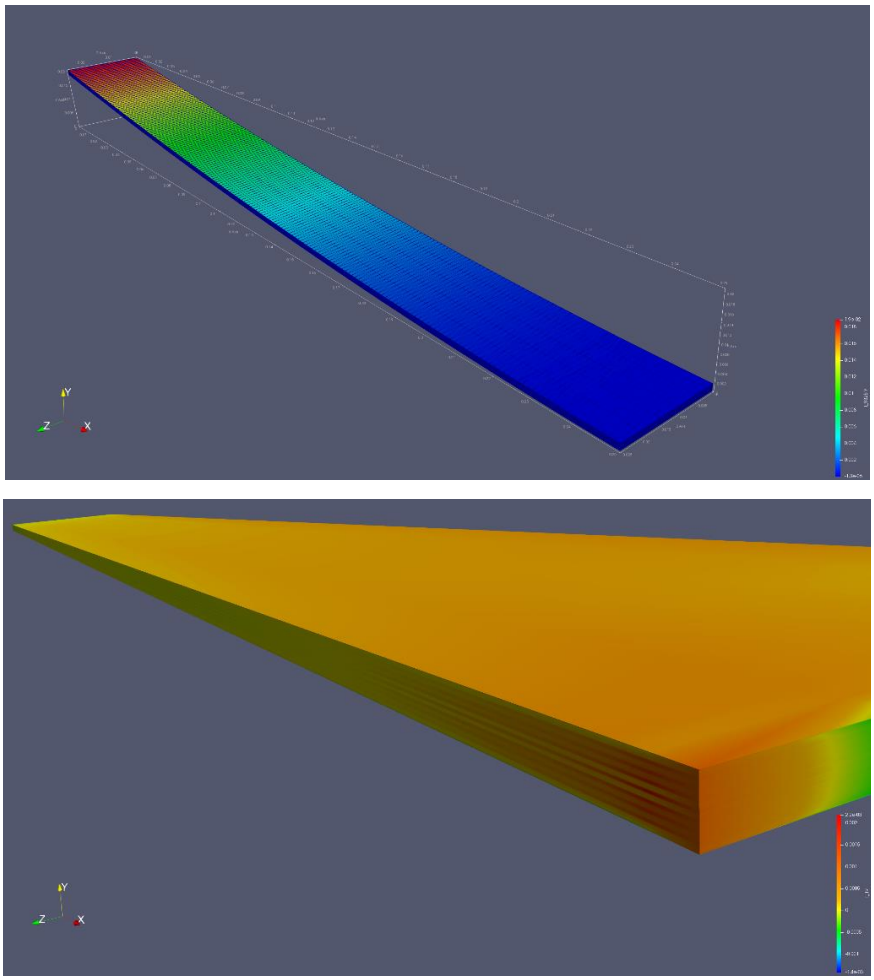

Figure 3.14 PRBM simulation in 3D. Above: Directional deformation y. Below: Shear strain xy

A step further achieved by the use of the PGD method, used to construct our PRBM, is the acceleration of change of scales, so they become more integrated. We explained already how the problem is solved first at the mesoscale, that is, through the thickness direction involving the interactions between layers and interfaces, to quickly obtain a 1D function. Then using the function through the longitudinal direction to compute a solution in the

macroscale; moreover, even if a PGD solution requires and enrichment process which implies iterating this process multiple times, the convergence is reached faster because both, the solution through the thickness direction and the solution through the longitudinal direction are in 1D.

3.6.3 Qualification of the PRBM for static behavior

Using the PGD method, the PRBM is created in about 300 seconds; this new model includes the parametrization of the stacking sequence and the number of layers. Then with the PRBM, fast simulations are computed to get particular solutions with a small error in comparison to equivalent models computed by the FEM. The error increases in the case of 6 layers suggesting that the deformations may be considered already too large. In Table 3-5, some particular results are presented and compared vs. the FEM solution, both regarding maximum deformation and computing time. In this table, it is noticed that each particular solution takes between 270 to 572 seconds to be computed using the FEM with a server, whereas fast test results are obtained from the PRBM.

Table 3-5. Validation of the PRBM Vs. FEM models using some particular results

Description	**FEM**		**PGD**		**Maximum deformation error**
			The time required to obtain the PRBM: 290 sec		
	Machine: Server Distributed processes: 16		Machine: Laptop No distributed processes		
Description	Maximum deformation	**Computing time**	Maximum deformation	**Post-processing time**	
Number of layers:10 Stacking sequence: [90, 00, 90, 90, 00]s*	14,43 mm	**572 sec**	14,54 mm	**11 sec**	0,76%

Table 3 5. (Continuation) Validation of the PRBM Vs. FEM models using some particular results

Number of layers:10 Stacking sequence: [00, 90, 00, 00, 90]s	7,12 mm	**442 sec**	7,13 mm	**11 sec**	0,14%
Number of layers:8 Stacking sequence: [00, 90, 90, 00]s	15,63 mm	**318 sec**	15,68 mm	**9 sec**	0,31%
Number of layers:8 Stacking sequence: [90, 00, 00, 90]s	22,84 mm	**370 sec**	22,72 mm	**9 sec**	0,52%
Number of layers:6 Stacking sequence: [00, 90, 00]s	30,92 mm	**316 sec**	30,71 mm	**6 sec**	0,67%
Number of layers:6 Stacking sequence: [90, 00, 90]s	75,86 mm	**270 sec**	73,48	**6 sec**	3,13%

We can see in the last table that the error is less than 1%, except the case with six layers, because the deformations are significant, it is a weak, thin beam.

3.7 Conclusion

The deterministic nature of the FEM increases the computing time, especially when a discrete sampling of several input conditions of properties is needed in order to obtain a probabilistic distribution interpretation of the results, for example for the application of the Monte Carlo Method. In other words, the FEM accepts only one discrete value for each input variable to produce a unique solution. As a consequence, the capacity of exploration and optimization over improved stacking sequences, imposed conditions or uncertainties at lower scales is diminished, and therefore virtual testing is also limited, making a designer to overestimate security factors and perform expensive experimental validations.

On the other side, we were able to develop a PRBM embedding multiscale information about the laminated structure. The PGD method does not require enormous computation capacities to produce a PRBM, and even less computational resources are needed to perform a simulation at the level of the interfaces between plies.

In the following chapter, a PRBM will be developed to analyze the same beam but under dynamic load, having a viscoelastic behavior in the interfaces.

Chapter 4

MULTIPHYSICAL MODELING: PRBM BASED SIMULATION OF THE DYNAMIC BEHAVIOR OF A LAMINATED COMPOSITE STRUCTURE

The work described in this chapter has been published in the international journal of Multiscale and Multidisciplinary Modeling, Experiments and Design. (See section personal publications)

4.1 Introduction

We aim to model the response of a laminated composite beam under dynamic load, incorporating further developments to the PRBM. The approach is not only separated but also multiphysical, because it is considering pure elastic response within the fibers and a viscoelastic behavior in the interfaces, so that the detailed stress and strain through the thickness direction may be analyzed at different material properties, ply orientation and number of plies.

The PRBM is constructed based on the PGD method; it also includes the parametrization of critical variables, this is the most remarkable and exciting property, because the resulting model requires low computing cost to obtain a

solution within seconds, thus an advantage solving time incremental integration schemes.

4.2 Viscoelastic behavior in a laminated composite structure

4.2.1 Experimental approach

This section studies a laminated composite beam under dynamic load by a dynamic experimental test. The beam is restrained at one end and loaded at the other end as shown in Figure 4.1. The lamination has eight unidirectional plies, symmetrically stacked [0, 90, 90, 0, 0, 90, 90, 0].

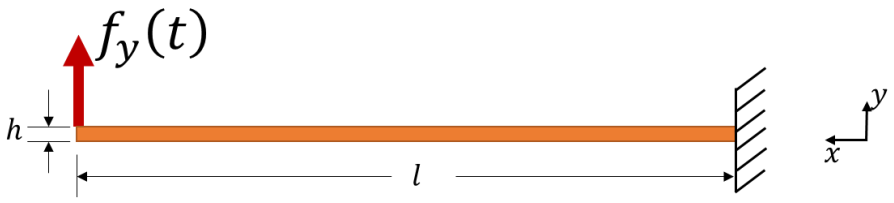

Figure 4.1 Beam under dynamic load

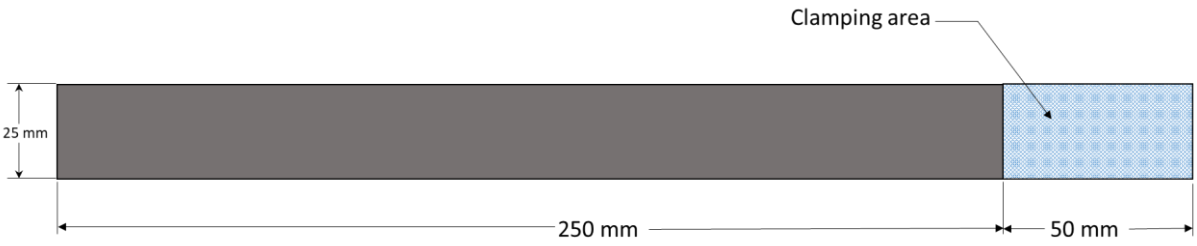

Figure 4.2 Beam dimensions similar to the recommendation of ASTM D3039 [178]

Ten samples of the laminated composite beam were built, all at the same time by Figure 4.2. Each beam is made of eight prepreg unidirectional carbon

fiber layers. The layers are of the type HexPly® M21/34%/UD200/T800S/150mm. Images of the resulting beams are shown in Figure 4.3.



Figure 4.3 Manufacturing the beam. (COMPOSITADOUR – ESTIA)

The test set up follows the recommendation of ISO 18437-3:2005 [179] for the characterization of the dynamic mechanical properties of viscoelastic materials, it is represented in Figure 4.4, and the actual set up is shown in Figure 4.5. The test was carried out at a controlled temperature of 25±2 C. The calibration of all the instrumentation and equipment used is regularly verified in accordance with an ISO 17025 [180] accreditation granted to the lab.

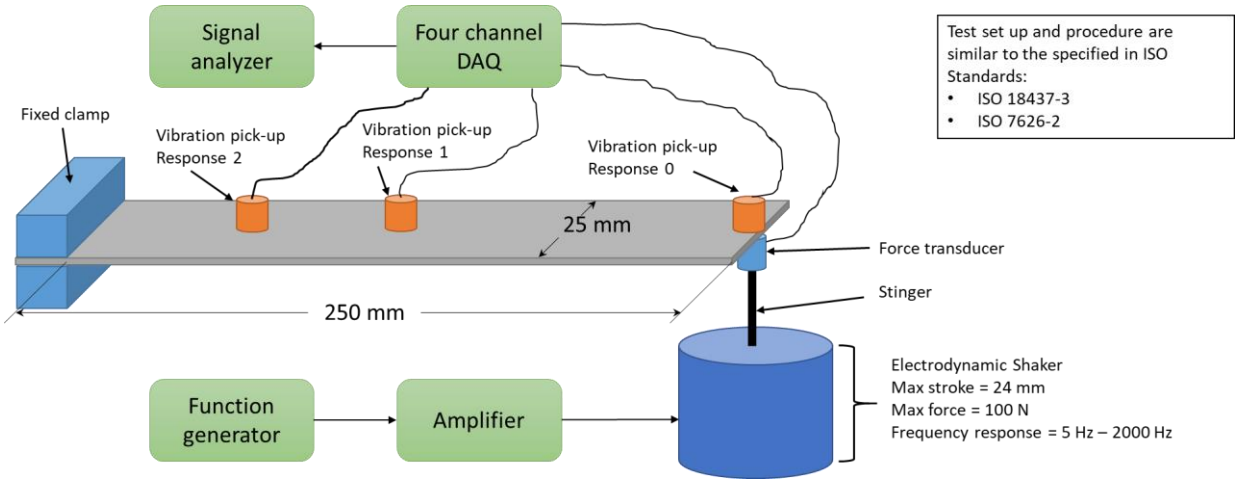

Figure 4.4 Experimental dynamic test set-up

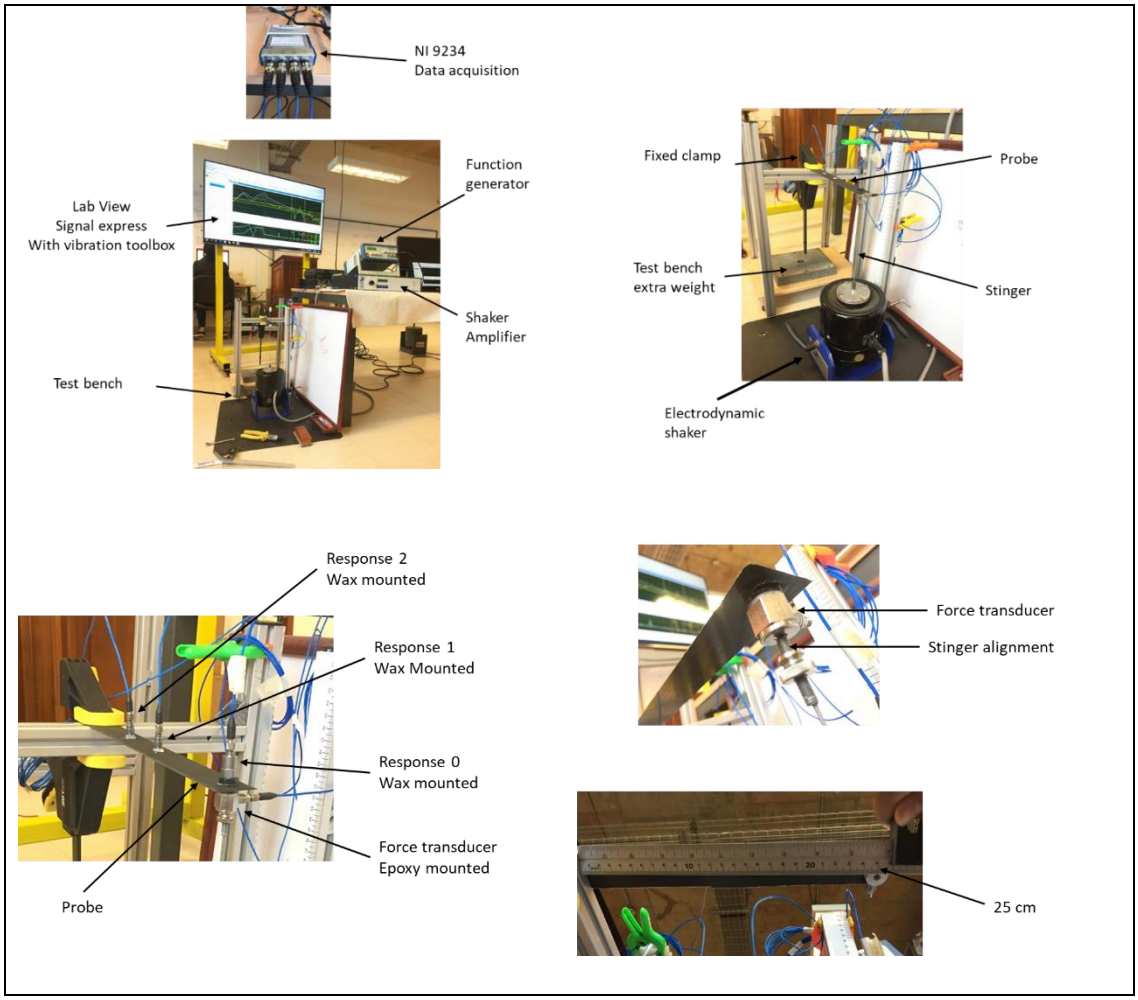

Figure 4.5 Actual dynamic test set-up

We need to choose an excitation frequency away from the natural frequencies so that the phase lag is more likely to be viscoelasticity. Therefore, Frequency Response Functions were measured following the procedure recommended by ISO 7626-2 (1990) [181]. The excitation force was measured with a force transducer PCB 208C01 installed between a shaker stinger and the free end of the bar. Simultaneous responses were captured with a PCB 35C34 accelerometer mounted at the same position of the excitation (drive point measurement) and two other PCB 352C68 located at the beam midpoint and the beam first quarter respectively (transfer point measurements). All the four sensors were aligned carefully to the center of the beams in order to diminish the influence of lateral and torsional modes on the responses, and they are

connected to a simultaneous four-channel data acquisition module NI 9234. Data was gathered using LabVIEW® Signal Express software.

4.2.2 Demonstration of viscoelasticity

After a visual inspection, the five most similar beams were selected to perform the same testing procedure. First, random vibration was induced into the beams, with an approximated constant force of 1 N through a frequency span of 2000 Hz. Three frequency response functions were available for each beam; they were named according to the convention indicated in Table 4-1.

Table 4-1. Convention to the Frequency Response Functions

Point FRF	$\frac{Response\ 0\ (\omega)}{Excitation\ force\ (\omega)}$
Transfer FRF 1	$\frac{Response\ 1\ (\omega)}{Excitation\ force\ (\omega)}$
Transfer FRF 2	$\frac{Response\ 2\ (\omega)}{Excitation\ force\ (\omega)}$

Three mobility FRF at each beam were computed using single integration from the accelerometer signals and applying 50 linear vector averages. The results of every beam were also averaged, and two of the most relevant mobility FRF are plotted in Figure 4.6.

We identified the first source of error in the sensor and wiring by mass interference on the beams; this is why miniature sensors were installed in positions 1 and 2, making the relationship between sensor to beam mass 0,2. Additionally, even if the instrumentation frequency response is good above 5Hz, from the coherence plots in Figure 4.6, it is possible to see some non-linear behavior below 11 Hz, this is a second limitation to the validity of the experimental data. The first resonance peak could cause this nonlinearity and some

compliance in the clamp needed to avoid producing damage in the beams, although still following a positive trend in the magnitude FRF in this first low-frequency zone, meaning a spring-like characteristic typical of cantilever beams.

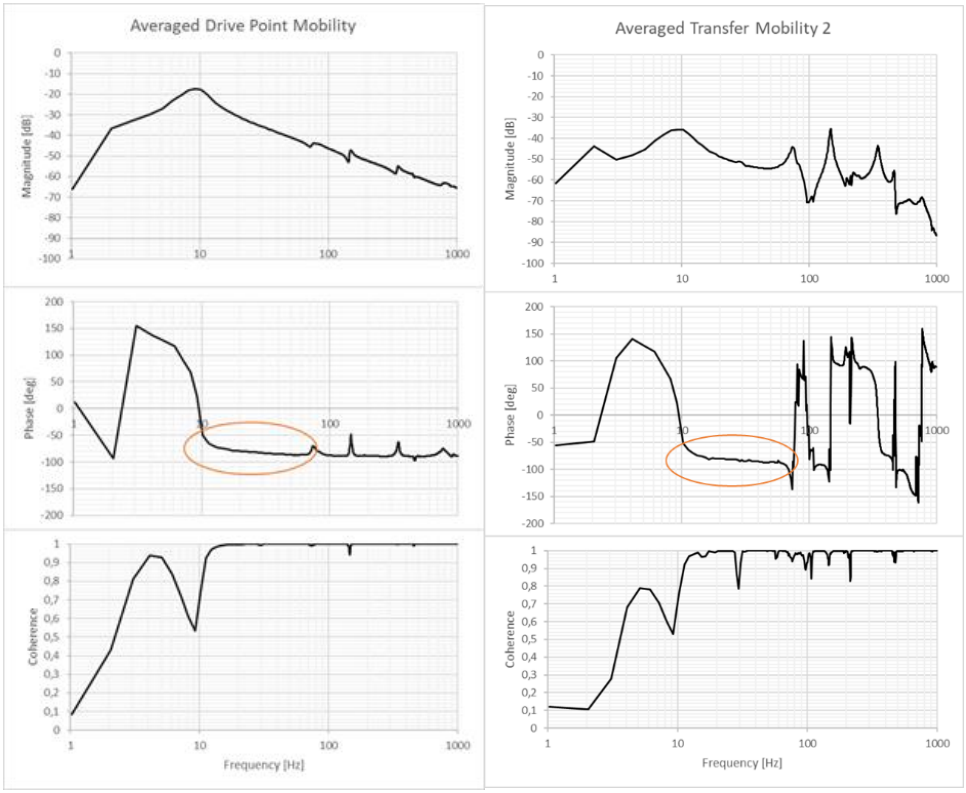

Figure 4.6 Mobility FRF. Left: Drive Point. Right: Transfer 2. Highlighted is the phase lag caused by viscoelasticity

At first glance, the identification of viscoelastic behavior in the beams is highlighted in Figure 4.6, showing the phase lag remaining outside the natural frequencies, it is quite evident between 20 Hz and 70 Hz, bearing in mind that the coherence function in this zone is one, indicating a good chance of linearity. Indeed, if no viscoelastic behavior were present there, the phase lag would be 90 degrees, corresponding to pure elastic behavior between the velocity response and the force excitation. In the same frequency response functions, an anti-resonance is identified at 72 Hz, followed by a second longitudinal resonance peak at 77 Hz. Besides, it is possible to identify torsional modes at 30 Hz and 58 Hz, but they are lightly excited due to the careful alignment of the sensors and

excitation force along the center of the beams. Torsional modes are not considered along this work in order to simplify the simulations under 2D plane strain assumption.

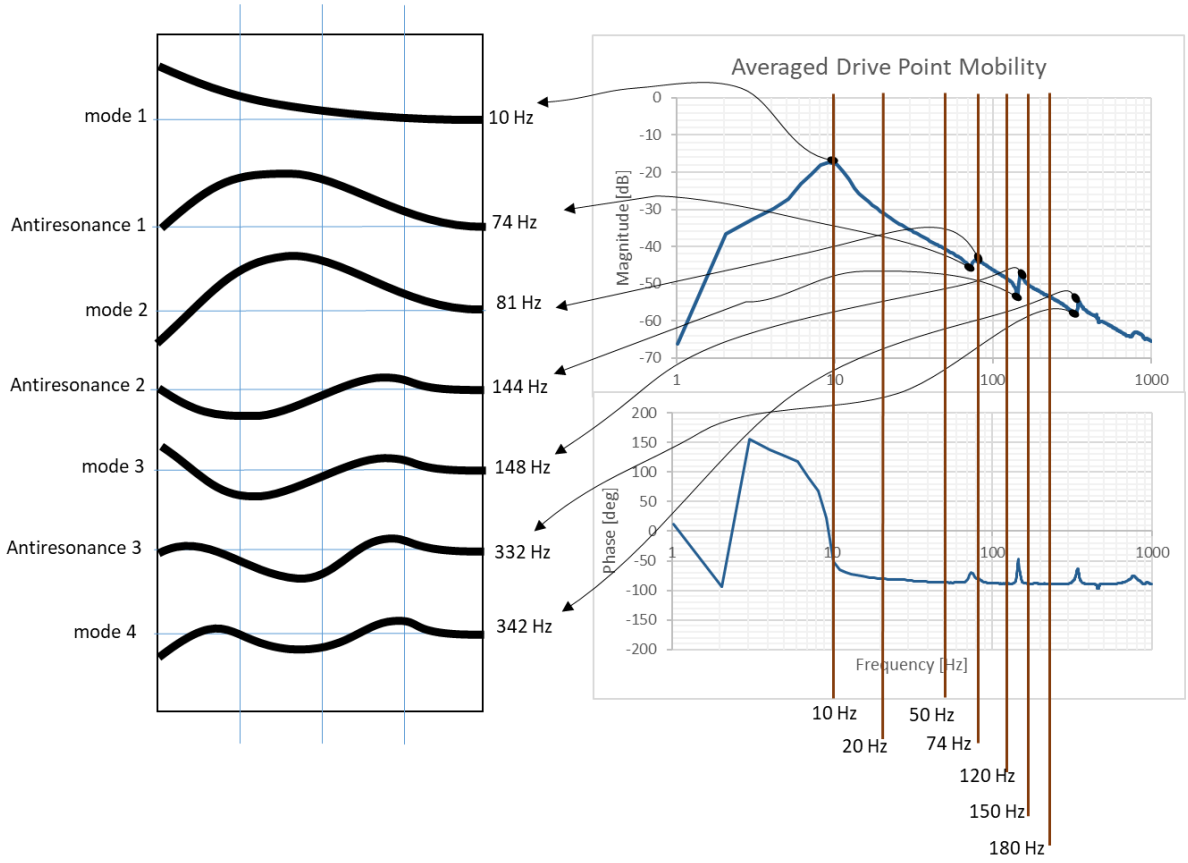

Figure 4.7 Modal shapes extracted from frequency response functions.

Using the information of magnitude and phase in the frequency response functions, we derived the modal shapes of the beams; this is shown in Figure 4.7. The information of the modal shapes helps to understand the behavior of the responses relative to the excitation force and to choose appropriate excitation frequencies for the simulations with our PRBM. Otherwise, the phase lags would become influenced by the resonances.

Taking the above into account, in Figure 4.8 the stiffness magnitude and phase are plotted for a narrower frequency span, where the best data quality is found regarding linear response and the viscoelastic behavior. Choosing the excitation frequency within this span allows better comparisons between

experimental and simulated data, mainly because the positive trend in FRF magnitude and phase indicates that the viscoelastic long-term mechanical property is expected to be higher than the equivalent property under static load.

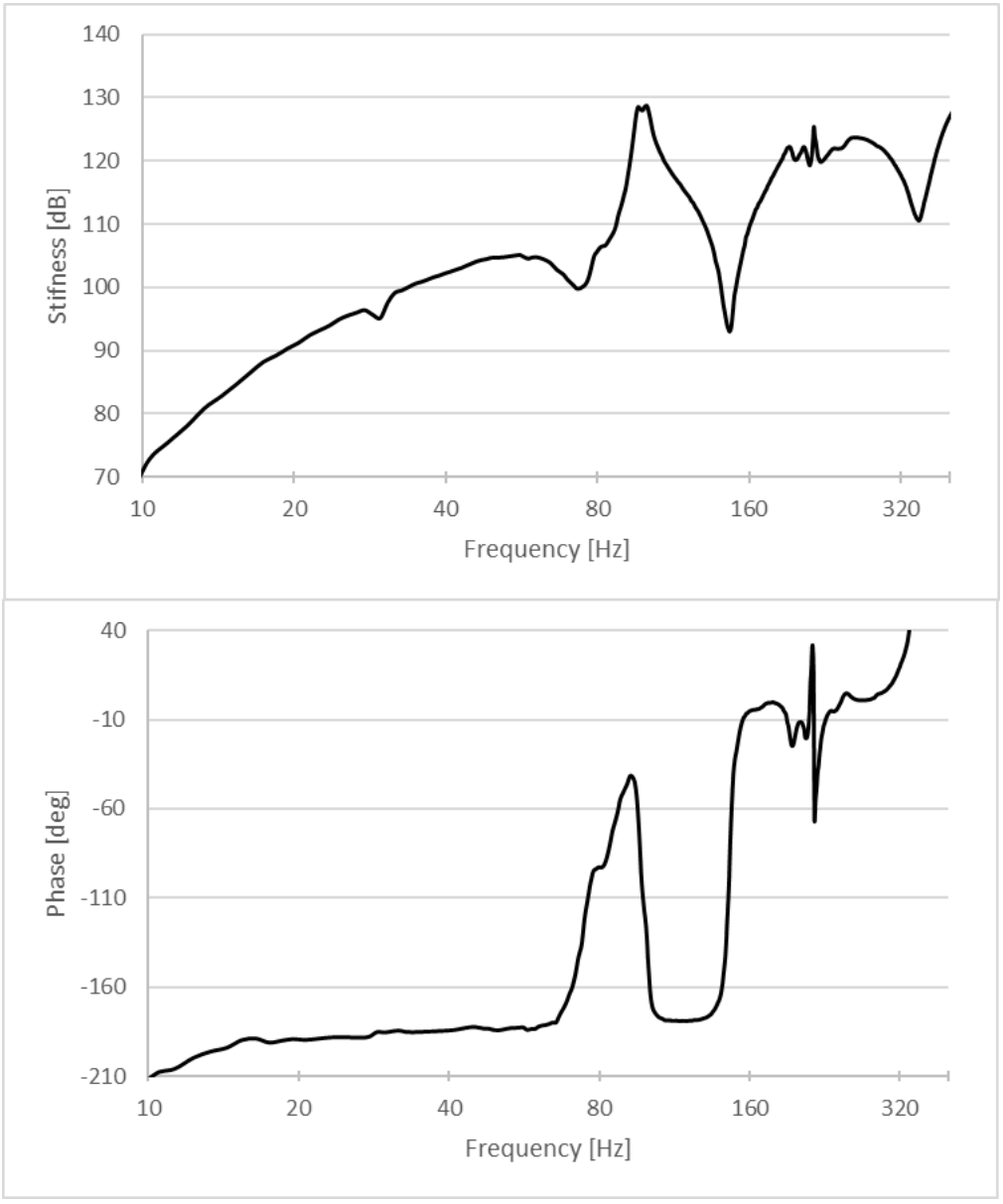

Figure 4.8 Stiffness magnitude (above) and phase (below) for FRF 2

4.3 PRBM construction for a multiphysical approach.

Under dynamic load, the interfaces between plies are playing a significant role: we demonstrated that a creeping behavior is occurring. The retarded behavior in the time is limiting the effect of deformation of the plate. In order to model the creeping induced by the interfaces, we developed a specific model being integrated into the PRBM using a fractional derivative; the procedure was detailed in Fontecha et al. [182].

To develop an equivalent FEM basis simulation, we should:

- Model a stack up of layers with finite solid elements,
- Link all the nodes of the adjacent layers with contact elements modeling internal friction. These elements add significant nonlinearities.
- Solve the model with an explicit approach costly in iteration and challenging to converge.

Developing a FEM model that converges under these circumstances is very time-consuming. In an incremental scheme, it requires monitoring the convergence along the computation, adjusting the configuration when the simulation is aborted and resumed. After many attempts, we were not able to run a model that converges.

On the other hand, despite the difficulties described above, the dynamic PRBM provided the solutions shown in Figure 4.9

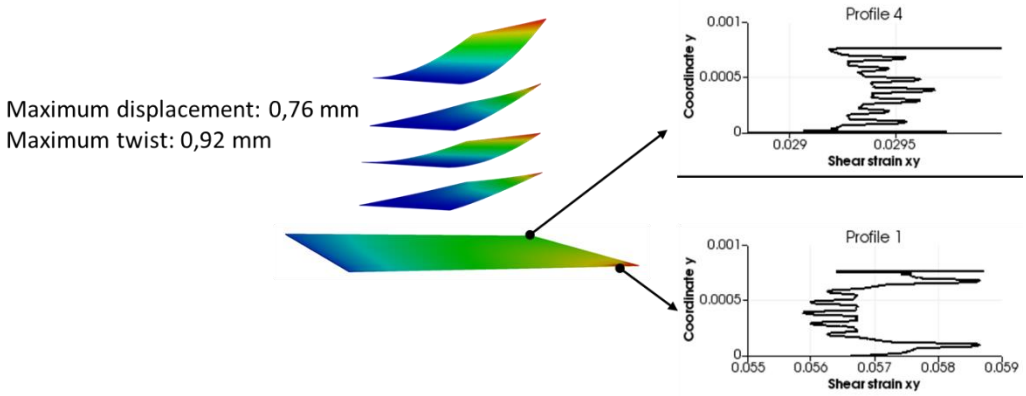

Figure 4.9. The dynamic behavior represented by the PRBM model.

In the case of the laminate used in this work with multiples bodies i interacting between each other, the principle of conservation of linear momentum defines the kinetics of the problem by the internal forces (as a function of the stress tensor $\boldsymbol{\sigma}$), inertia (as a function of the density ρ and the displacement U) and body forces B, as shown in equation 4.1.

$$\sum_{i=0}^{n} \nabla \cdot \boldsymbol{\sigma}^i + \sum_{i=0}^{n} \rho \frac{\partial^2 U}{\partial t^2} = B \tag{4.1}$$

Assuming that the displacement gradients are sufficiently small, the kinematics relating strain and displacement is defined by equation 4.2.

$$\boldsymbol{\varepsilon}^i(U) = \frac{1}{2}\left(\nabla U^i + \left(\nabla U^i\right)^T\right) \tag{4.2}$$

So by Hamilton's principle, the governing equation in the weak form is equation 4.3.

$$\int_\Omega \boldsymbol{\sigma}^i : \boldsymbol{\varepsilon}^i(U^*) \cdot d\Omega \cdot dt - \rho \int_\Omega \frac{\partial^2 U^i}{\partial t^2} \cdot U^* \cdot d\Omega \cdot dt = \int_\Omega B \cdot U^* \cdot d\Omega \cdot dt + \int_\Gamma R \cdot U^* \cdot d\Gamma \cdot dt \tag{4.3}$$

Where R represents the external forces in a boundary Γ

In the case of a viscoelastic body i, the stress tensor is not only a mechanism storing energy by elasticity according to the Hooke's law, but it is also a mechanism dissipating energy by viscoelasticity so we obtain equation 4.4.

$$\boldsymbol{\sigma}^i(t) = \boldsymbol{\sigma}^i(t)_{ela} + \boldsymbol{\sigma}^i(t)_{visc}$$

$$\boldsymbol{\sigma}^i(t)_{Ela} = \boldsymbol{H}^i \cdot \boldsymbol{\varepsilon}^i_{ela}(t) \text{ ; Elastic stress} \qquad 4.4$$

$$\boldsymbol{\sigma}^i(t)_{visc} = \boldsymbol{H}^i \cdot \boldsymbol{\varepsilon}^i_{visc}(t) \text{ ; Viscoelastic stress}$$

In section 1.5.2 we justified the use of the Zener model for viscoelasticity in solid materials, it is represented by equation 4.5.

$$\sigma(t) + \tau \frac{d\sigma(t)}{dt} = G_0 \varepsilon(t) + G_\infty \tau \frac{d\varepsilon(t)}{dt} \qquad 4.5$$

As described in Figure 4.10, in our model we make explicit the design variables determining:

- The nature of the multi-layer structure, this is the number of plies.
- The constitutive law of each ply being defined by the usual nine material characteristics for an orthotropic law.

With this we develop a first PRBM with the following characteristics:

- Parametrized, making explicit some design parameters.
- Multiscale, because the different design variables address different scales of the composite structure, but acting together on the overall behavior of the structure.

In order to achieve such a PRBM, we implement a numerical approach based on the variable separation principle. For this purpose, we choose the Proper Generalized Decomposition (PGD) method because it has the advantage to lead both, to a reduced model and parametrized.

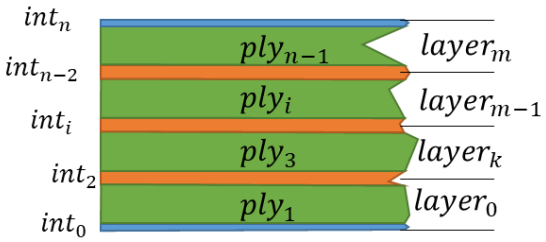

$m = number\ of\ layers - 1$
$k = 0;\ 1;\ 2;\ \cdots; m$
$n = 2 * m + 1$
$i = 0;\ 1;\ 2;\ \cdots; n$
$int_0; int_n = {}^{int_i}/_2$

Figure 4.10 Description of the lamination

4.4 Fractional derivative to model viscoelasticity

4.4.1 Modeling of creeping

In section 4.2, we demonstrated experimentally that the composite beam structure responds under creping. In order to represent this behavior in our PRBM, and according to the justification given in section 1.5.2, we adopt the fractional order Zener's model with four parameters expressed by equation 4.6.

$$\sigma(t) + \tau^{\alpha}\frac{d^{\alpha}\sigma(t)}{dt^{\alpha}} = G_0\varepsilon(t) + G_{\infty}\tau^{\alpha}\frac{d^{\alpha}\varepsilon(t)}{dt^{\alpha}} \qquad 4.6$$

Therefore, by the Riemann-Liouville definition, the fractional operator is equation 4.7. [183]

$$\frac{d^{\alpha}f(t)}{dt^{\alpha}} = \frac{1}{\Gamma(1-\alpha)}\frac{d}{dt}\int_0^t \frac{f(s)}{(t-s)^{\alpha}}ds \qquad 4.7$$

Where the gamma function Γ introduces a memory effect by equation 4.8.

$$n! = \Gamma(n+1) \qquad 4.8$$

Definition: **Memory effect**

> Under a change in external load, the memory effect is a characteristic reaction of a material, which is faded as time goes ("*hereditary response*," Gutierrez-Lemini [64]). The memory effect is responsible for the phase lag between the response of the structure to the change in load.

In a time integration scheme, the external force may change at each time step, so there is a memory effect to every time step. However, instead of the above equation, in a time integration scheme, we use the Grünwald approximation to the fractional operator (equation 4.9) (Galucio [184]), with incremental time steps $h = \Delta t$, so that the w_j are the non-integer infinite sum of binomial coefficients introducing the memory effect, this may be approximated finite if h is small enough.

$$\frac{d^\alpha f(t)}{dt^\alpha} \cong \frac{1}{h^\alpha}\sum_{j=0}^{N_t} w_j f(t-jh) \qquad 4.9$$

$$w_j = \frac{\Gamma(j-\alpha)}{\Gamma(-\alpha)\Gamma(j+1)} = \frac{j-(\alpha+1)}{j} w_{j-1}$$

Finally, using the Grünwald approximation as in Galucio [184], assuming only viscoelastic shear strain at each interfaces i between plies, from equation 4.4 we get equation 4.10,

$$\boldsymbol{\varepsilon}^{i}_{xy\,visc}(t) = \left(1 - \frac{\tau^{\alpha}}{\tau^{\alpha} + \Delta t^{\alpha}}\right)\frac{G_{\infty} - G_0}{G_{\infty}}\boldsymbol{\varepsilon}_{xy\,inst}(t) - \frac{\tau^{\alpha}}{\tau^{\alpha} + \Delta t^{\alpha}}\sum_{j=1}^{N_t} w_j \boldsymbol{\varepsilon}^{i}_{xy\,mem}(t - j\Delta t) \qquad 4.10$$

Definition: **Instantaneous effect**

> Under a change in load, the instantaneous effect is the initial response of a viscoelastic material (Gutierrez-Lemini [64]).

It is seen from the equation above, that the viscoelastic strain is composed both by an instantaneous effect and a memory effect computed at previous time steps, so it develops to equation 4.11.

$$\sigma^{i}_{xy}(t)_{visc} = \sigma^{i}_{xy}(t)_{inst} + \sigma^{i}_{xy}(t)_{mem}$$

$$\sigma^{i}_{xy}(t)_{inst} = 2G_0\left(1 + \frac{\tau^{\alpha}}{\tau^{\alpha} + \Delta t^{\alpha}}\right)\frac{G_{\infty} - G_0}{G_{\infty}}\boldsymbol{\varepsilon}_{xy\,inst}(t) \quad \text{Instantaneous stress} \qquad 4.11$$

$$\sigma^{i}_{xy}(t)_{mem} = 2\frac{G_{\infty}}{G_0}\frac{\tau^{\alpha}}{\tau^{\alpha} + \Delta t^{\alpha}}\sum_{j=1}^{N_t} w_j \boldsymbol{\varepsilon}^{i}_{xy\,mem}(t - j\Delta t) \quad \text{Memory stress}$$

We use the PGD method to produce a parametrized model solution incorporating an additional domain for each parametrized variable so that they can have a variation within a given probability distribution. An identification algorithm based on a function that minimizes the error between the experimental data and the simulated response could be used, but the primary objective of this work is to define the methodology to develop the PRBM, for further application in optimization algorithms (seen Chapter 5). Therefore, at a first instance, we keep

the relaxation time τ and the short term shear modulus G_0 constant, using the data published in Irazu and Elejabarrieta [185] , then we explore the best solution making direct variations on the fractional order α and the long term shear modulus G_∞, this is shown in Table 4-2.

Table 4-2. Data used for the fractional parameters representing viscoelasticity

$\tau = 1.031 \times 10^{-7}$ s
$G_0 = 3{,}24 \times 10^{6}$ Pa
$0 \leq \alpha \leq 1$
5×10^{7} Pa $\leq G_\infty \leq 5 \times 10^{9}$ Pa

4.4.2 Modeling viscoelasticity in the PRBM

For simplicity we present the mathematical model assuming 2D plane strain; therefore, the development of the PRBM implies that each domain x and y must be specified separately by 1D meshes, at the same time, each shall be defined in directions u and v as illustrated in Figure 4.11.

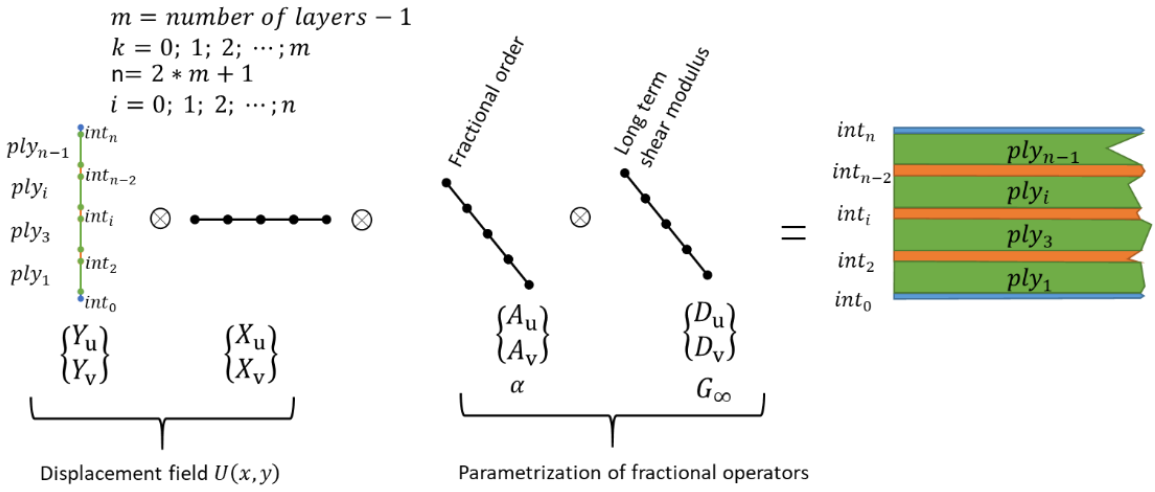

Figure 4.11 PGD implementation and parametrization of fractional operators

In this case, the incorporation of the fractional parameters implies representing the displacement field, equation 4.12.

$$U(x,y) \cong U^n(x,y,a,d)$$

$$U^n(x,y) = \sum_{i=1}^{n} \begin{Bmatrix} X_{\mathrm{u}}^i \cdot Y_{\mathrm{u}}^i \cdot A_{\mathrm{u}}^i \cdot D_{\mathrm{u}}^i \\ X_{\mathrm{v}}^i \cdot Y_{\mathrm{v}}^i \cdot A_{\mathrm{v}}^i \cdot D_{\mathrm{v}}^i \end{Bmatrix} \qquad 4.12$$

The approach adopted here is to assume orthotropic elastic plies and isotropic viscoelastic interfaces. In this case for an orthotropic material the Hooke's law is given by equation 4.13,

$$J = \frac{1}{1 - \vartheta_{xy}\vartheta_{yx}}$$

$$\left[\boldsymbol{H}^i\right] = J \begin{bmatrix} E_{xx} & E_{xx}(\vartheta_{yx}) & 0 \\ E_{xx}(\vartheta_{yx}) & E_{yy} & 0 \\ 0 & 0 & \dfrac{G_{xy}}{J} \end{bmatrix} \qquad 4.13$$

Mechanical properties are first assigned at the layer scale as a discrete function through the thickness domain y, keeping a unity function through the x domain. Just the separation of the shear modulus G_{xy}, decay time τ, long term modulus G_∞, and fractional order of the derivatives in the Zener model α are presented in equations 4.14 to 4.17. The other properties are handled similarly.

$G_{xy} = G_x \circ G_y \circ G_a \circ G_d$	Separation of properties	4.14
$G_x = G_a = G_d = 1$	For convenience, properties are only assigned through the thickness direction, domain y	
$G_{\mathrm{yu}i} = G_{xyi}\ if\ \ y = body_i$		
$\tau = \tau_x \circ \tau_y \circ \tau_a \circ \tau_d$	Separation of properties	4.15
$\tau_x = \tau_a = \tau_d = 1$	For convenience, properties are only	

$\tau_y = \begin{cases} 0 & if\ i \notin interface \\ 1.031 \times 10^{-7} & if\ i \in interface \end{cases}$	assigned through the thickness direction, domain y	
$G_\infty = G_{\infty x} \circ G_{\infty y} \circ G_{\infty a} \circ G_{\infty d}$	Separation of properties	4.16
$G_{\infty x} = G_{\infty y} = G_{\infty d} = 1$	For convenience, properties are assigned through domain d	
$5 \times 10^7\ Pa \leq G_{\infty d} \leq 5 \times 10^9\ Pa$		
$\alpha = \alpha_x \circ \alpha_y \circ \alpha_a \circ \alpha_d$	Separation of properties	4.17
$\alpha_x = \alpha_y = \alpha_d = 1$	For convenience, properties are assigned through domain a	
$0 \leq \alpha_a \leq 1$		

It is convenient to group the known terms to the right of the governing equation, so from equation 4.3 and making the body force $B = 0$, it is possible to redefine the load into the beam adding the memory load so we get equation 4.18,

$$R = R_{ext} + R_{mem} \qquad 4.18$$

$$R_{ext} = f_y(t) \qquad \text{External force}$$

$$R_{mem} = \frac{\tau^{(\alpha)}}{\tau^{(\alpha)} + \Delta t^{(\alpha)}} \frac{G_\infty}{G_0} G_{xy}^i \sum_{j=1}^{N_t} w_j U_{mem}^i (t - j\Delta t) \qquad \text{Memory force}$$

Summarizing, from equation 4.4, we get equation 4.19

$$\boldsymbol{\sigma}_{xx} = J \cdot \left(E_{xx} \boldsymbol{\varepsilon}_{xx} \left(1 - \vartheta_{yz}\vartheta_{zy}\right) + E_{xx} \boldsymbol{\varepsilon}_{yy} \left(\vartheta_{yx} - \vartheta_{zx}\vartheta_{yz}\right) \right)$$

$$\boldsymbol{\sigma}_{yy} = J \left(E_{yy} \boldsymbol{\varepsilon}_{yy} (1 - \vartheta_{xz}\vartheta_{zx}) + E_{xx} \varepsilon_{xx} \left(\vartheta_{yx} - \vartheta_{zx}\vartheta_{yz}\right) \right) \qquad 4.19$$

$$\boldsymbol{\sigma}_{xy} = 2G_{xy} \boldsymbol{\varepsilon}_{xy\ ela} + 2G_0 \left(1 + \frac{\tau^\alpha}{\tau^\alpha + \Delta t^\alpha}\right) \frac{G_\infty - G_0}{G_\infty} \boldsymbol{\varepsilon}_{xy\ ela}(t)$$

Note in equation 4.15 that the decay time $\tau = 0$ in the plies, therefore they are only elastic because the viscous part of the shear stress and the memory force vanish.

Now, incorporating in equation 4.19 the domains d and a of equation 4.12 and applying these to equation 4.3 , we get equations 4.20 to 4.23.

$$\begin{aligned}\boldsymbol{\sigma}_{xx} \cdot \boldsymbol{\varepsilon}_{xx}\left(U^*(x,y)\right) = J \cdot \Bigg(& E_{xx}\left(\left(\sum_{i=1}^{n-1}\left(\frac{dX_{\mathrm{u}}^{i}}{dx}\right)\cdot Y_{\mathrm{u}}^{i}\cdot D_{\mathrm{u}}^{i}\cdot A_{\mathrm{u}}^{i}\right)+\left(\frac{dX_{\mathrm{u}}^{p}}{dx}\right)\cdot Y_{\mathrm{u}}^{p-1}\cdot D_{\mathrm{u}}^{p-1}\cdot A_{\mathrm{u}}^{p-1}\right)\left(1-\vartheta_{yz}\vartheta_{zy}\right) \\ & + E_{xx}\left(\left(\sum_{i=1}^{n-1}X_{\mathrm{v}}^{i}\cdot\left(\frac{dY_{\mathrm{v}}^{i}}{dy}\right)\cdot D_{\mathrm{v}}^{i}\cdot A_{\mathrm{v}}^{i}\right)+X_{\mathrm{v}}^{p}\cdot\left(\frac{dY_{\mathrm{v}}^{p-1}}{dy}\right)\cdot D_{\mathrm{v}}^{p-1}\cdot A_{\mathrm{v}}^{p-1}\right)\left(\vartheta_{yx}-\vartheta_{zx}\vartheta_{yz}\right)\Bigg)\cdot\left(\frac{dX_{\mathrm{u}}^{*}}{dx}\right)\cdot Y_{\mathrm{u}}^{p-1}\cdot D_{\mathrm{u}}^{p-1}\cdot A_{\mathrm{u}}^{p-1}\end{aligned} \tag{4.20}$$

$$\begin{aligned}\boldsymbol{\sigma}_{yy} \cdot \boldsymbol{\varepsilon}_{yy}\left(U^*(x,y)\right) = J \cdot \Bigg(& E_{yy}\left(\left(\sum_{i=1}^{n-1}X_{\mathrm{v}}^{i}\cdot\left(\frac{dY_{\mathrm{v}}^{i}}{dy}\right)\cdot D_{\mathrm{v}}^{i}\cdot A_{\mathrm{v}}^{i}\right)+X_{\mathrm{v}}^{p}\cdot\left(\frac{dY_{\mathrm{v}}^{p-1}}{dy}\right)\cdot D_{\mathrm{v}}^{p-1}\cdot A_{\mathrm{v}}^{p-1}\right)\left(1-\vartheta_{xz}\vartheta_{zx}\right) \\ & + E_{xx}\left(\left(\sum_{i=1}^{n-1}\left(\frac{dX_{\mathrm{u}}^{i}}{dx}\right)\cdot Y_{\mathrm{u}}^{i}\cdot D_{\mathrm{u}}^{i}\cdot A_{\mathrm{u}}^{i}\right)+\left(\frac{dX_{\mathrm{u}}^{p}}{dx}\right)\cdot Y_{\mathrm{u}}^{p-1}\cdot D_{\mathrm{u}}^{p-1}\cdot A_{\mathrm{u}}^{p-1}\right)\left(\vartheta_{yx}-\vartheta_{zx}\vartheta_{yz}\right)\Bigg)\cdot X_{\mathrm{v}}^{*}\cdot\left(\frac{dY_{\mathrm{v}}^{p-1}}{dy}\right)\cdot D_{\mathrm{v}}^{p-1}\cdot A_{\mathrm{v}}^{p-1}\end{aligned} \tag{4.21}$$

$$\begin{aligned}\boldsymbol{\sigma}_{xy} \cdot 2\boldsymbol{\varepsilon}_{xy}\left(U^*(x,y)\right) = & \Bigg(G_{xy}\left(\left(\sum_{i=1}^{n-1}\left(X_{\mathrm{u}}^{i}\cdot\frac{dY_{\mathrm{u}}^{i}}{dy}\cdot D_{\mathrm{u}}^{i}\cdot A_{\mathrm{u}}^{i}+\frac{dX_{\mathrm{v}}^{i}}{dx}\cdot Y_{\mathrm{v}}^{i}\cdot D_{\mathrm{v}}^{i}\cdot A_{\mathrm{v}}^{i}+2G_{xy}\,\boldsymbol{\varepsilon}_{xy\ visc}\cdot D_{\mathrm{v}}^{i}\cdot A_{\mathrm{v}}^{i}\right)\right)+X_{\mathrm{u}}^{p}\cdot\frac{dY_{\mathrm{u}}^{p-1}}{dy}\cdot D_{\mathrm{u}}^{p-1}\cdot A_{\mathrm{u}}^{p-1} \\ & +\frac{dX_{\mathrm{v}}^{p}}{dx}\cdot Y_{\mathrm{v}}^{p-1}\cdot D_{\mathrm{v}}^{p-1}\cdot A_{\mathrm{v}}^{p-1}+2G_{xy}\,\boldsymbol{\varepsilon}_{xy\ visc}\cdot D_{\mathrm{v}}^{p-1}\cdot A_{\mathrm{v}}^{p-1}\Bigg)\Bigg) \\ & \cdot\left(X_{\mathrm{u}}^{*}\cdot\left(\frac{dY_{\mathrm{u}}^{p-1}}{dy}\right)\cdot D_{\mathrm{u}}^{p-1}\cdot A_{\mathrm{u}}^{p-1}+\left(\frac{dX_{\mathrm{v}}^{*}}{dx}\right)\cdot Y_{\mathrm{v}}^{p-1}\cdot D_{\mathrm{v}}^{p-1}\cdot A_{\mathrm{v}}^{p-1}\right)\end{aligned} \tag{4.22}$$

$$R = \left(f_y(t)+\frac{\tau^{(\alpha)}}{\tau^{(\alpha)}+\Delta t^{(\alpha)}}\frac{G_{\infty}}{G_0}G_{xy}^{i}\sum_{j=1}^{N_t}w_j\,U_{mem}^{i}\left(t-j\Delta t\right)\right)\cdot X_{\mathrm{v}}^{*}\cdot\left(\frac{dY_{\mathrm{v}}^{p-1}}{dy}\right)\cdot D_{\mathrm{v}}^{p-1}\cdot A_{\mathrm{v}}^{p-1} \tag{4.23}$$

Before the computation of the PRBM by the alternative direction strategy, a final important step in the PGD method is to reorganize the equation above, such that the domain x, y, a and d are grouped in separated terms, keeping the unknowns at the left part of the equation. Finally, after converging to a solution, from the individual 1D solutions, a new solution is mapped in 2D to the x direction and another one to the y direction. We used Fenics and ParaView for plotting

the results, so the solutions contained in the PRBM may be projected either to separated 2D function spaces or combined to a 2D vector function space.

4.4.3 Determination of the fractional parameters from experimentation

In order to find fractional derivative operators experimentally, we use the same set up shown in Figure 4.4; two sinusoidal excitation forces are generated with a maximum amplitude of 1 N. We choose the excitation frequencies based on the narrow frequency span presented in Figure 4.8, away from natural frequencies. The frequencies chosen are 50 Hz and 120 Hz, so they are apart from the resonances. The responses were passed through a high pass filter with a cut frequency of 10 Hz to avoid the low frequencies caused by the clamping. In order to compare the results, the simulated force was synchronized first with the excitation force gathered from the experiment.

Recalling that only the long-term relaxation module G_∞ and the fractional order derivative α are parametrized, a simple, direct search procedure over the solution scenario generated by the PRBM method was performed. This identification is done on post processing; the computing cost is very low since technically these are arrays projected on 2D FEM meshes. Some of the values gathered are presented in Table 4-3, and the results in Figure 4.13. (adjusting G_∞ with $\alpha = a1 = 0{,}9$ (see Table 4-3) and excitation force $f = 1\ N$ at a frequency of $50\ Hz$.) and in Figure 4.13. (adjusting α with $G_\infty = d3 = 7{,}1 \times 10^8\ Pa$ and excitation force $f = 1\ N$ at a frequency of 120Hz)

Table 4-3. Experimental Fractional parameter identification

	50 Hz			120 Hz	
G_∞ [Pa]	$d1 = 1 \times 10^8$	$d2 = 6 \times 10^8$	$d3 = 7{,}1 \times 10^8$	$d3 = 7{,}1 \times 10^8$	
α	$a1 = 0{,}9$			$a1 = 0{,}9$	$a2 = 0{,}63$

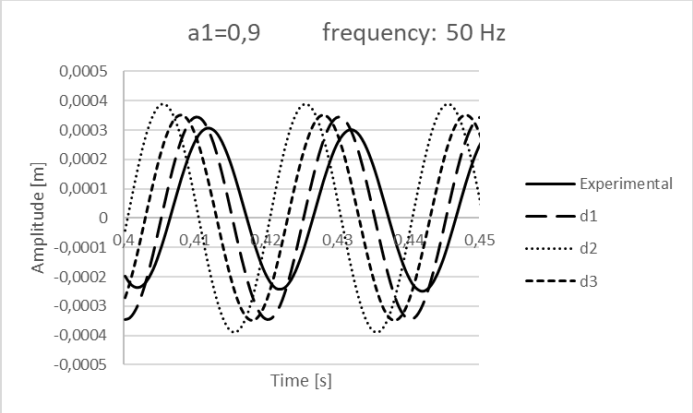

Figure 4.12. Adjustment of the long-term shear modulus G_∞

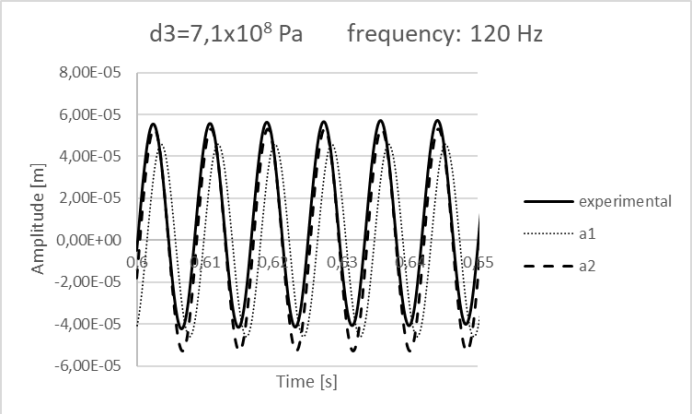

Figure 4.13 Adjustment of the fractional order α

As expected in this identification experiment, adjusting the long-term shear modulus increments the lagging of the simulated response at 50Hz; however, the results above show a better fit at 120 Hz if the loss factor is not related to an integer order of the strain derivative as it is in the classical Zener's model, but to a derivative of a diminished order ($\alpha = 0{,}63$), this trend agrees with the references analyzed in section 1.5. The data fit may be improved by incorporating the relaxation time to the PRBM and using an optimization algorithm that minimizes the error; with the advantage that every computed solution may be quickly calculated with light computing resources. This is a future working perspective.

4.5 PRBM based simulation of dynamic behavior in a composite structure

4.5.1 Study case

We simulate the same laminated composite beam described in section 4.2.1. Therefore, we propose a second PRBM making explicit the main design parameters of the laminated beam even if these parameters occur at different scales. The PRBM represents:

- The design parameters (Figure 4.14).
- The variables allowing to know the overall behavior of the laminated beam

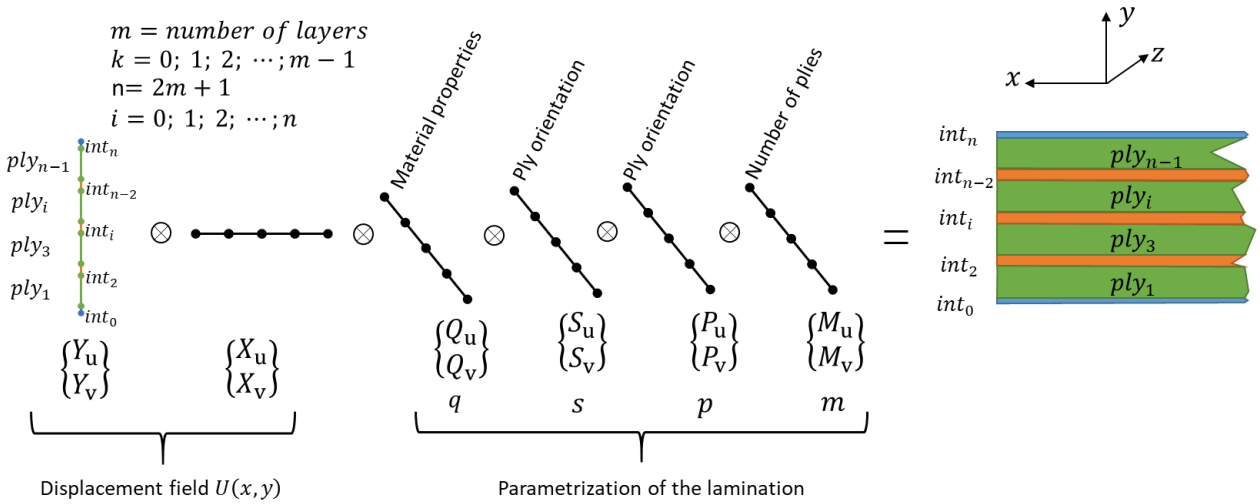

Figure 4.14. Design variables of the lamination model

4.5.2 A separated and reduced model of the dynamic behavior of the composite beam

The application of the PGD method adds the required dimensions. In this case, the displacement field is represented by equation 4.24,

$$U(x,y,q,s,p,m) \cong U^n(x,y,q,s,p,m)$$

$$U^n(x,y,q,s,p,m) = \sum_{i=1}^{n} \begin{Bmatrix} X_{\mathrm{u}}^i \cdot Y_{\mathrm{u}}^i \cdot Q_{\mathrm{u}}^i \cdot S_{\mathrm{u}}^i \cdot P_{\mathrm{u}}^i \cdot M_{\mathrm{u}}^i \\ X_{\mathrm{v}}^i \cdot Y_{\mathrm{v}}^i \cdot Q_{\mathrm{v}}^i \cdot S_{\mathrm{v}}^i \cdot P_{\mathrm{v}}^i \cdot M_{\mathrm{v}}^i \end{Bmatrix} \quad 4.24$$

For simplicity, in this work the model is limited to symmetrically oriented plies; additionally, the plies are grouped so they can be treated individually by coefficients on the appropriate dimension domain. Thus the computation of individual stresses needs to group the properties as shown for Young's modulus in Figure 4.15.

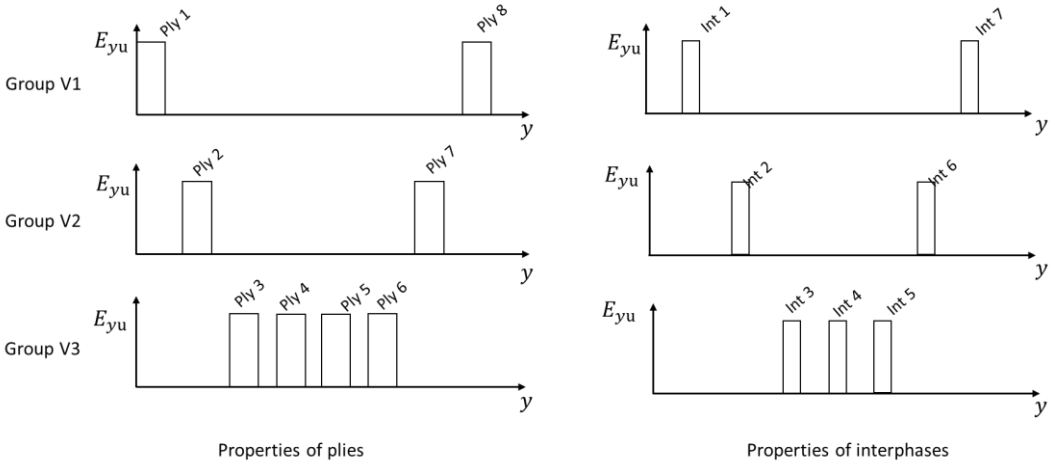

Figure 4.15. Properties assignment through the thickness direction.

Under these circumstances, Young's modulus is expressed by equations 4.25 to 4.32,

$E_{xx}^{i} = E_{x\mathrm{u}} \cdot E_{y\mathrm{u}}^{i} \cdot E_{q\mathrm{u}}^{i} \cdot E_{s\mathrm{u}}^{i} \cdot E_{p\mathrm{u}}^{i} \cdot E_{m\mathrm{u}}^{i}$		4.25
$E_{x\mathrm{u}} = 1$	Material properties direction u through domain x	4.26
$E_{y\mathrm{u}}^{i} = \begin{cases} E_{xx}^{i} \; if \;\; y = body_i \\ 0 \quad if \;\; y \neq body_i \end{cases}$	material properties direction u through domain y	4.27
$E_{q\mathrm{u}}^{i} = \begin{cases} q \quad if \;\; y = body_i \\ 1 \quad if \;\; y \neq body_i \end{cases}$	Variation of material properties	4.28
$E_{s\mathrm{u}}^{i} = \begin{cases} cos(\theta_s) + \dfrac{E_{zz}^{i}}{E_{xx}^{i}} sin(\theta_s) \quad body_i \in group\, V1 \\ 1 \qquad\qquad\qquad\qquad if \;\; body_i \notin group\, V1 \end{cases}$	Ply orientation of group V1	4.29
$E_{p\mathrm{u}}^{i} = \begin{cases} cos(\theta_p) + \dfrac{E_{zz}^{i}}{E_{xx}^{i}} sin(\theta_p) \quad if \;\; body_i \in group\, V2 \\ 1 \qquad\qquad\qquad\qquad if \;\; body_i \notin group\, V2 \end{cases}$	Ply orientation of group V2	4.30
$E_{m\mathrm{u}1}^{i} = \begin{cases} 1 \; if \; m \geq 8 \\ 1 \times 10^{-14} \; otherwise \end{cases}$	Presence of group V1	4.31
$E_{m\mathrm{u}2}^{i} = \begin{cases} 1 \; if \; m \geq 6 \\ 1 \times 10^{-14} \; otherwise \end{cases}$	Presence of group V2	4.32

4.5.3 Model processing for CAE

First, we developed a Finite Element Model to simulate the dynamic behavior of our laminated beam. The FEM models have been done with Ansys® by implementing a distributed parallel process. Table 4-4 is presenting the assessment of different models being developed, the cost processing, the advantages and inconvenient.

We realized (Table 4-4):

1. Overall orthotropic models with 3D elements, and then with 2D elements are not separated and cannot allow the user to represent the damping effect at the interfaces level.
2. When the behavior of each ply is represented separately, each ply is seen as a 2D plane.
3. When the behavior of the matrix between the plies is included within the model, the matrix is also represented by 2D planes having capacities of viscoelasticity

We were not able to compute a FEM viscoelastic separated model with more than two plies. Table 4-4 shows that two plies and one interface are computed in about 88 hours.

Secondly, we used our reduced and parametrized model. Table 4-5 compares the processing cost from the 2-plies laminated beam having a visco-elastic behavior. The models were implemented using:

- For the FEM model: An Intel® Xeon® CPU @ 2,5GHz, two processors, 16 cores, RAM: 40 GB, with parallel processes
- For the PRBM: An Intel® core i7 processor, four cores. RAM 16Gb, with any parallel processes.

Table 4-4. Assessment of FEM models

DESCRIPTION	MESH REPRESENTATION	COMPUTING COST	MODEL AND COSTS	COMMENTS
OVERALL MODEL	Full 3D model, One equivalent single layer Ten elements through the thickness direction	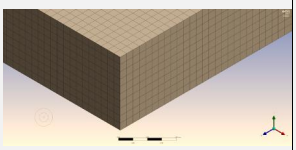	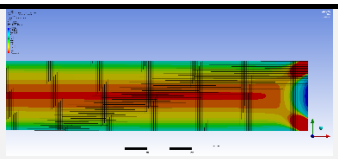 **Elements**: 2.622.780 **Nodes**: 2.904.660 **Max allocated memory**: 23,6 GB **Computing time**: 364 sec	**Impossible to compute the plies behavior separately and to represent the viscoelastic behavior due to the matrix**
	2D plane strain, one equivalent single layer	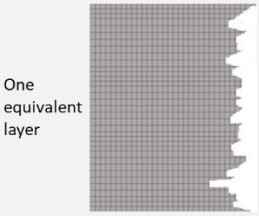	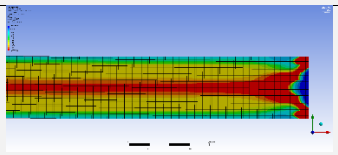 **Elements**: 256.000 **Nodes**: 262.000 **Max allocated memory**: 17,5 GB **Computing time**: 30 sec	
SEPARATED MODEL	2D plane strain, until 8 Layers	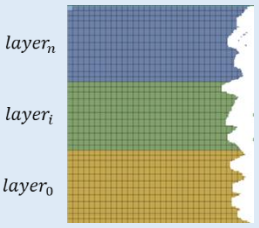	**<u>For two layers:</u>** **Elements**: 256.000 **Nodes**: 307,248 **Max allocated memory**: 17,5 GB **Computing time**: 32 sec	**The behavior of the plies has been separated, but the viscosity due to the matrix between the plies is not represented. Convergence difficulties due to mismatch of properties**
VISCO-ELASTIC SEPARATED MODEL	2D plane strain, 2 plies + 1 interface	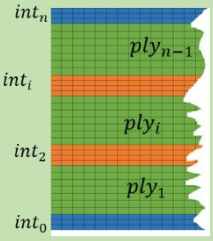	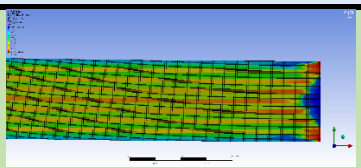 **<u>For two layers:</u>** **Elements**: 840.000 **Nodes**: 976.122 **Max allocated memory**: 19,5 GB **Computing time**: **88 hours and 21 minutes**	**The behavior of the plies have been separated, and the behavior of each ply interface is represented: also the viscosity is represented at the scale of the ply interface**

Table 4-5. Comparing FEM vs. PRBM results

	FEM		PRBM		Error
	Machine: Server Distributed processes: 16		Machine: Laptop No distributed processes		
	Max shear strain	Computing time	Max shear strain (m/m)	Post-processing time	
Number of layers: 2 **Stacking sequence:** **[90, 00,]**	$4{,}83 \times 10^{-5}$	71 h	$4{,}55 \times 10^{-5}$	15 s	5,8%

As an illustration, we used our new PRBM to simulate a laminated composite beam having more than two plies: our model is not limited. Figure 4.16 shows the detail of the shear strain distribution through the thickness direction in an 8-plies beam. The simulation was computed in a couple of seconds. An equivalent result was attempted using FEM, but it was impossible to run an explicit and non-linear model with more than two layers on the available computer resources.

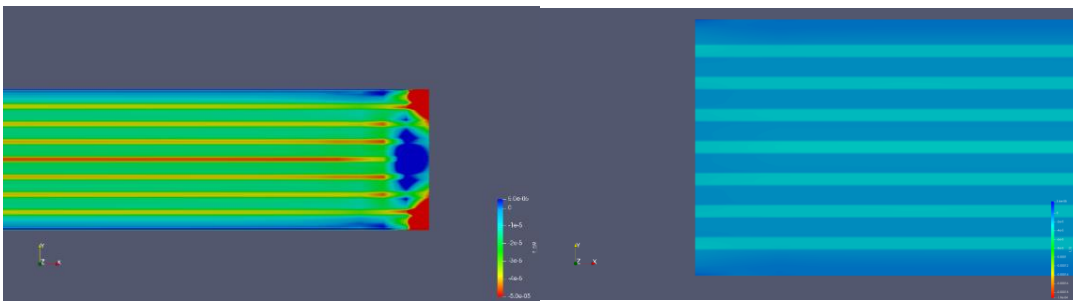

Figure 4.16 Shear strain distribution through the thickness direction

The difference between a regular model (FEM) and the proposed PRBM is that the FEM model is based on solid finite elements, this means that the number of equations to solve the problem raises exponentially to the number of dimensions (either 2D or 3D). Moreover, every solution is computed based on a

set of input variables, so if several input variables are to be tested, the model shall be computed again for each new set.

On the other hand, the PRBM is based on the principle of separation of variables (domains in our case), each made by 1D finite elements, so the number of equations to solve the problem rises proportionally (and not exponentially as in the FEM) to the number of degrees of freedom (either 2D or 3D). Additionally, if several input variables are to be tested, these may be introduced as additional domains. Thus the number of equations does not grow considerably, and the response is not a single solution but a reduced model able to compute particular solutions almost immediately using a few computational resources.

4.6 Conclusion

In this chapter, we addressed the problem of a laminated composite under dynamic load. First, we conducted a dynamic experiment to demonstrate the viscoelastic characteristic of the structure. Then we developed a PRBM linked to the fractional order Zener model to represent viscoelasticity being present within the interfaces between plies. This link is a new contribution by our work.

The PRBM allowed running a simple search to find the value of the fractional parameters. Finally, the PRBM is enriched with the parametrization of the number of plies, material properties and ply orientation.

We used a time integration incremental scheme to find solutions from the PRBM over time. Even if gathering solutions from the PRBM is fast, the generation of the PRBM itself demands considerable time, even though light computational resources were used.

In the following chapter, we link the PRBM to a knowledge model to find optimal solutions of a laminated composite plaque.

(This page is intentionally left blank)

Chapter 5

THE PRBM SUPPORTING DECISION MAKING IN THE DESIGN OF COMPOSITE STRUCTURES

The work described in this chapter has been published in two articles in the international journal of Applied Composite Materials. (See section personal publications).

5.1 Introduction

In this chapter, the optimization is interfaced with a reduced behavioral model, the PRBM, allowing fast reconstruction of full 3D displacement fields by designing the composite structure at the level of the plies and the interfaces between plies. Additionally, the PRBM is parametric within predefined intervals, meaning that the displacement field is a function of critical design parameters: the number of plies, the fiber orientation, the fiber volume fraction and the viscoelastic nature of the interfaces.

An evolutionary algorithm uses the PRBM to evaluate candidate solutions until achieving convergence on specific objectives. Two simple cases are presented to illustrate the flexibility of the approach when designing composite structures: one involving a static load and the other using a force oscillating over time.

We propose a solution allowing a designer to explore design spaces for an aimed behavior, described by the displacement field $U(x, y, z)$, representing the movement of every element of the composite structure in position (x, y, z).

5.2 PRBM for design

The Parametric and Reduced Behavior Model (PRBM) is a representation of the behavior of the laminated structure. From the governing equation 5.1, we generate the PRBM using the Proper Generalized Decomposition (PGD) method. The idea is to separate the spatial domains (x, y, z) into basis functions (X, Y, Z) on each domain in the governing equation, as shown in equation 5.2. In the same equation, the model becomes parametric because the PGD method allows the introduction of additional basis functions $(P1, P2, P3, P4, P5, P6, P7)$ in additional domains $(p_1, p_2, p_3, p_4, p_5, p_6, p_7)$ (Figure 5.3). These domains representing parameters are explained in section 5.3.1; these work in a similar way than section 4.4 and 4.5 and published by Fontecha-Dulcey et al. [182].

The resulting PRBM is reduced because the displacement field U is no longer computed from tensor operations relating stresses and strains. Instead, the displacement field is reconstructed by adding simple Kronecker products of the functions at each enrichment mode n as shown in equation 5.4.

$$\sum_{i=0}^{n} \nabla \cdot \boldsymbol{\sigma}^i + \sum_{i=0}^{n} \rho \frac{\partial^2 U}{\partial t^2} = B \tag{5.1}$$

$$\begin{aligned} U(x, y, z, p_1, p_2, p_3, p_4, p_5, p_6, p_7) &\cong U_{x,y,z,p_1,p_2,p_3,p_4,p_5,p_6,p_7} \\ &\cong \sum_{i=0}^{n} U^i (x, y, z, p_1, p_2, p_3, p_4, p_5, p_6, p_7) \end{aligned} \tag{5.2}$$

The domains defining the displacement U are listed in Table 5-1.

Table 5-1. Parameters describing the displacement field U

Domain	Description
x, y, z	Geometric domains
p_1, p_2, p_3, p_4	Parameters holding the constitutive law of the plies
p_5	Parameter handling the fiber volume fraction
p_6	Parameter handling the viscoelastic property
p_7	Parameter handling the number of plies

$$U(x, y, z, p_1, p_2, p_3, p_4, p_5, p_6, p_7) = \sum_{i=1}^{n} \{X_i(x) \circ Y_i(y) \circ Z_i(z) \circ P1_i(p1) \circ P2_i(p2) \circ P3_i(p3) \circ P4_i(p4) \circ P5_i(p5) \circ P6_i(p6) \circ P7_i(p7)\} \quad 5.3$$

In particular, applying the PGD method to our case of study, and considering a static case where the external load is constant over time, the displacement field is determined directly from the mechanical behavior law of the structure.

On the other side, when the external load changes over time we face a dynamic case, therefore the problem is solved using the Newmark's method as a time integration scheme. This incremental integration scheme is used because of the memory effect introduced by viscoelasticity. Therefore, the displacement field U is reconstructed in a separated form of one dimensional functions in domains x, y, z at each time step $t_i,\ i = 1.2, \cdots, n$.

The solution of the dynamic case also requires the density of the structure. In the lamination studied here, the density is determined from the density of the fibers ρ_f and from the density of the matrix ρ_m. We use a separated approach that leads us to consider the density ρ_m only at the level of the interfaces and the density ρ_f at the level of the plies; we do not use a mixture law, some experiments have demonstrated that this is sufficient to represent the dynamic behavior as shown in Figure 5.1.

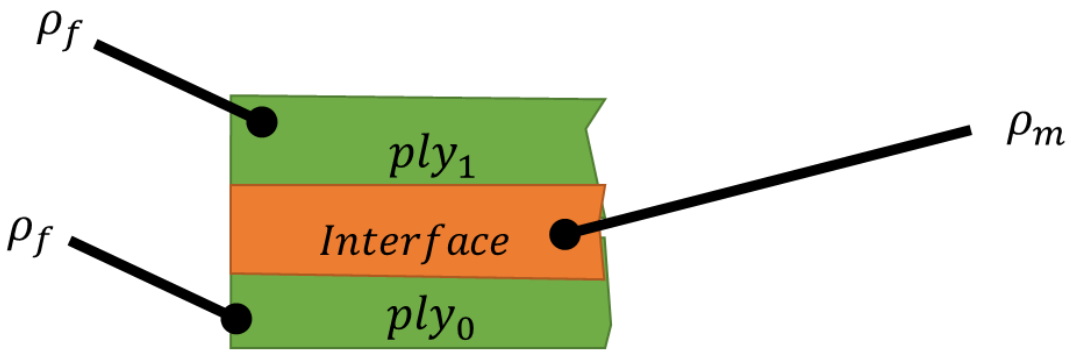

Figure 5.1 Density distribution

In our PRBM the parameters are introduced in the orthotropic constitutive law represented by $\bar{C}$.

5.3 A knowledge model to design

5.3.1 The parametric knowledge model

Variables and parameters are linked together by different behavioral laws or specific mathematical representations of experts' know-how. Together, these laws complete a knowledge model.

Definition: **Parametric Knowledge Model (PKM)**

> We name a Parametric Knowledge Model (PKM) a meta-model, a collection of models representing at the same time the behavior of a product as a function of its design parameters as well as the way a product is created.

From Figure 5.2, in our case, the PKM includes:

1. A representation of the behavior of the laminated structure under static and dynamic loading. It is the Parametric and Reduced Behavior Model (PRBM).
2. The laws are allowing building orthotropic constitutive laws of the laminated structure.

Parametric Knowledge model (PKM)

Parametric and Reduced Behavior Model (PRBM)	$U_{x,y,z,p1,p2,p3,p4,p5,p6,p7}$
Material law	$\boldsymbol{\sigma} = \overline{\boldsymbol{C}}\boldsymbol{\varepsilon}$
Geometric law	$\boldsymbol{\varepsilon}(U) = \frac{1}{2}(\nabla U + (\nabla U)^T)$
Oriented constitutive law for ply *i*	$E_x^i = f(E_l, E_t, \theta_i)$ $E_y^i = f(E_l, E_t, \theta_i)$
Ply constitutive law	$E_l = f(V_f, E_f, E_m)$ $E_t = f(V_f, E_f, E_m)$
Viscoelastic behavior at the interfaces	$P = f(G_0, G_\infty, \alpha, \tau)$

Figure 5.2 Parametric Knowledge model (PKM).

From the displacement field, and assuming small deformations, the strain is computed from equation 5.4,

$$\boldsymbol{\varepsilon}(U) = \frac{1}{2}(\nabla U + (\nabla U)^T) \qquad 5.4$$

Moreover, from the Hooke's law we obtain the stress in equation 5.5:

$$\boldsymbol{\sigma} = \overline{\boldsymbol{C}}\boldsymbol{\varepsilon} \qquad 5.5$$

We call these relations 'usual laws' because they are typically presented in a model able to produce a single solution, but the PRBM is parametric so that it may generate solutions within the interval of the parameters.

The stacking sequence is constrained to symmetric, so the stiffness at each ply is computed as a function of the ply orientation, the principal material properties, the fiber volume fraction and the function defining the number of plies. These stiffness values are specified in separated domains (p_1, p_2, p_3, p_4) as represented in Figure 5.3.

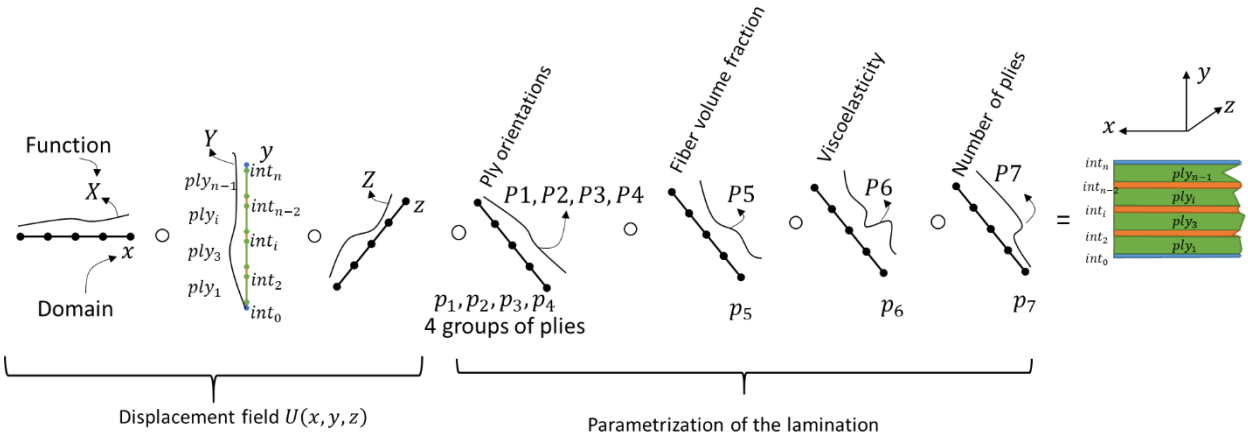

Figure 5.3 Parametrization of the knowledge model

The stiffness at each ply (i) in local coordinates, considering orthotropic behavior is given by equation 5.6.

$$J = \frac{1}{1 - \vartheta_{lt}\vartheta_{tl} - \vartheta_m\vartheta_m - \vartheta_{tl}\vartheta_{lt} - 2\vartheta_{tl}\vartheta_{tt}\vartheta_{tl}}$$

$$[\boldsymbol{C_i}] = J \begin{bmatrix} E_l(1-\vartheta_m\vartheta_m) & E_l(\vartheta_{tl}-\vartheta_{tl}\vartheta_m) & E_l(\vartheta_{tl}-\vartheta_{tl}\vartheta_m) & 0 & 0 & 0 \\ E_l(\vartheta_{tl}-\vartheta_{tl}\vartheta_m) & E_t(1-\vartheta_{lt}\vartheta_{tl}) & E_t(\vartheta_m-\vartheta_{lt}\vartheta_{tl}) & 0 & 0 & 0 \\ E_l(\vartheta_{tl}-\vartheta_{tl}\vartheta_m) & E_t(\vartheta_m-\vartheta_{lt}\vartheta_{tl}) & E_{zz}(1-\vartheta_{lt}\vartheta_{tl}) & 0 & 0 & 0 \\ 0 & 0 & 0 & {G_m}/{J} & 0 & 0 \\ 0 & 0 & 0 & 0 & {G_{lt}}/{J} & 0 \\ 0 & 0 & 0 & 0 & 0 & {G_{lt}}/{J} \end{bmatrix}^i \quad 5.6$$

In the equation above, the sub-index l means the direction of the fibers, t the direction perpendicular to the fibers and m is the matrix (Figure 1.2).

Additionally, the stiffness C_i is related to the transformed stiffness $\bar{C}_i$ in global coordinates using the transformation matrix D_i in equation 5.7.

$$\overline{\boldsymbol{C}}_i = \boldsymbol{D}_i \boldsymbol{C}_i \boldsymbol{D}_i^T \quad 5.7$$

$$D_i = \begin{bmatrix} cos^2\theta_i & 0 & sin^2\theta_i & 0 & 2\cdot sin\theta_i \cdot cos\theta_i & 0 \\ 0 & 1 & 0 & 0 & 0 & 0 \\ sin^2\theta_i & 0 & cos^2\theta_i & 0 & -2\cdot sin\theta_i \cdot cos\theta_i & 0 \\ 0 & 0 & 0 & cos\theta_i & 0 & -sin\theta_i \\ -sin\theta_i \cdot cos\theta_i & 0 & sin\theta_i \cdot cos\theta_i & 0 & cos^2\theta_i - sin^2\theta_i & 0 \\ 0 & 0 & 0 & 0 & 0 & cos\theta_i \end{bmatrix}$$

On the other hand, the interfaces between plies are considered isotropic, so the stiffness is given by equation 5.8.

$$J = \frac{E}{(1+v)(1-2v)}$$

$$[\boldsymbol{C}_{int}] = J \begin{bmatrix} 1-v & v & v & 0 & 0 & 0 \\ v & 1-v & v & 0 & 0 & 0 \\ v & v & 1-v & 0 & 0 & 0 \\ 0 & 0 & 0 & \frac{1-2v}{2} & 0 & 0 \\ 0 & 0 & 0 & 0 & \frac{1-2v}{2} & 0 \\ 0 & 0 & 0 & 0 & 0 & \frac{1-2v}{2} \end{bmatrix}^{i} \quad 5.8$$

The stiffness of plies and interfaces is therefore represented by equation 5.9**.**

$$\overline{\boldsymbol{C}} = f(\bar{C}_1(p_1), \bar{C}_2(p_2), \bar{C}_3(p_3), \bar{C}_4(p_4), C_{int}) \quad 5.9$$

To enforce symmetric lamination, the plies are grouped as shown in Figure 5.4. By this manner, the stiffness at each ply is represented by equations 5.10 to 5.14.

$\overline{\boldsymbol{C}}_1(p_1) = f(E_l, E_t, G_{lt}, \upsilon_m, \upsilon_{tl}, \upsilon_{lt}, \theta_1, Q(p_6), R1(p_7))$	Ply group 1, made by ply 1 and ply 8	5.10
$\overline{\boldsymbol{C}}_2(p_2) = f(E_l, E_t, G_{lt}, \upsilon_m, \upsilon_{tl}, \upsilon_{lt}, \theta_2, Q(p_6), R2(p_7))$	Ply group 2, made by ply 2 and ply 7	5.11
$\overline{\boldsymbol{C}}_3(p_3) = f\big(E_l, E_t, G_{lt}, \upsilon_m, \upsilon_{tl}, \upsilon_{lt}, \theta_3, Q(p_6)\big)$	Ply group 3, made by ply 3 and 6	5.12

$\bar{\boldsymbol{C}}_4(p_4) = f\left(E_l, E_t, G_{lt}, \upsilon_m, \upsilon_{tl}, \upsilon_{lt}, \theta_4, Q(p_6)\right)$	Ply group 4, made by ply 4 and 5	5.13
$\boldsymbol{C}_{int} = f\left(E_m, G_m, Visc(p_5), R1(p_7), R2(p_7)\right)$	See section 4.4	5.14

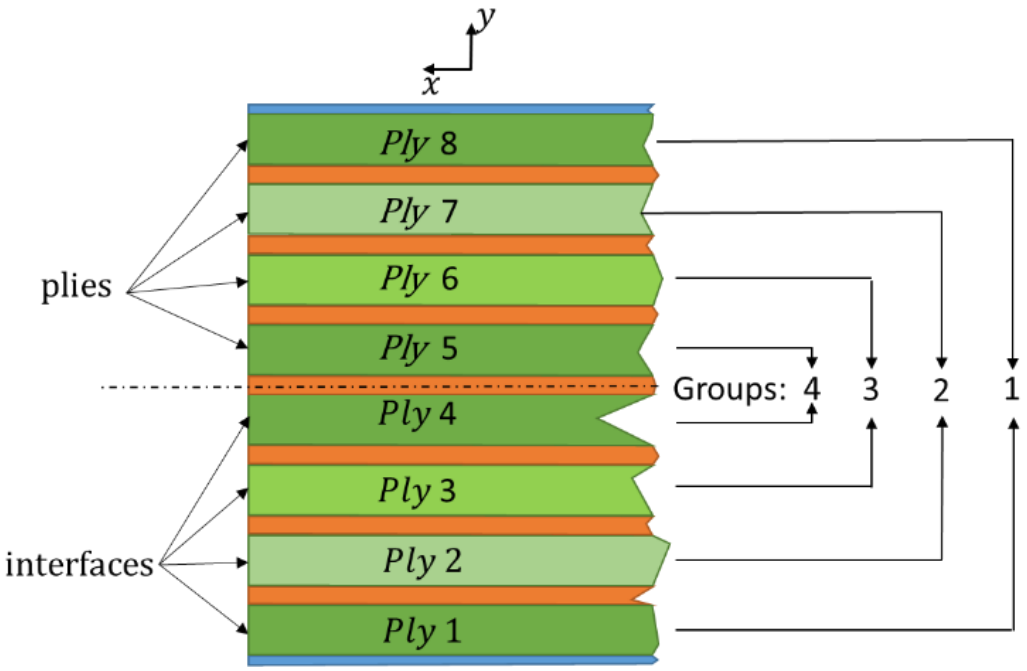

Figure 5.4 Lamination groups

Also, the mixture law [186] is used to introduce the variation of ply properties as a function of fiber fraction volume, fiber properties, and matrix properties, as shown in equation 5.15

$$Q(p_6) = E_m \frac{1}{\left(1 - V_f\right) + \frac{E_m}{E_f} V_f} \qquad 5.15$$

In the equation above, the sub-index f means the property of the fiber and the sub-index m means the property of the matrix.

Finally, taking into account the symmetry restriction, we fixed the number of plies to either 8 or 6 for the sake of simplicity in this work. However, the number of plies may be unlimited using the same methodology. Equations 5.16 and 5.17 are the functions in the domain p_7 modifying the number of plies.

$$R1(p_7) = \begin{cases} 1 \; if \; r \geq 8 \\ 1 \times 10^{-14} \; otherwise \end{cases} \quad 5.16$$

$$R2(p_7) = \begin{cases} 1 \; if \; r \geq 6 \\ 1 \times 10^{-14} \; otherwise \end{cases} \quad 5.17$$

After analyzing the displacement field in Chapter 4, we consider the particularity of viscoelasticity at the interfaces as both the phenomena of creeping and stress relaxation in the laminated structure. This viscoelastic behavior is modeled by the Zener's model (equation 5.18) at the level of the interfaces, having as variable parameter the fractional order of the derivatives.

$$\sigma(t) + \tau^{\alpha} \frac{d^{\alpha}\sigma(t)}{dt^{\alpha}} = G_0 \varepsilon(t) + G_{\infty}\tau^{\alpha} \frac{d^{\alpha}\varepsilon(t)}{dt^{\alpha}} \quad 5.18$$

Equation 5.9 is integrating for dynamic behavior and added an element named C_{int} (equation 5.19)

$$\boldsymbol{C}_{int} = f\left(E_m, G_m, Visc_{p5}, R1_{p7}, R2_{p7}\right) \quad 5.19$$

Equation 5.19 contains both the elastic behavior and the viscous behavior:

- The matrix makes the interfaces, therefore E_m, G_m represent the Young's modulus and shear modulus, both forming the elastic law of the interfaces. These interfaces have an isotropic behavior.
- $R1(p_7), R2(p_7)$ are intermediate functions allowing to control the number of interfaces in the laminated structure.

- The viscous parameter function P_5 (equation 5.19) uses the discrete version of the Zener's model with fractional derivatives (equation 5.20) as presented in section 4.4

$$Visc_{p5} = \left(1 - \frac{\tau^{\alpha}}{\tau^{\alpha} + \Delta t^{\alpha}}\right)\frac{G_{\infty} - G_0}{G_{\infty}}\boldsymbol{\varepsilon}_{xy\ inst}(t) - \frac{\tau^{\alpha}}{\tau^{\alpha} + \Delta t^{\alpha}}\sum_{j=1}^{N_t} w_j \boldsymbol{\varepsilon}^{i}_{xy\ mem}(t - j\Delta t) \qquad 5.20$$

By this manner, the short-term shear modulus G_0, the long term shear modulus G_∞ and the decay time τ are fixed,

$$\mathrm{G_0} = 3{,}24 \times 10^6\ \mathrm{Pa}$$

$$\mathrm{G_\infty} = 5 \times 10^9\ \mathrm{Pa}$$

$$\tau = 1.031 \times 10^{-7}\ \mathrm{s}$$

Moreover, the fractional operator α is a parameter, the nature of the interface.

$$0 < \alpha \leq 1$$

So far we have described the different variables, parameters and models making the PKM.

5.3.2 Modeling of design objectives

The objective function is different for the static or the dynamic case. Both versions are described in Table 5-2. Note that in this particular implementation, a weighted method was used to convert the multiple objectives into one. This assumes that the individual objectives are convex and that the Pareto front is well behaved. A rank-based approach could indeed be used to generate non-dominated solutions, so this is a future perspective. However, our goal was to

show that the methodology can produce a result, and our selected approach was the first try at coupling the PGD with an optimizer.

Table 5-2. Design objectives for the static and dynamic case

Static behavior		**Dynamic behavior**	
$F_0 = \varsigma R + \xi \mathcal{L}_{max} + c$	5.21	$F_0 = \varsigma R + \xi \mathcal{L}_{max} + \psi T_{max} + c$	5.22
The optimization problem establishes two design objectives, - Minimization of the number of plies (R) - Minimization of the maximum deformation in the vertical direction $(\mathcal{L}_{max})$ Moreover, a penalty function c introduces the constraints (see below)		The optimization problem establishes three design objectives as a function of time, - Minimization of the number of plies (R) - Minimization of the maximum deformation in the vertical direction $(\mathcal{L}_{max})$ - Minimization of the twist along the plate (T) Moreover, a penalty function c introduces the constraints (see below)	
The coefficients ς, ξ and ψ are weights assigned to the individual objectives according to the designer's experience and preference.			

Each potential solution is allocated a measure of adaptation or fitness calculated from the respective equations above.

5.3.3 Modeling of design constraints

Within the model, ply symmetry is enforced by specifying couples of mirror plies. On the other hand, the procedure evaluates the feasibility of every candidate solution by checking the Tsai-Hill as shown in equation (5.23) (Kamiński [187]):

$$\begin{cases} Th = \dfrac{\sigma_x^2}{T_x^2} + \dfrac{\sigma_y^2}{T_y^2} + \dfrac{\sigma_z^2}{T_z^2} - \sigma_y\sigma_z\left(\dfrac{1}{T_x^2} + \dfrac{1}{T_y^2} + \dfrac{1}{T_z^2}\right) - \sigma_x\sigma_z\left(\dfrac{1}{T_x^2} + \dfrac{1}{T_y^2} + \dfrac{1}{T_z^2}\right) \\ \qquad -\sigma_x\sigma_y\left(\dfrac{1}{T_x^2} + \dfrac{1}{T_y^2} + \dfrac{1}{T_z^2}\right) + \dfrac{\sigma_{yz}^2}{T_{yz}^2} + \dfrac{\sigma_{xz}^2}{T_{xz}^2} + \dfrac{\sigma_{xy}^2}{T_{xy}^2} \\ Th < 1 \end{cases} \quad 5.23$$

Then, the objective function is complemented by the penalty function shown in equation 5.24,

$$c = \begin{cases} 0;\ if\ Th < 1 \\ 10;\ if\ Th > 1 \end{cases} \quad 5.24$$

5.4 Optimization: a strategy to explore design spaces interactively

5.4.1 The choice of evolutionary approach

Given the nature and quantity of the design parameters, we use an evolutionary algorithm (EA) because contrary to a gradient-based optimization tied to the Finite Elements, these can handle discrete variables. Generally speaking, an EA perform searching loops through the following steps,

a) An initial population
b) A fitness evaluation of every candidate solution
c) A selection of the best suitable solutions produces a new population
d) An alteration of the population
e) Goes to b) until convergence is reached

The main particularity of a GA is the way the population is altered; it is based on Darwin's theory of evolution and natural selection and operated by

crossing genes between solutions to find improved children and to mutate genetic information to introduce noise in order to keep a certain degree of diversity within the population in new generations. The detailed steps defined by the GA are presented in Figure 5.5.

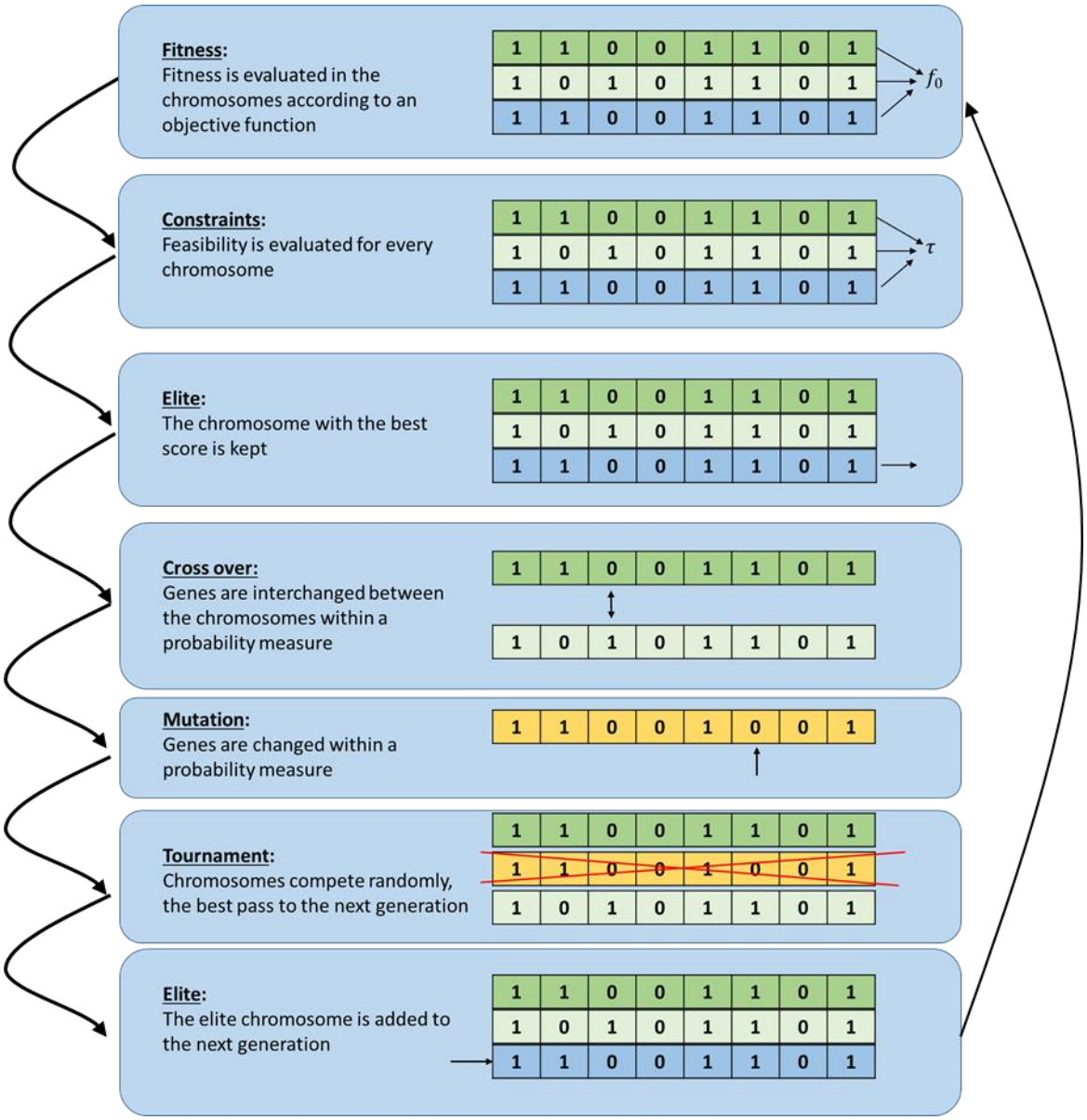

Figure 5.5. Genetic Algorithm routine

5.4.2 From the PKM to the optimization model

This work aims to use the Knowledge Model to compute the fitness of every candidate solution generated by the GA and evolve the solutions towards

an optimum. As the algorithm iterates, the new generations are distributed around the global optimum using the value (score) of the objective function, rather than the gradient, such as in the gradient-based approach.

Finally, our optimization model contains the PKM, the design objectives and the constraints. The optimization model is detailed in Figure 5.6

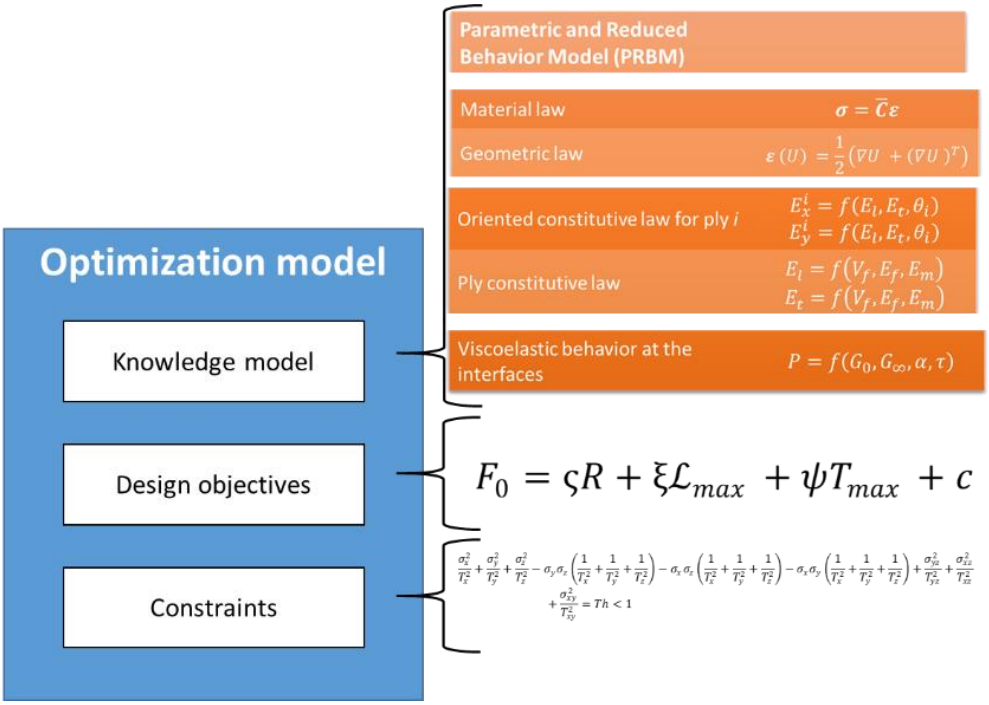

Figure 5.6 Optimization model.

5.5 Modeling a design problem for GA processing

5.5.1 Representation of the chromosome

In order to address the optimization problem described in the last section, we define a chromosome with seven genes as shown in Figure 5.7

Gene 1 Ply orientation $\theta 1$	Gene 2 Ply orientation $\theta 2$	Gene 3 Ply orientation $\theta 3$	Gene 4 Ply orientation $\theta 4$	Gene 5 Fiber volume fraction V_f	Gene 6 Viscous parameter α	Gene 7 Number of plies p_7

Figure 5.7 Representation of the chromosome.

Each gene is 8-bit long

Gene 1 - 4

Using as a reference the structure's x axes to define 0° (Figure 1.2), the first four genes shown in Figure 5.8 are reserved for ply orientation for one layer and its corresponding symmetric layer as shown in Figure 5.4. The orientation of the plies may range from -90° up to +90°. The number of bits (2^8) translates to 256 increments which, produces Δ_{ply} increments of,

$$\Delta_{ply} = \frac{180°}{256} \approx 0.7$$

These increments are rounded to the closest integer. In practice, these could still be small, but our interest is to find out if it is possible to define better configurations than the standard 30° increments, while we appreciate the difficulty of being able to be so precise in the manufacturing process.

Gene 1 Ply orientation $\theta 1$	Gene 2 Ply orientation $\theta 2$	Gene 3 Ply orientation $\theta 3$	Gene 4 Ply orientation $\theta 4$	Gene 5 Fiber volume fraction V_f	Gene 6 Viscous parameter α	Gene 7 Number of plies p_7

Figure 5.8 Genes related to ply orientation.

Note that gene 4 is affected by the number of plies, indeed if six plies are being considered, this gene is excluded from the computations. If additional plies are desired, the chromosome is extended to include more ply orientation genes using the same methodology.

Gene 5

The fiber fraction volume modifies the properties of all plies in gene 5 (Figure 5.9), as described by equation 5.15. In this relation, the fiber volume fraction can range from 50% to 60%. Considering an 8 bits gene, the 10% span is represented by 28 or 256 values and the increments Δ_f are,

$$\Delta_f = \frac{10}{256} \approx 0.04\%$$

Gene 1 Ply orientation $\theta 1$	Gene 2 Ply orientation $\theta 2$	Gene 3 Ply orientation $\theta 3$	Gene 4 Ply orientation $\theta 4$	Gene 5 Fiber volume fraction V_f	Gene 6 Viscous parameter α	Gene 7 Number of plies p_7

Figure 5.9 Gene related to fiber fraction volume.

Gene 6

The viscous nature of the interfaces between plies is chosen in Gene 6 (Figure 5.10). According to the explanation in section 5.3.1, the free parameter is the fractional order of the derivatives in the Zener model (α). This parameter may go from 0 to 1. Considering 8 bits, the increments Δ_α are,

$$\Delta_\alpha = \frac{1}{256} \approx 0.004$$

Gene 1 Ply orientation $\theta 1$	Gene 2 Ply orientation $\theta 2$	Gene 3 Ply orientation $\theta 3$	Gene 4 Ply orientation $\theta 4$	Gene 5 Fiber volume fraction V_f	Gene 6 Viscous parameter α	Gene 7 Number of plies p_7

Figure 5.10 Gene related to viscous parameter.

Gene 7

Finally, the number of plies is chosen by Gene 7 (Figure 5.11). This option is discrete. In this work, it is only possible to select either 6 or 8 plies. However, the number of plies may be expanded to many more using the same methodology. Indeed, the advantage of the GA is that it can handle either continuous or discrete parameters.

Gene 1 Ply orientation $\theta 1$	Gene 2 Ply orientation $\theta 2$	Gene 3 Ply orientation $\theta 3$	Gene 4 Ply orientation $\theta 4$	Gene 5 Fiber volume fraction V_f	Gene 6 Viscous parameter α	Gene 7 Number of plies p_7

Figure 5.11 Gene related to the number of plies.

5.5.2 Description of the optimization process.

The optimization problem is set with the configuration presented in Table 5-3

Table 5-3. Population characteristics.

Number of bits/genes	8
Population size	50

The process of optimization is based on the four common genetic operations being: (1) the Selection, (2) the Cross-over between chromosomes, (3) the gene Mutation, (4) the identification of Elites [188]**.**

The characteristics of the optimization process are given in Table 5-4.

Table 5-4. Population of the generation.

Number of generations	50
Crossover probability	80%
Mutation probability	4%

The algorithm strategy is such that an elite chromosome is kept at every generation, based on the best score out of the objective function. Equations (5.21- 5.22).

Most of the tests being implemented show the algorithm converges after around 40 some generations.

As a reminder, the problem is to design a composite plate such that:

- In static behavior, the values of design parameters that minimize both the number of plies and the maximum displacement are sought.

- In dynamic behavior, the values of design parameters that minimize the number of plies, the displacement and the twist at the free end are desired.

5.6 A design problem solving

5.6.1 Design problem details: a laminated composite plate

We consider a laminate plate 250 mm long (l) and 150 mm wide (w), shown in Figure 5.12, made by prepreg laminates of the type M21/T800. The plate is fixed at one end and subject to a load in one corner of the free end.

In the static case, a side load is imposed on one of the free edges, while in the dynamic case, the out of plane corner load is sinusoidal in magnitude. Our objective is to design the plate to minimize deflection and twist in both the static and dynamic cases Figure 5.12.

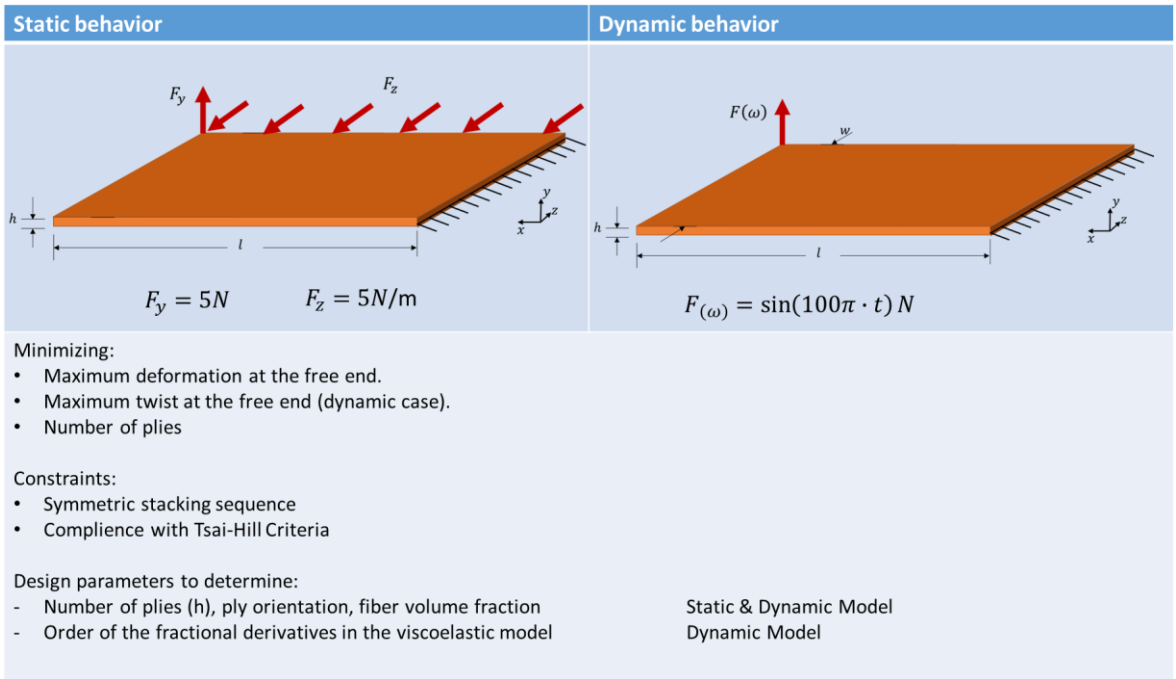

Figure 5.12. Plate under study

As mentioned earlier, we are using a genetic algorithm to solve the problem, connecting the PKM to the GA. We must, therefore, describe the encoding of the variables, and discuss the operators used before showing results.

5.6.2 Design solutions after optimization

From two optimization models:

- One for identifying the design solution from objectives in static behavior.
- The other one for identifying appropriate design solutions from objectives in dynamic behavior.

Both solutions are given in Table 5-5

Table 5-5. Design solutions

	Static behavior	**Dynamic behavior**
Behavior of the design solution	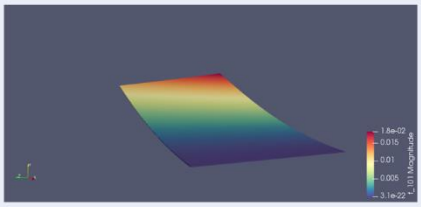 Maximum displacement: 18.12 mm	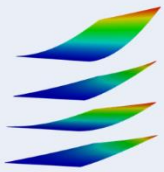 Maximum displacement: 0.76 mm Maximum twist: 0.92 mm
Design parameters	Number of plies: 8 Ply orientation: 20°/-28°/46°/22°/22°/46°/-28°/20° Carbon fiber: Matrix M21 (HexPly M21) Fraction of fiber volume: 57%	Number of plies: 8 Ply orientation: 5°/-12°/65°/-32°/-32°/65°/-12°/5° Carbon fiber: Matrix M21 (HexPly M21) Fraction of fiber volume: 52% Viscous Fractional parameter α: 0.66

We processed a discrete continuous optimization model: even if our approach is discrete because of the number of plies, all other objective variables are varying in continuous domains. Our approach is different from a standard finite element approach that cannot consider the number of plies as a parameter. In other words, the discrete approach based on a feasibility map is not our selected one because we can explore continuous domains for ply orientation,

fiber volume fraction and the viscosity parameter. Figure 5.13 presents the solution space when we are looking for good solutions in the case of static behavior: our solution space is discrete and also continuous.

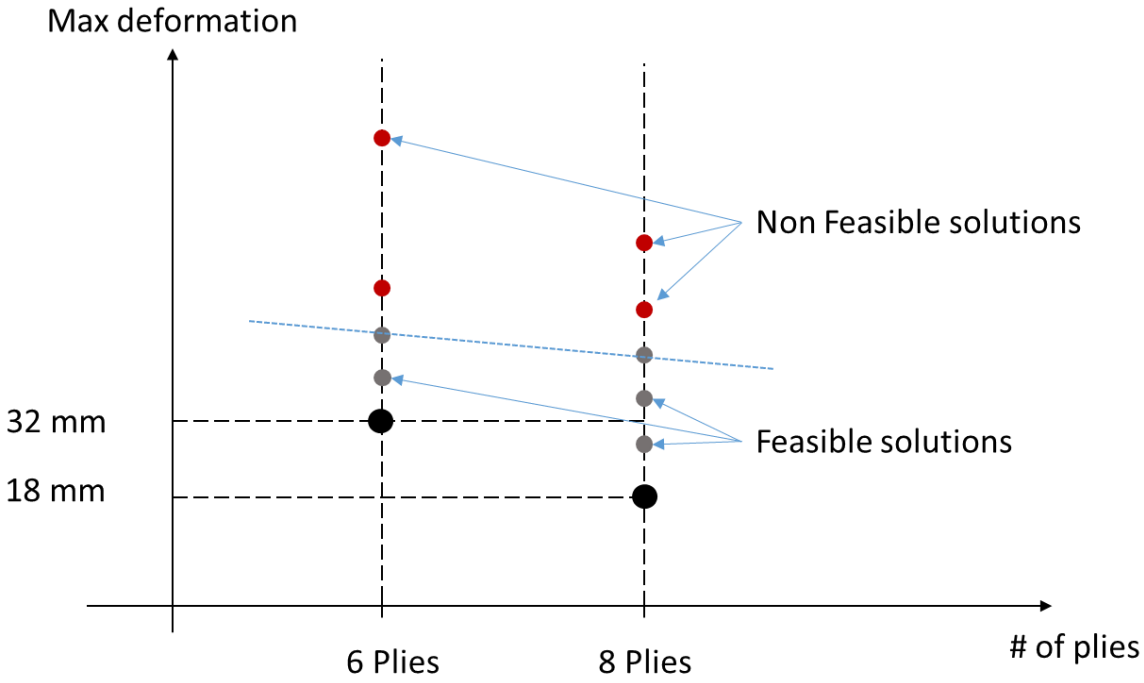

Figure 5.13 Two sets of solutions forming a non-dominated or possibly Pareto front in static behavior

In the following section we comment on the processing cost and design solution results.

5.6.3 Design of laminated composite structures from the PKM

Design optimization of laminated composites was addressed and carried out in this work. In order to maintain the computational cost reasonable, while targeting obtaining more detailed information on the behavior of the composite ply-by-ply significantly, we used a reduced behavior model that is also parametrized (the PRBM). This model is coupled with a Genetic algorithm to find optimal solutions. The results show that optimized solutions may be obtained at stacking orientations different from the common stacking sequences chosen in industry. The results also generate future perspectives to develop the viscoelastic

nature of the interfaces to obtain particular dynamic characteristics of the laminate structure.

We also showed that the PKM in the design of laminated composite materials is flexible because it may be used either as a regular fast solver for dimensioning in a standard design process or earlier as a DMSS during preliminary design Figure 5.14. The latter makes the PRBM able to skip the detailed design phase and the dimensioning phase, and directly obtain the information needed for the production of an optimized solution.

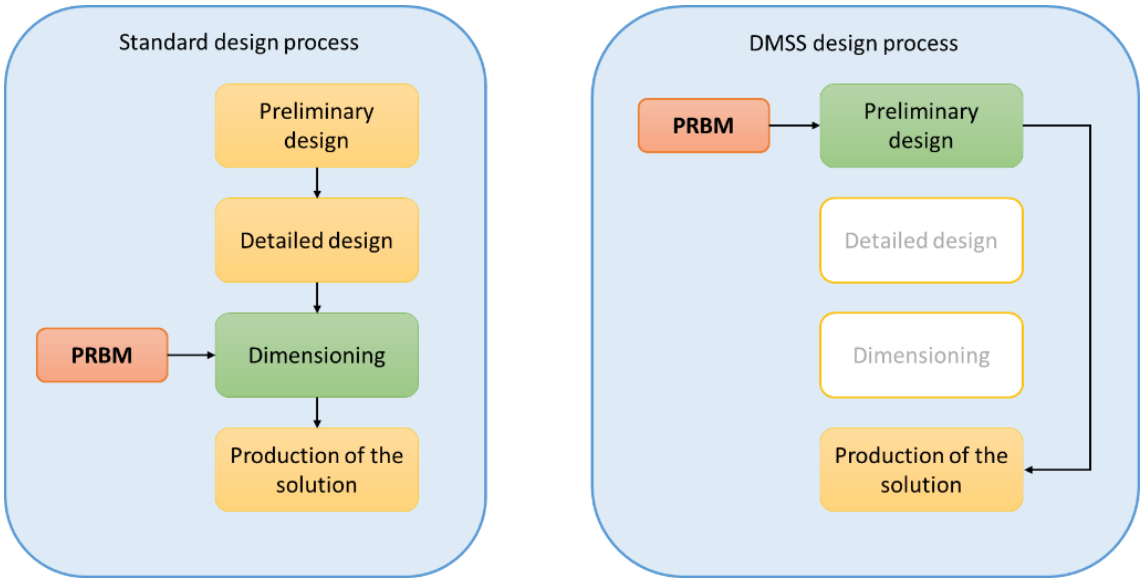

Figure 5.14. Supporting decision making during design

5.7 Qualification

Qualifying a model is analyzing the results regarding parsimony, accuracy, precision, and specialization; this is known as PEPS. Therefore, qualifying is not just validating a model; PEPS also embraces other variables as the complexity, computational cost and computing time. We aim at qualifying the dynamic results obtained from the optimization procedure in section 5.6. This qualification may be used for feasibility analysis in further developments.

5.7.1 Performance of the optimization process

The primary computational processing time relates to the generation of the PRBM. The computational cost is presented in Table 5-6.

The computations were run on a Pentium i7 laptop with 16 Gb of RAM, on a virtual machine set on Linux.

Table 5-6. Computation time of the optimization process

	Static behavior	Dynamic behavior
Time to build the PRBM (ready for simulation and processing)	25 min	360 min
Time searching optimized solutions	75 min	520 min

5.7.2 Qualification of the design solution having static behavior: validation from a FEM simulation

In order to validate the results obtained using the PRBM, we simulated a design solution obtained from the static behavior optimization using ANSYS ACP®, with shell elements. The difference between the PRBM solutions and ANSYS simulation is 5,8 % (Table 5-7).

Table 5-7 Comparison between PRBM and FE solutions in the static case

	Solution based on PRBM	FE Analysis
Behavior of the design solution	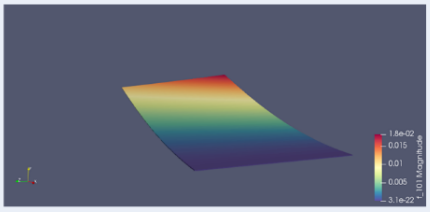 Maximum displacement: 18 mm	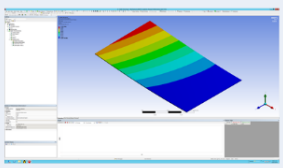 Maximum displacement: 17 mm

Our approach allows having a separated and multi-scale approach. So the results benefit this particularity by presenting nonstandard solutions.

The advantage of our modeling approach is that we can have information on the behavior ply-by-ply and interface-by-interface. We can reproduce the zig-zag behavior occurring in a laminated structure Figure 5.15. However, we were not able to validate the dynamic behavior of the optimized solution because we currently lack information on the viscous properties of each interface. Instead, we perform experimental tests to validate our simulation work in the following section.

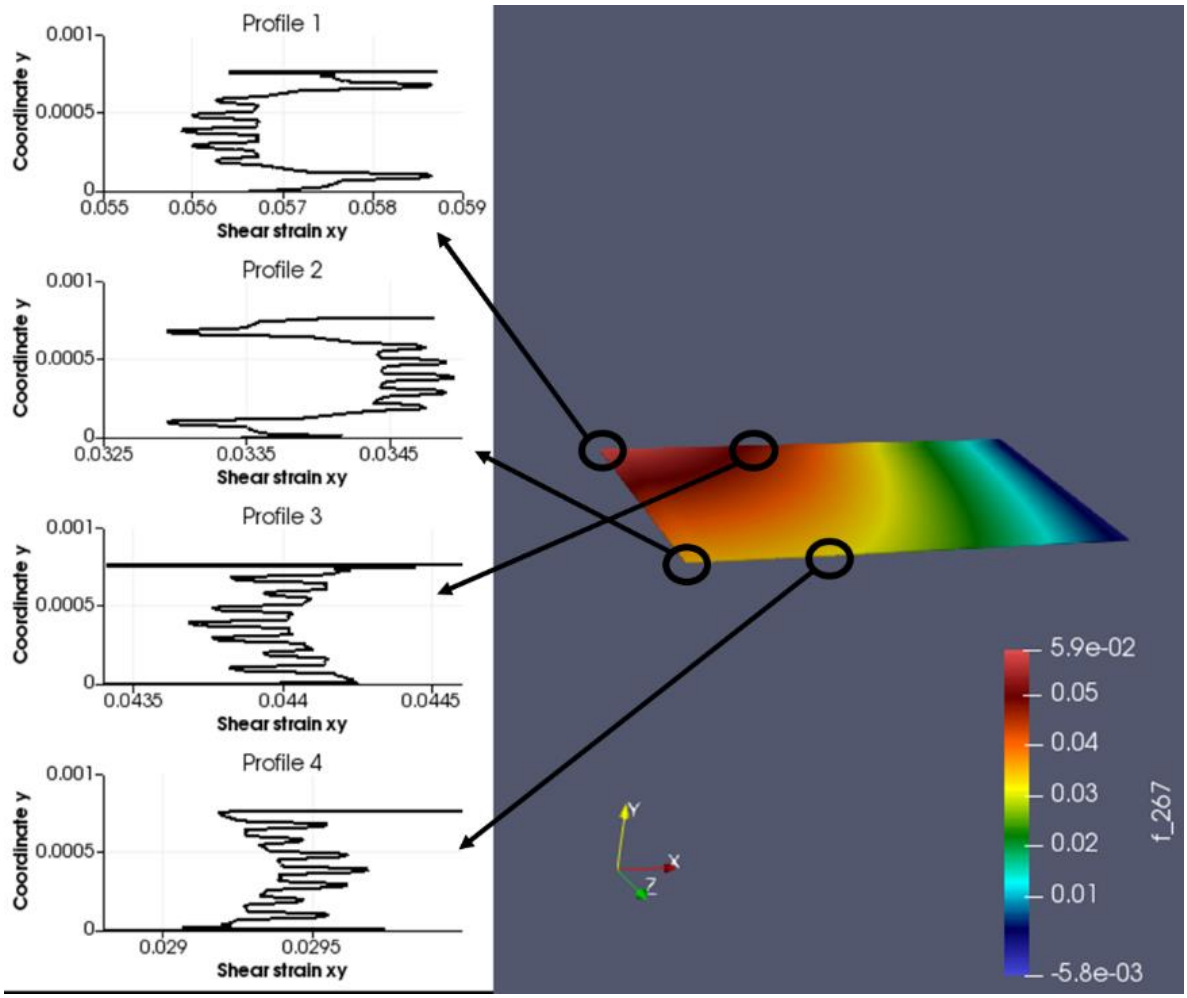

Figure 5.15 shear strain through the thickness

Qualification: **Laminated composite structure having a static behavior**

We qualified the design solution obtained by realizing design objectives for a product aiming at having a static behavior with the following statements:

- Reference for the qualification:
  FEM-based simulation of the design solution
  Error predicting maximum deformation: 5.5 %
  Time searching optimized solutions: 1h 15 min
- Terms of qualification
  The PRBM is qualified with a risk of
  The design method is qualified to lead to consistent design solutions

5.7.3 Qualification of the design solution having dynamic behavior: validation from experiments

In order to proceed with a dynamic experimental test, we manufactured a plaque with the overall characteristics presented in Table 5-8. These are obtained from the results of the optimization procedure in section 5.6.

Table 5-8. Overall characteristics of the optimized structure

Dimensions	Length: 250 mm Wide: 150 mm
Number of plies	8
Stacking sequence	[5 /-12 / 65 / -32 / -32 / 65 / -12 / 5]
Material type	Prepreg unidirectional,

	carbon fiber reinforcement
	Type Hexply M-21

The test set up follows the same recommendations of ISO 7626-2, described in section 4.2. The details are represented in Figure 5.16 and the actual set-up in Figure 5.17.

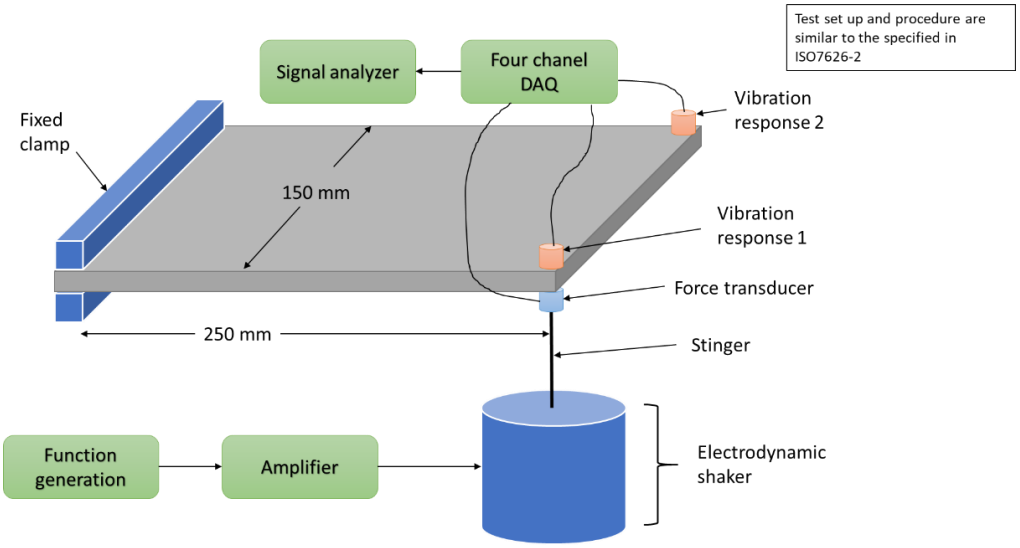

Figure 5.16. Experimental dynamic set-up

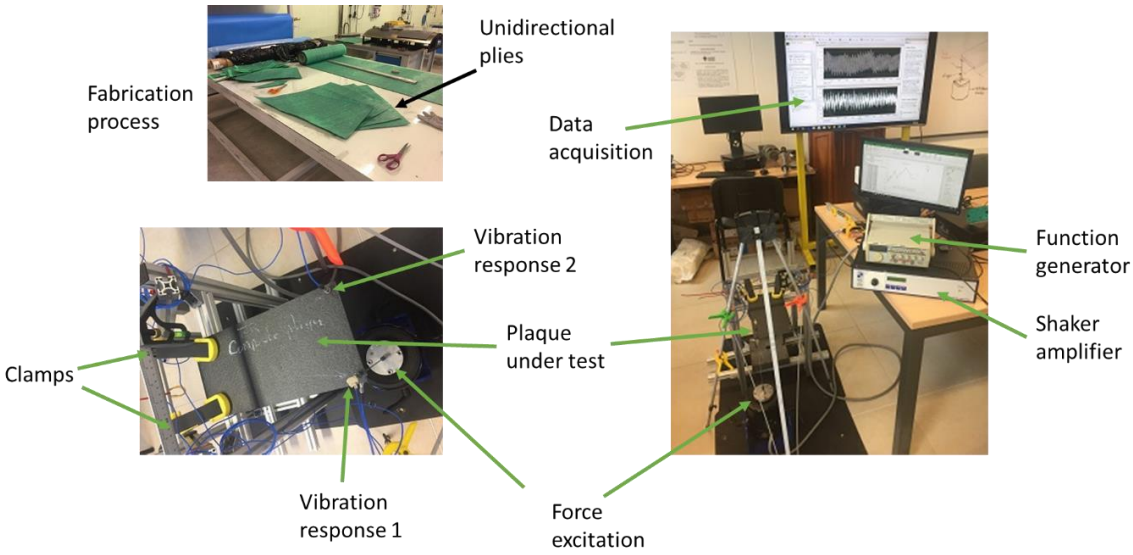

Figure 5.17. Actual dynamic set-up

The excitation was measured by a force transducer PCB 208C01 and the vibration responses by miniature accelerometers PCB 352C68.

The first test is verifying whether the excitation frequency used in the simulation is a resonance. Therefore, we need frequency response functions (FRF) to measure the natural frequencies nearby the frequency of the force used in the simulation (50 Hz). Table 5-9 defines the convention used for the FRF according to Figure 5.16 or Figure 5.17.

Table 5-9. Convention for the FRF. ω is the angular frequency

FRF 1	$\frac{vibration\ response\ 1\ (\omega)}{Force\ excitation\ (\omega)}$
FRF 2	$\frac{Vibration\ response\ 2\ (\omega)}{Force\ excitation\ (\omega)}$

Using the shaker, we performed a sinusoidal swept from 10 Hz to 80 Hz in 60 sec. The Bode plot in Figure 5.18 shows the resulting FRF1 and FRF2 using linear averaging. These two FRF reveal a first natural frequency of 25 Hz and a second of 59 Hz. Therefore, we know that the excitation simulated by the PRBM, with a force of 1 N at 50 Hz is not likely to represent a resonance frequency. Furthermore, in Figure 5.18 (phase plot) and Figure 5.20, we note a phase lag of 23° between excitation an vibration response, confirming the viscoelastic response of the structure.

From the bode plots in Figure 5.18, we can derive the modal shapes (Figure 5.19). They are essential because the vibration response of the plaque under an excitation frequency of 50 Hz is mostly a combination between the mode shape at the first natural frequency of 25 Hz, with a longitudinal mode, and the mode shape at the second natural frequency of 59 Hz, with a twist mode.

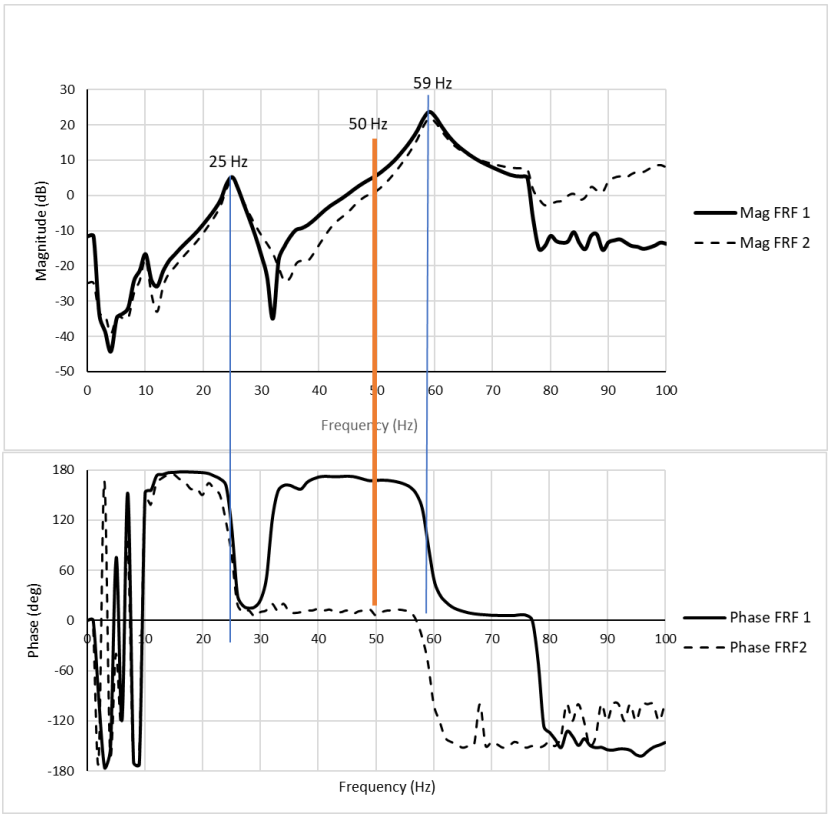

Figure 5.18. Frequency response functions. Above: magnitude response, below: phase.

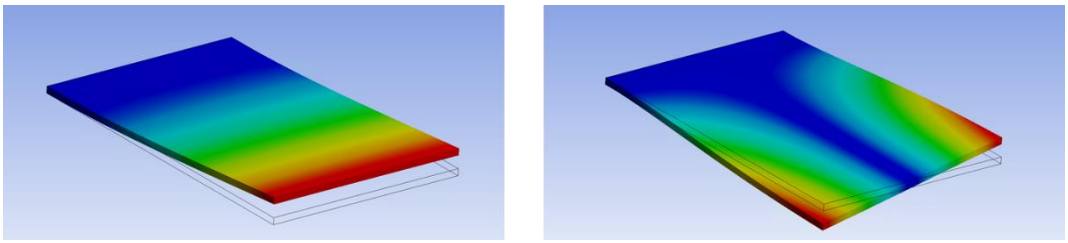

Figure 5.19. Mode shapes. Left: at natural frequency 1 (25 Hz).
Right: at natural frequency 2 (59 Hz)

The second step is to generate the same force simulated in the PRBM. So, from the shaker, we introduce a force of 1 N peak at 50 Hz. Figure 5.20 and Figure 5.21 show the excitation force and the displacement responses obtained by double integration of the signal from the accelerometers and by applying a high pass filter of order 2 with cut out frequency of 10 Hz.

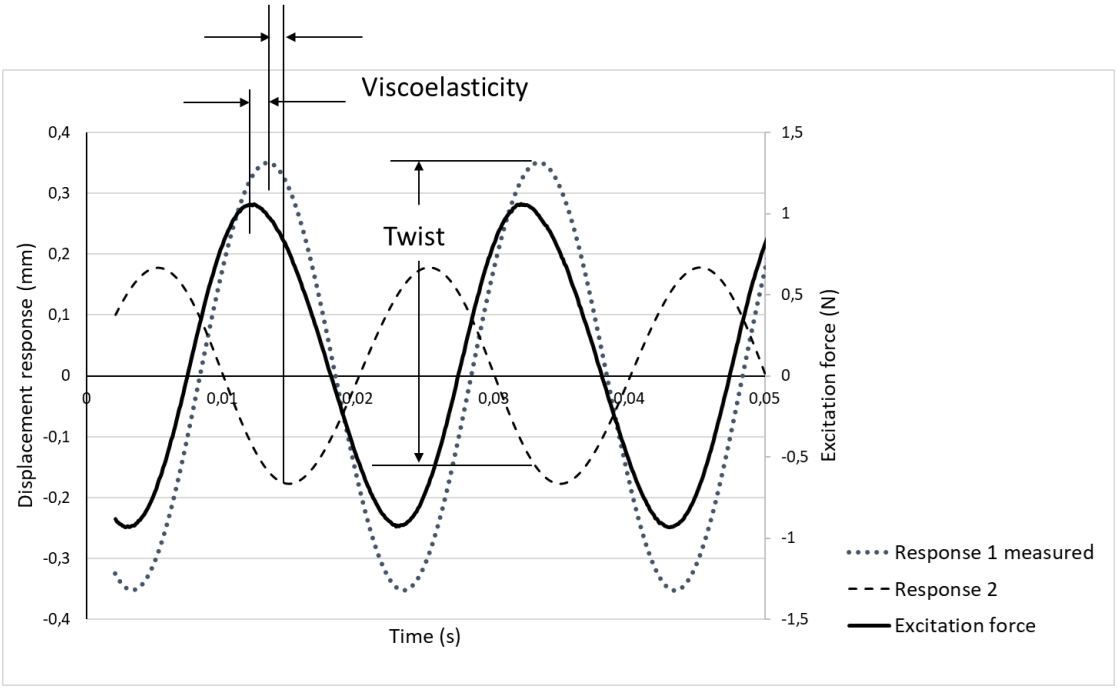

Figure 5.20. Excitation force and vibration responses.

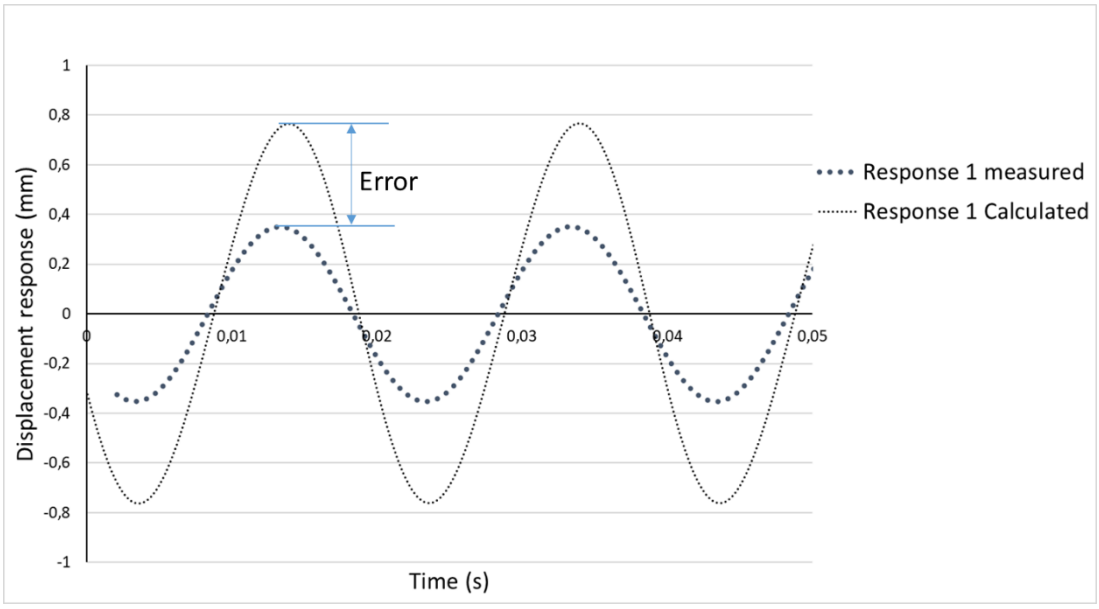

Figure 5.21. Simulated displacement vibration (response 1) vs. measured (response 1)

Table 5-10 summarizes the validation, regarding maximum displacement and twist.

Table 5-10. Comparing simulated vs. measured maximum displacement and twist.

	Predicted by the PRBM	Measured in the experimental test	Difference
Maximum displacement	0,76 mm	0,40	0, 35 mm
Maximum twist	0,92 mm	0,17 mm	0,52 mm

The differences between predicted vs. measured in Table 5-10 are not too high, considering the following sources of error:

1. The fabrication procedure is not strictly controlled; we did a hand layup.
2. The clamps used in the test set-up do not damage the plaque, but they introduce some compliance.
3. The vibration deformation responses of the structure were derived by double integration from accelerometers and by filtering. Improving the accuracy requires a laser vibrometer not available in our lab.
4. A process to control the viscoelastic fractional parameters of the interfaces between plies ($G_0, G_\infty, \tau, \alpha$) does not exist. This is a future perspective.

However, the most exciting results are related to the capacity of the optimization procedure to consider the fractional parameter α within the computations. In order to analyze this capacity, in Figure 5.22 we plotted the loss factor η as a function of frequency, using the methodology presented by Pritz [66] and by curve fitting using the half-power method on the first two natural frequencies of the plaque under study.

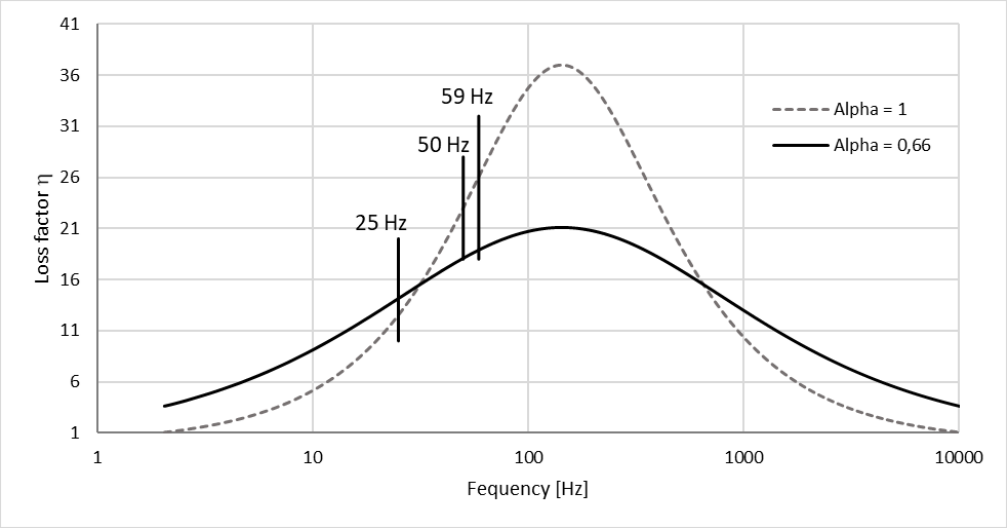

Figure 5.22. Loss factor η vs. frequency.

In Figure 5.22 we can see that the optimization algorithm was attempting to find the optimal α, such that the minimum twist with a forced excitation frequency of 50 Hz is achieved by maximizing the loss factor at the natural frequency presented in 59 Hz, with twisting mode shape (Figure 5.19, right); but at the expense of diminishing the lost factor of the first natural frequency presented with 25 Hz, thus increasing the influence of the longitudinal mode (Figure 5.19, left) over the maximum deformation.

The process of qualification in this approach is divided into two stages. The stage one is the development of the PRBM using the PGD method (Table 5-11). The stage two is about the use of the PRBM linked to a PKM in an optimization problem (Table 5-12).

Table 5-11. Qualifying the computation of the PRBM

Computing the PRBM	Evaluation
Parsimony	The computation of the PRBM is time consuming, both regarding human development and computing resources. The parsimony is high. (see Table 5-6)
Accuracy	This step is about computing a reduced model. Therefore accuracy does not apply.
Precision	This step is about computing a reduced model. Therefore precision does not apply
Specialization	The specialization required is exceptionally high because of the complex mathematical models and since the development of the PGD method is new.

Table 5-12. Qualifying the use of the PRBM in an optimization problem

Using the DMSS	Evaluation
Parsimony	We succeed in finding solutions using low computational resources in a short time. The parsimony is low. (see Table 5-6)
Accuracy	The accuracy on the maximum deformation and twist were not very accurate, mainly because of the difficulties during the manufacture of the plaque. However, the results showed the ability of the model to explore optimal viscoelastic parameters to find improved vibration response characteristics. The accuracy is good.
Precision	The model always converged towards the same results. Therefore the precision is good.
Specialization	The specialization required to operate the DMSS is low because it does not require sophisticated mathematical models. The solutions are already embedded in the knowledge model

Qualification: **Laminated composite structure having a dynamic behavior**

We qualified the design solution obtained by realizing design objectives for a product aiming at having a dynamic behavior with the following statements:

- Reference for the qualification:
  Experimental plan applied to the design solution
  Error to predict max deformation: 47 %
  Error to predict max twist: 81 %
  Creeping / phase difference: 2,2 %
  Time exploring optimized solutions: 8h 40 min
- Terms of qualification
  The PRBM is efficient regarding the creeping solution, but it does not integrate manufacturing parameters that modified the stiffness of the structure.
  The design method is qualified, it leads to consistent design solutions regarding the creeping behavior.

5.8 Conclusion

In this chapter, we developed a knowledge model having embedded a PRBM containing information about critical parameters of the design in a laminated structure. We demonstrated the use of the PRBM as a fast solver during the dimensioning phase on design, but also during preliminary design in a

process assisted by a DMSS. With this concept, we solved a design problem to find the optimal solution of a plate under static load and dynamic load.

This development is a new contribution; it allows a design engineer to explore optimal solutions interactively, while the complexities of the computations are embedded in the knowledge model.

Chapter 6

CONCLUSIONS AND PERSPECTIVES

6.1 Conclusions

In this thesis, we addressed the problem of the design of laminated composite materials. The objective was to develop a new numeric approach, such that a design engineer could manipulate every design parameter characterizing the composite structure, regardless of the scale where the parameter is relevant.

In a composite structure, the combination of fibers and resin implies that the mechanical performance highly depends on the internal microstructure, the fabrication process, and the thermal regime. Ideally, the development of advanced material technologies requires to account for all this, so the only option in design is to simulate the micromechanics; that is, increasing the level of detail at smaller scales in the simulations to link more related physical phenomena to bigger scales.

Our first step was to analyze current CAE tools used by engineers to design composite structures. Design engineers face the problem of whether simplifying their simulations to obtain only global perspectives, withdrawing many essential design parameters to known practices within the manufacturing process, or performing highly specialized and expensive simulations to account for lower scales.

The state of the art advances in simulation capacities for analysis made evident the interest in incorporating details of the composite structures at lower scales. Examples of these advances are the zig-zag theories and the use of high-performance computers to link into the macroscale representative volume elements of the microstructure. A trend is also devoted to incorporate multiphysical capabilities, precisely at the interfaces where the stress transfer between the components of the lamination occurs.

On the other hand, advances on DMSS are incorporating models to find optimal solutions of specialized laminated composites explicitly. However, their limitation is the vast amount of computations required by optimization algorithms, given the immense computational cost of each potential solution.

At this stage, we identified the need for a reduced model. For this purpose, we used the PGD method to produce a Spatial and Separated Model (SSM), the result is undoubtedly the acceleration on the changes of scales, making them more integrated, which is already a step further. We identify two additional advantages: first, the SSM is not only resulting in a single solution but within a slight increment of computing time, we obtain a parametric model containing a set of solutions. Second, the SSM executes fast simulations requiring very light computational resources to obtain a particular solution.

Then we incorporated multiphysical capabilities in the reduced model. In this manner, we obtain a Parametric and Reduced Base Model (PRBM). The PRBM was used to quickly solve the problem of a laminated composite under dynamic load, including viscoelastic behavior within the interfaces between plies. The new contribution is the use of the Zener model with fractional derivatives to represent the viscoelastic behavior of the matrix conforming the interfaces. Nevertheless, the manipulation of the multiphysical mechanics at different scales using the PGD still may imply significant computing resources and long waiting time to obtain a PRBM.

A new contribution is also integrating a PRBM to a Parametric Knowledge Model (PKM). This is a numerical approach for fast exploration of the design

parameters in different scales, finding optimal solutions of a laminated composite for the case of both, a static and a dynamic load. The PKM uses a genetic algorithm, and the optimization is continuous, so a design engineer may interactively set behavior objectives to obtain specialized configurations, without complex mathematical models. Finally, we validated the solutions versus a FEM model in the case of static load and a dynamic experimental test in the case of a dynamic load. We concluded from the experimental test that the optimization algorithm could adjust the fractional parameters to obtain optimized vibration characteristics.

6.2 Perspectives

Despite using harmonic force excitation loads for the solution of the dynamic problems, we implemented a time incremental scheme due to the non-linear character of the models. The first perspective for further development is to evaluate the feasibility of a non-linear non-incremental time-based PRBM, similarly to the approach proposed by Ladevèze [143]. Otherwise, the perspective would be using artificial intelligence to find harmonic response patterns, thus improving the performance of the PRBM in optimization routines.

A second perspective is to make the optimization problem muti-objective. The capability of the PRBM to compute fast solutions makes possible to find improved specialized structures, being able to respond to the multiple requirements coming from the engineers involved in product design.

In order to continue improving accuracy, a third perspective is going deeper into the microscale, including new physical phenomena into the PRBM. In order to achieve this challenge, it is necessary to develop parallel computational capacities when a PRBM is calculated using the PGD method. Additionally, the performance of the finite element computations needs to be improved to avoid spurious matrices.

We succeeded at incorporating fractional derivative parameters of the Zener model to represent viscoelasticity in the PRBM. A fourth perspective is to define methodologies to characterize the parameters of the matrices accurately, not only on laminates but also in other types of composites. Consequently, many manufacturing processes may be redefined to achieve specialized composites.

Other perspectives using a multiscale reduced model such as the PRBM are failure identification, condition monitoring or real-time control of composite structures.

Alternatively, another personal research interest is the analysis of the dynamics of rotors in critical machinery, with applications in machinery condition monitoring, diagnosis, and prediction. Following the work by Cherabi et al. [189], a perspective in this field is to develop a PRBM to address the problem of the non-linear viscous response of journal bearings, tied to artificial intelligence capabilities for prognosis and performance optimization.

PERSONAL PUBLICATIONS

International journals

1. G. Fontecha-Dulcey, X. Fischer, P. Joyot. “An Experiment Based Method for Parameter identification of a Reduced Multiscale Parametric viscoelastic model of a laminated composite beam” Multiscale and Multidisciplinary Modeling, Experiments and Design. Springer, Jun. 2018. DOI:10.1007/s41939-018-0018-8

2. G. Fontecha-Dulcey, X. Fischer, P. Joyot, G. Fadel. “Support for Decision Making in Design of Composite Laminated Structures. Part 1: Parametric Knowledge Model” Applied Composite Materials. Springer, DOI: 10.1007/s10443-018-9741-x

3. G. Fontecha-Dulcey, X. Fischer, P. Joyot, G. Fadel. “Support for Decision Making in Design of Composite Laminated Structures. Part 2: Reduced Parametric Model-Based Optimization” Applied Composite Materials. Springer, DOI: 10.1007/s10443-018-9742-9

International workshops

1. G. Fontecha. “Optimization Approach to Support Decision Making during Interactive Design of Laminated Composite Structures”. Virtual Concept International Workshop on innovation in Engineering and Sciences. Monterrey, Mexico, 10 – 12 December 2018

2. G. Fontecha. “Exploring Design Solution Spaces to Support the Design for Manufacturing Process of Laminated Composite Structures”. Virtual Concept International Workshop on Advanced Manufacturing process and design for X in Industry 4.0. Bordeaux, 29-30 April 2019.

(This page is intentionally left blank)

REFERENCES

[1] D. Scaravetti, “Formalisation préalable d’un problème de conception pour l’aide à la décision en conception préliminaire,” ENSAM, 2004.

[2] D. G. Ullman, *The mechanical design process*, Sixth edition. Independence, Oregon: David G. Ullman, 2018.

[3] B. Bognet, F. Bordeu, F. Chinesta, A. Leygue, and A. Poitou, “Advanced simulation of models defined in plate geometries: 3D solutions with 2D computational complexity,” *Comput. Methods Appl. Mech. Eng.*, vol. 201–204, pp. 1–12, Jan. 2012.

[4] G. Couégnat, E. Martin, J. Lamon, and N. Carrère, “Approche multiéchelle du comportement mécanique des matériaux composites à renfort tissé.,” *Univ. Sci. Technol. - Bordx. I*, 2009.

[5] E. Carrera, “Theories and finite elements for multilayered, anisotropic, composite plates and shells,” *Arch. Comput. Methods Eng.*, vol. 9, no. 2, pp. 87–140, Jun. 2002.

[6] Z. Cheng, A. K. Jemah, and F. W. Williams, “Theory for Multilayered Anisotropic Plates With Weakened Interfaces,” *J. Appl. Mech.*, vol. 63, no. 4, p. 1019, 1996.

[7] E. Pruliere, F. Chinesta, and A. Ammar, “On the deterministic solution of multidimensional parametric models using the Proper Generalized Decomposition,” *Math. Comput. Simul.*, vol. 81, no. 4, pp. 791–810, Dec. 2010.

[8] A. Ammar, F. Chinesta, E. Cueto, and M. Doblaré, “Proper generalized decomposition of time-multiscale models,” *Int. J. Numer. Methods Eng.*, vol. 90, no. 5, pp. 569–596, May 2012.

[9] F. Chinesta, R. Keunings, and A. Leygue, *The Proper Generalized Decomposition for Advanced Numerical Simulations*. Cham: Springer International Publishing, 2014.

[10] A. Chattopadhyay, H. S. Kim, and A. Ghoshal, “Non-linear vibration analysis of smart composite structures with discrete delamination using a

refined layerwise theory," *J. Sound Vib.*, vol. 273, no. 1–2, pp. 387–407, May 2004.

[11] Z. Lei, X. Li, F. Qin, and W. Qiu, "Interfacial Micromechanics in Fibrous Composites: Design, Evaluation, and Models," *Sci. World J.*, vol. 2014, pp. 1–9, 2014.

[12] P. F. Liu, Z. P. Gu, and X. Q. Peng, "A nonlinear cohesive/friction coupled model for shear induced delamination of adhesive composite joint," *Int. J. Fract.*, vol. 199, no. 2, pp. 135–156, Jun. 2016.

[13] B. A. Budiman, K. Takahashi, K. Inaba, and K. Kishimoto, "A new method of evaluating interfacial properties of a fiber/matrix composite," *J. Compos. Mater.*, vol. 49, no. 4, pp. 465–475, Feb. 2015.

[14] R. Ramos and C. P. Pesce, "A Consistent Analytical Model to Predict the Structural Behavior of Flexible Risers Subjected to Combined Loads," *J. Offshore Mech. Arct. Eng.*, vol. 126, no. 2, p. 141, 2004.

[15] S. Lenci and J. Warminski, "Free and forced nonlinear oscillations of a two-layer composite beam with interface slip," *Nonlinear Dyn.*, vol. 70, no. 3, pp. 2071–2087, Nov. 2012.

[16] J. N. Reddy, "An evaluation of equivalent-single-layer and layerwise theories of composite laminates," *Compos. Struct.*, vol. 25, no. 1–4, pp. 21–35, Jan. 1993.

[17] F.-X. Irisarri, "Stratégies de calcul pour l'optimisation multiobjectif des structures composites," Université de Toulouse.

[18] L. Galuppi and G. Royer-Carfagni, "Laminated beams with viscoelastic interlayer," *Int. J. Solids Struct.*, vol. 49, no. 18, pp. 2637–2645, Sep. 2012.

[19] A. R. Bunsell and J. Renard, *Fundamentals of fibre reinforced composite materials*. Bristol: Institute of Physics Publishing, 2005.

[20] E. Carrera and A. Ciuffreda, "A unified formulation to assess theories of multilayered plates for various bending problems," *Compos. Struct.*, vol. 69, no. 3, pp. 271–293, Jul. 2005.

[21] E. Carrera, "Historical review of Zig-Zag theories for multilayered plates and shells," *Appl. Mech. Rev.*, vol. 56, no. 3, p. 287, 2003.

[22] E. Carrera, "On the use of the Murakami's zig-zag function in the modeling of layered plates and shells," *Comput. Struct.*, vol. 82, no. 7–8, pp. 541–554, Mar. 2004.

[23] E. Carrera and S. Brischetto, "A Survey With Numerical Assessment of Classical and Refined Theories for the Analysis of Sandwich Plates," *Appl. Mech. Rev.*, vol. 62, no. 1, p. 010803, 2009.

[24] S. Brischetto and E. Carrera, "Advanced mixed theories for bending analysis of functionally graded plates," *Comput. Struct.*, vol. 88, no. 23–24, pp. 1474–1483, Dec. 2010.

[25] E. Carrera and M. Petrolo, “Guidelines and Recommendations to Construct Theories for Metallic and Composite Plates,” *AIAA J.*, vol. 48, no. 12, pp. 2852–2866, Dec. 2010.

[26] E. Carrera, M. Petrolo, and P. Nali, “Unified Formulation Applied to Free Vibrations Finite Element Analysis of Beams with Arbitrary Section,” *Shock Vib.*, vol. 18, no. 3, pp. 485–502, 2011.

[27] E. Carrera and M. Petrolo, “Refined One-Dimensional Formulations for Laminated Structure Analysis,” *AIAA J.*, vol. 50, no. 1, pp. 176–189, Jan. 2012.

[28] E. Carrera and F. Miglioretti, “Selection of appropriate multilayered plate theories by using a genetic like algorithm,” *Compos. Struct.*, vol. 94, no. 3, pp. 1175–1186, Feb. 2012.

[29] M. Filippi and E. Carrera, “Flutter analysis of fixed and rotary wings through a one-dimensional unified formulation,” *Compos. Struct.*, vol. 133, pp. 381–389, Dec. 2015.

[30] E. Carrera, A. Pagani, and J. R. Banerjee, “Linearized buckling analysis of isotropic and composite beam-columns by Carrera Unified Formulation and dynamic stiffness method,” *Mech. Adv. Mater. Struct.*, vol. 23, no. 9, pp. 1092–1103, Sep. 2016.

[31] D. H. Robbins, J. N. Reddy, and F. Rostam-Abadi, “Layerwise modeling of progressive damage in fiber-reinforced composite laminates,” *Int. J. Mech. Mater. Des.*, vol. 2, no. 3–4, pp. 165–182, Sep. 2005.

[32] M. H. Yas, M. Shakeri, M. Heshmati, and S. Mohammadi, “Layer-wise finite element analysis of functionally graded cylindrical shell under dynamic load,” *J. Mech. Sci. Technol.*, vol. 25, no. 3, pp. 597–604, Mar. 2011.

[33] J. N. Reddy, *Mechanics of laminated composite plates and shells: theory and analysis*, 2nd ed. Boca Raton: CRC Press, 2004.

[34] E. Andreassen and C. S. Andreasen, “How to determine composite material properties using numerical homogenization,” *Comput. Mater. Sci.*, vol. 83, pp. 488–495, Feb. 2014.

[35] X. S. Sun, V. B. C. Tan, Y. Chen, L. B. Tan, R. K. Jaiman, and T. E. Tay, “Stress analysis of multi-layered hollow anisotropic composite cylindrical structures using the homogenization method,” *Acta Mech.*, vol. 225, no. 6, pp. 1649–1672, Jun. 2014.

[36] E. A. de Souza Neto, P. J. Blanco, P. J. Sánchez, and R. A. Feijóo, “An RVE-based multiscale theory of solids with micro-scale inertia and body force effects,” *Mech. Mater.*, vol. 80, pp. 136–144, Jan. 2015.

[37] M. Mosby and K. Matouš, “Computational homogenization at extreme scales,” *Extreme Mech. Lett.*, vol. 6, pp. 68–74, Mar. 2016.

[38] U. Kushnir and O. Rabinovitch, “A Multiscale Approach to Nonlinearity in Piezoelectric-Ferroelectric Smart Structures: From Micromechanics to

Engineering," *Int. J. Multiscale Comput. Eng.*, vol. 6, no. 5, pp. 451–468, 2008.

[39] G. Puel and D. Aubry, "Efficient Fatigue Simulation Using Periodig Homogenization with Multiple Time Scales," *Int. J. Multiscale Comput. Eng.*, vol. 12, no. 4, pp. 291–318, 2014.

[40] F. Willot and D. Jeulin, "Elastic and Electrical Behavior of Some Random Multiscale Highly-Contrasted Composites," *Int. J. Multiscale Comput. Eng.*, vol. 9, no. 3, pp. 305–326, 2011.

[41] W. Hu, Y. D. Ha, and F. Bobaru, "Modeling Dynamic Fracture and Damage in a Fiber-Reinforced Composite Lamina with Peridynamics," *Int. J. Multiscale Comput. Eng.*, vol. 9, no. 6, pp. 707–726, 2011.

[42] D. Savvas and V. Papadopoulos, "Nonlinear Multiscale Homogenization of Carbon Nanotube Reinforced Composites With Interfacial Slippage," *Int. J. Multiscale Comput. Eng.*, vol. 12, no. 4, pp. 271–289, 2014.

[43] S. Sakata, F. Ashida, and K. Enya, "Perturbation-Based Stochastic Microscopic Stress Analysis Considering Uncertainty in Material Properties," *Int. J. Multiscale Comput. Eng.*, vol. 9, no. 4, pp. 395–408, 2011.

[44] F. Feyel, "Multiscale FE2 elastoviscoplastic analysis of composite structures," *Comput. Mater. Sci.*, vol. 16, no. 1–4, pp. 344–354, Dec. 1999.

[45] J. F. Unger, "An FE2-X1 approach for multiscale localization phenomena," *J. Mech. Phys. Solids*, vol. 61, no. 4, pp. 928–948, Apr. 2013.

[46] C. Soutis and P. W. R. Beaumont, Eds., *Multi-scale modelling of composite material systems: the art of predictive damage modelling*. Cambridge : Boca Raton: Woodhead : Maney Publishing ; CRC Press, 2005.

[47] C. Galiotis and Paipetis, "Interfacial damage modelling of composites," *Multi-Scale Model. Compos. Mater. Syst. 1st Ed Soutis C Beaumont*, pp. 33–64, 2005.

[48] L. N. McCartney, "Multi-scale predictive modelling of cracking in laminate composites," *Multi-Scale Model. Compos. Mater. Syst. 1st Ed Soutis C Beaumont*, pp. 65–98, 2005.

[49] M. J. Bogdanor, C. Oskay, and S. B. Clay, "Multiscale modeling of failure in composites under model parameter uncertainty," *Comput. Mech.*, vol. 56, no. 3, pp. 389–404, Sep. 2015.

[50] S. A. Hosseini Kordkheili, H. Toozandehjani, and Z. Soltani, "A progressive multi-scale fatigue model for life prediction of laminated composites," *J. Compos. Mater.*, vol. 51, no. 20, pp. 2949–2960, Aug. 2017.

[51] P. W. R. Beaumont, "On the Problems of Cracking and the Question of Structural Integrity of Engineering Composite Materials," *Appl. Compos. Mater.*, vol. 21, no. 1, pp. 5–43, Feb. 2014.

[52] C. H. Wang, “Progressive multi-scale modelling of composite laminates,” *Multi-Scale Model. Compos. Mater. Syst. 1st Ed Soutis C Beaumont*, pp. 33–64, 2005.

[53] D. Ivančević and I. Smojver, “Explicit multiscale modelling of impact damage on laminated composites – Part I: Validation of the micromechanical model,” *Compos. Struct.*, vol. 145, pp. 248–258, Jun. 2016.

[54] G. Pahl, K. Wallace, and L. Blessing, Eds., *Engineering design: a systematic approach*, 3rd ed. London: Springer, 2007.

[55] Z. Yuan, T. Jiang, J. Fish, and G. Morscher, “Reduced-Order Multiscale-Multiphysics Model for Heterogeneous Materials,” *Int. J. Multiscale Comput. Eng.*, vol. 12, no. 1, pp. 45–64, 2014.

[56] M. G. D. Geers, V. G. Kouznetsova, and W. A. M. Brekelmans, “Multi-scale computational homogenization: Trends and challenges,” *J. Comput. Appl. Math.*, vol. 234, no. 7, pp. 2175–2182, Aug. 2010.

[57] G. I. Barenblatt, “The Mathematical Theory of Equilibrium Cracks in Brittle Fracture,” in *Advances in Applied Mechanics*, vol. 7, Elsevier, 1962, pp. 55–129.

[58] A. Needleman, “Some Issues in Cohesive Surface Modeling,” *Procedia IUTAM*, vol. 10, pp. 221–246, 2014.

[59] S. C. Aduloju and T. J. Truster, “A variational multiscale discontinuous Galerkin formulation for both implicit and explicit dynamic modeling of interfacial fracture,” *Comput. Methods Appl. Mech. Eng.*, vol. 343, pp. 602–630, Jan. 2019.

[60] D. Kumar, R. Roy, J.-H. Kweon, and J. Choi, “Numerical Modeling of Combined Matrix Cracking and Delamination in Composite Laminates Using Cohesive Elements,” *Appl. Compos. Mater.*, vol. 23, no. 3, pp. 397–419, Jun. 2016.

[61] R. Venkatachalam and S. Balasivanandha Prabu, “Vibration and damping analysis of orthotropic sandwich shaft-disc system using finite element method,” *Int. J. Mech. Mater. Des.*, vol. 8, no. 3, pp. 287–296, Sep. 2012.

[62] S. R. Sahoo and M. C. Ray, “Analysis of smart damping of laminated composite beams using mesh free method,” *Int. J. Mech. Mater. Des.*, Jul. 2017.

[63] P. Lisandrin and M. van Tooren, “High-order finite elements reduced models for modal analysis of stiffened panels,” *Int. J. Mech. Mater. Des.*, vol. 3, no. 2, pp. 111–127, Jun. 2006.

[64] D. Gutierrez-Lemini, *Engineering viscoelasticity*. New York: Springer, 2014.

[65] A. E. Assie, M. A. Eltaher, and F. F. Mahmoud, “Modeling of viscoelastic contact-impact problems,” *Appl. Math. Model.*, vol. 34, no. 9, pp. 2336–2352, Sep. 2010.

[66] T. Pritz, “Analysis of four-parameter fractional derivative model of real solid materials,” *J. Sound Vib.*, vol. 195, no. 1, pp. 103–115, Aug. 1996.

[67] T. Pritz, “Five-parameter fractional derivative model for polymeric damping materials,” *J. Sound Vib.*, vol. 265, no. 5, pp. 935–952, Aug. 2003.

[68] K.-J. Bathe, *Finite element procedures*. Englewood Cliffs, N.J: Prentice Hall, 1996.

[69] Z.-Q. Qu, *Model order reduction techniques: with applications in finite element analysis*. London: Springer, 2010.

[70] B. Han *et al.*, “A refined quasi-3D zigzag beam theory for free vibration and stability analysis of multilayered composite beams subjected to thermomechanical loading,” *Compos. Struct.*, vol. 204, pp. 620–633, Nov. 2018.

[71] R. Kussmaul, M. Zogg, and P. Ermanni, “An efficient two-dimensional shear-lag model for the analysis of patched laminates,” *Compos. Struct.*, vol. 206, pp. 288–300, Dec. 2018.

[72] Y. Yan, E. Carrera, A. G. de Miguel, A. Pagani, and Q.-W. Ren, “Meshless analysis of metallic and composite beam structures by advanced hierarchical models with layer-wise capabilities,” *Compos. Struct.*, vol. 200, pp. 380–395, Sep. 2018.

[73] C. Bedon and M. Fragiacomo, “Numerical analysis of timber-to-timber joints and composite beams with inclined self-tapping screws,” *Compos. Struct.*, vol. 207, pp. 13–28, Jan. 2019.

[74] Z. Sápi, R. Butler, and A. Rhead, “Filler materials in composite out-of-plane joints – A review,” *Compos. Struct.*, vol. 207, pp. 787–800, Jan. 2019.

[75] X. C. Sun, L. F. Kawashita, A. S. Kaddour, M. J. Hiley, and S. R. Hallett, “Comparison of low velocity impact modelling techniques for thermoplastic and thermoset polymer composites,” *Compos. Struct.*, vol. 203, pp. 659–671, Nov. 2018.

[76] Q. Dong, G. Wan, L. Ping, Y. Guo, X. Yi, and Y. Jia, “Coupled thermal-mechanical damage model of laminated carbon fiber/resin composite subjected to lightning strike,” *Compos. Struct.*, vol. 206, pp. 185–193, Dec. 2018.

[77] K. Matouš, M. G. D. Geers, V. G. Kouznetsova, and A. Gillman, “A review of predictive nonlinear theories for multiscale modeling of heterogeneous materials,” *J. Comput. Phys.*, vol. 330, pp. 192–220, Feb. 2017.

[78] H.-Y. Kim and S.-Y. Lee, “Static and fatigue load performance of a pultruded GFRP deck panel reinforced with steel wires,” *Compos. Struct.*, vol. 207, pp. 166–175, Jan. 2019.

[79] Z. Song, J. Le, D. Whisler, and H. Kim, “Skin-stringer interface failure investigation of stringer-stiffened curved composite panels under hail ice impact,” *Int. J. Impact Eng.*, vol. 122, pp. 439–450, Dec. 2018.

[80] B. Raju, S. R. Hiremath, and D. Roy Mahapatra, “A review of micromechanics based models for effective elastic properties of reinforced polymer matrix composites,” *Compos. Struct.*, vol. 204, pp. 607–619, Nov. 2018.

[81] H. Molker, R. Gutkin, S. Pinho, and L. E. Asp, “Hot spot analysis in complex composite material structures,” *Compos. Struct.*, vol. 207, pp. 776–786, Jan. 2019.

[82] E. Carrera, S. Valvano, and M. Filippi, “Classical, higher-order, zig-zag and variable kinematic shell elements for the analysis of composite multilayered structures,” *Eur. J. Mech. - ASolids*, vol. 72, pp. 97–110, Nov. 2018.

[83] A. G. de Miguel, I. Kaleel, M. H. Nagaraj, A. Pagani, M. Petrolo, and E. Carrera, “Accurate evaluation of failure indices of composite layered structures via various FE models,” *Compos. Sci. Technol.*, vol. 167, pp. 174–189, Oct. 2018.

[84] A. Entezari, M. Filippi, E. Carrera, and M. A. Kouchakzadeh, “3D dynamic coupled thermoelastic solution for constant thickness disks using refined 1D finite element models,” *Appl. Math. Model.*, vol. 60, pp. 273–285, Aug. 2018.

[85] C. Yang, G. Jin, Y. Zhang, and Z. Liu, “A unified three-dimensional method for vibration analysis of the frequency-dependent sandwich shallow shells with general boundary conditions,” *Appl. Math. Model.*, vol. 66, pp. 59–76, Feb. 2019.

[86] M. Assarar, W. Zouari, R. Ayad, H. Kebir, and J.-M. Berthelot, “Improving the damping properties of carbon fibre reinforced composites by interleaving flax and viscoelastic layers,” *Compos. Part B Eng.*, vol. 152, pp. 248–255, Nov. 2018.

[87] M. Filippi, E. Carrera, and S. Valvano, “Analysis of multilayered structures embedding viscoelastic layers by higher-order, and zig-zag plate elements,” *Compos. Part B Eng.*, vol. 154, pp. 77–89, Dec. 2018.

[88] M. Hirsekorn, L. Marcin, and T. Godon, “Multi-scale modeling of the viscoelastic behavior of 3D woven composites,” *Compos. Part Appl. Sci. Manuf.*, vol. 112, pp. 539–548, Sep. 2018.

[89] M. K. Hazzard, R. S. Trask, U. Heisserer, M. Van Der Kamp, and S. R. Hallett, “Finite element modelling of Dyneema® composites: From quasi-static rates to ballistic impact,” *Compos. Part Appl. Sci. Manuf.*, vol. 115, pp. 31–45, Dec. 2018.

[90] F. Stojcevski, J. D. Randall, and L. C. Henderson, “Using variable interfacial adhesion characteristics within a composite to improve flexural strength and decrease fiber volume,” *Compos. Sci. Technol.*, vol. 165, pp. 250–258, Sep. 2018.

[91] T. Berton, S. Haldar, J. Montesano, and C. V. Singh, “Time-dependent damage analysis for viscoelastic-viscoplastic structural laminates under biaxial loading,” *Compos. Struct.*, vol. 203, pp. 60–70, Nov. 2018.

[92] F. Covezzi, S. de Miranda, S. Marfia, and E. Sacco, “Multiscale analysis of nonlinear composites via a mixed reduced order formulation,” *Compos. Struct.*, vol. 203, pp. 810–825, Nov. 2018.

[93] Z. Ullah, Ł. Kaczmarczyk, S. A. Grammatikos, M. C. Evernden, and C. J. Pearce, “Multi-scale computational homogenisation to predict the long-term durability of composite structures,” *Comput. Struct.*, vol. 181, pp. 21–31, Mar. 2017.

[94] S. Wulfinghoff, F. Cavaliere, and S. Reese, “Model order reduction of nonlinear homogenization problems using a Hashin–Shtrikman type finite element method,” *Comput. Methods Appl. Mech. Eng.*, vol. 330, pp. 149–179, Mar. 2018.

[95] R. R. Hiemstra, F. Calabrò, D. Schillinger, and T. J. R. Hughes, “Optimal and reduced quadrature rules for tensor product and hierarchically refined splines in isogeometric analysis,” *Comput. Methods Appl. Mech. Eng.*, vol. 316, pp. 966–1004, Apr. 2017.

[96] J. Oliver, M. Caicedo, A. E. Huespe, J. A. Hernández, and E. Roubin, “Reduced order modeling strategies for computational multiscale fracture,” *Comput. Methods Appl. Mech. Eng.*, vol. 313, pp. 560–595, Jan. 2017.

[97] P. Shakya, M. R. Sunny, and D. K. Maiti, “A parametric study of flutter behavior of a composite wind turbine blade with bend-twist coupling,” *Compos. Struct.*, vol. 207, pp. 764–775, Jan. 2019.

[98] U. Gul, M. Aydogdu, and F. Karacam, “Dynamics of a functionally graded Timoshenko beam considering new spectrums,” *Compos. Struct.*, vol. 207, pp. 273–291, Jan. 2019.

[99] J. Li, Y. Xue, F. Li, and Y. Narita, “Active vibration control of functionally graded piezoelectric material plate,” *Compos. Struct.*, vol. 207, pp. 509–518, Jan. 2019.

[100] S. Kumar, B. Dhas, and D. Roy, “Emergence of pseudo-ductility in laminated ceramic composites,” *Compos. Struct.*, vol. 204, pp. 664–676, Nov. 2018.

[101] H. Ahmadi and G. Rahimi, “Analytical and experimental investigation of transverse loading on grid stiffened composite panels,” *Compos. Part B Eng.*, vol. 159, pp. 184–198, Feb. 2019.

[102] A. Khan and H. S. Kim, “Assessment of delaminated smart composite laminates via system identification and supervised learning,” *Compos. Struct.*, vol. 206, pp. 354–362, Dec. 2018.

[103] X.-Y. Zhou, P. D. Gosling, Z. Ullah, L. Kaczmarczyk, and C. J. Pearce, “Stochastic multi-scale finite element based reliability analysis for laminated composite structures,” *Appl. Math. Model.*, vol. 45, pp. 457–473, May 2017.

[104] K. Liang, Q. Sun, and Y. Zhang, “Nonlinear buckling analysis of variable stiffness composite plates based on the reduced order model,” *Compos. Struct.*, vol. 206, pp. 681–692, Dec. 2018.

[105] X. Li, H. Wang, and G. Li, “Reanalysis assisted metaheuristic optimization for free vibration problems of composite laminates,” *Compos. Struct.*, vol. 206, pp. 380–391, Dec. 2018.

[106] M. Savran and L. Aydin, “Stochastic optimization of graphite-flax/epoxy hybrid laminated composite for maximum fundamental frequency and minimum cost,” *Eng. Struct.*, vol. 174, pp. 675–687, Nov. 2018.

[107] M. Montemurro, A. Pagani, G. A. Fiordilino, J. Pailhès, and E. Carrera, “A general multi-scale two-level optimisation strategy for designing composite stiffened panels,” *Compos. Struct.*, vol. 201, pp. 968–979, Oct. 2018.

[108] G. Gonzalez Lozano, A. Tiwari, and C. Turner, “A design algorithm to model fibre paths for manufacturing of structurally optimised composite laminates,” *Compos. Struct.*, vol. 204, pp. 882–895, Nov. 2018.

[109] D. Scheffold, C. Bach, F. Duddeck, G. Müller, and M. Buchschmid, “Vibration Frequency Optimization of Jointed Structures with Contact Nonlinearities using Hyper-Reduction,” *IFAC-Pap.*, vol. 51, no. 2, pp. 843–848, 2018.

[110] S. Cagin, “Reduced and Separated Meta-Models of the Scavenging by Ports in 2-Stroke Diesel Engines to use Evolutionary Algorithms in Search Space,” Bordeaux University, 2015.

[111] S. Zaghi, X. Martinez, R. Rossi, and M. Petracca, “Adaptive and off-line techniques for non-linear multiscale analysis,” *Compos. Struct.*, vol. 206, pp. 215–233, Dec. 2018.

[112] M. P. Limongelli, “The Surface Interpolation Method for damage localization in plates,” *Mech. Syst. Signal Process.*, vol. 118, pp. 171–194, Mar. 2019.

[113] S. Bhattacharjee and K. Matouš, “A nonlinear manifold-based reduced order model for multiscale analysis of heterogeneous hyperelastic materials,” *J. Comput. Phys.*, vol. 313, pp. 635–653, May 2016.

[114] M. A. Bessa *et al.*, “A framework for data-driven analysis of materials under uncertainty: Countering the curse of dimensionality,” *Comput. Methods Appl. Mech. Eng.*, vol. 320, pp. 633–667, Jun. 2017.

[115] R. Bostanabad *et al.*, “Computational microstructure characterization and reconstruction: Review of the state-of-the-art techniques,” *Prog. Mater. Sci.*, vol. 95, pp. 1–41, Jun. 2018.

[116] G. R. Liu, K. Zaw, Y. Y. Wang, and B. Deng, “A novel reduced-basis method with upper and lower bounds for real-time computation of linear elasticity problems,” *Comput. Methods Appl. Mech. Eng.*, vol. 198, no. 2, pp. 269–279, Dec. 2008.

[117] R. Milani, A. Quarteroni, and G. Rozza, “Reduced basis method for linear elasticity problems with many parameters,” *Comput. Methods Appl. Mech. Eng.*, vol. 197, no. 51–52, pp. 4812–4829, Oct. 2008.

[118] L. Iapichino and S. Volkwein, “Optimization strategy for parameter sampling in the reduced basis method,” *IFAC-Pap.*, vol. 48, no. 1, pp. 707–712, 2015.

[119] Y. Lu, N. Blal, and A. Gravouil, “Space–time POD based computational vademecums for parametric studies: application to thermo-mechanical problems,” *Adv. Model. Simul. Eng. Sci.*, vol. 5, no. 1, Dec. 2018.

[120] J. A. Hernández, M. A. Caicedo, and A. Ferrer, “Dimensional hyper-reduction of nonlinear finite element models via empirical cubature,” *Comput. Methods Appl. Mech. Eng.*, vol. 313, pp. 687–722, Jan. 2017.

[121] K. Samir, B. Brahim, R. Capozucca, and M. Abdel Wahab, “Damage detection in CFRP composite beams based on vibration analysis using proper orthogonal decomposition method with radial basis functions and cuckoo search algorithm,” *Compos. Struct.*, vol. 187, pp. 344–353, Mar. 2018.

[122] C.-M. Chang, T.-K. Lin, and C.-W. Chang, “Applications of neural network models for structural health monitoring based on derived modal properties,” *Measurement*, vol. 129, pp. 457–470, Dec. 2018.

[123] R. B. Hudson and A. Sinha, “An order reduction method for single-walled carbon nanotubes with multi-vacancy defects,” *Carbon*, vol. 138, pp. 81–89, Nov. 2018.

[124] J.-C. Michel and P. Suquet, “A model-reduction approach in micromechanics of materials preserving the variational structure of constitutive relations,” *J. Mech. Phys. Solids*, vol. 90, pp. 254–285, May 2016.

[125] M. Leuschner and F. Fritzen, “Reduced order homogenization for viscoplastic composite materials including dissipative imperfect interfaces,” *Mech. Mater.*, vol. 104, pp. 121–138, Jan. 2017.

[126] D. González, F. Masson, F. Poulhaon, A. Leygue, E. Cueto, and F. Chinesta, “Proper Generalized Decomposition based dynamic data driven inverse identification,” *Math. Comput. Simul.*, vol. 82, no. 9, pp. 1677–1695, May 2012.

[127] E. Nadal, F. Chinesta, P. Díez, F. J. Fuenmayor, and F. D. Denia, “Real time parameter identification and solution reconstruction from experimental data using the Proper Generalized Decomposition,” *Comput. Methods Appl. Mech. Eng.*, vol. 296, pp. 113–128, Nov. 2015.

[128] N. Bur, P. Joyot, and P. Villon, “Reduced-order model of optimal temperature control for the automated fibre placement process,” *Comptes Rendus Mécanique*, vol. 346, no. 7, pp. 556–570, Jul. 2018.

[129] A. Sibileau, A. García-González, F. Auricchio, S. Morganti, and P. Díez, “Explicit parametric solutions of lattice structures with proper generalized decomposition (PGD): Applications to the design of 3D-printed architectured materials,” *Comput. Mech.*, vol. 62, no. 4, pp. 871–891, Oct. 2018.

[130] E. Giner, B. Bognet, J. J. Ródenas, A. Leygue, F. J. Fuenmayor, and F. Chinesta, “The Proper Generalized Decomposition (PGD) as a numerical

procedure to solve 3D cracked plates in linear elastic fracture mechanics," *Int. J. Solids Struct.*, vol. 50, no. 10, pp. 1710–1720, May 2013.

[131] F. El Halabi, D. González, A. Chico, and M. Doblaré, "FE2 multiscale in linear elasticity based on parametrized microscale models using proper generalized decomposition," *Comput. Methods Appl. Mech. Eng.*, vol. 257, pp. 183–202, Apr. 2013.

[132] S. Metoui, E. Pruliere, A. Ammar, F. Dau, and I. Iordanoff, "A multiscale separated representation to compute the mechanical behavior of composites with periodic microstructure," *Math. Comput. Simul.*, vol. 144, pp. 162–181, Feb. 2018.

[133] E. Prulière, "3D simulation of laminated shell structures using the Proper Generalized Decomposition," *Compos. Struct.*, vol. 117, pp. 373–381, Nov. 2014.

[134] C. Ghnatios, E. Abisset-Chavanne, C. Binetruy, F. Chinesta, and S. Advani, "3D modeling of squeeze flow of multiaxial laminates," *J. Non-Newton. Fluid Mech.*, vol. 234, pp. 188–200, Aug. 2016.

[135] F. El Halabi, D. González, J. A. Sanz-Herrera, and M. Doblaré, "A PGD-based multiscale formulation for non-linear solid mechanics under small deformations," *Comput. Methods Appl. Mech. Eng.*, vol. 305, pp. 806–826, Jun. 2016.

[136] J. Zghal, A. Ammar, F. Chinesta, C. Binetruy, and E. Abisset-Chavanne, "High-resolution elastic analysis of thin-ply composite laminates," *Compos. Struct.*, vol. 172, pp. 15–21, Jul. 2017.

[137] S. Metoui, E. Pruliere, A. Ammar, and F. Dau, "A reduced model to simulate the damage in composite laminates under low velocity impact," *Comput. Struct.*, vol. 199, pp. 34–45, Apr. 2018.

[138] A. Leon, A. Barasinski, E. Abisset-Chavanne, E. Cueto, and F. Chinesta, "Wavelet-based multiscale proper generalized decomposition," *Comptes Rendus Mécanique*, vol. 346, no. 7, pp. 485–500, Jul. 2018.

[139] A. Ammar, A. Huerta, F. Chinesta, E. Cueto, and A. Leygue, "Parametric solutions involving geometry: A step towards efficient shape optimization," *Comput. Methods Appl. Mech. Eng.*, vol. 268, pp. 178–193, Jan. 2014.

[140] L. Chamoin, F. Pled, P.-E. Allier, and P. Ladevèze, "A posteriori error estimation and adaptive strategy for PGD model reduction applied to parametrized linear parabolic problems," *Comput. Methods Appl. Mech. Eng.*, vol. 327, pp. 118–146, Dec. 2017.

[141] M. H. Malik, D. Borzacchiello, J. V. Aguado, and F. Chinesta, "Advanced parametric space-frequency separated representations in structural dynamics: A harmonic–modal hybrid approach," *Comptes Rendus Mécanique*, vol. 346, no. 7, pp. 590–602, Jul. 2018.

[142] A. Ammar, A. Zghal, F. Morel, and F. Chinesta, “On the space-time separated representation of integral linear viscoelastic models,” *Comptes Rendus Mécanique*, vol. 343, no. 4, pp. 247–263, Apr. 2015.

[143] P. Ladevèze, “On reduced models in nonlinear solid mechanics,” *Eur. J. Mech. - ASolids*, vol. 60, pp. 227–237, Nov. 2016.

[144] R. M. Gutierrez, X. Fischer, and F. Bennis, “A Tutor Agent for supporting distributed knowledge modelling in interactive product design,” *Int. J. Intell. Syst. Technol. Appl.*, vol. 4, no. 3/4, p. 399, 2008.

[145] X. Fischer, J.-P. Nadeau, P. Sébastian, and P. Joyot, “Decision support in integrated mechanical design through qualitative constraints,” in *Integrated Design and Manufacturing in Mechanical Engineering*, P. Chedmail. G. Cgnet, C. Fortin, C. Mascle, J. Pegna, Kluwer., 2002, pp. 35–42.

[146] D. Bouyssou, Ed., *Decision-making process: concepts and methods*. London: ISTE [u.a.], 2009.

[147] A. Hambali, S. M. Sapuan, N. Ismail, and Y. Nukman, “Material selection of polymeric composite automotive bumper beam using analytical hierarchy process,” *J. Cent. South Univ. Technol.*, vol. 17, no. 2, pp. 244–256, Apr. 2010.

[148] A. Corona, B. Madsen, M. Z. Hauschild, and M. Birkved, “Natural fibre selection for composite eco-design,” *CIRP Ann.*, vol. 65, no. 1, pp. 13–16, 2016.

[149] E. A. Calado, M. Leite, and A. Silva, “Selecting composite materials considering cost and environmental impact in the early phases of aircraft structure design,” *J. Clean. Prod.*, vol. 186, pp. 113–122, Jun. 2018.

[150] R. Srinivasan, H. M. Karandikar, and F. Mistree, “Understanding design-manufacture interaction using compromise decision support problems—III. Design for manufacture of composite pressure vessels,” *Comput. Struct.*, vol. 40, no. 3, pp. 705–717, Jan. 1991.

[151] J. Sanz-Corretge, “A procedure to design optimum composite plates using implicit decision trees,” *Struct. Multidiscip. Optim.*, vol. 56, no. 5, pp. 1169–1183, Nov. 2017.

[152] A. E. Coronado Mondragon, C. E. Coronado Mondragon, P. J. Hogg, and N. Rodríguez-López, “A design process for the adoption of composite materials and supply chain reconfiguration supported by a software tool,” *Comput. Ind. Eng.*, vol. 121, pp. 62–72, Jul. 2018.

[153] M. Gascons, N. Blanco, J. A. Mayugo, and K. Matthys, “A Strategy to Support Design Processes for Fibre Reinforced Thermoset Composite Materials,” *Appl. Compos. Mater.*, vol. 19, no. 3–4, pp. 297–314, Jun. 2012.

[154] T. Macquart, V. Maes, M. T. Bordogna, A. Pirrera, and P. M. Weaver, “Optimisation of composite structures – Enforcing the feasibility of lamination parameter constraints with computationally-efficient maps,” *Compos. Struct.*, vol. 192, pp. 605–615, May 2018.

[155] T. A. Dutra and S. F. M. de Almeida, “Composite plate stiffness multicriteria optimization using lamination parameters,” *Compos. Struct.*, vol. 133, pp. 166–177, Dec. 2015.

[156] N. Ranaivomiarana, F.-X. Irisarri, D. Bettebghor, and B. Desmorat, “Concurrent optimization of material spatial distribution and material anisotropy repartition for two-dimensional structures,” *Contin. Mech. Thermodyn.*, Apr. 2018.

[157] X. Tong, W. Ge, and Y. Zhang, “Optimal fiber orientation and topology design for compliant mechanisms with fiber-reinforced composites,” *Proc. Inst. Mech. Eng. Part C J. Mech. Eng. Sci.*, vol. 231, no. 12, pp. 2302–2312, Jun. 2017.

[158] S. M. C. Monte, V. Infante, J. F. A. Madeira, and F. Moleiro, “Optimization of fibers orientation in a composite specimen,” *Mech. Adv. Mater. Struct.*, vol. 24, no. 5, pp. 410–416, Apr. 2017.

[159] J. N. Reddy, Ed., *Mechanics of Composite Materials*, vol. 34. Dordrecht: Springer Netherlands, 1994.

[160] S. Nikbakt, S. Kamarian, and M. Shakeri, “A review on optimization of composite structures Part I: Laminated composites,” *Compos. Struct.*, vol. 195, pp. 158–185, Jul. 2018.

[161] J. H. S. Almeida, M. L. Ribeiro, V. Tita, and S. C. Amico, “Stacking sequence optimization in composite tubes under internal pressure based on genetic algorithm accounting for progressive damage,” *Compos. Struct.*, vol. 178, pp. 20–26, Oct. 2017.

[162] F.-X. Irisarri, D. H. Bassir, N. Carrere, and J.-F. Maire, “Multiobjective stacking sequence optimization for laminated composite structures,” *Compos. Sci. Technol.*, vol. 69, no. 7–8, pp. 983–990, Jun. 2009.

[163] M. Miki and Y. Sugiyamat, “Optimum Design of Laminated Composite Plates Using Lamination Parameters,” *AIAA J.*, vol. 31, no. 5, pp. 921–922, May 1993.

[164] Z. Jing, X. Fan, and Q. Sun, “Stacking sequence optimization of composite laminates for maximum buckling load using permutation search algorithm,” *Compos. Struct.*, vol. 121, pp. 225–236, Mar. 2015.

[165] P. Ladevèze, “Multiscale modelling and computational strategies for composites,” *Int. J. Numer. Methods Eng.*, vol. 60, no. 1, pp. 233–253, May 2004.

[166] J. LLorca, C. González, J. M. Molina-Aldareguía, and C. S. Lópes, “Multiscale Modeling of Composites: Toward Virtual Testing … and Beyond,” *JOM*, vol. 65, no. 2, pp. 215–225, Feb. 2013.

[167] F. Cluzel, B. Yannou, and M. Dihlmann, “Using evolutionary design to interactively sketch car silhouettes and stimulate designer’s creativity,” *Eng. Appl. Artif. Intell.*, vol. 25, no. 7, pp. 1413–1424, Oct. 2012.

[168] G. Sirin, C. J. J. Paredis, B. Yannou, E. Coatanea, and E. Landel, “A Model Identity Card to Support Simulation Model Development Process in a Collaborative Multidisciplinary Design Environment,” *IEEE Syst. J.*, vol. 9, no. 4, pp. 1151–1162, Dec. 2015.

[169] B. Yannou and J.-F. Petiot, “A View of Design (and JMD): The French Perspective,” *J. Mech. Des.*, vol. 133, no. 5, p. 050301, 2011.

[170] F. O. Sonmez, “Optimum Design of Composite Structures: A Literature Survey (1969–2009),” *J. Reinf. Plast. Compos.*, vol. 36, no. 1, pp. 3–39, Jan. 2017.

[171] D. S. Dugdale, “Yielding of steel sheets containing slits,” *J. Mech. Phys. Solids*, vol. 8, no. 2, pp. 100–104, May 1960.

[172] “ANSYS Mechanical APDL Theory Reference. Release 17.0.” ANSYS, Inc., 2016.

[173] A. Konyukhov and R. Izi, *Introduction to computational contact mechanics: a geometrical approach*. Chichester, West Sussex: Wiley, 2015.

[174] K. Ordaz-Hernández, “Modelling Techniques for Virtual Prototyping on Interactive Design: Application to Non linear Dynamic behaviour of a Structure Under Deformation,” Nantes University, 2007.

[175] N. J. Pagano, “Exact Solutions for Rectangular Bidirectional Composites and Sandwich Plates,” *Mech. Compos. Mater.*, p. 16, 1966.

[176] E. Carrera and A. Pagani, “Multi-line enhanced beam model for the analysis of laminated composite structures,” *Compos. Part B Eng.*, vol. 57, pp. 112–119, Feb. 2014.

[177] A. Falcó, L. Hilario, N. Montés, and M. C. Mora, “Numerical strategies for the Galerkin–proper generalized decomposition method,” *Math. Comput. Model.*, vol. 57, no. 7–8, pp. 1694–1702, Apr. 2013.

[178] ASTM, “D3039/D3039M-14: Standard Test Method for Tensile Properties of Polymer Matrix Composite Materials.” 2016.

[179] ISO, “ISO 18437-3:2005 Mechanical vibration ando shock - Characterization of the dynamic mechanical properties of visco-elastic materials - Part3: Cantilever shear beam method.” International Organization for Standardization, 2005.

[180] ISO, “ISO/IEC 17025:2017 General requirements for the competence of testing and calibration laboratories.” International Organization for Standardization, 2017.

[181] ISO, “ISO 7626-2 Vibration and shock – Experimental determinationof mechanical mobility – Part 2: Measurements using single-point translation excitation with an attached vibration exciter.” 1990.

[182] G. Fontecha Dulcey, X. Fischer, and P. Joyot, “An experiment-based method for parameter identification of a reduced multiscale parametric

viscoelastic model of a laminated composite beam," *Multiscale Multidiscip. Model. Exp. Des.*, Jun. 2018.

[183] P. Ostalczyk, *Discrete fractional calculus: applications in control and image processing*. New Jersey: World Scientific, 2016.

[184] A. C. Galucio, J.-F. Deü, and R. Ohayon, "Finite element formulation of viscoelastic sandwich beams using fractional derivative operators," *Comput. Mech.*, vol. 33, no. 4, pp. 282–291, Mar. 2004.

[185] L. Irazu and M. J. Elejabarrieta, "The effect of the viscoelastic film and metallic skin on the dynamic properties of thin sandwich structures," *Compos. Struct.*, vol. 176, pp. 407–419, Sep. 2017.

[186] Y. W. Kwon, D. H. Allen, and R. Talreja, Eds., *Multiscale modeling and simulation of composite materials and structures*. New York: Springer, 2008.

[187] M. M. Kamiński, *Computational mechanics of composite materials: sensitivity, randomness, and multiscale behaviour*. London: Springer, 2005.

[188] Z. Michalewicz, *Genetic algorithms + data structures = evolution programs*, 2nd, extended ed ed. Berlin ; New York: Springer-Verlag, 1994.

[189] B. Cherabi, A. Hamrani, I. Belaidi, S. Khelladi, and F. Bakir, "An efficient reduced-order method with PGD for solving journal bearing hydrodynamic lubrication problems," *Comptes Rendus Mécanique*, vol. 344, no. 10, pp. 689–714, Oct. 2016.